TECHNISCHE UNIVERSITÄT DARMSTADT

N- and C-terminal domains in tobacco aquaporins – Analysis of protein-mediated water permeability *in vitro* and *in silico*

Vom Fachbereich Biologie der Technischen Universität Darmstadt
zur
Erlangung des akademischen Grades
eines *Doctor rerum naturalium*
genehmigte Dissertation von

M. Sc. Gabriel Glitsos
aus Korinth, Griechenland

1. Referent: Prof. Dr. Ralf Kaldenhoff
2. Referent: Prof. Dr. Heribert Warzecha

Tag der Einreichung: 16.11.2016
Tag der mündlichen Prüfung: 10.03.2017
Darmstadt 2017
D 17

Dedicated to Renata

“Perhaps it is better in this present world of ours that a revolutionary idea or invention instead of being helped and patted, be hampered and ill-treated in its adolescence – by want of means, by selfish interest, pedantry, stupidity and ignorance; that it be attacked and stifled; that it pass through bitter trials and tribulations, through the heartless strife of commercial existence. *So* do we get our light. So all that was great in the past was ridiculed, condemned, combated, suppressed – only to emerge all the more powerfully, all the more triumphantly from the struggle.”

Nikola Tesla. 1905. The transmission of electrical energy without wires as a means for furthering peace. *Electrical World and Engineer*. **Jan 7 1905:** 21-24.

I. Table of Contents

II. Table of Figures

III. List of Tables

IV. List of Abbreviations

(a)s	(anti)sense
A	ampere
A	amplitude
Å	Ångström
A1	NtAQP1
aa	amino acid(s)
ABA	abscisic acid
ABM	aquaporin based biomimetic membrane
AcP	acetyl phosphate lithium potassium salt
AFM	atomic force microscopy
Amp(R)	ampicillin (resistance)
AP	alkaline phophatase
APS	ammonium persulfate
AQP	aquaporin
Aqy	aquaporin (yeast)
ar/R	aromatic / arginine motif
At	*Arabidopsis thaliana*
ATP / ADP	adenosine tri(di)phosphate
AU	arbitrary unit(s)
b	bovine
BIB	drosophila big brain
bp	base pair(s)
Brij S20	polyethylene glycol octadecyl ether
BSA	bovine serum albumine
Bv	*Beta vulgaris*
°C	degrees Celsius
C	carboxyl (terminus)
CAPS	N-cyclohexyl-3-aminopropanesulfonic acid
CECF	continuous exchange cell-free expression
CFCF	continuous flow cell-free expression
CFE	cell-free expression
(c/ds)DNA	(complementary/double stranded) deoxyribonucleic acid
(c)GMP	(cyclic) guanosine monophosphate
CGSC	Coli Genetic Stock Center
cic	*Cicadella viridis*
Cs	*Camelina sativa*
CTP	cytidine triphosphate
Da	dalton (unified atomic mass unit)
D-CF	detergent based cell-free expression of membrane proteins
DDM	n-dodecyl-β-D-maltopyranoside
Δ_{osm}	molar quantification of an osmotic gradient
Δ(X)	deletion of X (nucleotides, amino acids or domain)
dem.	demineralized
(d)NTP	(deoxy)nucleoside triphosphate
ds	downstream
DTT	dithiothreitol
E. coli	*Escherichia coli*
E_{1-5}	elution step 1-5

ECM	electron cryomicroscopy
EDTA	ethylenediaminetetraacetic acid
e.g.	exempli gratia (for the sake of an example)
EMBL-EBI	European Molecular Biology Laboratory - European Bioinformatics Institute
ER	endoplasmatic reticulum
et al.	et alia (and others)
EtBr	ethidium bromide
EtOH	ethanol
F_D	(relative) fitting distance
Fig.	figure
FM	feeding mix
FT	flowthrough
fw	forward
g	gram
g	gravitational force (multiples of standard gravity)
GE	gel electrophoresis
GFP	green fluorescent protein
GLP	aquaglyceroporin (GlpF-like intrinsic protein)
GlpF	glycerol permease facilitator
GRAVY	Grand Average of Hydropathy
GST	glutathion S-transferase
GTP	guanosine triphosphate
h	hour(s)
h	human
HB/E	short helix B/E
HE	HEPES-EDTA
HEPES	4-(2-hydroxyethyl)-1-piperazineethanesulfonic acid
HGVS	Human Genome Variation Society
HIP	hybrid intrinsic protein
His_6	sixfold histidine affinity tag
HN	HEPES-NaCl
HXK	hexokinase
hν	photon energy = Planck`s constant * light frequency
i.e.	id est (that is)
IgG	immunoglobulin G
IMAC	immobilized metal ion affinity chromatography
IPTG	isopropyl-β-D-thiogalactopyranoside
k	rate constant
l	liter
lacI	lac repressor
lacO	lac operon
LA-E	loop A-E
LB	Lysogeny-Broth
L-CF	lipid based cell-free expression of membrane proteins
LIRMM	Montpellier Laboratory for Computer Science, Robotics, and Microelectronics
LN_2	liquid nitrogen
Lp_r	root hydraulic conductivity
lsiI	low silicon rice 1 (gene)
LUV	large, unilamellar liposome vesicle(s)
M	Molar

m	meter
Mc	*Mesembryanthemum crystallinum*
min	minute(s)
MIP	major intrinsic protein
MLV	large, multilamellar liposome vesicle(s)
MOE	Molecular Operating Environment
MP	membrane protein
mpstruc	Data Bank of Membrane Proteins with known 3D Structure
MQ-H_2O	MilliQ filtered and demineralized water
(m/t)RNA	(messenger/transfer) ribonucleic acid
MS	mass spectrometry
MWCO	molecular weight cut-off
N	amino (terminus)
n	sample quantity
n.d.	not discussed
NADP(H)	nicotinamide adenine dinucleotide phosphate
NiNTA	nickel-nitrilotriacetic acid
NIP	nodulin26-like intrinsic protein
NIP6	type-6 nodulin intrinsic protein
NMR	nuclear magnetic resonance spectroscopy
Nod26	Soybean Nodulin 26
NPA	asparagine-proline-alanine motif
ns	not significant
Nt	*Nicotiana tabacum*
OD	optical density
ori	origin of replication
Os	*Oryza sativa*
p	promoter
P	precipitate
p	statistical significance level
P1 - P5	Froger´s positions
P2	NtPIP2;1
Pa	Pascal
PAA	polyacrylamide
PAGE	polyacrylamide gel electrophoresis
PBS(T)	phosphate buffered saline (+ Tween)
PC	L-α-phophatidylcholine
P-CF	precipitation based cell-free expression of membrane proteins
PCR	polymerase chain reaction
PDB	Protein Data Bank
PE	polyester
PEG	polyethylene glycol
PEP	phosphoenolpyruvate monopotassium salt
P_f	water permeability factor [m/s]
Pf	*Plasmodium falciparum*
Pfu	*Pyrococcus furiosus*
pH	negative logarithm to base 10 of hydrogen ion molar concentration
PIP	plasma membrane intrinsic protein
PK	pyruvate kinase
PMSF	phenylmethylsulfonyl fluoride

POSS	polyhedral oligomeric silsesquioxanes
psi	pounds per square inch
PTM	post-translational modification
PVDF	polyvinylidene fluoride
RCWMDE	Arg, Cys, Trp, Met, Asp, Glu
RE	restriction endonuclease
rec.	reconstitution mix
RM	reaction mix
RMSD	root mean square distance
ROS	reactive oxygen species
rpm	revolutions per minute
Rs	*Raphanus sativus*
RT	room temperature
RuBisCO	ribulose-1,5-bisphosphate carboxylase/oxygenase
rv	reverse
s	second(s)
S	surface area
S	supernatant
SDS	sodium dodecylsulfate
SE	standard error
SF	(proteo)liposome sample ready for Stopped Flow measurement
SIB	Swiss Institute of Bioinformatics
SIP	small basic intrinsic protein
SLB	supported lipid bilayer
Sm	*Schistosoma mansoni*
SM	symbiosome membrane
So	*Spinacia oleracea*
SUV	small, unilamellar liposome vesicle(s)
t	terminator
T(7)RNAP	T7 RNA polymerase
TA	triacetate
TAE	triacetate-ethylenediaminetetraacetic acid
Taq	*Thermus aquaticus*
TEMED	tetramethylethylenediamine
TIP	tonoplast intrinsic protein
TM	transmembrane (helix)
Triton X-100	4-(1,1,3,3-tetramethylbutyl)phenyl-polyethylene glycol
us	upstream
UTP	uridine triphosphate
UV	ultraviolet
v/v	volume over volume
V_0	initial volume
Vw	partial molar volume of water
W	watt(s)
W	wash fraction
w/v	weight over volume
WT	wildtype
χ	difference between two data points
XIP	uncategorized intrinsic protein
Y_0	offset from point of origin

YTPG	yeast tryptone phosphate buffer
Zm	*Zea mays*

Proteinogenic Amino Acids

One Letter Code	Three Letter Code	Amino Acid
A	Ala	Alanine
R	Arg	Arginine
N	Asn	Asparagine
D	Asp	Aspartic acid
C	Cys	Cysteine
Q	Gln	Glutamine
E	Glu	Glutamic acid
G	Gly	Glycine
H	His	Histidine
I	Ile	Isoleucine
L	Leu	Leucine
K	Lys	Lysine
M	Met	Methionine
F	Phe	Phenylalanine
P	Pro	Proline
S	Ser	Serine
T	Thr	Threonine
W	Trp	Tryptophane
Y	Tyr	Tyrosine
V	Val	Valine
B	-	Asx type amino acids
Z	-	Glx type amno acids

Decimal unit prefixes

Prefix	Unit abbreviation	Decimal value
pico	p	10^{-12}
nano	n	10^{-9}
micro	µ	10^{-6}
milli	m	10^{-3}
centi	c	10^{2}
kilo	k	10^{3}
mega	M	10^{6}

V. Summary

Aquaporins are a subclass of a ubiquitous protein family, the major intrinsic proteins (MIPs), and are thus represented in all domains of life. Their primordial function as integral membrane channels is the passive mediation of water across lipid bilayer barriers. In addition, various alternative substrates, such as small uncharged molecules, gases, carbohydrates, metalloids or ions have been found to be transported via aquaporins. As such, they fulfill a wide range of physiological functions and are of growing interest as targets for medical, as well as industrial applications.

In plants, aquaporins are divided into five subclasses based on their localization, substrate specificity and sequence similarity: Plasma membrane intrinsic proteins (PIPs), tonoplast membrane intrinsic proteins (TIPs), Nodulin26-like intrinsic proteins (NIPs), small basic intrinsic proteins (SIPs) and uncategorized (X) intrinsic proteins (XIPs). PIPs as the largest group are further split up into PIP1 and PIP2 phylogenetic subcategories. The latter is differentiated from the former by a shorter N- and a longer C-terminus, an additional number of amino acids in the first extracellular loop A and a significantly higher overall water permeability. Furthermore, PIP2s have been described as rather strict water channels, whereas members of the PIP1 family are more likely to mediate alternative substrates.

As typical representatives of their respective PIP subclasses, NtAQP1 and NtPIP2;1 from tobacco were at the center of this thesis. A detailed *in silico* amino acid sequence analysis and comparison revealed the most significant variances in terms of domain length and sequence identity to be in the N- and C-termini, as well as loop A of these two aquaporins. A previous study found NtAQP1 water permeation to be unmodulated after its loop A was modified to resemble that of a PIP2 member. In addition, a multiple sequence alignment with various other MIPs helped identify all sequence motifs relevant for substrate specificity in NtAQP1 and NtPIP2;1. Interestingly, all of them were found to be identical between the two, thus giving way to the hypothesis that their terminal domains could play a significant role in their respective water permeation capabilities.

In order to test that hypothesis, an *E. coli* based continuous exchange cell free expression (CECF) system was established. A total of three different expression modes were tested for experimental applicability. The precipitation based mode (P-CF) without the inclusion of a hydrophobic environment served as a quick initial expression test for newly constructed vectors, as well as verification of individual reaction components. Detergent based cell free expression (D-CF) provided micelles for the direct solubilization of translated aquaporin, but was eventually dismissed as a viable option due to the complexity of its downstream processing. Finally, lipid based cell free expression (L-CF) provided both a liposome based hydrophobic environment for direct integration of translated protein and a downstream processing of comparably low complexity.

The water permeability of proteoliposomes containing either of the two tobacco aquaporin wildtypes or terminal domain mutant constructs, as well as empty control liposomes was measured via a Stopped Flow based assay. Therein, (proteo)liposome shrinkage via a hypoosmotic pressure gradient was analyzed via scattered light kinetics. Obtained raw data underwent nonlinear regression to an exponential rise function and thus allowed the calculation of the water permeability factor P_f for individual samples.

NtPIP2;1 and NtAQP1 showed water permeation rates in line with previously published results. While the former was a true aquaporin and demonstrated high water permeability, the latter indicated low transport rates barely above that of empty control liposomes. The deletion of either the N- or C-terminal domain in NtPIP2;1 caused a significant drop in water permeability to levels equivalent to NtAQP1 and the control (N) or slightly above that (C). Compared to that, the double deletion mutant demonstrated even lower water transport rates. In contrast, the removal of either of the NtAQP1 termini did not cause a significant shift in water permeation compared to the wildtype configuration. Deleting both domains, however, resulted in the lowest measured water

permeability of all tested constructs. Subsequently, terminal domains were exchanged between the two wildtypes and the impact on their mediation functionality was analyzed. P_f values for NtPIP2;1 constructs, where either of the termini were exchanged with NtAQP1 sequences did not differ significantly from their single deletion counterparts. However, the exchange of both PIP2 termini resulted in transport rates statistically equivalent to those of the wildtype NtAQP1 and thus significantly higher than NtPIP2;1 with both domains removed. Finally, all NtAQP1 terminal exchange mutants demonstrated increased water permeation in the following order, when compared with the wildtype: N exchange < C exchange < N & C exchange, with the latter closing two thirds of the water transport gap previously seen between the two wildtype aquaporins. Thus, all three NtAQP1 exchange mutants showed significantly higher transport rates than their deletion mutant equivalents.

Based on the obtained results, various types of previously reported aquaporin regulation were discussed in order to better interpret the role of terminal domains in the water permeability of NtPIP2;1 and NtAQP1. N-terminal acetylation / methylation as a type of post-translational modification, the interaction of termini with neighboring aquaporin monomers and a modification of mechanosensitivity were found to be options in the realm of possibility. In addition, a three-dimensional structure homology modeling of both wildtypes, as well as their respective double deletion and double exchange mutants allowed to spot potential conformation changes in transmembrane regions. In conclusion, both the mere presence, as well as the specific sequence makeup of the terminal domains seem to play a major role in the water transport functionality of both tobacco aquaporins.

VI. Zusammenfassung

Aquaporine sind eine Unterklasse einer ubiquitären Proteinfamilie, den *major intrinsic proteins* (MIPs), und sind als solche in allen Domänen des Lebens vertreten. Ihre ursprüngliche Funktion als integrale Membranproteine ist der passive Transport von Wasser durch Doppellipidmembranen. Darüber hinaus wurden weitere Alternativen wie kleine, ungeladene Moleküle, Gase, Kohlenhydrate, Metalloide oder Ionen als Substrate von Aquaporinen beschrieben. Dank dieses breiten Spektrums erfüllen die Membrankanäle eine große Bandbreite von physiologischen Funktionen und rücken vermehrt in den wissenschaftlichen Fokus als Targets für pharmakologische und industrielle Applikationen.

In Pflanzen wurde eine Aufteilung von Aquaporinen in insgesamt fünf Unterklassen durchgeführt, welche auf Lokalisation, Substratspezifität und Sequenzidentität basiert: *plasma membrane intrinsic proteins* (PIPs), *tonoplast membrane intrinsic proteins* (TIPs), *Nodulin26-like intrinsic proteins* (NIPs), *small, basic intrinsic proteins* (SIPs) und *uncategorized* (X) *intrinsic proteins* (XIPs). Die zahlenmäßig größte Gruppe der PIPs lässt sich weiter in die phylogenetischen Unterkategorien PIP1 und PIP2 einteilen. Letztere unterscheiden sich von Ersteren durch einen kürzeren N- und einen längeren C-terminus, zusätzlichen Aminosäuren in der ersten extrazellulären loop A und eine signifikant höhere intrinsische Wasserpermeabilität. Des Weiteren wurden PIP2 Aquaporine als strikte Wasserkanäle beschrieben während bei Mitgliedern der PIP1 Unterkategorie die Wahrscheinlichkeit höher ist, auch alternative Substrate zu vermitteln.

Im Fokus dieser Arbeit standen NtAQP1 und NtPIP2;1 aus *Nicotiana tabacum* als typische Repräsentanten ihrer jeweiligen Unterkategorien. Eine detaillierte *in silico* Analyse der beiden Aminosäuresequenzen mit anschließendem Vergleich offenbarte die größten Unterschiede bezüglich Sequenzlänge und -identität bei den N- und C-terminalen Proteindomänen sowie loop A dieser Aquaporine. Eine vorangegangene Studie demonstrierte eine unveränderte Wasserpermeabilität von NtAQP1, nachdem die Aminosäuresequenz von loop A an die eines PIP2 Aquaporins angepasst worden war. Unter Zuhilfenahme eines *multiple sequence alignments* mit diversen anderen MIPs wurden in der vorliegenden Arbeit alle für die Substratspezifität relevanten Sequenzmotive in NtAQP1 und NtPIP2;1 identifiziert. Interessanterweise stellte sich im Vergleich hierbei heraus, dass diese in allen Positionen identisch sind. Dies führte zur Formulierung der zentralen Hypothese dieser Arbeit, welche den terminalen Domänen der beiden Tabak-Aquaporine eine wichtige Rolle in der Modulation ihrer respektiven Wasserpermeabilität zusprach.

Um diese Hypothese zu testen, wurde ein *E. coli* basiertes *continuous exchange cell free expression* (CECF) System etabliert. Hierbei wurden drei unterschiedliche Expressions-Modi auf ihre experimentelle Anwendbarkeit überprüft. Ein Präzipitations-basierter Modus (P-CF) ohne hydrophobe Additive diente als Schnelltest, sowohl zur Ermittlung der generellen Expressionsviabilität von neu konstruierten Vektoren, als auch zur Verifizierung individueller Reaktionskomponenten. Detergenz-basierte zellfreie Expression (D-CF) stellte zwar Mizellen zur direkten Solubilisierung von translatiertem Aquaporin zur Verfügung, wurde letztendlich aufgrund der Komplexität des notwendigen *downstream processing* als unpraktikable Option aufgegeben. Schlussendlich bot ein Lipid-basierter Modus (L-CF) nicht nur ein Liposom-abhängiges, hydrophobes Mileu zur unmittelbaren Integration von produziertem Protein, sondern auch ein *downstream processing* von vergleichsweise niedriger Komplexität.

Die Wasserpermeabilität von Proteoliposomen mit eingebautem Wildtyp-Aquaporin oder entsprechenden Terminaldomän-Mutanten einerseits und leeren Kontroll-Liposomen andererseits wurde mittels eines *Stopped Flow* basierten Assays ermittelt. (Proteo)liposom-Schrumpfung wurde hierbei durch einen angelegten hypoosmotischen Gradienten ausgelöst und als Streulicht gemessen. Aufgenommene Rohdaten unterliefen eine nonlineare Regressionsanalyse anhand einer Exponential-Funktion und erlaubten somit die Kalkulation des Wasserpermeabilitätsfaktor P_f für individuelle Proben.

NtPIP2;1 und NtAQP1 demonstrierten Wasserpermeabilitätsraten übereinstimmend mit zuvor publizierten Daten. Während ersteres hohe intrinsischen Wassertransport zeigte, weiste letzteres sehr niedrige Permeabilität auf, welche nur geringfügig höher war als bei leeren Kontroll-Liposomen. Eine Deletion der N- oder C-terminalen Domäne führte bei NtPIP2;1 zu einem signifikanten Rückgang der Wasserpermeabilität, welche sich dann auf NtAQP1 Wildtyp-Level (N-Deletion) bzw. geringfügig darüber (C-Deletion) einpendelte. Im Vergleich dazu zeigte die Doppeldeletions-Mutante die geringsten Transportraten. Das Entfernen von einzelnen terminalen Domänen bei NtAQP1 hatte keine signifikante Änderung der Wasserpermeabilität zur Folge. Eine Deletion beider Domänen zeigte jedoch die niedrigsten Transportraten aller gemessenen Konstrukte. Im Anschluß wurden N- und C-terminale Domänen zwischen den beiden Wildtyp-Aquaporinen ausgetauscht und die Auswirkungen im Hinblick auf die Modulation der Wassertransportraten analysiert. P_f Werte von NtPIP2;1 Konstrukten, in denen eine von beiden terminalen Domänen mit NtAQP1 Sequenzen ausgetauscht wurde, unterschieden sich nicht signifikant von denen ihrer respektiven Einzeldeletionsmutanten. Allerdings resultierte der Austausch beider PIP2 Termini in Transportraten statistisch äquivalent zu Werten vom NtAQP1 Wildtyp und somit signifikant höher als der NtPIP2;1 Doppeldeletionsmutante. Alle terminalen Austauschmutanten von NtAQP1 zeigten höhere Wasserpermeabilität als der Wildtyp und ordneten sich in die folgende Reihenfolge ein: N-terminaler Austausch < C-terminaler Austausch < N- & C-terminaler Austausch. Letztere Mutante überbrückte damit zwei Drittel der ursprünglichen Permeabilitätslücke zwischen den Wildtypen. Folglich demonstrierten alle drei NtAQP1 Austauschmutanten signifikant höhere Transportraten als ihre Deletions-Äquivalente.

Basierend auf den erhaltenen Egebnissen wurden verschiedene Arten von bereits publizierten Regulationsmechanismen bei Aquaporinen diskutiert, um den Einfluss von terminalen Domänen auf die Wasserpermeabilität bei NtPIP2;1 und NtAQP1 interpretieren zu können. N-terminale Acetylierung / Methylierung als post-translationale Modifikation, die Interaktion von Termini mit benachbarten Aquaporin-Monomeren und eine Modifikation der Mechanosensitivität wurden hierbei als mögliche Optionen gefunden. Des Weiteren diente ein durchgeführtes *3D homology modeling* der beiden Wildtypen und ihrer respektiven Doppeldeletions- und Doppelaustauschmutanten als strukturelle Grundlage, um potenzielle Konformationsänderungen in Transmembranregionen nachzuweisen.

Abschliessend lässt sich sagen, dass sowohl die bloße Anwesenheit, als auch spezifische terminale Sequenzen ausschlaggebend sind für die Modulation der Wassertransportfunktionalität in beiden Tabak-Aquaporinen.

1. Introduction

1.1 Membrane Proteins

1.1.1 Classification and structural attributes

Biological membranes serve as selective, semipermeable barriers for whole cells and cellular compartments with a great variety of compositions pertaining to lipids, proteins and carbohydrates. With lipid:protein ratios ranging from 4:1 to 1:4 by mass [Tan *et al.* 2014], membrane proteins participate in a multifold of vital cellular processes, including protein/lipid biogenesis, cell shape regulation, transport, cell recognition, adhesion, energy production, homeostasis, signal transduction and electric impulse generation, as well as propagation [Pogozheva *et al.* 2014]. This functional diversity is not only the basis for their significant role in medical applications, responsible for more than 50 % of all drug targets [Overington *et al.* 2006], but also their general abundance in most genomes ranging from 20 to 30 % of all genes [Krogh *et al.* 2001].

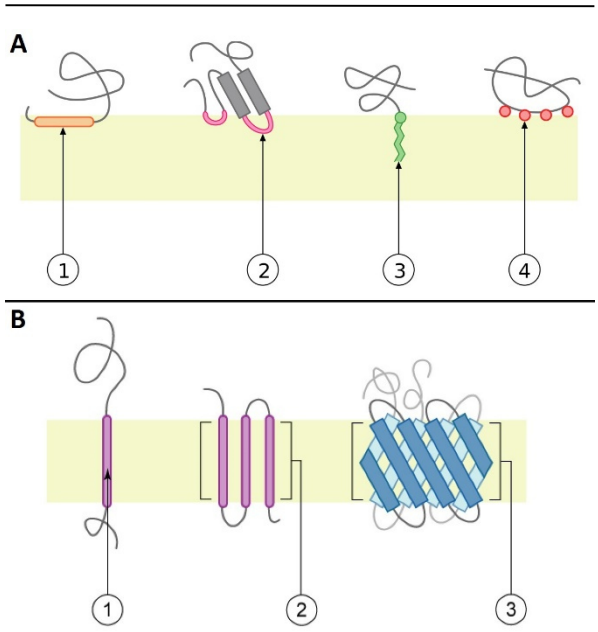

Fig. 1 – Schematic representation of peripheral, monotopic (A) and polytopic integral membrane proteins (B). A1 = peripheral membrane interaction of amphiphatic α-helix / A2 = peripheral membrane interaction of hydrophobic loop / A3 = monotopic integral interaction with a membrane lipid / A4 = peripheral electrostatic or ionic interaction with membrane lipids / B1 = single transmembrane α-helix / B2 = polytopic α-helical transmembrane protein / B3 = polytopic β-sheet transmembrane protein [Wikimedia Commons 2006]

The classification of membrane protein topology is dependent on the number of transmembrane segments (TM) and their orientation in or attachment quality to the respective membrane [Heijne 2006].

In total, there are suggested to be three topology types [Karp 2009], the first of which are integral membrane proteins that are permanently attached to their respective membranes. The resolvement of their anchored state is only possible through the usage of detergents, nonpolar solvents or denaturing agents. This group of membrane proteins consists of two subclasses: Firstly, integral polytopic proteins that span across the entire membrane at least once and exhibit one of two tertiary structures, namely α-helix bundles or β-sheets (Fig. 1, B1-3). The former are present in all biomembranes, whereas the latter are known to populate the outer membranes of Gram negative bacteria, as well as the cell walls of a few Gram positive bacterial species and the outer membranes of mitochondria and chloroplasts. Secondly, monotopic integral membrane proteins are attached to only one side of a membrane and thus do not span entirely across it (Fig. 1, A3).

Peripheral membrane proteins make up the second topology group (Fig. 1, A1-2, A4): hydrophobic, electrostatic and other non-covalent interactions enable them to temporarily attach themselves to lipid bilayers or integral membrane proteins. The dissociation of this group is easily obtainable through polar conditions, such as high salt concentration or a change in pH.

Lastly, the third topology class of membrane proteins are represented by polypeptide poreforming toxins. These include many antibacterial peptides and proteins involved in apoptosis. An interesting feature of this group is their ability to aggregate and associate with lipid bilayers in opposition to their overall water-soluble nature.

In a three-dimensional context, membrane proteins consist of mostly hydrophobic amino acid residues attached to the lipid bilayer with mostly hydrophilic residues protruding out of the membrane. The afore-mentioned

secondary structural motifs of α-helices and β-sheets satisfy the obligatory structural requirements for membrane insertion by saturating the hydrogen bonding potential of polar main chain groups. Due to this necessity of a hydrophobic environment, the overall structural diversity is restricted in so far that a 10-fold lower number of membrane protein families is suggested to exist when compared to their water soluble counterparts [Liu *et al.* 2004a]. According to estimates, 80 % of the total polytopic membrane protein sequence space may be covered by roughly 700 unique structures, whereas 70 – 80 % of the soluble protein domain would require more than 25,000 unique structures to achieve the same goal [Oberai *et al.* 2006].
Another feature that greatly differentiates TM proteins from water soluble complexes is frequent large-scale conformational transition. This is mostly due to their membrane integration or as a part of their functional regulation [Rollauer *et al.* 2012], i.e. during transport of substances or signals in transporters, receptors and channels [Vinothkumar & Henderson 2010]. This may involve local topology, such as inward or outward facing terminal regions [Marcoux et al. 2013], global topology in the form of individual subunits or whole protein complexes [Thøgersen & Nissen 2012], or gating as the (un)plugging of pores [Shi 2013].
50 to 70 % of membrane protein complexes form homo-oligomers [Venkatakrishnan *et al.* 2010], out of which homo-dimers represent the largest fraction at more than 65 % [Nishi *et al.* 2013]. TM protein association in the form of oligomerization increases overall structural stability and generates conductive TM pores. Such configurations are found in ion channels, bacterial secretion systems or toxins. Furthermore, it allows for the formation of ligand-binding sites at the oligomer interfaces, as well as for cooperativity between individual subunits and an additional level of regulation [Meng *et al.* 2009].

1.1.2 Key technologies in structure determination

The hydrophobic nature and generally low expression levels of membrane proteins make the solving of their atomic structures more difficult than with globular proteins [Carpenter *et al.* 2008]. Thus, they take up only 2.3 % of the total entries in the Protein Data Bank (PDB) as of February 2016 [Protein Data Bank of Transmembrane Proteins (PDBTM) 2016]. This stands in contrast to the suggested 20 to 30 % that membrane proteins would occupy of the total proteome [Membrane Proteins of Known 3D Structure (mpstruc) 2016]. However, the ever accelerating pace of membrane protein structure resolution is based on several key technologies covering both expression and purification, as well as the actual structure determination.
Escherichia coli (*E. coli*) as the most widely used protein expression organism in the scientific community represents a great tool for the characterization of prokaryotic targets. However, its easy handling is contrasted by its shortcomings when the need for post-translational modifications arises. Incorrect, as well as lacking glycosylation or the usage of specific lipids, among others, can cause incorrect folding of many eukaryotic membrane proteins, thus alternative systems based on yeast, insect and mammalian cells have been devised. Examples for such successful systems include the resolution of potassium channels [Long *et al.* 2005], P-type ATPases [Pedersen *et al.* 2007] and also aquaporins [Hiroaki *et al.* 2006 / Horsefield *et al.* 2008], among others. Another major hurdle in the area of expression and purification of TM proteins is the need for specific membrane insertion machinery to avoid a toxic overload of cells when producing large quantities of correctly folded insoluble protein targets [Vinothkumar & Henderson 2010]. Overcoming these unwanted side effects due to their open and accessible nature, cell free expression (CFE) systems have recently seen an increasing popularity in this field [Junge *et al.* 2008] and might be a viable option for future research in this area (see chapter 1.2 for further discussion on this topic).

The actual determination of three dimensional membrane protein structures via X-Ray crystallography as the method of choice is presented with the problem of obtaining such 3D crystals of sufficient size and order. Thus,

the choice of the hydrophobic environment is crucial for the correct folding of the expression target, e.g. a specific type of detergent or lipid membrane system [Kühlbrandt 1998 / Privé 2007].
Electron cryomicroscopy (ECM) is another method and offers the capability to analyze topologies in a more native environment, albeit only in a two dimensional realm. Nevertheless, various structures have already been resolved with this method, among them a few aquaporins [Murata *et al.* 2000 / Gonen *et al.* 2004]. At lower resolutions, ECM is a viable tool in combination with other sources, such as X-Ray crystallography as well as biochemical and evolutionary data to give a more complete picture of previously resolved structures [Fleishman *et al.* 2006]. It becomes especially advantageous when dealing with otherwise difficult to determine structures [Nogales *et al.* 1997], as well as following significant conformational changes in a protein complex. Both would induce disorder into 3D crystals and thus make them impossible to resolve via X-Ray crystallography [Subramaniam & Henderson 2000].
Nuclear magnetic resonance (NMR) spectrocropy as a solution based method is another viable alternative for resolving protein and nucleic acid structures in cases where partially disordered regions would prevent the proper formation of ordered crystals. In combination with freely mobile or attached paramagnetic tags it can also be used to determine the orientation and overall topology of membrane proteins [Schrank *et al.* 2013], although the inherent size limitation of solution NMR makes resolution of structures beyond 5 kDa difficult. However, membrane proteins present a challenge here due to detergent micelle interference [Vinothkumar & Henderson 2010]. Solid state NMR would then offer a unique possibility to study unmodified TM protein structures in their native environment of phospholipid bilayers under physiological conditions of temperature and pH [Opella 2013 / Zhou & Cross 2013]. Isolated characterization of amino acid side chains and backbones become possible, as well as in complexes with small molecules and other biopolymers. It is also important to note, that the liquid crystalline nature of membranes makes their study an almost exclusive application for NMR in structural biology [Radoicic *et al.* 2014].
Finally, mass spectrometry (MS) and atomic force microscopy (AFM) represent additional tools to identify post-translational modifications, protein-protein interactions and spatial organization of TM proteins [Schey *et al.* 2013]. Furthermore, they are able to obtain topographical surface data of protein structures in 2D [Trinh *et al.* 2012]. However, in combination with atomic coordinates, the latter enables the reconstruction of complex 3D models for large multidomain proteins.

1.2 Cell-free expression

In vitro or cell-free transcription / translation systems have an inherently open nature and thus not only provide easy access to reaction conditions, but also the potential for establishing high-thoughput protocols. They are of great interest in the production of difficult targets, such as toxic and transmembrane proteins, since the cellular metabolism does not have to be preserved and no cellular barriers restrict direct control of the translation apparatus. Hence, adaptation and modification of such systems is easily achieveable, i.e. through the addition of various supplements, such as chaperones [Ryabova *et al.* 1997 / Jiang *et al.* 2002], radioisotope labels [Cancedda & Schlesinger 1974], nanodiscs [Ritchie *et al.* 2009] or microsomes [Sachse *et al.* 2013 / Stech *et al.* 2012]. Furthermore, the possibility to alter the genetic code and the incorporation of non-canonical amino acids sets the foundation for enormous potential in biotechnology, as well as pharmaceutical research and applications [Quast *et al.* 2014 / Chin *et al.* 2003].

The first cell-free protein synthesis system was developed in the 1960s by Matthaei & Nirenberg and was based on *E. coli* extracts [1961]. Nowadays, cell-free expression systems derived from various organisms are available, including Archaea, prokaryotes, fungi, plants, insects and mammals [Carlson *et al.* 2012]. Table 1 provides an overview on these systems and their respective attributes.

Table 1 – Overview of current cell-free expression systems and their respective attributes. 1 = refers to obtainable amount of synthesized target protein / 2 = post-translational modifications / 3 = refers to presence of endogenous membranes for the direct synthesis and integration of membrane protein (MP) targets / n.d. = not discussed [Zemella *et al.* 2015, modified]

Extract origin	Yield[1]	Cost	Complexity	PTMs[2]	MP[3] integration	Scalability	distinctive features & applications
E. coli	high	low	simple & fast cultivation fast lysate preparation easy genetic engineering well-established	limited	no	high	- incorporation of non-canonical amino acids - human therapeutics, modified enzymes, protein polymers, ribosome display
Archaea	low	n.d.	n.d.	n.d.	n.d.	n.d.	- synthesis of thermostable proteins - high temperature conditions possible, thus reduced secondary mRNA structures
Protozoa	low	low	not well established less used	not well known	n.d.	high	- high throughput analysis by PCR based cell-free protein synthesis - high solubility of synthesized proteins
Yeast	low	n.d.	simple & fast cultivation simple & fast lysate preparation established cell engineering	yes (non-mammalian)	n.d.	n.d.	- production of virus like particles for anti-viral drug research - bioethanol and (S)-L-acetoxyalkan-2-ol production
Wheat germ	medium	high	well-known system laborious lysate preparation	limited	no	n.d.	- characterization of novel malaria vaccine candidates - on-chip protein synthesis, high-throughput applications, monoclonal antibodies - conformation analysis of ribosomes
Tobacco BY-2	medium	high	simple & fast lysate preparation not well established	yes	n.d.	n.d.	- novel cell-free system with high potential for future applications
Insect	n.d.	high	simple & fast lysate preparation	yes	yes	n.d.	- automated production of membrane proteins - integration of non-canonical amino acids - formation of giant unilamellar vesicles for study of membrane protein models
Rabbit reticulocyte	low	n.d.	well-established	yes (with microsomes)	yes (with microsomes)	n.d.	- protein microarrays, display and screening technologies - protein-molecule interaction studies
Chinese Hamster Ovary	low	high	well-known cell line	yes	yes	n.d.	- novel cell-free system with high potential for future applications
Human	low	high	laborious cultivation highly sensitive cells	yes	yes	n.d.	- facilitation of high molecular weight protein synthesis - antiviral drugs & investigation of viral replication mechanisms

All cell-free expression systems are based on the same underlying principle: Crude extracts are firstly generated from cultured cells, that are depleted from endogenous DNA and mRNA and are subsequently supplemented with energy regenerating components and free amino acids, as well as tRNA. Translation is then initiated by the addition of a suitable template, i.e. linear or circular DNA or mRNA [Sawasaki et al. 2002 / Rosenblum & Cooperman 2014] and is carried out at the appropriate temperature for the chosen system. Specific reaction conditions differ for each and every individual target protein and have to be adjusted accordingly to its needs in terms of complexity, folding and post-translational modifications. Formats for cell-free expression systems range from simple classical batch setups with short reaction times, limited protein yields, but easy handling and scalability [Kim & Swartz 1999] to more complex dialysis systems known as continuous flow cell-free (CFCF) [Spirin *et al.* 1988] and continuous exchange cell-free systems (CECF) [Kim & Choi 1996 / Stech *et al.* 2014]. The latter provide integrated dialysis systems that allow prolonged reaction lifetimes and thus higher protein yields up to several mg/ml. Additionally, easy removal of inhibitory products, such as inorganic phosphates, is ensured,

while at the same time replenishing low molecular weight energy regenerating components and free amino acids. Fig. 2 provides a schematic overview of different cell-free production setups.

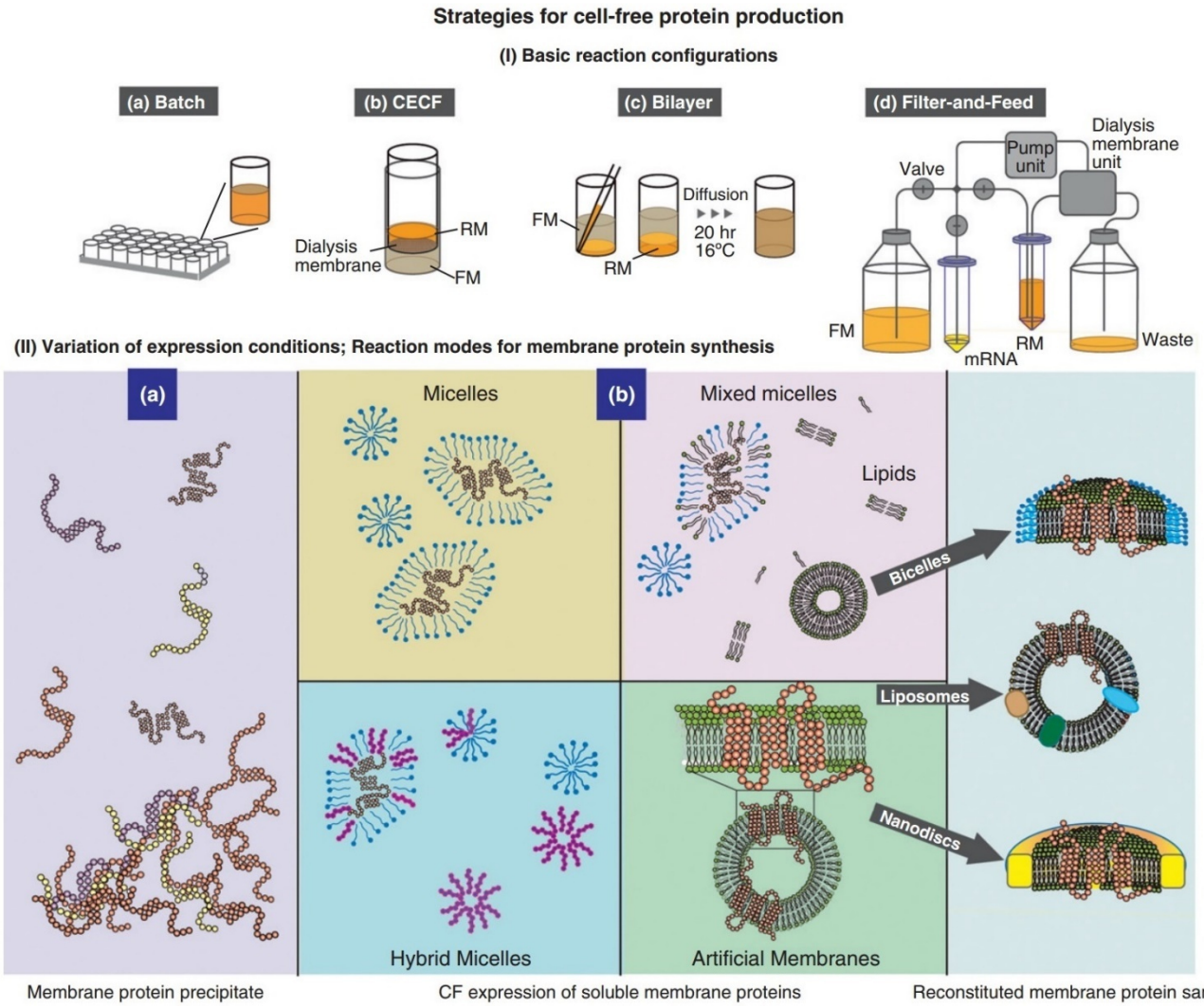

Fig. 2 – Setups and strategies for cell-free protein production. Ia = Batch system for preparative expression or optimization screenings / Ib = Two-compartment CECF setup with a reaction mixture (RM) separated from a feeding mixture (FM) by a dialysis membrane / Ic = Biphasic configuration with high-density RM and low-density FM for improved protein synthesis by slow diffusion mixing / Id = Automated setup with dialysis membrane allows for programmed intermittent exchange of FM and mRNA / IIa = Production of a membrane protein target in precipitated form / IIb = Production of a membrane protein target solubilized with detergent micelles, hybrid micelles (mixture of detergents and surfactants), or with artificial membranes (bicelles, liposomes, nanodiscs) [Bernhard & Tozawa 2013, modified]

Cell-free expression systems based on *E. coli* derived extracts represent the "workhorse" for both prokaryotic and eukaryotic membrane protein production. As such, their lack of a natural membrane impedes the production of membrane bound targets, which makes supplementation with membrane mimicking structures necessary. These include micelle-forming detergents, nanodiscs, liposomes or exogenous microsomes [Junge *et al.* 2011 / Geller & Wickner 1985]. The absence of such supplements results in initial precipitation and requires laborious additional protein purification and re-solubilization protocols to obtain functional targets [Klammt *et al.* 2007]. To circumvent the refolding problem, detergents were screened for suitability and Brij, as well as Tween derivatives, n-dodecyl-β-D-maltopyranoside (DDM), digitonin and Triton X-100 were found to form micelles at defined concentrations able to enclose the respective membrane protein [Berrier *et al.* 2004]. In contrast, artificial hydrophobic environments, such as liposomes and nanodiscs, provide improved membrane protein folding and functionality. Nanodiscs as phospholipid bilayers surrounded by membrane scaffold proteins [Bayburt & Sligar 2010] can contribute to increased stability for target proteins and are a powerful tool for

measuring quantitative binding kinetics with ligands. In comparison, liposomes are especially useful for functional studies including transporter assays and ion channel characterization [Geller & Wickner 1985]. In these, processes are analyzed, that involve the regulated passage of solutes across lipid bilayers, e.g. ions and small molecules.

1.3 Aquaporins – A ubiquitous and diverse class of membrane proteins

1.3.1 Classification, nomenclature, phylogeny

The discovery of the archetype molecular water channel aquaporin1 (AQP1) in mammals goes back to the late 1980s and early 1990s and is mainly attributed to the group around Peter Agre [Denker *et al.* 1988 / Preston *et al.* 1992 / Agre *et al.* 1993]. Afterwards, genome and transcriptome sequencing projects found evidence of this class of membrane protein in all three domains of life: eukaryotes, bacteria and archaea [Finn & Cerda 2015].
Early evolutionary studies recognized the Major Intrinsic Protein (MIP) superfamily [Tyerman *et al.* 1999] to consist of two major phylogenetic groups, namely water-selective aquaporins or AQPs and glycerol facilitators [Park & Saier 1996 / Froger *et al.* 1998 / Heymann & Engel 1999], also known as aquaglyceroporins or GLPs. Later on, this subdivision was slightly devised, in that the MIP superfamily would contain a total of three water channel protein related subfamilies [Benga 2012]. Aside from the water-selective or specific “orthodox” aquaporins, aquaglyceroporins were classified based on their permeability to water, but also to other small uncharged solutes, particularly glycerol. The latter included the subgroup of glycerol permease facilitators (GlpF) and demonstrated a differing signature amino acid residue in the otherwise highly conserved pore region, which would expand it to accept molecules larger than water to pass through [Ishibashi *et al.* 2011]. Additionally, the so-called “unorthodox” S-aquaporins were found to have little conserved amino acid sequences around the active center of the pore region, making them unclassifiable into the first two subfamilies, which were deemed to be the primordial, ancestral groups of the MIP family [Ishibashi 2006 / Nozaki *et al.* 2008].
Bacteria and Archaea generally retain that ancestral condition and have one AQP and one GLP each [Abascal *et al.* 2014]. Gene duplications in eukaryotes, however, led to great diversifications in terms of protein structure and functionality [Zardoya 2005]. The best known examples are found in vertebrates and flowering plants, where expansions of the MIP family are linked to subfunctionalization of different paralogues in various tissues [Ishibashi *et al.* 2011 / Johanson *et al.* 2001 / Quigley *et al.* 2002]. Analyses of animal MIPs indicate that maximum diversity, in terms of total number of subfamilies (AQP0 to AQP12), is achieved in fishes [Tingaud-Sequeira *et al.* 2010] and land vertebrates [Zardoya 2005] as a result of several rounds of whole genome duplication. While invertebrate major intrinsic proteins have been described almost exclusively in insects before [Tomkowiak & Pienkowska 2010 / Spring *et al.* 2009], a more recent report depicted the first putative orthodox aquaporins in gastropods [Pienkowska *et al.* 2014], further confirming the virtually ubiquitous nature of the MIP superfamily.
Comparing AQPs to GLPs phylogenetically, it was found that the latter is a rather compact group, where diversification with regard to paralog subfamilies is most evident in vertebrates (see Fig. 3). In contrast to that, AQPs, particularly in plants and animals, experienced successive events of gene duplication accompanied by sequence and functional divergences. Some AQP subgroups, such as plant small basic intrinsic proteins (SIPs) and Nodule26-like intrinsic proteins (NIPs), as well as the mammal AQP11 and AQP12 clusters are hardly even recognizable as members of the MIP superfamily.

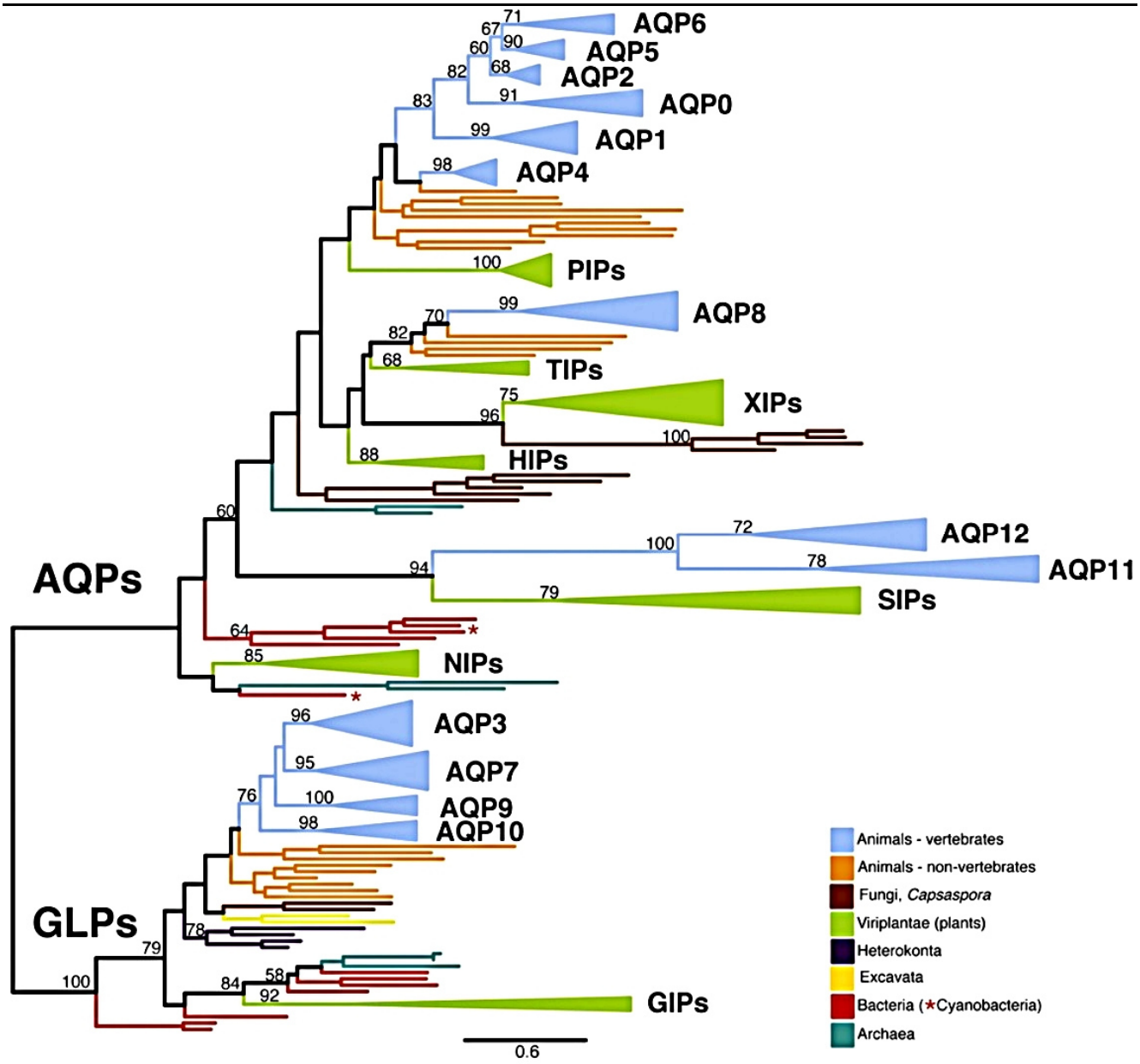

Fig. 3 – General phylogeny of MIPs. Major subfamilies are shown as collapsed sets of nodes with their branches colored according to the taxonomy in the accompanying legend. Numbers above nodes indicate bootstrap support from 1000 pseudoreplicates in percentage. The scale bar represents the amount of genetic change in terms of substitutions per respective sequence lengths. AQP = aquaporin / GLP = GlpF-like intrinsic protein / PIP = plasma membrane intrinsic protein / TIP = tonoplast intrinsic protein / XIP = uncategorized (X) intrinsic protein / HIP = hybrid intrinsic protein / SIP = small basic intrinsic protein / NIP = Nodulin26-like intrinsic protein [Abascal *et al.* 2014, modified]

1.3.2 Molecular structure and function

Aquaporins as integral membrane channels that facilitate a selective and passive transport of water and other small, mostly uncharged molecules along concentration gradients exhibit a conserved tertiary and quaternary structure. Their core domains, as individual water pore subunits, assemble into homo- or heterotetrameric protein complexes [Verbavatz *et al.* 1993 / Neely *et al.* 1999 / Fetter *et al.* 2004]. This formation into tetramers creates a central fifth pore, through which ions, such as K^+, Cs^+, Na^+ and tetramethylammonium (Fig. 4 D) might be transported [Saparov *et al.* 2001 / Yool & Weinstein 2002].

The integral membrane region of each monomer is composed of 6 transmembrane domains TM 1 – 6, three extracellular loops A, C, E and two intracellular loops B, D (Fig. 4 A, B, C). Two inverted hemihelices on loops B and E project opposing Asn-Pro-Ala (NPA) motifs to regulate single file conductance of water molecules through the central monomer pores. At the same time, they serve as excluding selectivity filters for cations and protons

[Murata *et al.* 2000 / Ho *et al.* 2009 / Tani *et al.* 2009 / Wree *et al.* 2011]. An additional proton selectivity filter is located in the outer channel vestibule, typically consisting of aromatic residues and an arginine (ar/R motif), that determine, which molecular permeant can traverse the pore [Fu *et al.* 2000 / Sui *et al.* 2001 / Beitz *et al.* 2006 / Almasalmeh *et al.* 2014].

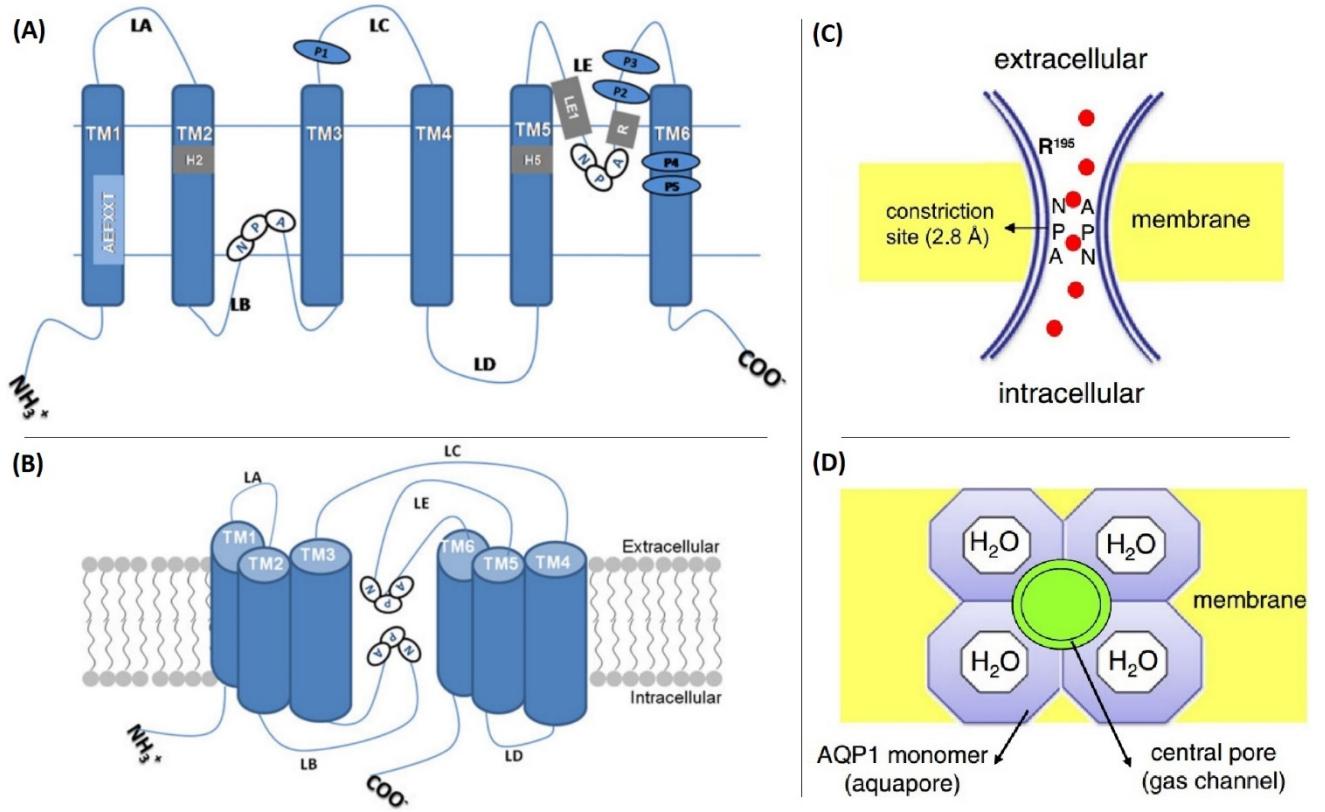

Fig. 4 – Molecular structure of aquaporins. (A) MIP monomer side view with 6 transmembrane helices connected by three extracellular (LA, LC, LE) and two intracellular loops (LB, LD). NPA motifs as conserved filter residues are shown in white ovals. Grey rectangles depict the four residues of the ar/R filter 2 constriction, whereas P1 – P5 positions are shown in blue ovals. (B) The NPA motifs in the two short helices HE and HB of loops LE and LB folds inwards to form the water conducting pore. (C) Side view of NPA constriction side, where water molecules (red dots) pass in single file. The arginine in position 195 (R195) provides fixed positive charges which prevent proton passage. (D) Top view of aquaporin tetramer, where each monomer transports water and the central fifth pore is suggested to conduct ions or gases [Hove & Bhave 2011, modified / Herrera & Garvin 2011, modified]

The arrangement of these ar/R residues correlates with the overall porin functionality: classical aquaporins, such as AQP0, 1, 2, 4 and 5 in mammals display a tight ar/R cluster, reducing the water conducting pore to a diameter of 1.5 Å and thus rendering it impermeable for glycerol [Ho *et al.* 2009]. On the other hand, aquaglyceroporins such as AQP3, 7, 9, and 10 in mammals show a more open structure [Verma *et al.* 2015]. In addition to the NPA motifs and the ar/R selectivity filter, there are up to five relatively conserved amino acid residues P1 to P5 [Froger *et al.* 1998], out of which the aspartic acid designated as P2 and located after the second NPA box is crucial in increasing the size of the central monomer pore to allow passage of larger molecules such as glycerol [Hub & de Groot 2008]. Although aquaporin sequences of resolved 3D structures are diverse in both configuration and functionality of the represented proteins, they all adopt a unique hour-glass shaped helical fold [Gonen & Walz 2006]. Global alignment of multiple MIP sequences show that highly conserved regions are predominantly on the cytoplasmic hemipore of the hour-glass shape, while sites responsible for pore selectivity (including the ar/R filter) mostly concentrate on the extracellular half of the protein structure [Abascal *et al.* 2014]. It was suggested that the hour-glass shape is the result of natural selection towards optimal hydrodynamic transport, demonstrating a combination of seemingly antagonist functions of high selectivity and high permeability

pertaining to water molecules [Gravelle *et al.* 2013]. This is due to conical entrances with suitable opening angles providing a maximum possible overall channel permeability.

Experimental determination of aquaporin permeability for various substrates was obtained from homologous or heterologous expression in amphibian oocytes, cultured cell lines, yeast cells and reconstituted targets in liposomes. Although the majority of prokaryotic and eukaryotic aquaporins are able to transport water, there are various exceptions to the rule. Those exceptions have either expanded their ancestral water transport functionality to other substrates or abolished their primordial substrate altogether in favor of alternatives. Examples include, but are not restricted to the transport of: gases like CO_2 [Geyer *et al.* 2013], NH_3 [Holm *et al.* 2005], NO [Herrera *et al.* 2006] and methylamine [Zeuthen *et al.* 2006]; small, uncharged solutes like glycerol [Tingaud-Sequeira *et al.* 2010], urea [Virkki *et al.* 2002], H_2O_2 [Almasalmeh *et al.* 2014] and formamide [Wallace & Roberts 2005]; complex carbohydrates like polyols and trehalose [Drake *et al.* 2015], as well as organic acids and bases like lactate [Bienert *et al.* 2013], purines and pyrimidines [Tsukaguchi *et al.* 1999]. Furthermore, metalloids have been described to pass through aquaporins, namely in the form of boric acid [Bienert *et al.* 2011], silicic acid [Mitani *et al.* 2008], arsenites [Liu *et al.* 2002] and antimonites [Sanders *et al.* 1997]. The regulation of aquaporins and the influence of their permeability function is either executed through post-translational modifications [Yukutake & Yasui 2010], interactions with metal ions [Verdoucq *et al.* 2008] or inhibition by selected drugs [Kato *et al.* 2013]. Additionally, the quality and composition of their lipid environment play an important role [Ton *et al.* 2013], together with protein-protein interactions [Sjöhamn & Hedfalk 2014] and the conformation of specific loops in their 3D structure [Jozefcowicz *et al.* 2013 / Törnroth-Horsefield *et al.* 2006].

1.3.3 Physiological functions

MIPs facilitate the movement of water and mostly non-ionic solutes across membranes and are required for osmoregulation, water conductance, gas and nutrient uptake, as well as translocation, metalloid homeostasis and signal transduction in eubacteria, archaea, fungi, plants and animals. The transport of water plays the most important role in the regulation of osmolarity, which in turn contributes to cellular homeostasis [Alleva *et al.* 2012]. Examples include the uptake and clearance of extracellular fluid in the mammalian brain by AQP4 [Manley *et al.* 2000], the crucial role of AQP0 in water transport and cell-to-cell adhesion in the fiber cells of the mammalian ocular lens [Gonen *et al.* 2004] or the abundant expression of AQPs in renal collecting ducts of birds [Lau *et al.* 2009], fishes [Engelund & Madsen 2015] and mammals [Matsuzaki *et al.* 2016] for the purpose of urine concentration. Furthermore, inherent water transport of AQPs has an essential impact in mammalian sweat glands [Takata *et al.* 2004] or the salinity-dependent regulation of aquaporins in fish intestines to mediate acclimatization to differing water salinity [Sundell & Sundh 2015]. Rather indirect consequences of aquaporin-regulated water transport encompass the participation of AQP1 in mice cell migration through the facilitation of rapid cell volume changes together with actin polymerization at the leading edge of migrating cells [Saadoun *et al.* 2005]. Furthermore, the mediation of water conservation in extant tetrapoda via MIPs supported overcoming the major physiological barrier of dessication in an aerial environment when aquatic organisms adapted to terrestrial life [Finn *et al.* 2014].

Aside from water transport, aquaporins play a significant role in the mediation of gases across biological membranes. Passive diffusion is relatively inefficient due to the hydrophobic nature of most physiologically relevant gases, with the consequence of the molecules being trapped in the lipid phase of the bilayer and thus unable to reenter the aqueous phase [Herrera & Garvin 2011]. Human AQP1, for example, has been shown to alleviate major resistances to the respiratory gases CO_2 and O_2 in the form of cholesterol in lipid bilayer cell membranes [Itel *et al.* 2012]. The physiologically normal cell membrane content of 30-50% cholesterol significantly impairs CO_2 diffusion by 2 orders of magnitude, especially so during phases of exercise [Endeward

et al. 2006]. Thus, the achievement of higher CO_2 permeabilities can only be executed by lowering the overall cholesterol content or by the integration of protein gas channels. This is even more critical for O_2 due to its 24-fold lower solubility in water compared to CO_2. NO as another example of aquaporin-mediated gas shows paracrine effects on neighboring cells, thus an efficient and fast facilitated diffusion would be physiologically preferred to free diffusion [Herrera & Garvin 2011]. AQP1 has been shown to transport NO three times faster than free diffusion would allow [Herrera *et al.* 2006], potentially playing a role in endothelium-based contractility control of vascular smooth muscle cells [Palmer *et al.* 1987 / Herrera & Garvin 2007]. Furthermore, NO and O_2 conductance via AQP4 in the mammalian brain suggests a potentially important role in neurotransmittance and signaling, that are physiologically important in sleep, learning and memory processes [Wang & Tajkhorshid 2010 / Pacher *et al.* 2007]. NO is also considered to be a fundamental messenger in the modulation of blood flow, thrombosis and neural activity in all vertebrates [Ignarro 2002 / Murad 2004], further confirming the critical role of aquaporins in this physiological area.

In addition to water and gases, major intrinsic proteins have been demonstrated to mediate the transport of other physiologically important molecules, one of which involves the import of lactic acid in lactobacilli by GlpF type proteins [Bienert *et al.* 2013] or by AQP9 and SmAQP in humans [Tsukaguchi *et al.* 1999] and trematodes [Faghiri *et al.* 2010], respectively. The transport of lactic acid is generally connected to energy production, i.e. via lactate-proton symport and is also involved in the metabolism of glycerol and dihydroxyacetone [Otto *et al.* 1980]. Silicon as an abundant and differentially distributed element in animals is believed to play a role in various important biological functions, including the regulation of bone mineral density [Jugdaosingh *et al.* 2004], cell differentiation [Carlisle 1982] and collagen synthesis [Reffitt *et al.* 2003], among others. Both human AQP7, AQP9 and AQP10 aquaglyceroporins [Garneau *et al.* 2015], as well as LsiI from rice [Ma *et al.* 2006] have been found to efficiently transport silicon through cell membranes. Further examples include the transport of HCO_3^- by AQP1 in proximal tubules of animal kidneys [Skelton *et al.* 2010], which plays a role in arterial pH regulation during metabolic acidosis [Xu *et al.* 2011]; or the release and uptake of glycerol into and from the blood stream by AQP7 and AQP9, respectively, during lipolysis [Rodriguez *et al.* 2006 / Hibuse *et al.* 2006], which is especially critical for gluconeogenesis during starvation [Carbrey *et al.* 2003]. Interestingly, metalloid arsenite and antimonite in solution mimic inorganic glycerol molecules and are thus also facilitated by many aquaglyceroporins in *E. coli* [Meng *et al.* 2004], yeast [Wysocki *et al.* 2001], mammals [Liu *et al.* 2004b] and fish [Hamdi *et al.* 2009] alike. Due to their high toxicity and significant accumulation in fish [Kuehnelt *et al.* 2003] in opposition to terrestrial animals, such as cattle or chickens [Dabeka et al. 1993], the study of marine based MIPs could provide the first steps in deciphering the metabolism and transport of such toxins in the food chain.

1.3.4 Medical implications

Due to the multifold molecular functionality and localization of aquaporins (as discussed in chapters 1.3.2 and 1.3.3), their impact on various medical conditions is quite significant. MIPs as potential pharmacological targets include areas of neuropsychiatric disorders, ocular conditions or gastrointestinal deficits, but also play a role in pain perception, memory and sleep processes (see Table 2). Additionally, new approaches are under way to treat parasitic diseases, such as malaria, sleeping sickness or leishmaniasis by specifically targeting protozoan aquaporins [Beitz 2005]. The idea is to disable the pathogen´s osmotic protection, lipid synthesis and glycolysis with an ensured high specificity of developed drugs due to significantly dissimilar protein structures accessible at the aquaporin pore entrances. The medical potential can be extended to the usage as drug vehicles, providing an entry pathway for cytotoxic compounds. Proofs of priciple have already been established with hydroxyurea [Pavlovic-Djuranovic *et al.* 2003] and trivalent hydroxyantimony [Gourbal *et al.* 2004]. In conclusion, the application of aquaporin modulators at different phases of a medical condition could have the capacity of amplifying favorable physiological outcomes or of attenuating undesirable ones. The next major hurdle in this

area will be to develop fast and simple high-throughput methods of identifying such modulators. Recently, initial steps have already been taken in this regard in the form of a freeze-thaw cycle assay based on the viability of yeast cells in dependence of aquaporin functionality [To *et al.* 2015].

Table 2 – Exemplary overview on aquaporins and their involvement as potential drug targets in various human medical conditions.

Aquaporin	Origin	Medical condition	Involvement	References
AQP0	*Homo sapiens*	Ocular cataract formation	cell adhesion, formation of square array and gap junctions	Biswas *et al.* 2014 Kumari *et al.* 2013
AQP1		Autosomal dominant polycystic kidney disease	water flow into cysts	Terryn *et al.* 2011
		Hydrocephalus	formation and regulation of cerebrospinal fluid	Tait *et al.* 2008
		Peripheral pain perception	abundant expression in peripheral nervous system	Ma *et al.* 2012
		Glaucoma	regulation of intraocular pressure, degeneration of optical nerve	Huber *et al.* 2012 Frigeri *et al.* 1995
		Atrophic gastritis	low expression levels in stomach disturb nutrient digestion and absorption	Laforenza 2012
AQP2		Hereditary nephrogenic diabetes insipidus	urine concentration	Deen *et al.* 1994
AQP4		Ischemic stroke	regulation of brain water homeostasis, formation of brain edemas	Manley *et al.* 2000 Verkman 2005
		Delirium	glymphatic clearance, regulation of brain water homeostasis	Sfera & Osorio 2014
		Neuroinflammation	formation of brain edemas, opening of blood-brain-barrier	Tourdias *et al.* 2011
		Alzheimer´s disease	regulation of astrocyte plasticity	Yang *et al.* 2012 Iliff *et al.* 2012
		Parkinson disease	gene deletion leads to decreased amount of CD4(+) and CD25(+) T-cells	Thenral & Vanisree 2012 Chi *et al.* 2011
		Depression	deficiency suppresses hippocampal neurogenesis	Kong *et al.* 2009 Eisch & Petrik 2012
		Cocaine-induced addiction	change in extracellular dopamine levels, negative neurogenesis regulation	Li *et al.* 2006 Xie *et al.* 2009
	Homo sapiens *Zea mays* *Glycine max* *Spinacia oleracea* *Solanum lycopersicum*	Multiple Sclerosis	antibody production against endogenous and environmental AQP4 proteins, cytotoxicity, tissue damage, demyelation of optic nerve and spinal cord, opening of blood-brain-barrier	Vojdani *et al.* 2015 Jarius *et al.* 2008

1.3.5 Industrial applications

After the first landmark publication in 2007, which demonstrated the use of aquaporins in polymeric membranes [Kumar *et al.* 2007], significant research is under way in order to create aquaporin-based biomimetic membranes (ABMs) with potentially superior performance to conventional membranes in terms of water flux and solute rejection [Zhao *et al.* 2012 / Sun *et al.* 2013 / Wang *et al.* 2013]. The development of such ABMs requires three major components: Protein water channels, amphiphilic molecules for their embedment and a polymer support structure (Fig. 5). Di- and triblock copolymers have predominantly been investigated as polymer support materials due to their superior performance in terms of flexibility and stability [Kita-Tokarczyk & Meier 2008]. Additionally, polyhedral oligomeric silsesquioxanes (POSS) are explored as well-defined nano-scale organic-inorganic structures for the construction of membranes for molecular separation processes at elevated temperatures [Raaijmakers *et al.* 2014], as well as models with anti-fouling properties [Ajit *et al.* 2015].

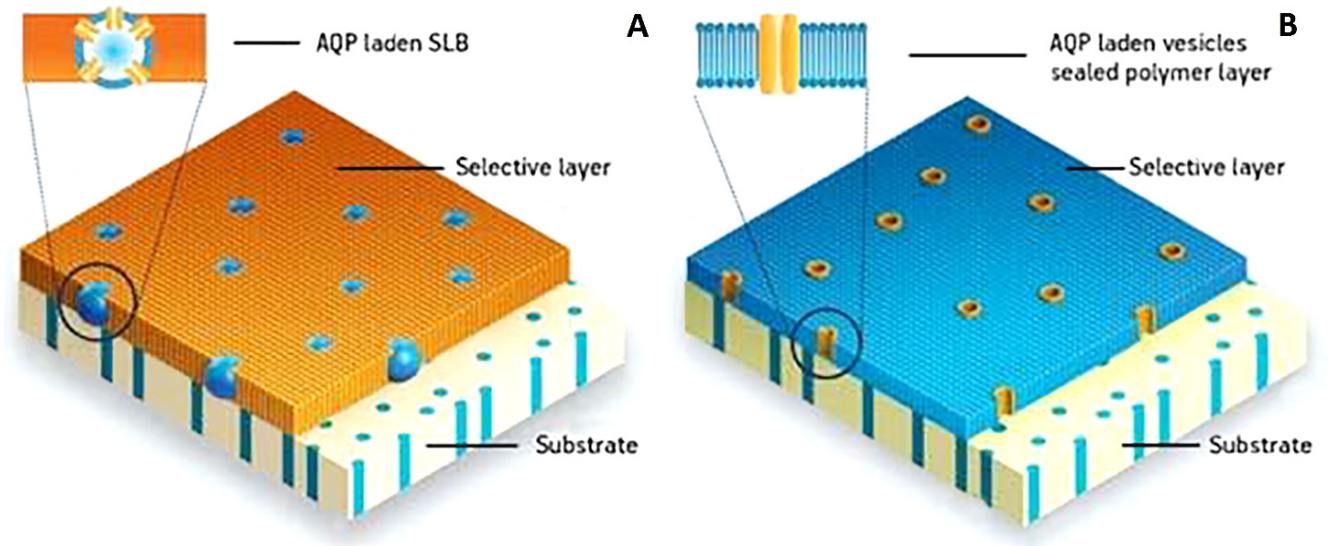

Fig. 5 – Schematic representation of aquaporin-based biomimetic membranes. A = Vesicles (blue) with embedded protein water channels (yellow) are immobilized in a polymer layer (orange) on a porous support substrate (beige). B = A membrane layer with aquaporins (yellow) is embedded in a flat layer (blue), which in turn is supported by a porous matrix (beige). SLB = supported lipid bilayer / AQP = aquaporin / [Perry *et al.* 2015 / Tang *et al.* 2015, modified]

Commercially available ABMs are already produced, for example by the Copenhagen-based company Aquaporin A/S (www.aquaporin.dk), for the usage of both traditional reverse osmosis and cutting edge forward osmosis systems. Application examples, where conventional technology fails, cover various areas [Perry *et al.* 2015]:

- Forward osmosis in diary industries as a pre-treatment step to remove urea from process water streams
  - ➔ Conventional reverse osmosis membranes only show urea rejection rates of roughly 40 % [Yoon & Lueptow 2005]
- Forward osmosis in the recycling of astronaut urine in space
  - ➔ Conventional methods are either too bulky or inefficient [Hill & Taylor 2012]
- Forward osmosis for direct dewatering of challenging industrial waste waters in biorefinery industries
  - ➔ Conventional reverse osmosis membranes are not applicable here due to their fouling propensity
- Reverse osmosis for low-pressure household water purifiers gives additional room for improvement over conventional solutions, that have currently reached their performance limits
- Forward osmosis as a more energy-efficient alternative for current amine-based CO_2 absorption methods for the recycling of Na_2CO_3 via crystallization [Luis *et al.* 2012]

Although current developments in this field are very promising, there are several challenges that have to be tackled in order to promote wider adoption of aquaporin-based biomimetic membranes. These include not only efficient upscaling techniques for the production of both the protein water channels, as well as the block copolymers, but also the economic issue of AQP-solubilizing detergents [Habel *et al.* 2015]. Furthermore, understanding the interactions and compatibility of aquaporins with various types of matrix materials is crucial for ensuring long-term stability of biomimetic hybrid assemblies and thus determine scalability and production costs [Hall *et al.* 2010]. The adaptation of wildtype aquaporins to synthetic alien environments via directed evolution and the development of high-throughput functional assays are important for extended operational shelf-life, resistance to chemicals, overall compatibility with synthetic polymers and subsequently, packaging and production yields [To & Torres 2015]. Molecular dynamics simulations have already started a discussion about carbon nanotubes as a suggested artificial, all synthetic alternative approach to aquaporins for the application in nanofluidic systems [Zuo *et al.* 2010].

1.4 Aquaporins in plants

1.4.1 Classification, nomenclature, phylogeny

The first identification of water channel proteins in plants dates back to the early 1990s [Maurel *et al.* 1993], shortly after their discovery in animals. In general, higher plant aquaporins can be organized into five subfamilies: Plasma membrane intrinsic proteins (PIPs), tonoplast intrinsic proteins (TIPs), Nodulin26-like intrinsic proteins (NIPs), small basic intrinsic proteins (SIPs) (Fig. 6) and the uncategorized (X) intrinsic proteins (XIPs).

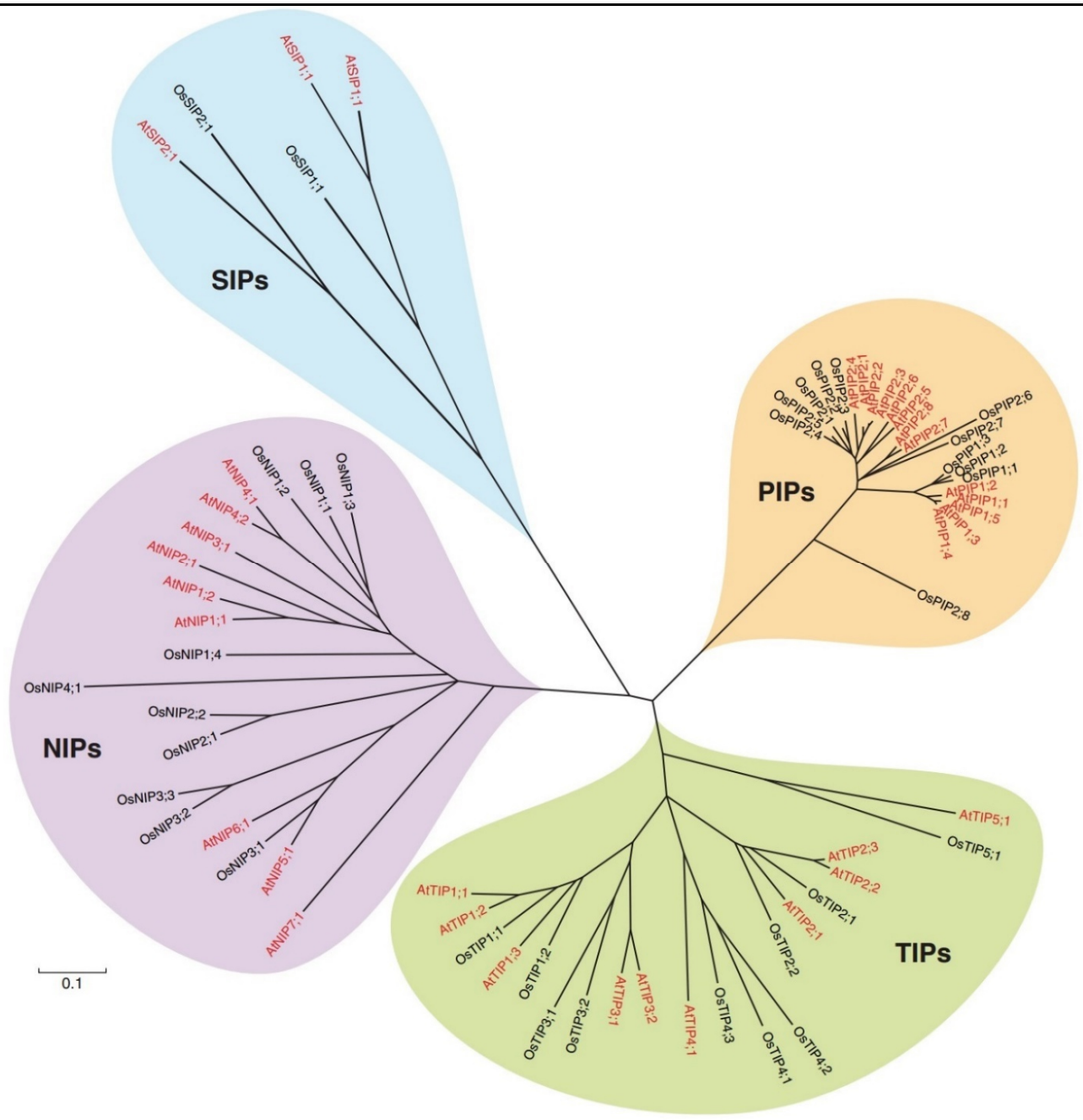

Fig. 6 – Phologenetic tree of the *Arabidopsis* (red) and rice (black) aquaporin families. A total of 1000 replicates were used to generate the bootstrap consensus tree and represent the evolutionary history of the analyzed taxa. The scale bar represents the amount of genetic change in terms of amino acid substitutions per respective sequence lengths. SIPs = small basic intrinsic proteins / PIPs = plasma membrane intrinsic proteins / NIPs = Nodulin26-like intrinsic proteins / TIPs = tonoplast intrinsic proteins [Maurel *et al.* 2015, modified]

PIPs, TIPs and NIPs have been well described with respect to protein localization and function, whereas SIPs and XIPs were discovered more recently, with the latter being absent in some higher plant species, such as monocots

or *Brassicacaea* [Johanson & Gustavsson 2002 / Danielson & Johanson 2008]. Genomic studies have provided additional insights into aquaporins of algae, such as *Chlamydomonas* and *Chlorella* species, and early branched land plants, such as mosses, that somewhat differ in their subcategorization when compared to higher plants [Anderberg *et al.* 2011 & 2012 / Danielson & Johanson 2008]. In contrast to animal and bacterial MIPs, that are broadly categorized into aquaporin and aquaglyceroporin clades, higher plant MIPs fall exclusively into the former [Maurel *et al.* 2015]. Phylogenetic analyses found the evolution of plant aquaporins in bacterial, as well as algal origin, possibly involving horizontal gene transfer [Gustavsson *et al.* 2005]. Certain subclasses though, such as TIPs, seem to have emerged during land plant evolution, possibly from a common PIP ancestor. The subdivision of PIPs and TIPs may have occurred early in evolution, since they seem to be conserved through all higher plants (Fig. 6). In contrast, XIPs may have evolved much later, as they show taxon-specific clade divergences [Lopez *et al.* 2012].

As the nomenclature of the plasma membrane intrinsic proteins implies, their localization is mainly in the plasma membrane of all parts of the plant like roots or leaves [Schäffner 1998]. There are two phylogenetic subgroups named PIP1 and PIP2, that differ in the length of their N- and C-termini, as well as their apparent water permeability when measured in different heterologous expression systems [Zardoya 2005]. PIP1 isoforms of *Arabidopsis* show an immense 90 % amino acid sequence identity [Johanson *et al.* 2001], whereas PIP2 members generally possess a shorter amino- and a longer carboxy-terminal region. Furthermore, 4-10 additional amino acid residues in their first extracytosolic loops separate them from PIP1 aquaporins [Kaldenhoff & Fischer 2006].

Plants of the *Leguminosae* family can be infected by nitrogen fixing bacteria in nitrogen-limited soil conditions. Infection results in the formation of nitrogen-fixing root organs, so called nodules [Stougaard 2000 / Hirsch *et al.* 2001], that contain symbiosome membranes (SMs) as the foremost location of NIPs, although transcripts of this aquaporin subclass have also been found in seed coats, shoots and roots [Schuurmans *et al.* 2003 / Weig *et al.* 1997]. The symbiosome membrane takes part in the efflux of fixed nitrogen to the plant and carbon supply in the opposite direction. The plant hereby produces Nodulin proteins and transfers them to the SM during nodule formation [Fortin *et al.* 1985]. Soybean Nodulin 26 (Nod26) was described as a major integral protein of the SM, constituting approximately 10 % of the total membrane protein [Weaver *et al.* 1991]. Subsequently, Nod26 was classified into the MIP cluster and represents the archetype of the NIP subfamily, thus all proteins related to Nodulin26-like intrinsic proteins were renamed accordingly.

The plant vacuole as a cellular storage compartment is responsible for turgor regulation, signaling and degradation processes and its tonoplast membrane is the paramount location of TIPs [Maurel *et al.* 1993 / Maurel et al. 1997 / Gerbeau *et al.* 1999].

Small basic intrinsic proteins were firstly identified by database mining and phylogenetic analysis [Johanson & Gustavsson 2002]. This subfamily is comprised of very small molecular size proteins, which is mainly derived from a comparably short cytosolic N-terminal region. They are mainly located in the endoplasmatic reticulum (ER) of *Arabidopsis* [Ishikawa *et al.* 2005].

1.4.2 Molecular function, organization and cellular localization

PIPs and TIPS are multifunctional water channels that are able to transport not only water, but also other compounds, such as H_2O_2, CO_2 (PIPs), NH_3, urea (TIPs), glycerol (both) and additional substrates. A comprehensive listing of substrate specificity in plant aquaporins is discussed in Maurel *et al.* 2015 and Perez Di Giorgio *et al.* 2014. PIP1 aquaporins show an overall low intrinsic water permeability [Chaumont *et al.* 2000 / Temmei *et al.* 2005], but divergent functionality when it comes to gas and small solute transport [Uehlein *et al.* 2003 / Biela *et al.* 1999]. In contrast, members of the PIP2 subfamily show significantly higher water transport rates, as shown in heterologous *Xenopus* oocytes or yeast expression systems [Weig *et al.* 1997 / Otto *et al.* 2010]. Heteromerization of different PIP1 isoforms has been shown to increase their overall intrinsic water

permeability in maize plasma membranes [Fetter *et al.* 2004], implying that this might be a requisite for this subclass to function as proper water channels. NIPs, in contrast to PIPs and TIPs, show an at most reduced water permeability, transporting mainly small organic solutes and mineral nutrients [Ma *et al.* 2006 / Takano *et al.* 2006]. In particular, they mediate the diffusion of beneficial (B, Si, Se) or toxic (As, Sb) metalloids [Bienert *et al.* 2008 / Zhao *et al.* 2010]. The functional characterization of SIPs has only revealed a moderate water transport activity [Johanson & Gustavsson 2002 / Noronha *et al.* 2014], whereas XIPs appear to be multifunctional channels permeable to water, metalloids and reactive oxygen species (ROS) [Bienert *et al.* 2011 / Lopez *et al.* 2012]. In contrast to mammalian AQP6, which has shown true ion permeability [Ikeda *et al.* 2002], no such functionality has been described in any plant aquaporins so far. Mercury was identified as the most common aquaporin blocker in plants and is thought to inhibit the water permeability through binding to the thiol groups in Cys residues, although is has recently been reported to target His residues in the rice aquaporin OsNIP3;1 [Katsuhara *et al.* 2014]. Some exceptions lack the critical Cys residues identified in other isoforms [Daniels *et al.* 1994], whereas SoPIP2;1 was shown to be Cys independently activated rather than inhibitied by mercury, suggesting a mechanical gating via effects on the lipid environment [Frick *et al.* 2013a].

Cryoelectron microscopy of PIPs and TIPs confirmed their molecular organization into tetramers made up of four identical monomer subunits, each containing an individual transmembrane pore [Daniels *et al.* 1999 / Kukulski *et al.* 2005]. However, members of the same aquaporin subclass may potentially assemble into heterotetramers due to the high structural similarity of the individual subunits, enabling multiple molecular and functional combinations. This was suggested for PIPs and TIPs from functional coexpression in *Xenopus* oocytes or yeast [Fetter *et al.* 2004 / Murozuka *et al.* 2013]. Molecular modeling of PIPs points to a critical role of loop A in oligomer interactions, contributing to a disulfide bond that stabilizes PIP dimers and subsequently allows them to assemble as tetramers [Bienert *et al.* 2012]. Site-directed mutations in this loop modified the interaction behavior of PIP1s and PIP2s in *Beta vulgaris* (common beet) [Jozefkowicz *et al.* 2013].

Concerning the cellular localization of plant aquaporins, the plasma membrane harbors three subclasses, namely PIPs, NIPs and XIPs [Bienert *et al.* 2011], most of which are expressed over the entire cell surface. Vacuoles as the most voluminous intracellular plant organelles harbor TIPs and provide proteolytic or nutrient storage functions [Wudick *et al.* 2009]. The expression of TIPs in the tonoplast is not uniform, however, but preferentially observed in intravacuolar bulbs and opposing regions of adjacent vacuoles [Beebo *et al.* 2009 / Saito *et al.* 2002], suggesting privileged exchanges between neighboring organelles of this type. Most aquaporins are observed in the ER during their biogenesis and transfer to their destination membranes. SIPs and NIPs seem to be residents in this compartment [Ishikawa *et al.* 2005 / Mizutani *et al.* 2006], although their particular function at that location is yet unknown. Thorough proteomic analyses of *Arabidopsis* have suggested the presence of PIPs in the inner envelope of chloroplasts, with TIPs being suspected in the thylakoid membranes [Ferro *et al.* 2003 & 2010].

1.4.3 Physiological functions

When it comes to physiological functions of plant aquaporins on a cellular level, osmoregulation is surely one of the most important aspects to consider. It has even been suggested that aquaporins localized in the plasma or tonoplast membranes may serve as osmosensors, i.e. in guard cells during stomatal movements or in growing pollen tubes [MacRobbie 2006 / Shachar-Hill *et al.* 2013]. TIPs also play a role in ROS detoxification, modulating a plant´s resistance towards oxidative stress, as shown by their ability to transport H_2O_2 [Bienert *et al.* 2007], as well as the increased sensitivity when overexpressed [Wang *et al.* 2014] or lowered sensibility when inactivated in plant tissues [Schüssler *et al.* 2008]. Furthermore, TIPs are suggested to contribute to vacuolar storage functions and the mobilization of nitrogen metabolites due to their ability to mediate NH_3 and urea diffusion [Gerbeau *et al.* 1999 / Liu *et al.* 2003 / Loque *et al.* 2005]. Another key area of cellular plant aquaporin physiology

involves the passive transport of solutes in chloroplasts [Fig. 7]. The protein channels are hypothesized to support the steady uptake of water required for the refilling of thylakoid lumen. This is in light of one of the key reactions in chloroplasts, namely the oxidation of water to molecular oxygen, where the daily conversion amount represents the 60 to 170-fold volume of the thylakoid lumen [Beebo *et al.* 2013]. Additionally, PIP1 aquaporins may ease the diffusion of CO_2 in chloroplasts, since their antisense inhibition in tobacco plants has been shown to reduce the CO_2 permeability of chloroplast membranes by 90 % [Uehlein *et al.* 2008]. In the context of CO_2 diffusion this is highly restricted throughout plant cells due to several physical and biochemical factors, including cell wall composition, unstirred layers in membranes, carbonic anhydrase activity in membrane vicinity or the CO_2 permeability of membranes themselves [Evans *et al.* 2009]. In this regard, the chloroplast envelope represents a critical CO_2 barrier, limiting carboxylation reactions in the stroma via the Calvin-Benson cycle. An additional involvement of aquaporins in the chloroplast has been suggested in the area of ROS dissipation during high-intensity light conditions: namely the H_2O_2 transport into the cytosol through the chloroplast envelope [Mubarakshina-Borisova *et al.* 2012].

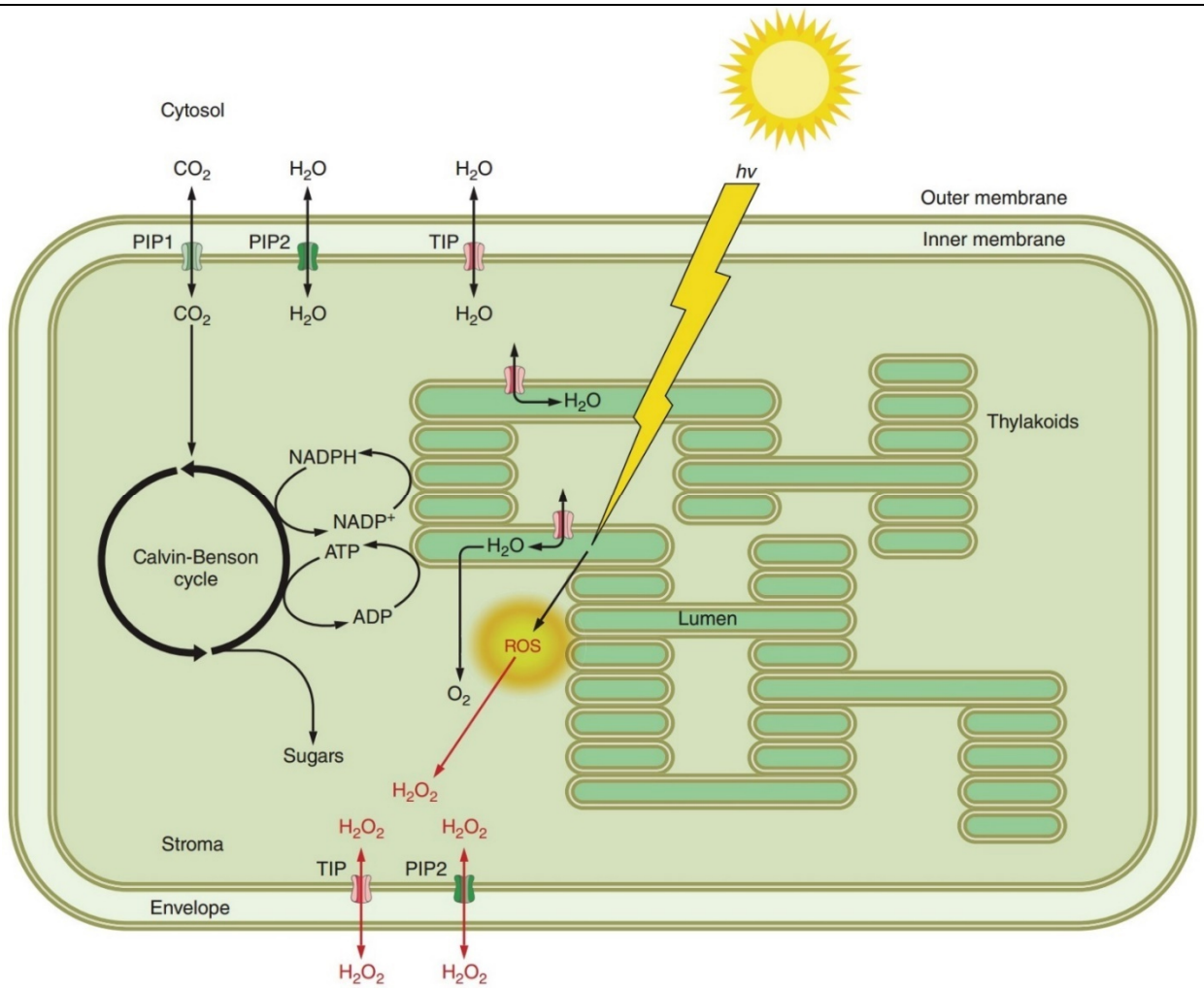

Fig. 7 – Putative functions of aquaporins in the chloroplast. PIPs and TIPs may contribute to water transport into the stroma and thylakoid lumen, having been localized in the inner envelope and thylakoid membranes. A role of PIP1s in the transport of CO_2 is also indicated, contributing to carbon fixation through carboxylation reactions in the Calvin-Benson cycle. Finally, H_2O_2 export by PIPs and TIPs potentially takes part after the buildup of ROS as byproducts of photosynthetic activities. [Maurel *et al.* 2015, modified]

The water transport in roots is characterized by the root hydraulic conductivity (Lp_r), which is based on apoplastic paths of water along the cell walls inside the root and transcellular paths, which are aquaporin-dependent. The transcellular parths have been shown to vary in significance across plant species and aquaporins contribute up to 60 % of their throughput in tomato and *Arabidopsis*, as demonstrated by mercury as an aquaporin blocker

[Maggio & Joly 1995 / Sutka *et al.* 2011]. Although mercury is toxic and has numerous secondary effects, thus potentially influencing results, inhibitors with different modes of action, such as weak acids or azide, yielded similar estimates of the aquaporin-dependent water transport path. A direct exposure of roots to water stress can either result in inhibition of aquaporin activity and thus water transport at a cellular or whole organ level [Boursiac *et al.* 2005 / Hachez *et al.* 2012], or an enhancement of Lp_r [Hachez *et al.* 2012 / Sutka *et al.* 2011]. An increased root hydraulic conductivity during the early phase of drought can help optimize water uptake, whereas long-term inhibition could help preserve the plant´s water resources. When it comes to nutrient availability, root water transport and aquaporin activity have been demonstrated to be highly sensitive, with Lp_r values decreasing during phosphorus, nitrogen or sulfur starvation [Carvajal *et al.* 1996 / Di Pietro *et al.* 2013]. This regulation may enhance the nutrient flux to roots in soil zones enriched in nutrients.

In leafs, expression studies have revealed a high abundance of aquaporins, especially in the vascular bundles of many plant species and to a lesser extent in the mesophyll [Besse *et al.* 2011 / Hachez *et al.* 2008]. Three PIP isoforms have been identified in *Arabidopsis*, contributing to leaf hydraulics and concentrated mostly in the hydrautically limiting xylem veins, as opposed to the rather conductive mesophyll [Prado *et al.* 2013]. Reversible changes of guard cell volumes adjust the opening and closing of stomata, thus playing a major role in plant transpiration. PIP1 and TIP isoforms in transgenic *Arabidopsis* and wild type sunflower guard cells have been found to significantly influence stomatal aperture [Cui *et al.* 2008 / Sarda *et al.* 1997]. The regulation of aquaporin expression also seems to contribute to circadian variations in osmotic water permeability of *Samanea saman* motor cells and the petiole of tobacco, influencing diurnal and epinastic leaf movements, respectively [Moshelion *et al.* 2002 / Siefritz *et al.* 2004]. Furthermore, aquaporin-mediated water transport has been suggested to play a role in embolism repair, thus refilling damaged xylem after intense drought or tissue freezing in winter [Lovisolo & Schubert 2006 / Sakr *et al.* 2003 / Secchi & Zwieniecki 2010].

The allocation of nutrients and toxic metalloids is another area, where plant aquaporins fulfill physiological functions. Boron, for example, is necessary for plant growth and to reinforce cell walls. NIP and XIP type aquaporins mediate B transport and have been shown to play a critical role in *Arabidopsis*, maize and tobacco plants during boron deficient conditions and growth phases [Takano *et al.* 2006 / Durbak *et al.* 2014 / Bienert *et al.* 2011]. In cereal plants, the accumulation of silicon has a growth promoting function and serves to build up resistances against biotic and abiotic stresses. For instance, the addition of Si alleviates drought stress in *Sorghum* by enhancing water uptake and aquaporin activity [Liu *et al.* 2014]. The opposite effect on plant health has been demonstrated by the accumulation of toxic arsenic and selenium via NIP type aquaporins in *Arabidopsis* and rice [Kamiya *et al.* 2009 / Ma *et al.* 2008 / Zhao *et al.* 2010].

When it comes to biotic interactions, TIPs and NIPs are important for root nodule formation in *Rhizobium*-Legume symbiosis [Gavrin *et al.* 2014] and osmoregulation. In addition, they provide support in the assimilation of atmospheric nitrogen via NH_3 uptake in fully differentiated symbiosome membranes [Guenther & Roberts 2000 / Ikeda *et al.* 2002]. *Mycorrhizae* as soil fungi help optimize soil exploration and nutrient capture, while profiting from carbon metabolites provided by the plant root. Root aquaporin inhibition and water conservation was enhanced in maize by interactive effects of *Mycorrhizae* and plant abscisic acid [Ruiz-Lozano *et al.* 2009]. Additionally, enhanced interspecies exchange of glycerol and NH_3 between plants and microbes was examined through gene profiling, which suggested an activation of aquaporin genes.

1.4.4 Biotechnology applications

Aquaporins represent attractive targets for plant molecular breeders due to their influence on water and nutrient uptake as major traits in crop improvement [Martinez-Ballesta & Carvajal 2014]. Examples of already applied genetic plant improvement include:

- Enhanced drought resistance in *Arabidopsis* and tobacco by overexpression of a *Vicia faba* PIP1 or a wheat PIP2, respectively [Cui *et al.* 2008 / Zhou *et al.* 2012]
- Enhanced growth performance of transgenic tomato plants under both normal and stress conditions via constitutive expression of stress-responsive tomato TIP [Sade *et al.* 2008]
- Higher tolerance of root and leaf growth to salt stress in rice plants by moderate constitutive expression of a rice PIP1 [Liu *et al.* 2013]
- Enhanced root hydraulics, transpiration and shoot growth of grapevine in control conditions with normal water conservation responses under water stress through overexpression of a root PIP1 [Perrone *et al.* 2012]

While many approaches in aquaporin biotechnology lead to remarkable progress and strain improvement, their exploration is most often accompanied by arising undesireable pleiotrophic effects. The problem was represented by a potentially detrimental influence of the transgenic target upon the native or normally regulated aquaporins. For instance, tobacco plants overexpressing *Arabidopsis* AtPIP1;2 grew better than control plants under optimal conditions, but became dramatically more sensitive to water deprivation [Aharon *et al.* 2003]. Another example was the expression of cucumber and figleaf gourd aquaporins in *Arabidopsis* having either beneficial effects during plant dehydration or detrimental effects when the plant was under salt stress conditions [Jang *et al.* 2007].

1.5 Tobacco aquaporins

1.5.1 NtPIP2;1

The first molecular characterization of the tobacco water channel NtPIP2;1 was performed by Bots *et al.* in 2005 [2005a] who found the aquaporin to be localized in sexual reproductive organs of tobacco plants. When expressed in *Xenopus* oocytes, it proved to be an efficient water channel with an 8-fold increase of water permeability when compared to controls.

NtPIP2;1 shows a high sequence similarity to the spinach aquaporin SoPIP2;1 [Fischer & Kaldenhoff 2008] and possesses all the residues required for the pH gating mechanism postulated to be conserved in all plant aquaporins by Törnroth-Horsefield *et al.* in 2006 (Fig. 8). The gating mechanism is based on the observation that a decrease of cytosolic pH in plants leads to a reduction in hydraulic permeability [Kamaluddin & Zwiazek 2004 / Zhang & Tyerman 1999]. The sensitivity of that reaction to heavy metal ions suggested the involvement of aquaporins with direct evidence for their pH regulation having been obtained through the analysis of AtPIP1;2, AtPIP2;2 and AtPIP2;3 in *Xenopus* oocytes. Replacing a histidine residue with alanine or aspartic acid in loop D at position 197 prevented pH sensitivity in such setups [Tournaire-Roux et al. 2003]. Based on the X-ray structure of SoPIP2;1 and the fact that the histidine residue in loop D is found in many plant aquaporin species, this gating mechanism was thus postulated to be universal for protein-based plant water facilitators [Törnroth-Horsefield *et al.* 2006]. It circumstantiates a displacement of loop D in the closed conformation of the aquaporin and an opening of a hydrophobic gate, which in turn blocks the water channel entrance. This closed conformation occurs, when two highly conserved serine residues are dephosphorylated or when these are phosphorylated in combination with the afore-mentioned His residue being protonated, i.e. during cellular acidification of flooded plant root cells [Tournaire-Roux et al. 2003] (Fig. 8). Possessing both conserved serine residues, as well as the His required for pH gating, NtPIP2;1 was indeed shown to modulate its water permeability dependent on pH. In a heterologous yeast system a 50 % reduction in transport rates was observed when lowering the pH by 0.33 [Fischer & Kaldenhoff 2008]. Although modulated, the mediated water diffusion did not shut down completely as postulated, but was still about 115-fold higher than the included control. This pH sensitivity could be eliminated by exchanging His_{196} with an alanine residue. As for the two conserved serine residues, their

substitution for alanine either showed a reduction of water permeability to control levels ($Ser_{118}Ala$) or elevated transport rates ($Ser_{277}Ala$). The corresponding double mutant containing $Ser_{277}Ala$ and $His_{196}Ala$ modifications demonstrated a resistance against pH modulation of NtPIP2;1, although water permeability was found to be elevated in comparison to the single $His_{196}Ala$ mutant. In conclusion, the phosphorylation state of the two serines did not alter His_{196} protonation dependent modification of AQP activity.

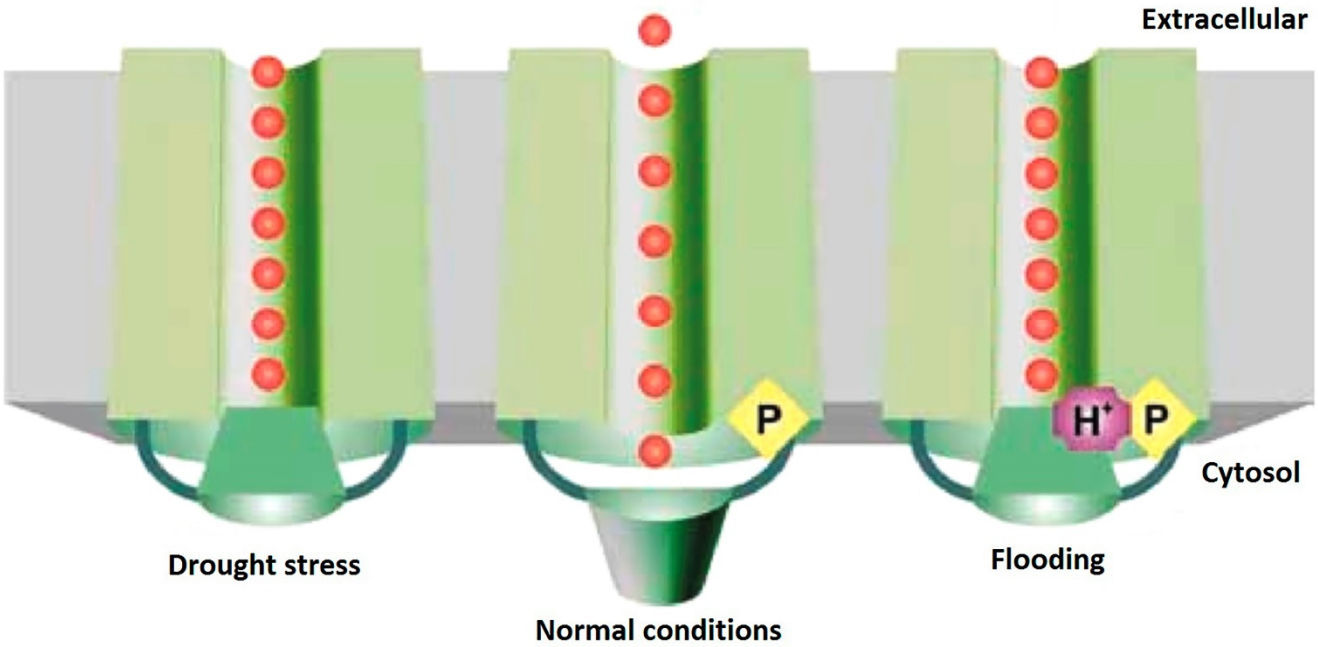

Fig. 8 – Structural mechanism of pH and phosphorylation dependent aquaporin gating in plant plasma membranes. Two highly conserved Ser residues are desphosphorylated in plant PIPs during periods of drought stress, leading to the closing of their water pores. Flooding, in turn, leads to the same conclusion in response to the protonation of a conserved His residue. [Törnroth-Horsefield *et al.* 2006, modified]

In 2008, Mahdieh *et al.* were able to confirm NtPIP2;1´s high water permeability using *Xenopus* oocytes, with rates being 8-fold higher than controls. Its activity was not found to be regulated by phosphorylation of Ser_{118} and Ser_{277}, as demonstrated by unmodulated water diffusion rates when protein phosphatase or protein kinase inhibitors were added. Co-expression with NtPIP1;1 greatly enhanced NtPIP2;1´s water mediation compared to the values obtained with individual aquaporins, suggesting heteromerization of the two in the form of heterotetrameric configuration or homotetrameric interaction.

Further investigations into artificially forced heteromerization of NtPIP2;1 on a gene level were performed by Otto *et al.* in 2010. Once more, the tobacco aquaporin was demonstrated to behave as a true aquaporin with high water permeability, but did now show any CO_2 transport ability. Heterotetramer constructs together with NtAQP1 showed that a single NtPIP2;1 monomer subunit was sufficient to significantly increase water transport activity of tetramers. Once more NtPIP2;1 monomers were added, this resulted in a sigmoidal saturation curve. This revealed the monomer subunits to be the functional units for water transport, which was thus found not to be exclusively dependent on a tetramer configuration.

Though not established in the former investigation, Uehlein *et al.* [2012] were able to show a 12-fold increase in CO_2 permeability for NtPIP2;1 compared to controls when it was integrated in gas-tight triblock copolymer membranes. This experimental setup abolished the inherent CO_2 diffusion that yeast membranes had in previous control measurements.

The first study to produce NtPIP2;1 in an *E. coli* based cell free expression system performed an analysis of diffusion rates for water and CO_2 in lipid bilayer liposomes in dependence of cholesterol and stigmasterol integration [Kai & Kaldenhoff 2014]. The addition of these sterols significantly decreased both water and CO_2 permeability in dependence of their molar incorporation ratios. However, insertion of NtPIP2;1 increased water

permeability of lipid vesicles 8-fold and 4-fold with and without sterols, respectively. In contrast, CO_2 permeability was unchanged in lipid bilayers with sterols, whereas during their absence a 50 % decrease was observed.

In a physiological context, NtPIP2;1 was first found to be expressed in reproductive organs of tobacco plants, specifically accumulating in most anther tissues [Bots *et al.* 2005a]. Water movement between cells or tissues is involved in several processes during sexual reproduction of higher plants. For instance, the anther and pollen undergo dehydration before the release of mature pollen at dehiscence, thus a likely involvement of PIP2 aquaporins was suggested in this process [Bots *et al.* 2005b]. Immunolocalization of PIP2 aquaporins in tobacco showed that expression is modulated during anther development, whereas RNA interference lines showed anther dehydration to be slower with dehiscence occurring significantly later when compared to wildtype plants. More specifically, NMR analysis of water content development in single anthers demonstrated a difference of 25-35 % in a time frame of 20 h.
NtPIP2;1 transcripts were found to be significantly reduced in number in tobacco plants undergoing drought stress, leading to an overall reduction of stomatal conductance, transpiration, water potential, turgor pressure in leafes, sap flow rate and osmotic hydraulic conductance in roots, whereas leaf osmotic pressure was increased [Mahdieh *et al.* 2008]. Rewatering the plants reinstated NtPIP2;1 transcription levels, as well as water relation parameters to those of control plants in regular watering conditions. In conclusion, the downregulation of this aquaporin reduces osmotic hydraulic conductance in the roots of tobacco plants under drought stress to help conserve water reservoirs under such conditions.
A later study examined the water transport properties in tobacco roots and the expression of NtPIP2;1 in dependence of abscisic acid (ABA) application, which modifies hydraulic root conductivity by increasing water flux [Mahdieh & Mostajeran 2009]. A significant increase of NtPIP2;1 transcripts could be detected after application, although no significant effect was apparent on expression levels in leafs. Subcellular localization of NtPIP2;1-GFP constructs by mesophyll chloroplast transformation showed the integration of the aquaporin into the plasma membrane.

1.5.2 NtAQP1

The first characterization of NtAQP1 included a plasma membrane localization and an apparent molecular monomer size of around 28 kDa, which was slightly smaller than the calculated 30 kDa based on its cDNA sequence [Biela *et al.* 1999]. It showed to moderately mediate water transport in *Xenopus* oocytes, with water permeability values (P_f) double that of controls, but only half of AtPIP2;2. Diffusion of glycerol was also detected, but not of Na^+, K^+ and Cl^- ions, making NtAQP1 the first plant aquaporin to be characterized as both a water and solute mediator. Although the number and position of Cys residues are identical to those in mercury sensitive AtPIP1;2 and AtPIP2;2, NtAQP1´s water permeability and selectivity could not be modulated by the addition of mercurial, protein kinase inhibitors or protein phosphatase inhibitors, classifying it both mercury-insensitive and impervious to regulation by phosphorylation. A subsequent study showed additional functionality with urea mediation in *Xenopus* oocytes [Eckert *et al.* 1999].
Siefritz *et al.* [2001] continued the analysis of NtAQP1 and suggested its insensitivity to mercury with moderate water permeability to be based on its comparably long N-terminus and short loop A. These features placed it in opposition of aquaporins with short N-terminal regions and an elongated loop A, that former experiments had shown to be highly water permeable and sensitive to mercury. While the deletion of 81 N-terminal amino acid residues and the insertion of an AGGDV motif into loop A did not alter the water flux capabilities of NtAQP1, a substitution of Thr_{233} with a Cys residue conferred mercury sensitivity comparable to AtPIP2;2. This study also was the first to speculate about NtAQP1´s potential to mediate CO_2.

Following in the footsteps of those speculations, a later publication was then able to demonstrate actual CO_2 permeability of NtAQP1 in *Xenopus* oocytes at 145 % of control values [Uehlein *et al.* 2003]. These levels were comparable to that of human AQP1 [Nakhoul *et al.* 1998], with which the plant aquaporin was shown to share a high amino acid similarity in the pore region [de Groot & Grubmüller 2001]. Integrated into gas-tight triblock-copolymer membranes impermeable for CO_2, NtAQP1 managed to transport CO_2 at rates 21-fold higher than controls [Uehlein *et al.* 2012]. Cell-free expressed NtAQP1 was able to completely restore CO_2 diffusion rates in lipid bilayer liposomes upon the incorporation of sterols decreased those in a concentration dependent manner [Kai & Kaldenhoff 2014]. Interestingly, the plant aquaporin decreased P_f values of lipid vesicles by 30 %, whereas CO_2 permeability was unchanged or restored to control values without and with sterols, respectively. Otto *et al.* [2010] undertook further investigations into the CO_2 mediation of NtAQP1 by heterologous expression in yeast cells, observing no difference in water transport between cells expressing the plant aquaporin and controls, but significant CO_2-triggered intracellular acidification. Artificial tetramers made up of varying ratios of NtPIP2;1 and NtAQP1 monomers showed that CO_2 mediated diffusion was a cooperative effect of the PIP1 monomers, resulting in an almost linear curve, the more cooporin subunits were added. These results suggested an alternative route of CO_2 transport in aquaporin tetramer structures when compared with water, the former potentially using the central fifth pore instead of the individual subunit channels of the latter (compare Fig. 4D). When analyzed for potential pH gating functionality in heterologous yeast cells (see chapter 1.5.1 and Fig. 8), NtAQP1 did not exhibit any sensitivity in its wildtype or conserved Ser_{129}Ala mutant configuration [Fischer & Kaldenhoff 2008]. However, its low intrinsic water permeability at only 4-5 fold that of controls complicated drafting clear cut conclusions about the underlying regulatory mechanism. Mahdieh *et al.* [2008] were able to confirm the negligible water permeability of NtAQP1 in *Xenopus* oocytes, with P_f values approximately double that of controls, but only 23 % of NtPIP2;1. Additionally, co-expression of the two plant aquaporins did not enhance transport rates.

Pertaining to its physiological functions, Biela *et al.* [1999] provided the first hint for the nature of NtAQP1´s regulatory role by detecting highly abundant transcripts in the roots and flowers of tobacco plants, but significantly lower levels in leafs and stems. Enlarging on that, Otto & Kaldenhoff [2000] were able to localize NtAQP1 mRNA in roots, stems and leafs with decreasing signal intensity. The intensity in roots was limited to the foremost part, where cell elongation and differentiation takes place. In older root tissues, NtAQP1 mRNA was found to be localized at the outer border of the xylem with an additional faint signal in phloem cells. Similar to roots, respective translation products were detected in the xylem and phloem cells of young shoots with an overall low concentration in leafs and clear accumulations around stomatal cavities. It was concluded that NtAQP1 could be important for the transition of water and small solutes between the apoplast and symplast. A subsequent study found NtAQP1 expression to be highest in flower petals and roots, followed by stems and leafs [Siefritz *et al.* 2001]. Additional experiments at a subcellular level revealed a definitive plasma membrane localization of the plant aquaporin with GFP fusion tags.

A succeeding series of experiments described the role of this protein based facilitator on the cellular and whole plant level [Siefritz *et al.* 2002]. Expression levels of NtAQP1 and NtPIP1;1, a 95 % sequence homologue, were significantly lowered in antisense lines, whereas PIP2 and TIP aquaporins appeared to be unaffected. Swelling assays on root protoplasts revealed a significantly reduced water permeability in NtAQP1 antisense cells. Analogously, root hydraulic conductivity decreased by 50 %, although no morphological changes could be observed in any antisense plant organs. A contribution of NtAQP1 gene products to water stress tolerance could be demonstrated under drought stress conditions, where wildtype plants seemed unaffected while antisense lines started to wilt prematurely.

A role of NtAQP1 in photophysiology was first proposed by Lorenz *et al.* in 2003 when the plant aquaporin, expressed as a GST-fusion product in *E. coli*, showed the capacity to bind 7-fold higher amounts of riboflavin than the GST only control. Similarly, but even more pronounced, membrane vesicle preparations from tobacco plant leafs overexpressing NtAQP1 demonstrated a 23-fold higher binding capacity for riboflavin when compared with samples drawn from NtAQP1 antisense lines. Substantiating the hypothesis above, Uehlein *et al.* [2003] were the first to indicate a significant physiological function of NtAQP1 in photosynthesis and stomatal opening of tobacco plants in conditions, where the CO_2 membrane gradient is small, i.e. between atmosphere and the inside of plant cells. Overexpression of the PIP1 heightened membrane CO_2 permeability *in vivo*, as demonstrated via increased $^{14}CO_2$ incorporation rates when comparing such plants to antisense lines. Similarly, net photosynthesis rates were reduced in antisense plants to 45 %, whereas overexpression lines exhibited an increase by 36 % under ambient CO_2 conditions. Furthermore, the longitudinal leaf growth of NtAQP1 overexpression plants more than doubled compared to controls, when neither overall height nor root mass showed significant growth differences, suggesting either a heightened photosynthetic capacity or a synergistic effect of both improved CO_2 and water permeability in plant tissues. In order to analyze the influence on mesophyll CO_2 conductance, which has been recognized to be finite and variable depending on environmental conditions, Flexas *et al.* [2006] conducted additional experiments with NtAQP1 antisense and overexpression tobacco lines. Photosynthetic rates at saturated light conditions were 13 % lower in antisense plants compared to wildtype controls, whereas NtAQP1 overexpressing lines showed a 20 % increase. *In vitro* studies revealed no alterations in RuBisCO activity or ribulose-1,5-biphosphate levels, that could have potentially attributed to the photosynthetic differences. Chlorophyll fluorescence and online ^{13}C discrimination supported the results obtained for photosynthesis rates with 20 % decreased and 30 % elevated CO_2 mesophyll conductance in antisense and overexpression lines, respectively. Despite these observed differences, no other morphological or physiological anomalies were visible between the plant lines. A subsequent study was able to not only localize NtAQP1 to plasma membranes, but also to inner chloroplast membranes in mesophyll and guard cells of tobacco plants [Uehlein *et al.* 2008]. Plasma membranes of tobacco leafs did not show a significant difference in CO_2 conductance when comparing wildtype with RNAi samples, whereas chloroplast envelopes showed a 90 % reduction. This result was easily discussed in consideration of the fact that chloroplast envelopes are less conductive to CO_2 than plasma membranes by a factor of 5. Water permeability showed an opposite tendency, with plasma membranes seeing a significant reduction in RNAi lines, whereas chloroplast envelopes did not. Photosynthetic rates in leafs were lowered by 15 % in NtAQP1 RNAi plants, suggesting a reduction in mesophyll conductance calculated to be based on a 20 % lower overall CO_2 transport ability. More recently, Kelly *et al.* [2014] analyzed the relationship between Hexokinase 1 from *Arabidopsis* (AtHXK1) and NtAQP1 in the regulation of photosynthesis and plant growth by expressing both gene targets in tomato. At that point it was already known that NtAQP1 increases both the rate of photosynthesis and transpiration, whereas AtHXK1, aside from sugar sensing, is able to decrease expression of photosynthetic genes and the rate of transpiration, as well as inhibit growth. Tomato plants expressing the two complementary gene products indeed demonstrated AtHXK1 to decrease root hydraulic conductivity and leaf mesophyll conductance of CO_2, whereas NtAQP1 significantly improved growth and increased transpiration rates in shoots. However, the latter only had a marginal effect on the root hydraulic conductivity, suggesting the complementary effect of the plant aquaporin being unrelated to shoot water transport.

After Siefritz *et al.* [2001] identified an upstream promotor element that enables phytohormone dependent NtAQP1 gene regulation via gibberellic and abscisic acids, Mahdieh & Mostajeran [2008] were able to confirm a significant increase of both NtAQP1 transcripts and gene products in tobacco roots after the application of ABA. However, no effect was seen on expression levels in leafs.

A key role of NtAQP1 in diurnal epinastic leaf movement was proposed by Siefritz *et al.* in 2004. Since aquaporin mediated water transport is an important component in rapid plant cell elongation, it was suggested to drive differential growth on the upper and lower leaf surface and thus highly influence epinastic leaf movement. NtAQP1-luciferase assays in combination with Northern & Western blotting indeed revealed diurnal and circadian oscillation of gene product expression in tobacco leaf petioles coinciding with leaf unfolding. Additionally, the water permeability of petiole protoplasts was found to be high in the morning during the unfolding reaction and low in the evening. As a consequence, diurnal epinastic leaf movement was significantly reduced in NtAQP1 antisense tobacco lines.

An investigation of mycorrhizal, fungal colonization patterns and their symbiotic efficiency in NtAQP1 antisense tobacco plants was undertaken by Porcel *et al.* in 2005 under well-watered and drought-stress conditions. Root colonization was found to be similar in both situations, although wildtype plants grew faster under drought stress than their antisense counterparts. Gas exchange analysis showed decreased transpiration and photosynthetic rates for antisense lines when compares to wildtype plants, both being in fungal symbiosis. It was implicated that NtAQP1 is enhancing symplastic water transport and its impact on the efficiency of symbiosis under drought stress conditions seems to be far reaching.

Further analysis of tobacco plants in drought-stress situations showed increased NtAQP1 transcript accumulation, suggesting a role in the transport of remaining water resources, as well as alternative substrates, such as CO_2, urea or glycerol [Mahdieh *et al.* 2008]. A later study pointed out a role of NtAQP1 in plant water use efficiency, stress resistance and productivity [Sade *et al.* 2010]. Expression of the tobacco aquaporin in tomato resulted in higher stomatal conductance, whole plant transpiration and leaf net photosynthesis. Root hydraulic conductivity under salt stress decreased to 30 % in control plants, whereas NtAQP1 expressing lines were able to level out at double that value under identical conditions. Reciprocal grafting experiments provided novel evidence for NtAQP1´s role in preventing hydraulic failure and maintaining whole plant transpiration rates. Additionally, constitutive expression of the tobacco aquaporin in greenhouse grown *Arabidopsis* and tomato plants resulted in overall higher yields in terms of biomass, as well as total mass and number of fruits under both normal and salt stress conditions. In conclusion, NtAQP1 was able to improve a stressed plant´s transpiration rate by three independent, but complementary means: Increasing CO_2 mesophyll conductivity (corresponding to increased photosynthetic rate), increasing stomatal aperture (corresponding to higher water and CO_2 conductance) and maintenance of near constant hydraulic conductivity under normal conditions or moderating a decrease of the same under salt stress. A subsequent study of the same group confirmed these results in *Arabidopsis* plants expressing NtAQP1 and showing enhanced photosynthesis rates and mesophyll CO_2 conductance in both normal and salt-stress conditions [Sade *et al.* 2014].

1.6 N- and C-terminal regulation of aquaporins

The regulation of aquaporins via their cytosolic N- and C-terminal sequences are quite multifold in nature and have been demonstrated to have various impacts on the molecular or physiological functions of the respective channels themselves or their immediate environment. The type of terminal modification during such regulatory processes not only include the deletion or truncation of amino acid residues and biochemical modifications, such as phosphorylation, palmitoylation, acetylation or methylation; they can also provide binding sites for other proteins, energy equivalents or ions. The impact of these modifications are equally diverse, most of which influence trafficking of the respective aquaporin to its target membrane or its intrinsic permeability and specificity for substrates by modulating its secondary and tertiary structures in the pore region, so called gating. Additional effects include alterations to the overall quaternary configuration of aquaporin tetramers or an efficiency increase in a metabolic pathway by binding proteins capable of processing the aquaporin facilitated

substrates. Table 3 gives an exemplary overview on aquaporins in mammalia, plants, insects, as well as unicellular eukaryotes and prokaryotes and their N- and C-terminally dependent regulatory mechanisms.

Table 3 – Overview on N- and C-terminally dependent regulation of aquaporins. 1 = Aquaporin / 2 = N- or C-terminus involved in regulation / 3 = Specific amino acid residues involved in regulation.

AQP[1]	Source	N / C[2]	Residues[3]	Type of Modification	Regulatory Impact	Physiological context	Reference
AQP0	*Homo sapiens*	C	235-261 / 239-261 244-261	Deletion	Plasma membrane trafficking	fluid distribution, cell adhesion	Ball *et al.* 2003
			Arg_{233}	Calmodulin Binding	Enhanced water permeability	mutation causes cataract formation	Hu *et al.* 2012
	Ovis aries		220-263	Deletion	Formation of lens fiber cell junctions	cell adhesion	Gonen *et al.* 2004
AQP1	*Homo sapiens*		Asp_{237} / Lys_{243}	cGMP Binding	Channel activation for cation conductance	water homeostasis in bile duct	Boassa & Yool 2003
			238-269 / 255-269	Deletion	Structural instability		Fotiadis *et al.* 2002
				Calmodulin Binding	Plasma membrane trafficking		
	Bos taurus		238-271 / 262-271	Deletion	Structural instability		
				Calmodulin Binding	Plasma membrane trafficking		
AQP2	*Homo sapiens*		Gly_{721} / 763-772 812-818	Deletion		urine concentration, diabetes insipidus	Kuwahara *et al.* 2001
			253-256	Phosphorylation	Apical membrane trafficking		Kuwahara *et al.* 2005
			262-271 / 268-271	Deletion PDZ Binding Motif			
	Rattus		Ser_{256}	Phosphorylation			Arthur *et al.* 2015
	Mus		230-272	Deletion			Shi *et al.* 2007
			Ser_{256}	Phosphorylation			
		N	1-29	Domain Exchange	Basolateral membrane trafficking		Rai *et al.* 2005
AQP3			20-23	Point Mutation		renal water homeostasis	
AQP4	*Rattus*	C	276-280	Deletion	Plasma membrane trafficking	mammalian brain	Nakahama *et al.* 2002
			299-301	PDZ Binding Motif			
	Homo sapiens		Ser_{276} / Ser_{285} Thr_{289} / Ser_{316}	Phosphorylation		water and K^+ homeostasis	Kadohira *et al.* 2008
	Rattus	N	Cys_{13} / Cys_{17}	Palmitoylation	Tetramer assembly into square arrays		Suzuki *et al.* 2008
AQP5	*Mus*	C	251-265	Prolactin-inducible Protein Binding	Apical membrane trafficking	lacrimal gland fluid distribution, Sjögren´s syndrome	Ohashi *et al.* 2008
	Rattus	N	1-12	Domain Exchange			Wellner *et al.* 2005
		C	227-265		Expression of gene product		
AQP8		N	1-38		Decreased water permeability	pancreas & colon water homeostasis	
		C	247-263				

AQP[1]	Source	N / C[2]	Residues[3]	Type of Modification	Regulatory Impact	Physiological context	Reference
AQPcic	*Cicadella viridis*	C	C-terminus + half of TM6	Domain Exchange	Decreased water permeability Tetramer to monomer configuration change	filter chamber water homeostasis	Duchesne *et al.* 2002
GlpF	*Escherichia coli*				Abolished glycerol transport	glycerol metabolism	
Aqy1	*Pichia pastoris*	N	Tyr_{31}	Hydrogen Bond Interaction	Occlusion of channel pore	improved cell survival	Fischer *et al.* 2009
Aqy1-1p	*Saccharomyces cerevisiae*	C	310-327	Deletion	Plasma membrane trafficking	during freezing	Laize *et al.* 1999
AtPIP1;1-4	*Arabidopsis thaliana*	N	Met_1	Nα-acetylation	Pore gating and subcellular trafficking	photosynthesis	Santoni *et al.* 2006
AtPIP2;2				Deletion		hydraulic root conductivity, salt & oxidative stress, signal transduction	
AtPIP2;4							
AtPIP2;1			Lys_3	Deletion Di- / Monomethylation			
			Met_1 / Lys_3 Glu_6	Point Mutation	Decrease of water permeability		
		C	Ser_{283}	Phosphorylation	Plasma membrane trafficking		Prak *et al.* 2008
		N	Glu_{31} / Asp_{28}	Divalent Cation & Proton Binding	Induction of closed-pore formation		Verdoucq *et al.* 2008
CsPIP2;1	*Camelina sativa*	C	Ser_{273}	Phosphorylation	Increased water permeability	salt & drought stress	Jang *et al.* 2014
Nod26	*Glycine max*		248-271	Glutamine Synthetase Binding	Enhanced ammonia assimilation	nitrogen fixation in soybean nodules	Masalkar *et al.* 2010
RsPIP1;3	*Raphanus sativus*	N	Ser_{27}	Phosphorylation	Decreased water permeability	salt & water stress	Suga & Maeshima 2004
RsPIP2;2		C	Ser_{278}		Increased water permeability		
SoPIP2;1	*Spinacia oleracea*		Ser_{274}	Phosphorylation		cell turgor, apoplastic water potential	Johansson *et al.* 1998
ZmPIP2;4	*Zea mays*	N	Asp_4-Ile_5-Glu_6	Point Mutation	Plasma membrane trafficking	mesophyll chloroplasts	Zelazny *et al.* 2009
ZmPIP2;5							

1.7 Thesis aim

The primary aim of this thesis was to gain insight into the regulatory impact of the cytosolic N- and C-terminal sequences on the intrinsic water permeability of the tobacco aquaporins NtPIP2;1 and NtAQP1 (see chapters 1.3 through 1.6). For this purpose, continuous exchange cell free expression protocols were established (see chapter 1.2) with the goal to obtain sufficient amount of target protein, followed by the functional integration into lipid bilayer liposomes. Additional methodologies included the generation of terminal domain deletion and exchange mutants, measurement of intrinsic water permeability via a hyperosmotic liposome shrinkage assay and the application of various *in silico* tools in order to get a better understanding of the structure-function relationships in these two plant aquaporins.

2. Material and Methods

2.1 Strains, Plasmids, Oligonucleotides

Table 4 – Strains used during the course of this thesis. Nomenclature of genes in strains 5-10 is as follows: *a1* = *ntaqp1* / *p2* = *ntpip2;1* / *(n)* = cytosolic N-terminus / *(c)* = cytosolic C-terminus. Thus, for instance, gene *(n)a1_p2_(c)a1* of strain 5 describes TM 1-6 of *ntpip2;1* with the cytosolic N- and C-terminal sequences of *ntaqp1*. The column for the relevant genotypes of the respective strains includes more detailed information on the mutated sequences as follows: c. = specifies a mutation in coding DNA / 1_168 = specifies nucleotides 1 to 168 / con = indicates type of mutation, in this case a conversion or substitution of more than one nucleotide. Thus, the genotype of strain 8, *ntaqp1*[c.1_168conAF440272:c.1_129] describes the conversion of *ntaqp1* nucleotides 1 to 168 to ntpip2;1 nucleotides 1 to 129 by referencing the respective genbank accession number (ntaqp1 = AJ001416 / ntpip2;1 = AF440272). Mutated gene nomenclature is based on HGVS [2016]. 1 = Derived from OpenWetWare [2016] and CGSC [2016] / 2 = Clone list accession number in the strain collection of Prof. Dr. Ralf Kaldenhoff at Applied Plant Sciences, TU Darmstadt, Darmstadt, Germany / 3 = Thermo Fisher Scientific, Waltham, Massachusetts, USA / 4 = Merck KGaA, Darmstadt, Germany.

#	Strain	Relevant genotype[1]	Clone[2]	References
1	*E. coli* DH5α	F⁻ *endA1 glnV44 thi-1 recA1 relA1 gyrA96 deoR nupG purB20* ϕ80d*lacZ*ΔM15 Δ(*lacZYA-argF*)U169, hsdR17($r_K^-m_K^+$), λ⁻	30	Thermo Fisher Scientific[3]
2	*E. coli* DH5α pET-21a(+)	F⁻ *endA1 glnV44 thi-1 recA1 relA1 gyrA96 deoR nupG purB20* ϕ80d*lacZ*ΔM15 Δ(*lacZYA-argF*)U169, hsdR17($r_K^-m_K^+$), λ⁻ pET-21a(+) (Amp^R)	295	Thermo Fisher Scientific[3], Merck[4]
3	*E. coli* DH5α pET-21a(+)::*ntpip2;1*(His)	F⁻ *endA1 glnV44 thi-1 recA1 relA1 gyrA96 deoR nupG purB20* ϕ80d*lacZ*ΔM15 Δ(*lacZYA-argF*)U169, hsdR17($r_K^-m_K^+$), λ⁻ pET-21a(+) (Amp^R) *ntpip2;1*(His)	1195	Thermo Fisher Scientific[3], Merck[4], Kai & Kaldenhoff 2014
4	*E. coli* DH5α pET-21a(+)::*ntaqp1*(His)	F⁻ *endA1 glnV44 thi-1 recA1 relA1 gyrA96 deoR nupG purB20* ϕ80d*lacZ*ΔM15 Δ(*lacZYA-argF*)U169, hsdR17($r_K^-m_K^+$), λ⁻ pET-21a(+) (Amp^R) *ntaqp1*(His)	1303	
5	*E. coli* DH5α pYES-DEST52::*(n)a1_p2_(c)a1*	F⁻ *endA1 glnV44 thi-1 recA1 relA1 gyrA96 deoR nupG purB20* ϕ80d*lacZ*ΔM15 Δ(*lacZYA-argF*)U169, hsdR17($r_K^-m_K^+$), λ⁻ pYES-DEST52 (Amp^R) *ntpip2;1*[c.1_129conAJ001416:c.1_168; c.783_852conAJ001416:c.816_861]	1126	Thermo Fisher Scientific[3], Priem 2011
6	*E. coli* DH5α pYES-DEST52::*(n)p2_a1_(c)p2*	F⁻ *endA1 glnV44 thi-1 recA1 relA1 gyrA96 deoR nupG purB20* ϕ80d*lacZ*ΔM15 Δ(*lacZYA-argF*)U169, hsdR17($r_K^-m_K^+$), λ⁻ pYES-DEST52 (Amp^R) *ntaqp1*[c.1_168conAF440272:c.1_129; c.816_861conAF440272:c.783_852]	1128	
7	*E. coli* DH5α pYES-DEST52::*(n)a1_p2*	F⁻ *endA1 glnV44 thi-1 recA1 relA1 gyrA96 deoR nupG purB20* ϕ80d*lacZ*ΔM15 Δ(*lacZYA-argF*)U169, hsdR17($r_K^-m_K^+$), λ⁻ pYES-DEST52 (Amp^R) *ntpip2;1*[c.1_129conAJ001416:c.1_168]	1124	
8	*E. coli* XL-1 Blue pYES2/CT::*(n)p2_a1*	*endA1 gyrA96*(nal^R) *thi-1 recA1 relA1 lac glnV44* F'*[::Tn10 proAB⁺ lacI^q Δ(lacZ)M15] hsdR17(r_K^- m_K^+)* pYES2/CT (Amp^R) *ntaqp1*[c.1_168conAF440272:c.1_129]	667	Bullock *et al.* 1987, Thermo Fisher Scientific[3], Fischer 2007
9	*E. coli* DH5α pYES-DEST52::*p2_(c)a1*	F⁻ *endA1 glnV44 thi-1 recA1 relA1 gyrA96 deoR nupG purB20* ϕ80d*lacZ*ΔM15 Δ(*lacZYA-argF*)U169, hsdR17($r_K^-m_K^+$), λ⁻ pYES-DEST52 (Amp^R) *ntpip2;1*[c.783_852conAJ001416:c.816_861]	1121	Thermo Fisher Scientific[3], Priem 2011
10	*E. coli* DH5α pYES-DEST52::*a1_(c)p2*	F⁻ *endA1 glnV44 thi-1 recA1 relA1 gyrA96 deoR nupG purB20* ϕ80d*lacZ*ΔM15 Δ(*lacZYA-argF*)U169, hsdR17($r_K^-m_K^+$), λ⁻ pYES-DEST52 (Amp^R) *ntaqp1*[c.816_861conAF440272:c.783_852]	1100	
11	*E. coli* A19	*rna-19*, *gdhA2*, *his-95*, *relA1*, *spoT1*, *metB1*	-	Gesteland 1966
12	*E. coli* BL21 pAR1219::*t7rnap*	B F⁻ *ompT gal dcm lon hsdS$_B$*($r_B^-m_B^-$) [*malB*⁺]$_{K\text{-}12}$(λ^S) pAR1219 (Amp^R) *t7rnap*	1060	Bullock *et al.* 1987, Thermo Fisher Scientific[3], Li *et al.* 1999

Table 5 – Recombinant strains generated during the course of this thesis. For nomenclature of strains 1-6, see Table 4 description. Additionally, strains 7-12 include deletions designated by Δ(n) or Δ(c) pertaining to cytosolic N- and C-terminal sequences, respectively. This is also reflected in more detail (as to the respective nucleotides) in the relevant genotypes by the addition of "del". For further reference, see Table 4 description. 1 = Derived from OpenWetWare [2016] / 2 = Thermo Fisher Scientific, Waltham, Massachusetts, USA / 3 = Merck KGaA, Darmstadt, Germany.

#	Strain	Relevant genotype[1]	References
1	*E. coli* DH5α pET-21a(+)::*(n)a1_p2_(c)a1*(His)	F⁻ *endA1 glnV44 thi-1 recA1 relA1 gyrA96 deoR nupG purB20* ϕ80d*lacZ*ΔM15 Δ(*lacZYA-argF*)U169, hsdR17($r_K^-m_K^+$), λ⁻ pET-21a(+) (Amp^R) *ntpip2;1*[c.1_129conAJ001416:c.1_168; c.783_852conAJ001416:c.816_861](His)	Thermo Fisher Scientific[2], Merck[3], this thesis
2	*E. coli* DH5α pET-21a(+)::*(n)p2_a1_(c)p2*(His)	F⁻ *endA1 glnV44 thi-1 recA1 relA1 gyrA96 deoR nupG purB20* ϕ80d*lacZ*ΔM15 Δ(*lacZYA-argF*)U169, hsdR17($r_K^-m_K^+$), λ⁻ pET-21a(+) (Amp^R) *ntaqp1*[c.1_168conAF440272:c.1_129; c.816_861conAF440272:c.783_852](His)	
3	*E. coli* DH5α pET-21a(+)::*(n)a1_p2*(His)	F⁻ *endA1 glnV44 thi-1 recA1 relA1 gyrA96 deoR nupG purB20* ϕ80d*lacZ*ΔM15 Δ(*lacZYA-argF*)U169, hsdR17($r_K^-m_K^+$), λ⁻ pET-21a(+) (Amp^R) *ntpip2;1*[c.1_129conAJ001416:c.1_168](His)	
4	*E. coli* DH5α pET-21a(+)::*(n)p2_a1*(His)	F⁻ *endA1 glnV44 thi-1 recA1 relA1 gyrA96 deoR nupG purB20* ϕ80d*lacZ*ΔM15 Δ(*lacZYA-argF*)U169, hsdR17($r_K^-m_K^+$), λ⁻ pET-21a(+) (Amp^R) *ntaqp1*[c.1_168conAF440272:c.1_129](His)	

#	Strain	Relevant genotype[1]	References
5	*E. coli* DH5α pET-21a(+)::*p2_(c)a1*(His)	F⁻ *endA1 glnV44 thi-1 recA1 relA1 gyrA96 deoR nupG purB20* ϕ80d*lacZ*ΔM15 Δ(*lacZYA-argF*)U169, hsdR17($r_K^-m_K^+$), λ⁻ pET-21a(+) (Amp^R) *ntpip2;1*[c.783_852conAJ001416:c.816_861](His)	Thermo Fisher Scientific[2], Merck[3], this thesis
6	*E. coli* DH5α pET-21a(+)::*a1_(c)p2*(His)	F⁻ *endA1 glnV44 thi-1 recA1 relA1 gyrA96 deoR nupG purB20* ϕ80d*lacZ*ΔM15 Δ(*lacZYA-argF*)U169, hsdR17($r_K^-m_K^+$), λ⁻ pET-21a(+) (Amp^R) *ntaqp1*[c.816_861conAF440272:c.783_852]	
7	*E. coli* DH5α pET-21a(+)::*Δ(n)_p2_Δ(c)*(His)	F⁻ *endA1 glnV44 thi-1 recA1 relA1 gyrA96 deoR nupG purB20* ϕ80d*lacZ*ΔM15 Δ(*lacZYA-argF*)U169, hsdR17($r_K^-m_K^+$), λ⁻ pET-21a(+) (Amp^R) *ntpip2;1*[c.1_129del; c.783_852del](His)	
8	*E. coli* DH5α pET-21a(+)::*Δ(n)_a1_Δ(c)*(His)	F⁻ *endA1 glnV44 thi-1 recA1 relA1 gyrA96 deoR nupG purB20* ϕ80d*lacZ*ΔM15 Δ(*lacZYA-argF*)U169, hsdR17($r_K^-m_K^+$), λ⁻ pET-21a(+) (Amp^R) *ntaqp1*[c.1_168del](His)	
9	*E. coli* DH5α pET-21a(+)::*Δ(n)_p2*(His)	F⁻ *endA1 glnV44 thi-1 recA1 relA1 gyrA96 deoR nupG purB20* ϕ80d*lacZ*ΔM15 Δ(*lacZYA-argF*)U169, hsdR17($r_K^-m_K^+$), λ⁻ pET-21a(+) (Amp^R) *ntpip2;1*[c.1_129del](His)	
10	*E. coli* DH5α pET-21a(+)::*Δ(n)_a1*(His)	F⁻ *endA1 glnV44 thi-1 recA1 relA1 gyrA96 deoR nupG purB20* ϕ80d*lacZ*ΔM15 Δ(*lacZYA-argF*)U169, hsdR17($r_K^-m_K^+$), λ⁻ pET-21a(+) (Amp^R) *ntaqp1*[c.1_168del; c.816_861del](His)	
11	*E. coli* DH5α pET-21a(+)::*p2_Δ(c)*(His)	F⁻ *endA1 glnV44 thi-1 recA1 relA1 gyrA96 deoR nupG purB20* ϕ80d*lacZ*ΔM15 Δ(*lacZYA-argF*)U169, hsdR17($r_K^-m_K^+$), λ⁻ pET-21a(+) (Amp^R) *ntpip2;1*[c.783_852del](His)	
12	*E. coli* DH5α pET-21a(+)::*a1_Δ(c)*(His)	F⁻ *endA1 glnV44 thi-1 recA1 relA1 gyrA96 deoR nupG purB20* ϕ80d*lacZ*ΔM15 Δ(*lacZYA-argF*)U169, hsdR17($r_K^-m_K^+$), λ⁻ pET-21a(+) (Amp^R) *ntaqp1*[c.816_861del](His)	

Table 6 – Plasmids used within this thesis. For details on nomenclature of relevant features, see descriptions of Tables 4 and 5. 1 = Clone list accession number in the strain collection of Prof. Dr. Ralf Kaldenhoff at Applied Plant Sciences, TU Darmstadt, Darmstadt, Germany / 2 = Merck KGaA, Darmstadt, Germany / 3 = Thermo Fisher Scientific, Waltham, Massachusetts, USA.

#	Plasmid	Relevant features	Size [kbp]	Clone[1]	References
1	pET-21a(+)	(Amp^R)	5.44	295	Merck[2]
2	pET-21a(+)::*ntpip2;1*(His)	(Amp^R) *ntpip2;1*(His)	6.27	1195	Merck[2], Kai & Kaldenhoff 2014
3	pET-21a(+)::*ntaqp1*(His)	(Amp^R) *ntaqp1*(His)	6.28	1303	
4	pYES-DEST52::*(n)a1_p2_(c)a1*	(Amp^R) *ntpip2;1*[c.1_129conAJ001416:c.1_168; c.783_852conAJ001416:c.816_861]	8.49	1126	Thermo Fisher Scientific[3], Priem 2011
5	pYES-DEST52::*(n)p2_a1_(c)p2*	(Amp^R) *ntaqp1*[c.1_168conAF440272:c.1_129; c.816_861conAF440272:c.783_852]	8.47	1128	
6	pYES-DEST52::*(n)a1_p2*	(Amp^R) *ntpip2;1*[c.1_129conAJ001416:c.1_168]	8.51	1124	
7	pYES2/CT::*(n)p2_a1*	(Amp^R) *ntaqp1*[c.1_168conAF440272:c.1_129]	6.79	667	Thermo Fisher Scientific[3], Fischer 2007
8	pYES-DEST52::*p2_(c)a1*	(Amp^R) *ntpip2;1*[c.783_852conAJ001416:c.816_861]	8.45	1121	Thermo Fisher Scientific[3], Priem 2011
9	pYES-DEST52::*a1_(c)p2*	(Amp^R) *ntaqp1*[c.816_861conAF440272:c.783_852]	8.51	1100	
10	pET-21a(+)::*(n)a1_p2_(c)a1*(His)	(Amp^R) *ntpip2;1*[c.1_129conAJ001416:c.1_168; c.783_852conAJ001416:c.816_861](His)	6.21	-	Merck[2], this thesis
11	pET-21a(+)::*(n)p2_a1_(c)p2*(His)	(Amp^R) *ntaqp1*[c.1_168conAF440272:c.1_129; c.816_861conAF440272:c.783_852](His)	6.28	-	
12	pET-21a(+)::*(n)a1_p2*(His)	(Amp^R) *ntpip2;1*[c.1_129conAJ001416:c.1_168](His)	6.30	-	
13	pET-21a(+)::*(n)p2_a1*(His)	(Amp^R) *ntaqp1*[c.1_168conAF440272:c.1_129](His)	6.27	-	
14	pET-21a(+)::*p2_(c)a1*(His)	(Amp^R) *ntpip2;1*[c.783_852conAJ001416:c.816_861](His)	6.20	-	
15	pET-21a(+)::*a1_(c)p2*(His)	(Amp^R) *ntaqp1*[c.816_861conAF440272:c.783_852](His)	6.29	-	
16	pET-21a(+)::*Δ(n)_p2_Δ(c)*(His)	(Amp^R) *ntpip2;1*[c.1_129del; c.783_852del](His)	6.00	-	
17	pET-21a(+)::*Δ(n)_a1_Δ(c)*(His)	(Amp^R) *ntaqp1*[c.1_168del](His)	6.00	-	
18	pET-21a(+)::*Δ(n)_p2*(His)	(Amp^R) *ntpip2;1*[c.1_129del](His)	6.07	-	
19	pET-21a(+)::*Δ(n)_a1*(His)	(Amp^R) *ntaqp1*[c.1_168del; c.816_861del](His)	6.04	-	
20	pET-21a(+)::*p2_Δ(c)*(His)	(Amp^R) *ntpip2;1*[c.783_852del](His)	6.13	-	
21	pET-21a(+)::*a1_Δ(c)*(His)	(Amp^R) *ntaqp1*[c.816_861del](His)	6.16	-	

Table 7 – Oligonucleotides used during the course of this thesis. 1 = Primer list accession number in the strain collection of Prof. Dr. Ralf Kaldenhoff at Applied Plant Sciences, TU Darmstadt, Darmstadt, Germany / 2 = Restriction endonuclease site included in the respective primer for cloning purposes (indicated via underlined nucleotides in primer sequence).

#[1]	Name	Sequence (5´-3´)	RE[2]	Utilization
66	T7	TAATACGACTCACTATAGGG	-	Sequencing
353	NtAQP1-s-HindIII	AAGCTTATGGCAGAAAACAAAGAAGAAGATG	HindIII	Validation PCR
354	NtAQP1-as- Eco47III	AGCGCTAAGACGACTTGTGGAATGGA	Eco47III (AfeI)	
491	NtPIP2.1-XhoI_s	TATCTCGAGATGTCAAAGGACGTGATTGAAG	XhoI	Validation PCR

#[1]	Name	Sequence (5´-3´)	RE[2]	Utilization
492	NtPIP2.1XbaI_as	TAATCTAGATTAGTTGGTTGGGTTACTGCG	XbaI	Validation PCR
709	T7 terminator as	AAAACCCCTCAAGACCCGTT	-	Sequencing
1203	NtAQP1 nP2cP2P1-pET21a-fw	GCGCAAGCTTATGTCAAAGGACGTGATTG	HindIII	Initial PCR of *(n)p2_α1, (n)p2_α1_(c)p2*
1207	NtPIP2;1 nP1cP1_P2-pET21a-fw	GTTGGATCCATGGCAGAAAACAAAGAAGAAG	BamHI	Initial PCR of *(n)α1_p2_(c)α1*
1208	NtPIP2,1 nP1cP1_P2-pET21a-rv	GTGCGGCCGCAGACGACTTGTGGAATGGAATGGC	NotI	Initial PCR of *(n)α1_p2_(c)α1, (n)p2_α1*
1211	NtAQP1 P1cP2-pET21a-fw	GCGCGGATCCATGGCAGAAAACAAAGAAGAA	BamHI	Initial PCR of *α1_(c)p2*
1215	NtPIP2,1 P2cP1-pET21a-fw	AAAGCTAGCATGTCAAAGGACGTGATTGAAGAAGGACAAG	NheI	Initial PCR of *p2_(c)α1*
1216	NtPIP2,1 P2cP1-pET21a-rv	TTTCTCGAGAGACGACTTGTGGAATGGAATGGCTCTGATG	XhoI	
1219	NtPIP2,1 nP1P2-pET21a-fw	GCGCGGATCCATGGCAGAAAACAAAGAAGA	BamHI	Initial PCR of *(n)α1_p2*
1220	NtPIP2,1 nP1P2-pET21a-rv	AAAACTCGAGGTTGGTTGGGTTACTGCGGA	XhoI	Initial PCR of *(n)α1_p2, α1_(c)p2, (n)p2_α1_(c)p2*
1376	NtAQP1 –N pET21a_fw_XbaI	GCGCTCTAGAAAGGAGATATACATATGGCAGAATTTATGGCTACTTTCTT	XbaI	Initial PCR of *Δ(n)_α1, Δ(n)_α1_Δ(c)*
1377	NtAQP1 +N pET21a_fw_XbaI	GCGCTCTAGAAAGGAGATATACATATGGCAGAAAACAAAGAAGAAGATGT	XbaI	Initial PCR of *α1_Δ(c)*
1378	NtAQP1 -C pET21a_rv_XhoI	AAAACTCGAGAACTGCAGCAAGTGCAGCTCCAATGAATGGTCCAACCCAA	XhoI	Initial PCR of *α1_Δ(c), Δ(n)_α1_Δ(c)*
1379	NtAQP1 +C pET21a_rv_XhoI	AAAACTCGAGAGACGACTTGTGGAATGGAATGGCTCTGATGATTATTTGA	XhoI	Initial PCR of *Δ(n)_α1*
1380	NtPIP2;1 -N pET21a_fw_XbaI	GCGCTCTAGAAAGGAGATATACATATGGCTGAGTTCATTGCTACTCTTCT	XbaI	Initial PCR of *Δ(n)_p2, Δ(n)_p2_Δ(c)*
1381	NtPIP2;1 +N pET21a_fw_XbaI	GCGCTCTAGAAAGGAGATATACATATGTCAAAGGACGTGATTGAAGAAGG	XbaI	Initial PCR of *p2_Δ(c)*
1382	NtPIP2;1 –C pET21a_rv_XhoI	AAAACTCGAGTACTGCTGCTACCAATGCTCCCACAAATGGTCCAACCCAG	XhoI	Initial PCR of *p2_Δ(c), Δ(n)_p2_Δ(c)*
1383	NtPIP2;1 +C pET21a_rv_XhoI	AAAACTCGAGGTTGGTTGGGTTACTGCGGAAAGAACCCAATGCCTTAATT	XhoI	Initial PCR of *Δ(n)_p2*

2.2 Media, Antibiotics, Cell Cultivation & Storage

Lysogeny-Broth (LB) and Yeast tryptone phosphate buffer (YTPG) media were used for the cultivation of bacterial cells. All batches were autoclaved at 121 °C for 20 min at 121 °C and then stored at room temperature (RT). 1.5 % (w/v) agar was added prior to autoclaving whenever solid medium plates were needed.

LB Medium [Sambrook & Russell 2001]	
NaCl	10 g/l
Tryptone	10 g/l
Yeast extract	5 g/l

2x YTPG Medium [Kim & Choi 2001]	
Tryptone	16 g/l
Yeast extract	10 g/l
NaCl	5 g/l
Glucose	100 mM
K_2HPO_4 / KH_2PO_4	40 mM / 22 mM

Ampicillin was exclusively used in cultivation as the antibiotic of choice at concentrations of 50 µg/ml or 100 µg/ml. 1000x stocks (w/v) were prepared with demineralized water ($H_2O_{dem.}$) and stored at -20 °C.

The cultivation of bacterial cells was performed at 37 °C and 170-250 rpm with incubation times of overnight cultures ranging from 16 to 22 hours at volumes of 3 ml up to 400 ml, depending on the utilization of the culture (glycerol stocks, mini or midi plasmid isolation, etc.). The ratio of the liquid cell culture volume to the volume of its Erlenmeyer flask was kept at 1:5 or lower to ensure sufficient aeration rates. Long-term storage of bacterial cell cultures was realized by the addition of 1 ml sterile glycerol (50 % v/v) per ml culture, followed by shock-freezing in liquid nitrogen (LN_2) and storage at -80 °C.

2.3 Generation of chemically competent *E. coli* cells [Hanahan 1983]

For the generation of chemically competent *E. coli* cells, 20 ml of LB medium were inoculated with 100 µl competent cells from the stock culture and cultivated to an OD_{600} value in the range of 0.3 to 0.5. Following an incubation on ice for 10 min to significantly slow down growth rates, the culture was then harvested by centrifugation at 3,500 *g* for 15 min at 4 °C. The sedimented cells were resuspended in 10 ml ice cold 0.1 M $CaCl_2$ and kept on ice for another 30 min. Subsequently, cells were harvested as above, followed by a resuspension in 2 ml of ice cold 0.1 M $CaCl_2$ containing 25 % (v/v) glycerol. Lastly, 100 µl aliquots were transferred to 1.5 ml Eppendorff reaction tubes, shock frozen in LN_2 and stored at -80 °C.

2.4 Measurement of culture growth through optical density determination

The optical density (OD) of a bacterial cell culture was monitored at 600 nm wavelength (OD_{600}) using a spectrophotometer calibrated to a preassigned reference or blank value (e.g. cell free medium, buffer, etc.). Whenever necessary, samples were diluted to obtain values inside the linear measurement range of up to OD_{600} = 0.3.

2.5 Handling and modification of DNA

2.5.1 Isolation of bacterial plasmid DNA

For verification, cloning and transformation purposes, plasmid DNA was isolated from *E. coli* cultures using the alkaline lysis method according to Birnboim [1983]. 3 ml overnight cultures were harvested by centrifugation at 16,000 *g* for 1 min at 4 °C in 1.5 ml Eppendorff reaction tubes. The resuspension of precipitated cells in 300 µl P1 resuspension buffer initiated enzymatic digestion of RNA and preliminary cell lysis, which was then completed by adding 300 µl P2 lysis buffer, carefully inverting the suspension 20 times and then incubating it on ice for 5 min. 300 µl of P3 neutralization buffer, repeated inversion and the subsequent incubation on ice for 10 min ensured a lowering of pH and thus the precipitation of genomic DNA and proteins, which were then removed by centrifugation at 16,000 *g* at 4 °C for at least 15 min. 750 µl of the remaining supernatant was transferred into a fresh 1.5 ml reaction tube and ice cold isopropanol was added in a ratio of 1:1 in order to precipitate the contained DNA. A centrifugation step followed at 16,000 *g* for at least 30 min at 4 °C, the supernatant was removed and the precipitated DNA was washed twice with 500 µl ice cold 70 % ethanol (EtOH) to remove unwanted salts. The ensuing DNA pellet was dried for 10 min at 37 °C, resuspended in 50 µl MilliQ filtered, demineralized water (MQ-H_2O) and then stored at -20 °C.

P1 Resuspension Buffer		P2 Lysis Buffer		P3 Neutralization Buffer	
Tris/HCl, pH 8.0	50 mM	NaOH	200 mM	CH_3CO_2K	3 M
EDTA	10 mM	SDS	1 % (w/v)	Glacial acetic acid	pH 5.5
RNase A	100 µg/ml	store at RT		store at 4 °C	
store at 4 °C					

For sequencing purposes, plasmids were further purified using either the Isolate PCR & Gel Kit by Bioline in London, UK or the PCR clean-up Gel extraction Kit by Macherey-Nagel GmbH & Co, KG in Düren, Germany. In either case, the protocol for the isolation of PCR products and PCR clean-up, respectively, was applied, resulting in a total of three elution steps of 10-20 µl MQ-H_2O each per utilized column. Similarly, purification of PCR products or gel elution was performed using the same kits.

Since the preparation of plasmid DNA for cell free expression of proteins requires significantly higher purity, midiprep kits by Macherey & Nagel in Düren, Germany (Nucleobond PC 100 DNA Kit) or Nippon Genetics in Tokyo, Japan (FastGene Xpress Plasmid Kit) were employed. Based on 150 ml and 400 ml cultures, the low copy plasmid protocols were applied in both cases, resulting in final elution volumes of 150 µl and 400 µl in MQ-H_2O, respectively.

2.5.2 Qualitative and quantitative spectrophotometric analysis of isolated plasmid DNA with regard to concentration and purity

Plasmid DNA samples were analyzed with regard to their concentration and purity using a Biowave S2100 diode array spectrophotometer (WPA Ltd., Cambridge, UK). A measured absorption value of 1 would thus equal 50 µg/µl dsDNA [Davis *et al.* 1980]. Sample purity was evaluated based on the respective 260 nm / 280 nm and 260 nm / 230 nm ratios with a value of 1.8 corresponding to non-existent protein contamination and contamination by organic compounds (e.g. phenolate ion and thiocanates), respectively.

2.5.3 Enzymatic restriction of circular plasmids and via PCR amplified, linear DNA

The restriction of DNA was conducted by utilization of the type II restriction endonucleases listed in Table 8 for the purpose of plasmid verification and restriction based cloning. 1 to 5 units of enzyme were applied to 0.5 – 5 µg of DNA for each preparation using the appropriate buffers and followed by an incubation time of 16-21 hours at the listed temperature.

Table 8 – DNA restriction enzymes used during the course of this thesis. All enzymes were manufactured by Thermo Fisher Scientific (Waltham, Massachusetts, USA). 1 = recommended reaction buffer for 100 % enzyme activity / 2 = alternative reaction buffer with 50 – 100 % enzyme activity, i.e. for double digest formulations / 3 = reaction conditions, in which the respective restriction enzyme relaxes or alters its cleavage specificity.

Enzyme	Buffer 1[1]	Buffer 2[2]	Temperature [°C]	Star activity[3]
BamHI	unique	green	37	low salt / glycerol >5% / pH >8.0 / >5-fold enzyme excess
BclI	green	tango (2x)	55	> 15-fold enzyme excess
EcoRI	unique	orange / tango (2x)	37	no
HindIII	red	-		
NheI	tango	blue		
NotI	orange	-		
PagI (BspHI)				
PstI	red	orange		
PvuII	green	-		> 15-fold enzyme excess
RsaI	tango			
VspI (AseI)	orange	tango (1x/2x)		no
XbaI	tango	-		
XhoI	red	tango (2x)		

2.5.4 Ligation of DNA

The ligation of target genes into linearized plasmid DNA was performed with T4 DNA Ligase (Thermo Fisher Scientific, Waltham, Massachusetts, USA). 5 units of this enzyme were added to each 20 µl preparation, together with 60 ng of linearized and purified vector and the 3 – 10-fold amount of the respective target gene (mol/mol). DNA concentrations were estimated based on densiometric comparison to an included size standard of known concentration. Incubation at 22 °C for 1 h followed with a subsequent switch to 16 °C and an additional overnight incubation.

2.5.5 DNA transfer into competent bacterial cells via *heat shock* transformation

For the transformation of competent cells with plasmid DNA [Hanahan 1983], 100 µl aliquots of the same were thawed on ice in 1.5 ml Eppendorff reaction tubes, prior to the addition of 40 ng of manually isolated plasmid. The cells were subsequently incubated on ice for 30 min and then heat shocked at 42 °C for 90 s. Afterwards, the cells were cooled on ice for 2 min and mixed with 600 µl sterile LB medium. Recuperation was performed at 37 °C, 1,000 rpm for 60 min, followed by centrifugation at 6,*000 g* for 5 min and the disposal of 600 µl supernatant. The resuspended cells were then plated on LB-agar plates containing the appropriate antibiotics and incubated overnight at 37 °C. To ensure viability of the cells, each transformation batch included a negative control (without added plasmid DNA), which was plated on LB-agar not containing antibiotics. Cell competence was verified through transformation with pET-21a plasmids that did not include any target genes.

2.5.6 Polymerase chain reaction (PCR)

DNA was amplified through the polymerase chain reaction method (PCR) [Innis *et al.* 1990] for the purpose of initial aquaporin gene amplification or verification of subsequently obtained potential clones, using Pfu (Thermo Scientific, Waltham, Massachusetts, USA) or Taq Polymerase (Biotherm Taq by Genecraft GmbH, Lüdinghausen, Germany and DreamTaq by Thermo Fisher Scientific, Waltham, Massachusetts, USA), respectively. The reaction mixtures and applied cycle parameters were as follows:

Initial aquaporin gene amplification

Reaction mix		Cycle parameters		
10x Pfu Buffer + $MgSO_4$	2 µl	1x	95 °C	3 min
dNTPs (2.5 mM each)	1 µl		95 °C	30 s
Template DNA (40 ng)	1 µl	35x	60 °C	30 s
Forward primer (10 µM)			72 °C	2 min / kbp
Reverse primer (10 µM)		1x	72 °C	15 min
Pfu DNA Polymerase (0.5 U)	0.2 µl	1x	8 °C	∞
MQ-H_2O	ad 20 µl			

Verification of potential clones (validation PCR)

Reaction mix		Cycle parameters		
10x Buffer incl. $MgCl_2$	2 µl	1x	95 °C	5 min
dNTPs (2.5 mM each)	1 µl		95 °C	30 s
Template DNA (1 colony)	1 µl	30x	60 °C	30 s
Forward primer (10 µM)			72 °C	1 min / kbp
Reverse primer (10 µM)		1x	72 °C	10 min
DNA Polymerase (0.5 U)	1 µl	1x	8 °C	∞
MQ-H_2O	ad 20 µl			

2.5.7 DNA Sequencing

The sequencing of DNA samples was outsourced to SeqLab Sequence Laboratories GmbH in Göttingen, Germany. Prepared samples with a total volume of 15 µl consisted of 3 µl fw or rv primer (10 µM), 720 – 1200 ng DNA template and MQ-H_2O. "Extended HotShot" was the sequencing program of choice, with the option for "GC-rich" sequence processing disabled.

2.6 Electrophoretic methods

2.6.1 Agarose gel electrophoresis

Agarose gel electrophoresis was utilized for the separation of DNA based on its molecular size [Sambrook & Russel 2001]. 0.8 % (w/v) agarose gels were cast in 1x triacetate-Ethylenediaminetetraacetic acid (TA-EDTA / TAE) buffer containing 50 ng/ml ethidium bromide (EtBr) and samples were prepared by adding 5x loading dye (2.2 mM Orange G, 7.5 % (v/v) glycerol). Hyperladder 1 kb (Bioline, London, UK) was used as the DNA standard. Detection was carried out under UV (254 nm).

TAE buffer (50x)	
Tris	242 g
Glacial acetic acid	57.1 ml
0.5 M EDTA (pH 8.0 /w NaOH)	100 ml
$H_2O_{dem.}$	ad 1000 ml
HCl / NaOH	pH 8.5

2.6.2 Discontinuous sodium dodecylsulfate-polyacrylamide gel electrophoresis (SDS-PAGE)

Samples were analyzed and separated with regards to the molecular size of their protein content by utilization of discontinuous sodium dodecylsulfate-polyacrylamide gel electrophoresis (SDS-PAGE) [Laemmli 1970]. Therefor, appropriate gels were prepared using Mighty Small 4-Gel SE200 series chambers manufactured by Hoefer Pharmacia Biotech, San Francisco, California, USA.

Collection Gel (4.1 % (w/v), 40 ml Stock)	
Collection gel buffer	10 ml
Acrylamide solution (30 % (w/v))	5.3 ml
$H_2O_{dem.}$	22.7 ml
SDS (10 % (w/v))	0.4 ml
Bromophenole blue (1 % (w/v))	20 µl
Tetramethylethylenediamine (TEMED)	2.8 µl / 3.5 ml
Ammonium persulfate (APS, 40 % (w/v))	4.55 µl / 3.5 ml
1x Collection Gel = 3.5 ml Stock	

1x Separation Gel (12.1 % (w/v))	
Separation gel buffer	1.875 ml
Acrylamide solution (30 % (w/v))	3 ml
$H_2O_{dem.}$	2.5 ml
SDS (10 % (w/v))	75 µl
TEMED	13.3 µl
APS	26.7 µl

4x Collection Gel Buffer	
Tris	500 mM
$H_2O_{dem.}$	ad 1000 ml
HCl	pH 6.8

4x Separation Gel Buffer	
Tris	1.5 M
$H_2O_{dem.}$	ad 1000 ml
HCl	pH 8.8

10x Electrode Buffer	
Tris	250 mM
Glycine	1.9 M
SDS	1 % (w/v)
$H_2O_{dem.}$	ad 1000 ml

Prior to loading, each sample was mixed with SDS protein denaturation buffer and heated to 37 °C for a minimum of 20 min. Gel runs were performed through submersion of cast and loaded gels in electrode buffer and application of 10 mA (single collection gel) and 20 mA (single separation gel), respectively. PageRuler Prestained Protein Ladder (Thermo Scientific, Waltham, Massachusetts, USA) and ProteMix (Anamed Elektrophorese GmbH, Groß-Bieberau, Germany) were the utilized protein standards. After run completion, gels were dyed in Coomassie brilliant blue solution [Weber & Osborn 1969] for a minimum of 20 min with subsequent double decolorization, one hour each, in 10 % (v/v) acetic acid aequous solution containing an additional 30 % (v/v) methanol.

SDS Protein Denaturation Buffer (4x)	
SDS	8 % (w/v)
Dithiothreitol (DTT)	400 mM
Glycerol	40 % (v/v)
Bromophenole blue	0.2 % (w/v)
Tris	250 mM
HCl	pH 6.8

Coomassie Brilliant Blue Dye	
Coomassie Brilliant Blue	1.5 g
Methanol	500 ml
Acetic acid	100 ml
$H_2O_{dem.}$	ad 1000 ml
Dye underwent filtration prior to use	

2.6.3 Western Blotting and immunodetection of His_6-tagged protein samples

The immunological detection of His_6-tagged aquaporins was performed through Western Blotting [Towbin *et al.* 1979 / Burnette 1981]. Therefor, an SDS-polyacrylamide (PAA) gel was equilibrated in transfer buffer after completion of its SDS-PAGE run, while its dimensions were carefully measured and respective sheets of Whatman filtering paper and polyvinylidene fluoride (PVDF) membrane with a pore size of 0.45 µm (Carl Roth GmbH & Co KG, Karlsruhe, Germany) were prepared accordingly. A "blotting sandwich" was then assembled, consisting of two sheets Whatman filtering paper, a PVDF membrane, the afore mentioned SDS-PAA gel and an additional three sheets of filtering paper, in that exact order. In order to avoid internal air pockets, the sandwich was gently flattened using a glass test tube, prior to assemblage of the blotting chamber (Mini Trans-Blot Cell by Bio-Rad, Hercules, California, USA) with the SDS-PAA gel facing the cathode and the PVDF membrane on the anode side.

Blotting was performed at a voltage of 40 for a minimum of 150 min at 4 °C under constant stirring. Verification of a successful transfer was obtained by visual inspection of the membrane for the prestained protein ladder (see chapter 2.6.2). Membrane binding sites were then blocked by overnight incubation in skim milk blocking solution at 4 °C while being agitated. Application of a primary antibody (Mouse anti-polyHis IgG by Sigma-Aldrich, St. Louis, Missouri, USA) was performed at a dilution of 1:6,000 in blocking solution and the membrane incubated for 1-2 h at RT under continuous horizontal agitation. Three washing steps with phosphate buffered saline containing Tween 20 (PBST) followed (10 min each, while agitating), prior to binding of a secondary antibody (alkaline phosphatase-conjugated goat-anti-mouse IgG by Sigma-Aldrich, St. Louis, Missouri, USA) at a dilution of 1:50,000 in blocking solution for 1 h under continuous horizontal agitation. Three additional washing steps with PBST were conducted, followed by two equilibration steps in Assay B for 5 min each under shaking. In order to enhance the subsequent chemiluminescence detection, a 1:20 dilution of Tropix Nitro-Block II by Thermo Fisher Scientific (Waltham, Massachusetts, USA) in Assay B was applied onto the PVDF membrane for 5 min, before it was again washed twice with Assay B for 5 min each under shaking. Finally, the addition of a 1:50 dilution of the AP substrate Tropix CDP-Star (Thermo Fisher Scientific, Waltham, Massachusetts, USA) in Assay B onto the PVDF membrane and its incubation for 5 min preceded the actual detection of chemiluminescent signals via a ChemiDoc XRS imaging system by Bio-Rad (Hercules, California, USA) with exposure times ranging 30 s - 10 min.

Transfer Buffer	
N-cyclohexyl-3-aminopropanesulfonic acid (CAPS)	10 mM
Methanol	10 % (v/v)
NaOH	pH 11.0

PBS(T)	
Na_2HPO_4	46 mM
NaH_2PO_4	15 mM
NaCl	68.5 mM
(Tween 20)	(0.5 % (v/v))

Skim Milk Blocking Solution	
Skin milk powder	2 % (w/v)
PBST	ad 50 ml

Assay B	
Tris	20 mM
$MgCl_2$	2 mM
HCl	pH 9.8

2.7 Cell-Free Expression of aquaporins

2.7.1 Preparation of *E. coli* A19 derived S30 extract

The preparation of the *E. coli* A19 derived S30 extract [Kai *et al.* 2012] for the cell free expression of aquaporins was performed on the premises of the research group lead by Prof. Dr. Volker Dötsch and Dr. Frank Bernhard at the Institute of Biophysical Chemistry on the Biocenter Campus of the Goethe University Frankfurt, Frankfurt am Main, Germany.

Therefor, a fermenter by B. Braun Melsungen AG in Melsungen, Germany was inoculated with 10 l of sterilized Yeast tryptone phosphate buffer (YTPG) medium together with 100 ml of a fresh *E. coli* A19 overnight culture. The incubation at 37 °C with intensive aeration and stirring was continuously monitored via OD_{600} and the cell broth was initiated to be chilled down to 10 – 14 °C before mid-log phase at an OD_{600} in the range of of 3 to 5 in order to avoid reaching the stationary growth phase. Cells were harvested via centrifugation at 7,000 *g* for 15 min at 4 °C and the resulting pellets were kept at 4 °C for all following steps, alternatively being frozen at -80 °C and stored in thin aluminium foil wraps for later processing.

Cell extraction was initiated by gentle resuspension of the cell pellets in a total of 300 ml pre-cooled S30-A buffer, followed by a centriguation step at 7,000 *g* for 10 min at 4 °C. The resulting supernatant was discarded and the washing step repeated twice, with the final centrifugation being extended to 30 min. Another resuspension followed, this time in 110 % (v/w) pre-cooled S30-B buffer before cell disruption was carried out via the utilization of a French pressure cell at 1,000 psi. To obtain cleared cell lysates, they werecentrifuged at 30,000 *g* for 30 min at 4 °C with one repetition using the resulting supernatant. The final supernatant was then adjusted stepwise to a final NaCl concentration of 400 mM and incubated at 42 °C for 45 min in a water bath. This caused significant precipitation of proteins, as well as dissociation of ribosomes from mRNA templates and the subsequent degradation of those templates, resulting in a higher quality final extract. An overnight dialysis step followed, placing the turbid extract against 100-fold excess of pre-cooled S30-C buffer by using a membrane with a molecular weight cut-off (MWCO) value of 12 – 14 kDa and a total of two buffer exchanges. Subsequently, extracts were cleared from aggregates by centrifugation for 30 min at 30,000 *g* and 4 °C, with the obtained supernatants dispensed into aliquots of 300 µl in plastic reaction tubes. Shock-freezing in LN_2 and storage at -80 °C ensured a shelf life of at least one year. The final protein concentration of the S30 extract was ideally between 20 and 40 mg/ml with a stepwise adjustment of contained Mg^{2+} and K^+ ions calibrated to test cell free expression batches.

40x S30-A/B/C Buffers		
Tris	400 mM	S30-A/B/C
$Mg(OAc)_2$	560 mM	
KCl	2.4 M	
Acetic acid	pH 8.2	
β-mercaptoethanol	6 mM	S30-A
DTT	1 mM	S30-B
Phenylmethylsulfonyl fluoride (PMSF)	1 mM	
DTT	0.5 mM	S30-C

2.7.2 Preparation and purification of T7 RNA Polymerase

As with the S30 extract, the T7 RNA Polymerase used for the cell free expression of aquaporins in this thesis was produced on the premises of the research group lead by Prof. Dr. Volker Dötsch and Dr. Frank Bernhard at the Institute of Biophysical Chemistry on the Biocenter Campus of the Goethe University Frankfurt, Frankfurt am Main, Germany.

Since it is one of the most expensive components in the utilized CECF system, it was overproduced in *E. coli* and purified by ion exchange chromatography [Kai *et al.* 2012], resulting in 0.5 to 1.0x10^6 units per liter of culture. For the purpose of prolonged shelf life, the purification was only partial, thus eluates included impurities.

1 l of LB medium was inoculated with 10 ml of an overnight culture containing strain BL21 pAR1219 (Table 4, strain 12) and grown at 37 °C to an OD_{600} of 0.6 – 0.8. Gene expression was induced via addition of 1 mM isopropyl-β-D-1-thiogalactopyranoside (IPTG), after which an additional incubation of 5 h followed. Cell harvest was performed via centrifugation at 8,000*g* for 15 min at 4 °C with the resulting pellets kept at -80 °C until further use.

30 ml of TRNAP-A buffer were used to resuspend the pellets, which were then disrupted by French pressure cell application at 1,000 psi or by sonication. The removal of cell debris was achieved by centrifugation at 20,000*g* for 30 min at 4 °C, the same temperature as all subsequent purification steps. Stepwise addition of a 20 % streptomycin sulfate stock solution to the obtained lysate supernatant resulted in a final concentration of 4 % in order to precipitate nucleic acid contaminants. After gentle mixing and a 5 min incubation on ice, the solution was centrifuged at 20,000*g* for 30 min at 4 °C. The resulting supernatant was loaded onto a Q-sepharose column (GE Healthcare, Chicago, Illinois, USA) with a bed volume of 40 ml, which had been equilibrated with TRNAP-B buffer. The same buffer was used to wash the column extensively before eluting the T7 RNA Polymerase with an NaCl gradient ranging 50 to 500 mM in TRNAP-C buffer in 10 column volumes at a flow rate of 3 – 4 ml/min. Fractions were collected and analyzed via SDS-PAGE before T7RNAP containing fractions were pooled and dyalized against TRNAP-D buffer overnight, adjusted to a glycerol concentration of 10 % and concentrated to 3 – 4 mg/ml total protein content by ultrafiltration at a MWCO of 30 kDa. After adjustment to a final glycerol concentration of 50 %, stock aliquots were stored at -80 °C with working stocks being transferred to -20 °C prior to actual usage.

TRNAP Buffers

	A	B	C	D
Tris	30 mM	30 mM	30 mM	-
NaCl	50 mM	50 mM	1 M	10 mM
EDTA	10 mM	1 mM	1 mM	0.5 mM
β-mercaptoethanol	10 mM	10 mM	10 mM	-
Glycerol	5 % (v/v)	5 % (v/v)	5 % (v/v)	5 % (v/v)
HCl	pH 8.0	pH 8.0	pH 8.0	-
K2HPO4 / KH2PO4	-	-	-	10 mM, pH. 8.0
DTT	-	-	-	1 mM

2.7.3 Small, unilamellar liposome vesicles

The generation of small, unilamellar liposome vesicles (SUV) was based on their formation from thin lipid films when hydrated and stacks of liquid crystalline bilayers become fluid and swell (Fig. 9). Hydrated lipid sheets detach during agitation and self-assemble to form large, multilamellar vesicles (MLV), which prevents interaction of water with the hydrocarbon core of the bilayer at the edges. A size reduction and homogenization of formed particles requires energy input in the form of sonication or, like in this case, extrusion (see chapter 2.8.6).

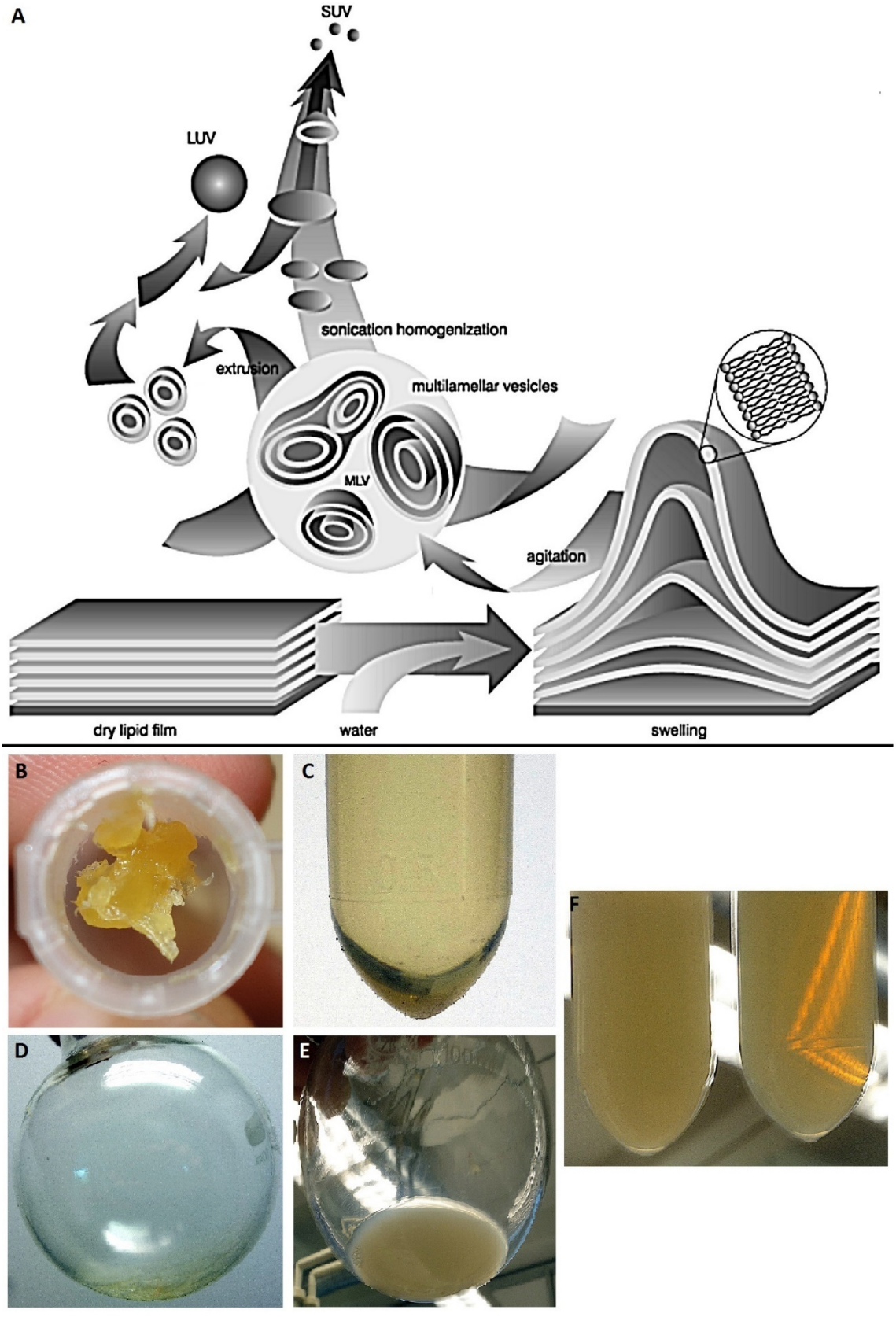

Fig. 9 – Generation of small, unilamellar liposome vesicles (SUV). (A) = Bilayers of a previously dried lipid film swell, detach and self-close to form large, multilamellar vesicles (MLV) when rehydrated under agitation. Energy input in the form of sonication or extrusion induces a size reduction and transformation into large, unilamellar vesicles (LUV) and finally into SUV / (B) = Pure L-α-phosphatidylcholine (PC) lipids / (C) = PC solubilized in chloroform / (D) = Dried, thin PC lipid layer in round bottom flask / (E) = Rehydrated PC MLV / (F) = Rehydrated PC as MLV before (left) and as SUV after extrusion (right). [(A) = Avanti Polar Lipids, avantilipids.com, modified]

For this purpose, 80 mg of soybean-derived L-α-phosphatidylcholine (PC) lipids (Type IV-S, ≥ 30% (enzymatic) by Sigma-Aldrich, St. Louis, Missouri, USA) were solubilized in 2 ml of chloroform by intensive vortexing and then

transferred to a 100 ml glass round bottom flask. Utilizing a rotation evaporator, a light vacuum (open pressure valve) was applied for 10 min at a rotational speed of 160 rpm in order to remove the bulk of the chloroform while letting a formation of a thin lipid layer take place. An additional 60 min under hard vacuum (closed pressure valve) and 130 rpm allowed any residual chloroform to be removed before 2 ml of HN buffer were used to rehydrate the lipid layer for 2.5 h at 160 rpm and ambient pressure for a final concentration of 40 mg/ml. FInally, the rehydrated lipids were extruded (see chapter 2.8.6) and stored at 4 °C for a maximum of 24 hours before usage in order to avoid hydrolysis.

HN Buffer	
4-(2-hydroxyethyl)-1-piperazineethanesulfonic acid (HEPES)	25 mM
NaCl	50 mM
NaOH	pH 7.5

2.7.4 Preparation of other chemical and enzyme stocks

Additional chemical and enzyme stocks required for cell free expression, but not mentioned above are listed in Table 9. All aqueous solutions were exclusively set up with MQ-H_2O.

Table 9 – Chemical and enzyme stocks for the cell-free expression of aquaporins. 1 = Sigma-Aldrich, St. Louis, Missouri, USA / 2 = AppliChem GmbH, Darmstadt, Germany / 3 = Roche Diagnostics, Risch-Rotkreuz, Switzerland / 4 = Thermo Fisher Scientific, Waltham, Massachusetts, USA.

Component	Manufacturer	Function	Stock conc.	Preparation	Storage
S30-C buffer	-	Buffering agent	1x	see chapter 2.7.1	-20 °C
Polyethylene glycol octadecyl ether (Brij S20)	Sigma-Aldrich[1]	Membrane protein solvent in D-CF mode	15 % (w/v)	dissolve in MQ-H_2O	
Arg, Cys, Trp, Met, Asp, Glu (RCWMDE)	AppliChem[2]	Protein translation	16.7 mM each	heat up to 60 °C to dissolve in MQ-H_2O	
Amino acid mix (20 natural, proteinogenic)	AppliChem[2]		25 mM each	heat up to 60 °C to dissolve in MQ-H_2O (remains turbid)	
Acetyl phosphate lithium potassium salt (AcP)	Sigma-Aldrich[1]	High-energy phosphate donor,	1 M	pH 7.0 (1 % (v/v) 10 M KOH)	
Phosphoenylpyruvate monopotassium salt (PEP)	AppliChem[2]	NTP regeneration	1.5 M	pH 7.0 (53 % (v/v) 10 M KOH)	
Nucleoside triphosphate (NTP) mix	Roche Diagnostics[3]	mRNA generation	75x	90 mM ATP, 60 mM CTP / GTP / UTP each, pH 7.0 (NaOH)	
DTT	Roche Diagnostics[3]	Reducing agent	0.5 M	dissolve in MQ-H_2O	
Folinic acid calcium salt	Sigma-Aldrich[1]	Initiation of protein synthesis	10 mg/ml	dissolve in MQ-H_2O (remains turbid)	
Complete, EDTA-free protease inhibitor cocktail	Roche Diagnostics[3]	Inhibition of target protein degradation	50x	dissolve 1 tablet in 5 ml MQ-H_2O	
HE buffer	-	Buffering agent	24x	2.4 M HEPES, 20 mM EDTA, pH 8.0 (KOH)	4 °C
$Mg(OAc)_2$	-	Enzyme cofactors, Transcription / translation efficiency	1 M	dissolve in MQ-H_2O	
KOAc	-		4 M		
Polyethylene glycol (PEG)-8000	-	mRNA stability	40 % (v/v)	mix with MQ-H_2O	
NaN_3	-	NTPase inhibition	10 % (w/v)	dissolve in MQ-H_2O	-20 °C
Plasmid DNA	-	Transcription template	~ 500 - 800 ng/µl	see chapter 2.5.1	
RiboLock Rnase inhibitor	Thermo Fisher Scientific[4]	Inhibition of RNases	40 U/µl	aliquot from stock bottle, use directly	
tRNA from *E. coli* MRE600	Sigma-Aldrich[1]	Protein translation	40 mg/ml	dissolve in MQ-H_2O	
Pyruvat kinase (PK)	Roche Diagnostics[3]	NTP regeneration	10 mg/ml	aliquot from stock bottle, use directly	

2.7.5 Reactor assembly, pipetting scheme and expression modes

Mini CECF reactors made of acrylic glass (produced at the Biology Campus workshop of the TU Darmstadt, Darmstadt, Germany) with a reaction mix (RM) capacity of 55 µl were used for the cell-free expression of aquaporins (Fig. 10), while 24-well plates by Greiner Bio-One GmbH, Kremsmünster, Austria served as containers for the feeding mixtures (FM) with a volume of 850 µl each. Between the two, a single layer of 25 mm wide Spectra/Por dialysis membrane with a MWCO of 12 - 14 kDa (Spectrum Labs, Rancho Domniguez, California, USA), which was attached to the CECF reactors by a tight-fitting teflon ring, mediated the continuous exchange of used up and fresh small molecular substrates, respectively, at the same time keeping high-molecular weight enzymes and ribosomes in the RM compartment. A layer of parafilm prevented any unwanted dissipation of liquid during the minimum of 21 hours incubation time at 30 °C and 170 rpm.

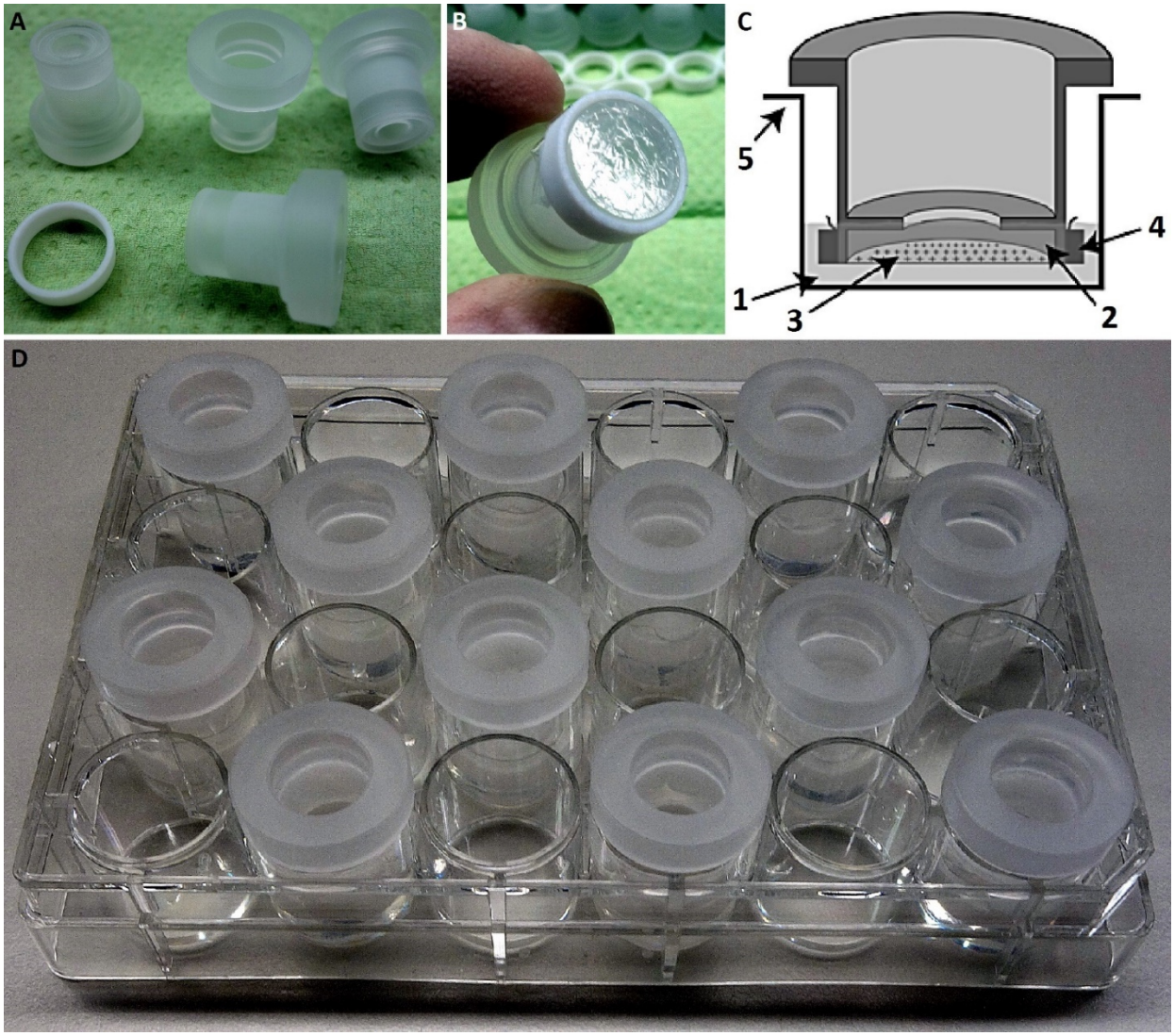

Fig. 10 – Individual parts and assembly thereof for the continuous exchange cell-free expression (CECF) of aquaporins. A = Mini CECF reactors made of acrylic glass, depicted together with a teflon ring / B = Mini CECF reactor assembled with teflon ring and single layer of dialysis membrane / C = Schematic crossview of assembled mini CECF reactor in 24-well plate. 1 = Feeding mix (FM) compartment, 2 = RM compartment, 3 = Dialysis membrane, 4 = Teflon ring, 5 = 24-well plate / D = Mini CECF reactors assembled with teflon rings and dialysis membranes in 24-well plate. [C = Kai *et al.* 2012, modified]

Since the RM contained all constituents of the FM, the latter was prepared first without the addition of water and S30-C buffer, which allowed for an aliquot to be transferred as a basis for RM setup. All individual preparations were calculated with an overhead of 10 % in order to make up for pipetting losses. The detailed RM and FM makeup was as follows:

Component	FM	RM
S30-C buffer	35 % (v/v)	-
Brij-S20	6.67 % (v/v)	6.67 % (v/v)
RCWMDE	1 mM	1 mM
Amino acid mix	0.5 mM	0.55 mM
AcP	20 mM	20 mM
PEP	20 mM	20 mM
NTP mix	1.33 % (v/v)	1.33 % (v/v)
DTT	2 mM	2 mM
Folinic acid	0.1 mg/ml	0.1 mg/ml
Complete protease inhibitor	2 % (v/v)	2 % (v/v)
HE buffer	4.17 % (v/v)	4.17 % (v/v)
$Mg(OAc)_2$	11.1 mM	11.1 mM
KOAc	130 mM	130 mM
PEG-8000	5 % (v/v)	5 % (v/v)
NaN_3	0.5 % (v/v)	0.5 % (v/v)
PC SUV liposomes	-	9.51 mg/ml
S30 extract	-	35 % (v/v)
Plasmid DNA	-	30 mg/ml
RNase inhibitor	-	100 U/ml
T7 RNA polymerase	-	80 µg/ml
E. coli tRNA	-	0.7 mg/ml
PK	-	80 µg/ml
MQ-H_2O	ad FM total volume	ad RM total volume

It should be noted, that all volume percentages given are derived from the respective component´s stock as described in chapters 2.7.1 through 2.7.4 and dependent on the total RM and FM volumes, respectively. Thus, 35 % (v/v) of a 1x S30-C buffer stock would result in 297.5 µl of a total FM volume of 850 µl. The addition of L-α-phosphatidylcholine derived small, unilamellar liposome vesicles in the RM (PC SUV) or Brij-S20 in both RM and FM were restricted to L-CF and D-CF formulations, respectively. Omission of both components would thus result in a P-CF mode setup. Fig. 11 details the three cell-free expression modes and their characteristics.

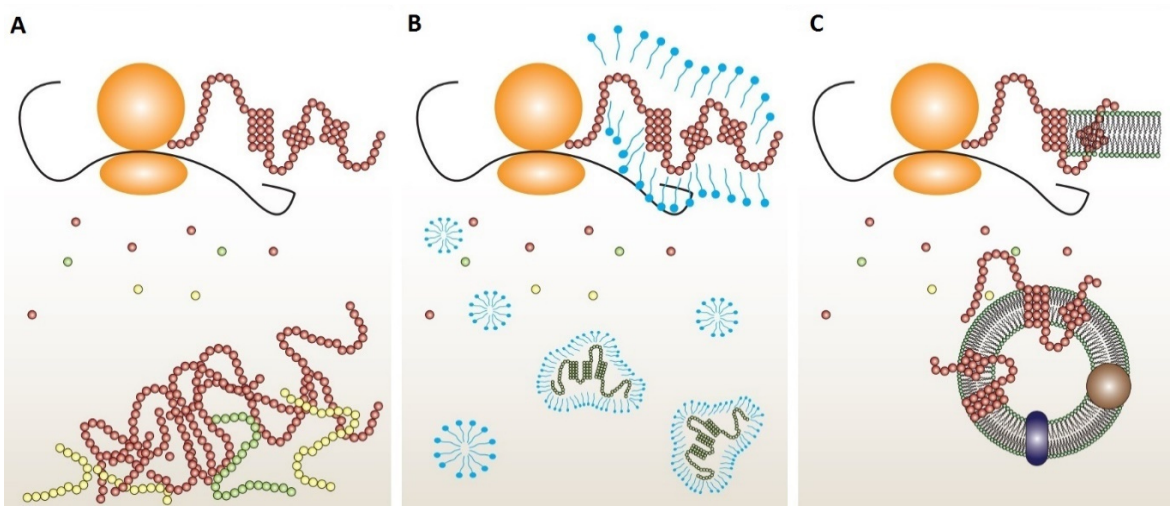

Fig. 11 – Cell-Free Expression modes used during the course of this thesis. The production of membrane protein targets without any additives results in their Precipitation (A) in P-CF mode, with the necessity of subsequent refolding protocols for proper functionality. The use of Detergents in D-CF mode (B) allows for a hydrophobic environment in the form of micelles, into which translated membrane proteins can transfer. Similarly, preformed Liposomes in L-CF mode (C) can provide a more native environment for membrane protein targets. [Kai *et al.* 2014, modified]

Dialysis membranes for the compartmentalization of RM and FM were processed / pretreated according to the following procedure:

Preparation of dialysis membranes for Mini CECF reactors

0. Usage of gloves required for all steps
1. Cut dialysis tubing to desired length
2. Wash thoroughly with $H_2O_{dem.}$
3. Incubate overnight in 2 l $H_2O_{dem.}$ under slow stirring
4. Immerse in 2 l $NaHCO_3$ with 1 mM EDTA and boil for 10 min
5. Rinse thoroughly with $H_2O_{dem.}$
6. Boil in 2 l $H_2O_{dem.}$ for 10 min
7. Remove $H_2O_{dem.}$ and replace with 20 % EtOH for long-term storage at 4 °C
8. Before usage with CECF reactors, cut tubing in half for single layers and wash thoroughly with MQ-H_2O

2.8 Downstream processing of Cell-Free Expression samples

2.8.1 General workflow of different expression mode samples

After completion of the CECF reaction, reactors were harvested by pipetting and washing the latter with 1 RM volume (= 55 µl) S30-C buffer in order to obtain any leftover target protein, all identical RM samples were pooled and centrifuged at 16,000*g* for 60 min at 4 °C. Depending on the performed expression mode, subsequent downstream-processing was carried out in variations, which are depicted in Fig. 12.

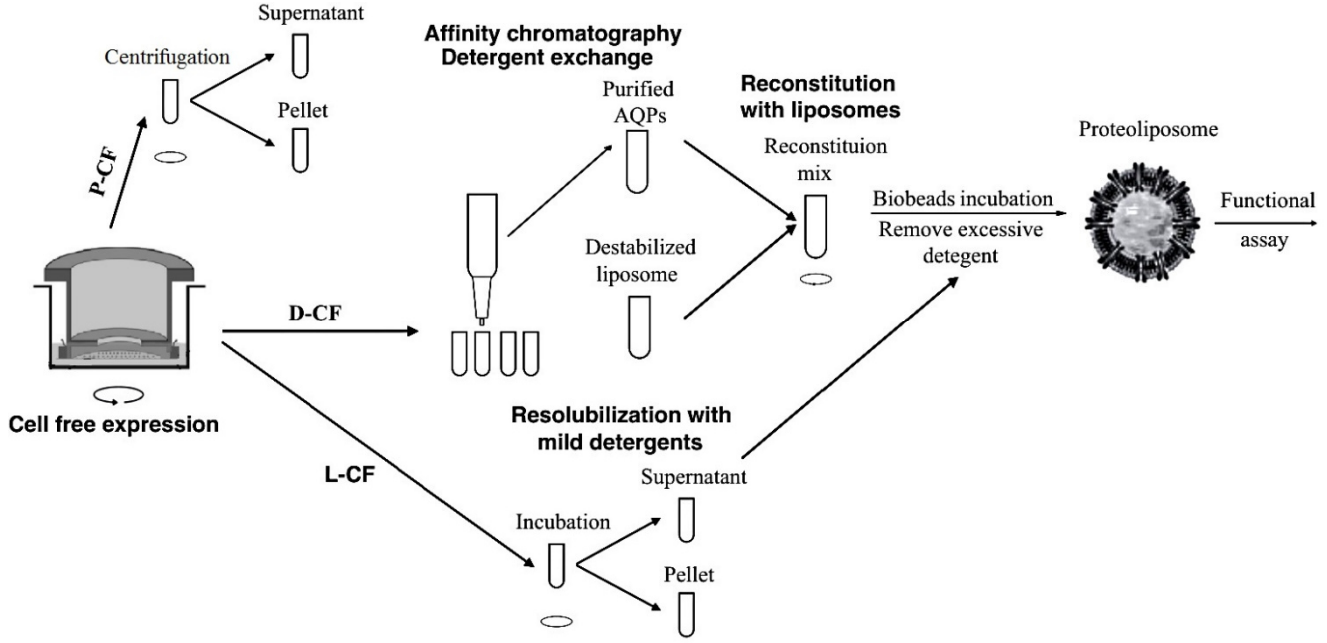

Fig. 12 – Overview on downstream-processing steps of cell-free expression samples in different modes. The precipitate cell-free expression mode (P-CF) without any hydrophobic additives was exclusively used for testing purposes regarding the expression efficiency of new constructs, thus no functional assays were performed with P-CF samples. Detergent cell-free expression (D-CF) included Brij-S20 micelles in the RM and FM, thus an IMAC based chromatographic step was necessary to provide sufficient purity of the respective aquaporin targets (AQPs) and also perform a detergent exchange with n-dodecyl β-D-maltoside (DDM). Subsequently, reconstitution of the purified protein with previously by 4-(1,1,3,3-tetramethylbutyl)phenyl-polyethylene glycol (Triton X-100) destabilized PC liposomes preceded incubation with polystyrene biobeads in order to remove excessive detergent and continue with the functional water permeability assay of the formed aquaporin proteoliposomes. In comparison, the liposome cell-free expression mode (L-CF) allowed direct integration of translated protein, thus a simple step using mild detergent (Triton X-100) in order to separate proteoliposomes from non-integrated, precipitated protein was sufficient to continue onto biobeads incubation and subsequently the functional assay. [Kai *et al.* 2012 / 2014, modified]

The **P-CF** mode was applied for the validation of newly cloned constructs, as well as the efficiency of CECF components. Thus, it did not result in any actual water permeability measurements of aquaporins. After harvesting and initial centrifugation, P-CF supernatants were usually discarded and their respective precipitates washed twice with 1 ml MQ-H_2O including intermittent centrifugation steps at 16,000*g* for 30 min at RT in order to remove any leftover soluble RM components. The resulting protein pellets were then resuspended in 1x SDS

protein denaturation buffer for subsequent analysis via SDS-PAGE and Western Blotting (see chapters 2.6.2 through 2.6.3).

Similar to P-CF, **D-CF** derived samples were centrifuged after harvesting and the resulting pellets washed with MQ-H_2O twice to remove excessive detergent for subsequent analysis via SDS-PAGE and Western Blotting. Small aliquots of the supernatants underwent acetone precipitation of their protein content (see chapter 2.8.2) for electrophoretic analysis, whereas the rest was used for IMAC purification of its His_6-tagged aquaporin targets (see chapter 2.8.3). The resulting eluates were analyzed regarding their protein content via SDS-PAGE in comparison with defined amounts of bovine serum albumin (BSA) in order to calculate the appropriate protein-detergent-liposome ratios for the subsequent reconstitution as proteoliposomes (see chapter 2.8.4). Excessive detergent in the reconstitution mixtures was removed by incubation with non-polar polystyrene biobeads (see chapter 2.8.4 through 2.8.5). Ultracentrifugation of the formed proteoliposomes at 500,000*g* for 45 min at RT allowed them to be washed with 1.6 ml HN buffer once (see chapter 2.7.3), before another ultracentrifugation step and final resuspension in 1.6 ml HN buffer. Before samples were measured via Stopped Flow (see chapter 2.9)., proteoliposomes underwent homogenization via extrusion (see chapter 2.8.6)

L-CF precipitates obtained after harvest and centrifugation were first washed with 55 µl S30-C buffer per CECF Mini reactor and centrifuged once more at 16,000*g* for 30 min at 4 °C. Resuspension in HN buffer followed, adjusting the final liposome concentration to 4 mg/ml before the addition of 0.41 % (v/v) Triton X-100 and incubation at 1400 rpm for 60 min at RT on a thermoshaker. This allowed for the separation of successfully formed liposomes from non-integrated, and thus non-functional target protein. Subsequent centrifugation at 16,000*g* for 30 min at RT preceded MQ-H_2O washing of the resulting pellets for Triton X-100 removal and SDS-PAGE, as well as Western Blotting analysis. The respective supernatants underwent aliquotation for the same purpose, in parallel to detergent removal via biobeads incubation. As with D-CF derived samples, homogenization of L-CF proteoliposomes via extrusion was the last step before functional water permeability analysis via Stopped Flow. Isolating protein from homogenized L-CF proteoliposomes for the purpose of SDS-PAGE and Western blotting analysis required a 2 phase organic solvent extraction with methanol and chloroform (see chapter 2.8.7).

2.8.2 Acetone precipication of aquaporins in detergent micelles

For proper detergent removal of RM and FM supernatants derived from D-CF samples, their protein content was precipitated with acetone [Pierce Biotechnology 2004]. Ice-cold acetone stored at -20 °C was added in 4-fold excess to the respective sample, vortexed thoroughly and then incubated at -20 °C for 60 min. After centrifugation at 16,000*g* for 15 min at 4 °C, the resulting supernatant was carefully decanted and discarded and the precipitate incubated at 37 °C for 10 min in order for any leftover acetone to evaporate. The dried pellet was recolubilized in 1x protein denaturation buffer for analysis via SDS-PAGE and Western Blotting.

2.8.3 Immobilized metal ion affinity chromatography (IMAC) purification of His_6-tagged aquaporins

As mentioned in chapter 2.8.1, IMAC purification of His_6-tagged aquaporins was performed after their generation in D-CF mode as a preparatory step for subsequent reconstitution into liposomes. All resin preparation and purification steps were carried out on ice with intermittent centrifugation steps at 500*g* for 1 min at 4 °C. The column enclosure used was Mobicol F by MoBiTec GmbH (Göttingen, Germany).

First, Chelating Sepharose Fast Flow beads (GE Healthcare, Chicago, Illinois, USA) were manually charged with Ni^{2+} ions. For that, the beads were washed with two resin volumes of MQ-H_2O before two resin volumes of 0.2 M $NiCl_2$ (with MQ-H_2O) were applied. Two washing steps followed in order to remove loosely bound ions, each consisting of five resin volumes, with MQ-H_2O and acidic resin charging buffer, respectively.

For the actual purification, a total of 100 µl resin was used for 8 RM volumes of D-CF expressed aquaporin. Equilibration of the beads with 5 resin volumes of binding buffer preceded the addition of the D-CF supernatant containing the respective solubilized aquaporin. An additional 1:10 dilution with binding buffer decreased the relative amount of Brij-S20 detergent contained in the sample (see chapter 2.7.5). Overnight incubation at 4 °C under constant shaking ensured efficient binding of the His_6-tagged protein to the resin matrix. Before the subsequent loading of the sample, the Mobicol F column was washed and equilibrated with 600 µl each of 20 % (v/v) EtOH, MQ-H_2O and binding buffer in that exact order. To remove unspecifically binding components from the resin matrix, 10 resin volumes of washing buffer were then applied to the column. Target aquaporin samples were eluted by the application of 6 resin volumes elution buffer.

Acidic Resin Charging Buffer	
NaOAc	20 mM
NaCl	150 mM
HCl	pH 4.0

Binding / Washing / Elution Buffer		
Tris	20 mM	
NaCl	150 mM	
Glycerol	10 % (v/v)	
DDM	0.05 % (v/v)	
Imidazole	10 mM	Binding
	50 mM	Washing
	400 mM	Elution
HCl	pH 7.5	

2.8.4 Reconstitution of D-CF derived, IMAC purified aquaporins into liposomes

The reconstitution protocol for purified aquaporins into liposomes was based on Ziedel *et al.* [1994] with modifications according to Kai *et al.* [2010]. Protein eluates (chapter 2.8.3) were mixed with HN buffer (see chapter 2.7.3), Triton X-100 and extruded PC liposomes (see chapter 2.7.3) in defined ratios and incubated at 25 °C and 1400 rpm for 30 min before the addition of biobeads for detergent removal. The detailed reconstitution mix setup was as follows:

Reconstitution Mix	
Triton X-100	1 or 4 mM
PC Liposomes	1 or 4 mg/ml
Triton X-100 / Liposome ratio	1 mM/mg·ml^{-1}
Purified AQP	5 - 100 µg/mg liposomes
HN Buffer	ad 0.8 - 2.0 ml

Triton X-100 as a mild detergent destabilized the liposomes and enabled the release of membrane protein from DDM micelles in the elution buffer, thereby allowing the autoassembly of proteoliposomes. The amount of aquaporin in the elution fractions was determined via trace quantity analysis of SDS-PAGE signals using the software Quantity One v4.6.3 (Bio-Rad, Hercules, California, USA). BSA served as a quantification standard, with samples containing 1, 2.5, 5 and 10 µg being loaded onto the same PAA gel as the respective elution fractions. Subsequent linear regression was based on BSA signals at an apparent molecular weight of 66 kDa and aquaporin monomer, dimer and tetramer signals at apparent kDa values of 27, 55 and 95, respectively.

2.8.5 Detergent removal by non-polar polystyrene biobeads

The application of BioBeads SM-2 hydrophobic and polar interaction adsorbents (Bio-Rad, Hercules, California, USA) was utilized for D-CF and L-CF aquaporin samples in order to remove excessive detergent contents, that could interfere with subsequent water permeability measurements (chapter 2.9) [Rigaud *et al.* 1998]. With an average pore diameter of 9 nm, these polystyrene-divinyl-benzene beads have a Triton X-100 binding capacity

in the range of 100 – 300 mmol/g coupled with a high specificity for any kind of polar detergents in aequous solutions.

Before initial usage, each batch of biobeads was thoroughly vortexed in an excess of methanol for 30 s, followed by three washing steps in MQ-H_2O for cleansing and equilibration purposes. An additional equilibration step involved the overnight saturation in an excess volume of 4 mg/ml homogenized PC liposomes (chapter 2.7.3) at 30 °C and 170 rpm to minimize adsorption of same in subsequent detergent removal steps [Rigaud *et al.* 1998]. 15.6 mg of biobeads were added for each mmol Triton X-100 contained in D-CF derived reconstitution mix samples (chapter 2.8.4), whereas L-CF derived samples underwent an evenly distributed four-step addition (1 h each), amounting to a final biobeads concentration of 160 mg/ml sample (see chapter 2.8.1). Subsequently, all samples were sealed in reaction tubes with parafilm in order to avoid unwanted evaporation and incubated overnight at 25 °C and 170 rpm.

After usage, biobeads could be regenerated following the respective Bio-Rad manual. Each batch was washed five times in an n-hexane / isopropanol solution (3:2 v/v) of equal volume by thorough vortexing for 30 s each. This was followed by an additional five washing steps with 100 % EtOH and ten steps with MQ-H_2O, removing any leftover detergents, lipids and proteins from previous utilizations. Beads regenerated in this way were stored in MQ-H_2O at RT in sealed reaction tubes until reuse.

2.8.6 Homogenization of (proteo)liposomes by extrusion

Uniform size homogenization of utilized L-α-phosphatidylcholine liposomes was accomplished by extrusion. Fig.13 details the individual parts of the Mini Extruder (Avanti Polar Lipids, Alabaster, Alabama, USA), its assembly, as well as the exemplary change of initial particle size distribution in a liposome sample when extruded repeatedly.

During extrusion a lipid suspension is repeatedly forced through a polycarbonate filter of defined pore size to yield particles with a mean diameter near the pore size of the filter used. 1 ml Hamilton glass syringes were equilibrated with HN buffer (see chapter 2.7.3) prior to usage. Filter supports (Whatman Drain Disc 10 mm PE, GE Healthcare, Chicago, Illinois, USA) and polycarbonate membranes (Whatman Nuclepore Track-Etch Membrane 19 mm, GE Healthcare, Chicago, Illinois, USA) with pore sizes of 800 and 200 nm underwent the same by submersion in HN buffer. Assembly of the central extrusion element was performed under careful exclusion of any air bubbles between the O-rings of the internal membrane supports, filter supports and the polycarbonate filter itself. After installment into the heating block, together with a syringe containing the liposome sample on one side and an empty syringe on the other, the setup as a whole was slowly heated to the lipid transition temperature at approximately 40 °C in order to avoid any potential membrane fouling.

Once the temperature was reached, repeated extrusion steps were performed by pushing the liposome sample from one syringe into the other and back again. Only an odd number of extrusion steps were performed in order to ensure the liposome sample ending up in the initially empty syringe and thus any potential contaminants, such as precipitated / non-integrated protein, staying in the original sample syringe. During the preparation of SUV liposomes (see chapter 2.7.3), solutions were passed through a 200 nm membrane 21 times. (Proteo)liposome samples for subsequent Stopped Flow water permeability measurements were

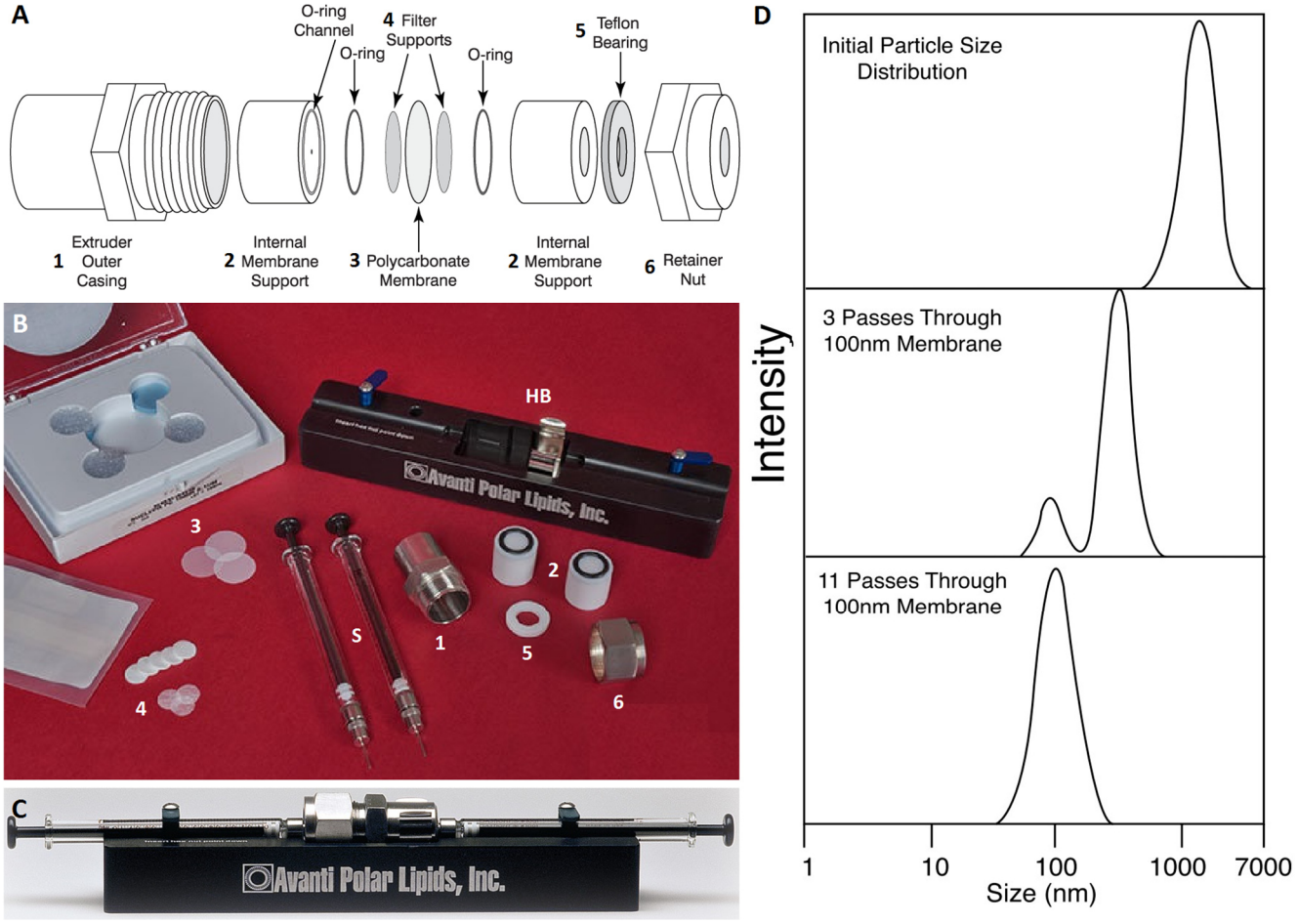

Fig. 13 – Uniform size homogenization of liposomes by extrusion. A = Individual parts making up the central extruder element / B = Individual extruder parts with 1 ml Hamilton glass syringes (S) and heating block (HB) / C = Assembled Mini Extruder / D = Change of initial particle size distribution in a liposome sample after repeated extrusion passes [Avanti Polar Lipids, avantilipids.com, modified]

passed through an 800 nm membrane once for improved subsequent filter passage before additional 21 passes through 200 nm membranes. One 800 nm membrane with four filter supports was used per batch of samples, whereas one 200 nm membrane with four fresh filter supports was used for each individual sample. Between samples, the central extrusion element with all individual parts, as well as both syringes were thoroughly washed with $H_2O_{dem.}$ and equilibrated anew with HN buffer. Extruded samples were stored at 4 °C for a maximum of 24 hours before usage.

2.8.7 Chloroform / methanol extraction of aquaporins in proteoliposomes

Proteoliposome samples obtained from D-CF and L-CF modes (see chapters 2.7.5 through 2.8.1) underwent a two-phase chloroform / methanol liquid-liquid extraction in order to isolate the contained protein for further analysis via SDS-PAGE and Western Blotting (see chapters 2.6.2 and 2.6.3). The protocol was adpoted from Wessel & Flügge [1984] and is based on the solubility of contained lipids in chloroform, whereas any protein would precipitate in the biphasic system with methanol.

Each addition step included thorough vortexing for 30 s, as well as a centrifugation step at 16,000 *g* for 1 min at RT. First, 4 volumes of methanol were added for each volume of proteoliposome sample, followed by 2 volumes of chloroform. Finally, 3 volumes of MQ-H_2O were added, resulting in the formation of a biphasic system after vortexing and centrifugation, with the interphase containing the precipitated protein. The upper methanol containing phase was removed and discarded and replaced by 3 sample volumes of fresh methanol.

A centrifugation step at 16,000 *g* for 60 min at RT formed a small, but distinct protein pellet, which was dried at 37 °C for 10 min before the resuspension in 1x SDS protein denaturation buffer for further processing.

2.9 Stopped Flow water permeability measurements of (proteo)liposomes

Stopped Flow spectrophotometry is one of currently six established assays to measure aquaporin water permeability. Table 10 gives an overview on these assays.

Table 10 – Overview on currently established aquaporin water permeability assays. [To & Torres 2015, modified]

Assay	Membrane component	Signal type measured	Throughput	Characteristics
Stopped Flow	(Proteo)liposomes, vesicles, cells (e.g. yeast)	Light scattering, fluorescence change	Low (10 samples / h)	specialized instrumentation required
Transepithelial	Cell monolayers on porous support	Dilution of indicator dye	Low (12 wells / plate)	virtually artefact-free, laborious
Fluorescence-based	Cell monolayers on solid support	Cytoplasmic fluorescence change	Medium (96-well plates)	potential artefacts due to compound-reporter interaction, easy handling
Oocyte swelling	*Xenopus laevis* oocytes	Oocyte imaging	Low (2-5 samples / d)	prone to artefacts, challenging
Erythrocyte lysis	Erythrocytes	Cell lysis	High (96-well plates)	restricted to AQP1 measurements
Yeast freeze-thaw	Yeast cells	Cell viability	High (96-well plates)	generic, easy to perform

Its principle is based on creating an osmotic gradient by rapidly mixing two solutions (dead time approx. 10 – 20 ms), which induces a shrinking or swelling of the included membrane components. In this case, homogenized (proteo)liposome samples in HN buffer (see chapters 2.7.3 and 2.8) were mixed with the same buffer containing 400 mM sucrose. Since sucrose cannot permeate the liposomes, the hyperosmotically induced gradient causes them to shrink. The shrinkage rate is then measured via light scattering and is characterized by a curve following an exponential saturation equation [Kai *et al.* 2010]. Fig. 14 gives an overview on the experimental setup and an example of the obtained raw data.

The Stopped Flow spectrophotometer used within this thesis was a model SFM-300 by Biologic (Claix, France), which was connected to an electric arc light source (Type H-1061 UV by Jobin Yvon Horiba, Longjumeau, France) set to emit light at a wavelength of 436 nm. An MPS-60 microprocessor unit handled manual control of the Stopped Flow syringe motors via its panel, as well as remote control using a connected computer terminal. The whole system was temperature-controlled via a RC 6 CS low-temperature thermostat (Lauda Dr. R. Wobser GmbH & Ko KG, Lauda-Königshofen, Germany). BioKine32 software v4.51 by BioLogic was used to set measurement parameters, remote control the Stopped Flow syringe motors and record light scattering curves. Finally, a PMS-250 signal amplifier by BioLogic allowed the manual fine tuning of the voltage-converted scattered light signal, which enabled to maintain the desired range.

Prior to measurements, (proteo)liposome samples previously homogenized by extrusion (see chapter 2.8.6) were diluted with HN buffer to equal OD_{436} values in the range of 0.065 to 0.15. This was done in order to equalize any concentration changes the samples went through during downstream processing (see chapter 2.8) and thus provide a common initial measurement baseline. Final OD_{436} values depended on sample volumes and were chosen to ensure sufficient material for individual measurements. Before sample loading, the Stopped Flow spectrophotometer was washed with 20 ml $H_2O_{dem.}$ per syringe access point and respective reservoir to purge air bubbles. This was followed by an equilibration step with the respective buffers used in the subsequent measurements: S1 served as the access point for the (proteo)liposome samples and was thus washed with 20 ml HN buffer; S2 was left unused during measurements and was washed with 20 ml $H_2O_{dem.}$; S3 contained the hyperosmotic HN buffer with 400 mM sucrose and was washed accordingly.

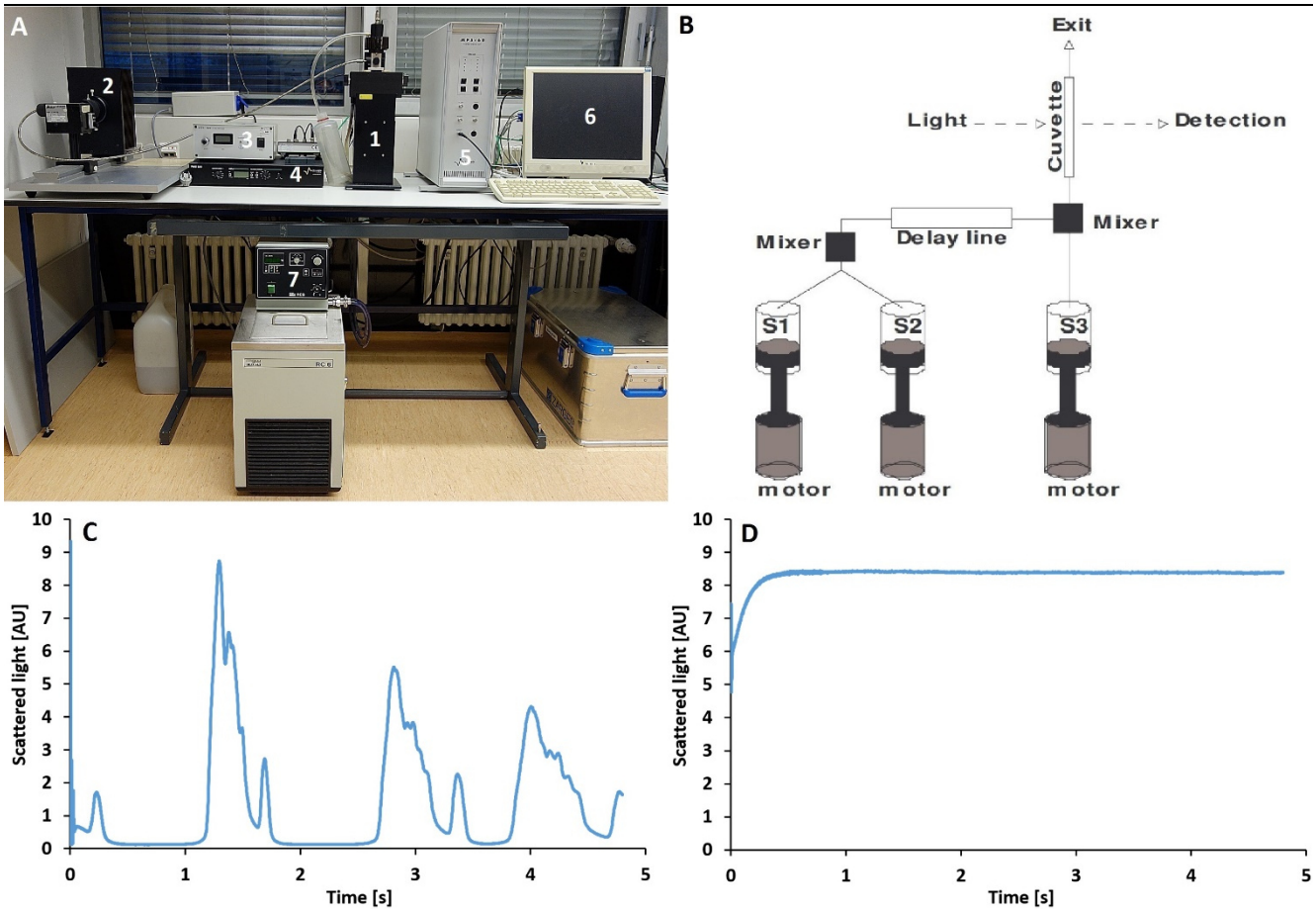

Fig. 14 – Experimental setup of Stopped Flow water permeability assay and exemplary obtained raw data. A = Experimental setup / 1 = BioLogic SFM-300 Stopped Flow / 2 = Jobin Yvon Horiba Type H-1061 electrical arc light source / 3 = light source wattage meter / 4 = BioLogic PMS-250 signal amplifier / 5 = BioLogic MPS-60 microprocessor unit / 6 = BioKine workstation for SFM-300 remote control and data acquisition / 7 = MWG Lauda RC 6 CS low-temperature thermostat / B = SFM-300 internal schematic: Three motorized syringe access points with respective reservoirs can transfer (proteo)liposome samples and hyperosmotic buffer through high-speed mixers into a quartz cuvette. Light at a wavelength of 436 nm hits the cuvette and scattered light signals are registered by a detector at an angle of 90 ° perpendicular to the light source, subsequently being converted into an electrical voltage signal. / C & D = Visual comparison of a pre-equilibration curve (C) to an actual raw data curve obtained from Stopped Flow measurements. Scattered light signals are given in arbitrary units [AU] as a function of time in seconds. Ideal characteristics of a raw data curve include an initial mixing phase with one upward and one downward facing spike lasting anywhere between 10 – 20 ms, followed by y continuous rise and a steady state. [B = BioLogic 2008, modified]

The subsequent loading of the (proteo)liposome sample and the hyperosmotic buffer into the respective syringe reservoirs went in parallel with ensuring the system´s measurement stability. In order to avoid fluctuations in the scattered light signal, the cooling unit´s temperature setting at 10 °C and the electrical arc light source`s wattage at a minimum of 145 W were visually confirmed. The experimental parameters set via BioKine software were as follows:

Menu	Parameter	Value
Mixing sequence	Mixing ratio	S1 = 1 S2 = 0 S3 = 1
	Total volume / shot	100 µl (50 µl per syringe)
	Total flow rate	10 ml/s
	Start of data aqcuisition	10 ms before stop
Data acquisition setup	Acquisition mode	Fluorescence & Volts
	Sampling period	1 = 200 µs (4000 data points) 2 = 2 ms (2000 data points) total shot time = 4.8 s

Consequently, each sample was divided into 50 µl shots and mixed at a flow rate of 10 ml/s with an equal amount of hyperosmotic buffer during individual water permeability measurements lasting a total of 4.8 s each. The first several curves obtained of each sample did not contain any viable data due to the system firstly having to attain equilibrium and were thus just used to manually fine tune the amplifier to a voltage range of ideally between 7 and 9. Single shots were manually engaged until equilibrium was reached and the amplifier set to the desired range, from which point on the system was switched to autorun until the sample was depleted. Between different samples, the S1 syringe access was thoroughly washed with 20 ml HN buffer, whereas S3 containing the hyperosmotic buffer was periodically refilled before depletion. The obtained light scattering data was subsequently exported to Excel 2016 (Microsoft, Redmond, Washington, USA) and analyzed as described in chapter 2.10.1.

2.10 Software & *in silico* methods

2.10.1 Calculation of (proteo)liposome water permeability by non-linear regression analysis of light scattering shrinkage kinetics

Shrinkage kinetics of (proteo)liposomes from Stopped Flow light scattering measurements (see chapter 2.9) were imported into Excel 2016 (Microsoft, Redmond, Washington, USA) and the first several pre-equilibration curves of each sample manually sorted out. Each individual raw data curve was then cropped to only include data points between 23.4 ms and 523.4 ms, erasing pre-kinetic mixture artefacts and redundant steady-state data points. To counteract kinetic fluctuations, the first data point was then normalized to the point of origin (= 0 %), whereas the average value of all data points between 0.45 and 0.5 s was equated to 100 %. Aside from visualization purposes, this normalization allowed previously undiscovered pre-equilibration curves to be identified and sorted out. Fig. 14 shows a normalized result including a pre-equilibration curve.
Cropped raw data curves normalized to the point of origin were subsequently fitted to an exponential rise function using non-linear regression:

$$Y = Y_0 + A \cdot (e^{-kx})$$

Y_0 is equivalent to each curve´s offset from the point of origin and A represents the amplitude from lowest to highest data point on the y-axis. The rate constant k [s^{-1}] describes the steepness of the slope and is the base for calculating each sample´s water permeability. Hence, a high rate constant would describe a very steep slope and thus a high water permeability of the analyzed sample. Only data points up to 0.1 s were included in the fitting process to ensure data robustness [Fischer & Kaldenhoff 2008 / Otto *et al.* 2010]. This is due to the fact that the initial water efflux rate opposing the osmotic gradient is not constant and thus changes during the course of a kinetic measurement. In general, a wider fitting range would not capture the initial rate constant as effectively as a narrow one, with both starting at the first data point. However, the latter would demonstrate a significantly higher variance between individual measurements of the same sample due to the relatively higher kinetic fluctuations. It is thus critical to choose a fitting range that ensures a precise calculation of the initial rate constant while keeping the variance between individual measurements at an acceptable level.
The fitting procedure was carried out by utilizing the Solver Add-In of Excel 2016, which was set to find the optimal values of the three variables described beforehand. Calculating the sum of squared differences between each raw and fitted data point, referred to as $\Sigma\chi^2$, allowed the modulation of the three variables until a global minimum for $\Sigma\chi^2$ was found via the GRG non-linear method. This ensured that the fitted curve represented the raw data as precisely as possible.

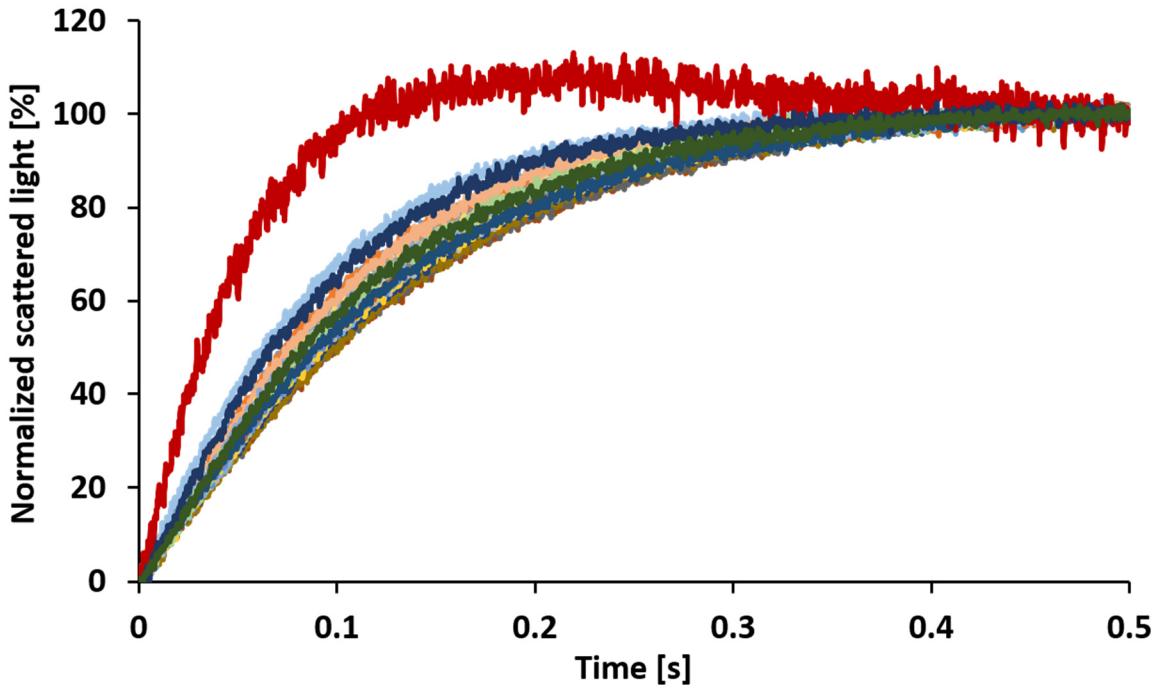

Fig. 15 – Cropped and normalized shrinkage kinetics obtained from Stopped Flow water permeability measurements of a PC liposome sample. Raw data curves as shown in chapter 2.9 were cropped to include a total of 2501 data points between 23.4 ms and 523.4 ms, leaving out pre-kinetic mixture artefacts and redundant steady-state data points. The first data point of each cropped curve was then normalized to 0/0 and the average value of all data points between 0.45 and 0.5 s equated to 100 %. Aside from visualization purposes, this normalization process allowed previously undiscovered pre-equilibration curves to be identified and sorted out (red curve in this example).

In order to convey the quality of each fit, a χ dependent variable was introduced: the relative fitting distance F_D was determined by calculating the average distance between the raw and fitted data points in ± [%] values of the averaged absolute values in raw and fitted data point pairs. It thus defines the area, in which the raw data curve fluctuates around the fitted curve as a standard deviation (Fig. 16).

The obtained set of a sample´s rate constant values allowed the calculation of an arithmetic mean with standard deviations. This was used as the basis to define and sort out outlier curves, that demonstrated k values located farther than three standard deviations from the arithmetic mean. The remaining rate constants were subjected to a mathematical conversion into the water permeability factor P_f. Unlike k, P_f allows an objective water permeability comparison independent from individual experimental factors and outputs the speed of the initial water efflux or influx in distance per unit of time. The P_f conversion was based on the following formula [van Heeswijk & van Os 1986 / Borgnia *et al.* 1999]:

$$P_f = \frac{k}{\frac{S}{V_0} \cdot V_w \cdot \Delta_{osm}}$$

$\frac{S}{V_0}$ represents the initial surface-to-volume ratio of the measured (proteo)liposome vesicles, while V_w is the partial molar volume of water at 18 $\frac{cm^3}{mol}$. The value of Δ_{osm} was set to 200 mM due to the osmotic gradient created when mixing 50 µl of a (proteo)liposome sample suspended in HN buffer with an equal volume of the same buffer containing 400 mM sucrose during Stopped Flow measurements (see chapter 2.9). The particle size of empty PC liposomes and proteoliposomes containing NtPIP2;1 or NtAQP1 aquaporins had previously been determined by dynamic light scattering [Kai & Kaldenhoff 2014, Supplement]. The predominant diameter class of the former was found to be at 115 nm, while the latter showed most vesicles to be 130 nm in size.

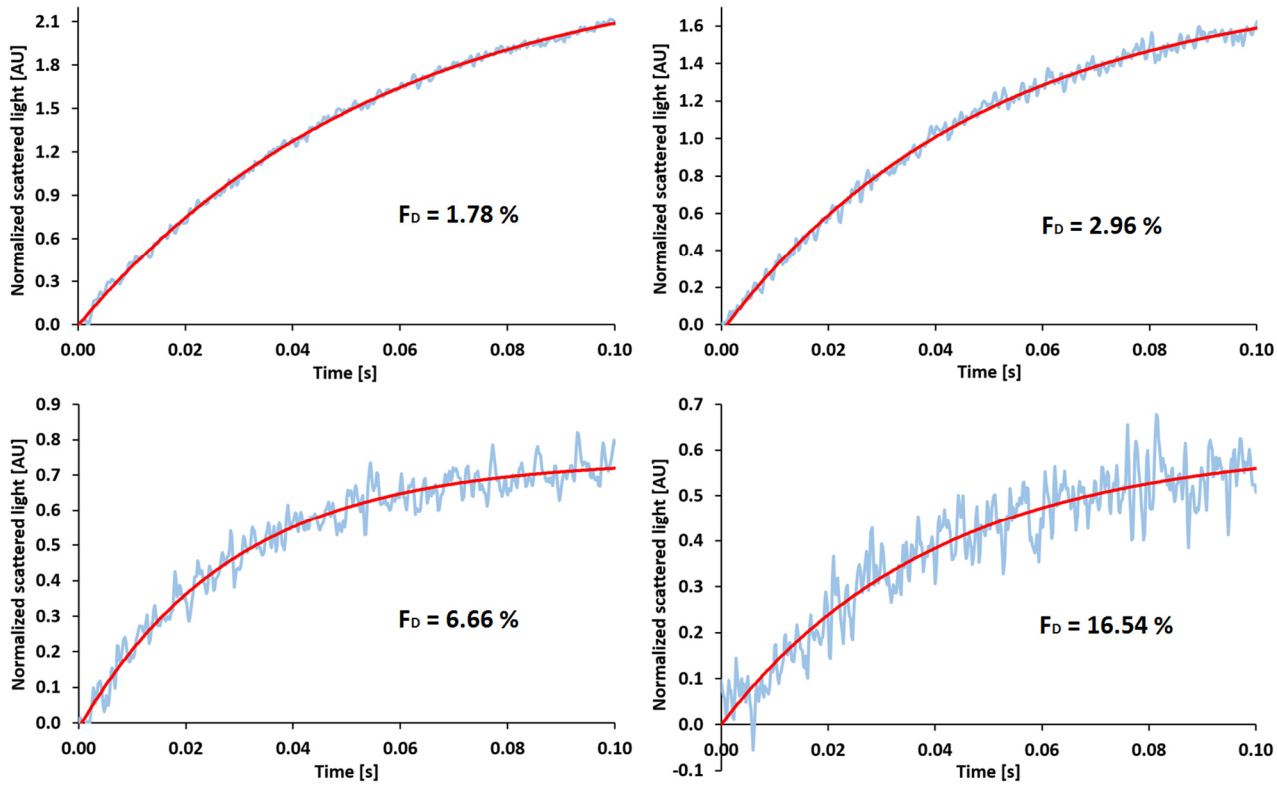

Fig. 16 – Visual demonstration of various relative fitting distance (F_D) values. A fitted curve based on an exponential rise equation (red) was derived from a cropped raw data curve (blue) by minimizing the sum of squared differences ($\Sigma\chi^2$) between their individual data points. F_D as a χ dependent indicator for the fit quality was determined by calculating the differences between the raw and fitted data points as ± [%] values of the averaged raw and fitted data point pairs. The output thus defines the area, in which the raw curve fluctuates around the fitted curve as a standard deviation.

Statistically significant differences between two sets of obtained P_f values were determined by applying an F-Test followed by a Student´s t-test. The former determines, whether two sets of data points share an equality of variances. The threshold was set at p = 0.05, below which heteroscedasticity and thus differing variances were given. Based on this result, a homo- or heteroscedastic Student´s t-test with a two-tailed distribution was performed. This determined the probability of two P_f value populations sharing an identical ($p \geq 0.05$) or a differing parent population ($p < 0.05$). The following significance levels were set based on the obtained p values [GraphPad Prism 2014]:

P value	Wording	Abbreviation
< 0.0001	extremely significant	****
0.0001 - < 0.001	extremely significant	***
0.001 - < 0.01	very significant	**
0.01 - < 0.05	significant	*
≥ 0.05	not significant	ns

2.10.2 Miscellaneous software tools

Table 11 gives an overview on the software tools used during the course of this thesis. Listed are details on software version, author or source link, references and the area of application in this work. All tools were used with default settings, unless otherwise stated.

Table 11 – Overview on software tools used during the course of this thesis. 1 = Microsoft Corporation, Redmont, WA, USA / 2 = PerkinElmer Inc., Waltham, MA, USA / 3 = Expert Protein Analysis System, Swiss Institute of Bioinformatics (SIB), University of Lausanne, Switzerland / 4 = Montpellier Laboratory of Computer Science, Robotics, and Microelectronics, Montpellier, France / 5 = European Bioinformatics Institute, European Molecular Biology Laboratory, Hinxton, Cambridgeshire, UK / 6 = Bio-Rad, Hercules, California, USA / 7 = Thermo Fisher Scientific, Waltham, Massachusetts, USA / 8 = Wollscheid Lab, Institute of Molecular Systems Biology, Department of Biology, ETH Zurich, Zurich, Switzerland.

Tool	Version	Source	Link	Application	References
CCTOP	1.00	Institute of Enzymology, Budapest, Hungary	cctop.enzim.ttk.mta.hu	Transmembrane topology prediction	Dobson *et al.* 2015a, Dobson *et al.* 2015b
Excel	2016	Microsoft[1]	products.office.com	Non-linear regression analysis	-
FinchTV	1.4.0	Geospiza (PerkinElmer[2])	www.geospiza.com/ftvdlinfo.html	Analysis of DNA sequencing traces	-
JalView	2.9.0b2	School of Life Sciences, University of Dundee, UK	www.jalview.org/Download	Visualisation of multiple sequence alignments	Waterhouse *et al.* 2009
LALIGN	-	ExPASy, SIB[3]	embnet.vital-it.ch/software/LALIGN_form.html	Local & global pairwise sequence alignment	Huang & Miller 1991
LIRMM	-	LIRMM[4]	phylogeny.lirmm.fr/phylo_cgi/index.cgi	Phylogenetic tree generation	Dereeper *et al.* 2008
MUSCLE	-	EMBL-EBI[5]	www.ebi.ac.uk/Tools/msa/muscle	Multiple sequence alignment	Edgar 2004a, Edgar 2004b
Pepstats	-	EMBL-EBI[5]	www.ebi.ac.uk/Tools/seqstats/emboss_pepstats	Computation of protein parameters	Rice *et al.* 2000, McWilliam *et al.* 2013, Li *et al.* 2015
Plasm	2.0.4.29	Biofreesoftware	biofreesoftware.com	Generation of Plasmid Maps	-
ProtParam	-	ExPASy, SIB[3]	web.expasy.org/protparam	Computation of protein parameters	Gasteiger *et al.* 2005
Protter	1.0	ETH Zurich[8]	http://wlab.ethz.ch/protter/start/	Vosualization of aquaporin wiltdtype and mutant proteins	Omasits *et al.* 2014
Quantity One	4.6.3	Bio-Rad[6]	www.bio-rad.com/en-us/product/quantity-one-1-d-analysis-software	Agarose GE, SDS-PAGE. Western Blot signal quantification	-
SerialCloner	2.6.1	Serial Basics	serialbasics.free.fr/Serial_Cloner.html	*In silico* cloning	-
Tm calculator	-	Applied Biosystems (Thermo Fisher Scientific[7])	www6.appliedbiosystems.com/support/techtools/tm_calculator.cfm	Calculation of PCR primer melting temperatures	-
TMPred	-	ExPASy, SIB[3]	www.ch.embnet.org/software/TMPRED_form.html	Transmembrane topology prediction	Hofmann & Stoffel 1993

3. Experiments and Results

3.1 NtPIP2;1 & NtAQP1 *in silico* sequence analysis

In order to provide a detailed overview on the primary amino acid sequences of the two tobacco aquaporins NtPIP2;1 and NtAQP1, a range of *in silico* tools were used to analyze them. Table 12 shows a sequence comparison of the two MIPs via ProtParam, Pepstats and CCTOP.

Table 12 – NtPIP2;1 and NtAQP1 amino acid sequence comparison based on ProtParam, PepStats and CCTOP. 1 = The aliphatic index of a protein is defined as the relative volume occupied by aliphatic side chains (A, V, I, and L) [Ikai 1980] / 2 = Grand Average of Hydropathy for a given protein is the sum of the individual amino acid hydropathy values divided by its total number of residues [Kyte & Doolittle 1982] / 3 = Z in this case represents the one letter code for Glx type amino acid residues / 4 = B in this case represents the one letter code for Asx type amino acid residues.

	NtPIP2;1	NtAQP1	Δ
Overall Characteristics (ProParam)			
Length [aa]	284	287	+ 1 %
Mw [Da]	30486	30822	
pI [pH]	9.05	8.29	- 8 %
Aliphatic Index[1]	105.42	98.64	- 6 %
GRAVY[2]	0.467	0.414	- 11 %
Residues (Pepstats)			
Aliphatic (I/L/V)	76	69	- 9 %
Aromatic (F/H/W/Y)	43	41	- 5 %
Non-polar (A/C/F/G/I/L/M/P/V/W/I)	194	195	+ 1 %
Polar (D/E/H/K/N/Q/R/S/T/Z[3])	90	92	+ 2 %
Charged (B[4]/D/E/H/K/R/Z[3])	46	46	± 0 %
Basic (H/K/R)	30	27	- 10 %
Acidic (B[4]/D/E/Z[3])	16	19	+ 19 %
Domains [number of aa residues] (CCTOP)			
N-Terminus	41	54	+ 32 %
Transmembrane Helix 1	18	18	± 0 %
Loop A	19	17	- 11 %
Transmembrane Helix 2	18	18	
Loop B_1	3	3	
Short Helix B	14	14	
Loop B_2	9	9	
Transmembrane Helix 3	18	18	
Loop C	27	27	
Transmembrane Helix 4	18	18	± 0 %
Loop D	14	14	
Transmembrane Helix 5	18	18	
Loop E_1	4	4	
Short Helix E	14	14	
Loop E_2	10	10	
Transmembrane Helix 6	18	18	
C-terminus	21	13	-38%

The obtained data indicate an apparent sequence similarity between the two aquaporins. At almost identical sequence length and molecular weight, the isoelectric points differ only slightly and correlate well with the

makeup of the individual amino acid residues, with NtAQP1 being marginally more acidic in nature than NtPIP2;1. Similarly, NtAQP1 shows a somewhat smaller aliphatic index value, as well as a slightly lower overall hydrophobicity than NtPIP2;1, which is also mirrored in their individual amino acid breakdown. A topology analysis including the localization of membrane spanning regions via CCTOP affirms the high sequence similarity of the two plasma membrane proteins. Aside from loop A, the only differences in domain lengths are restricted to the N- and C-termini, pointing towards a potential role in the diverging substrate specificity of NtPIP2;1 and NtAQP1 (see chapter 1.5). Since Siefritz *et al*. [2001] were already able to show that an elongation of the NtAQP1 loop A domain did not confer enhanced water permeation, this shifts the focus even more towards the N- and C-termini.

A combined TMPred and CCTOP analysis of the two plant aquaporins further illustrates the high sequence and domain similarity in the form of hydrophobicity plots (see Fig. 17).

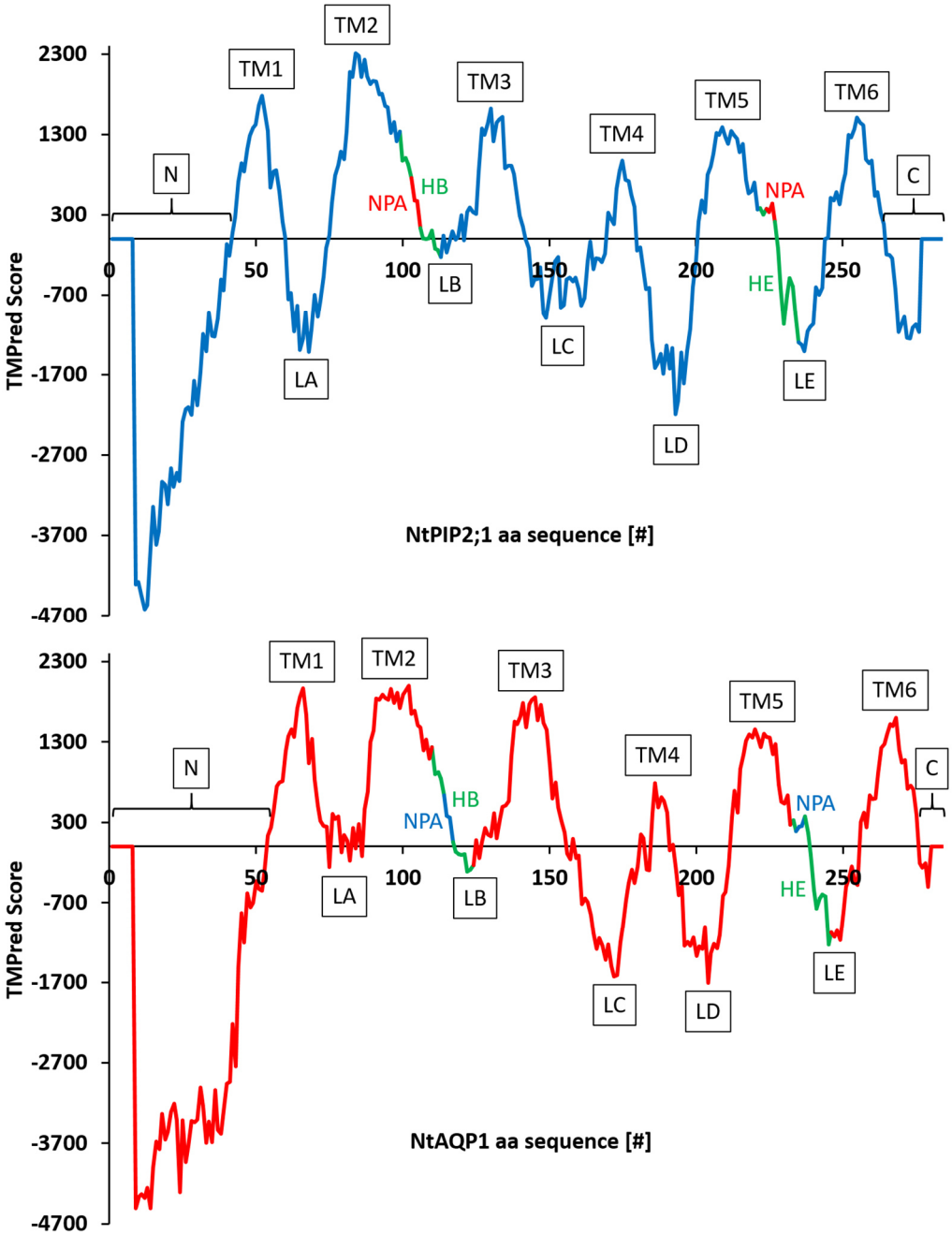

Fig. 17 – Hydrophobicity plots of NtPIP2;1 and NtAQP1 amino acid sequences derived from TMPred and CCTOP analysis. Visualized are the TMPred scores of the individual aquaporin amino acids as a function of their respective positions in the primary sequence. The TMPred scores are an indicator of residue hydrophobicity, thus a higher score implies a higher probability in membrane contact and/or integration. N = Amine-terminus / C = Carboxyl-terminus / TM = Transmembrane helix / LX = Loop X / HX = Short helix X / NPA = Asn-Pro-Ala motif.

The plots clearly show a near identical hydrophobicity and positioning of the NPA motifs and their surrounding short helices B and E in both aquaporins, which are essential components of the MIP family (see chapter 1.3.2). Similarly, the six membrane spanning helices show a very high similarity in their hydrophobicity and location in both membrane proteins. The only discernible differences between NtPIP2;1 and NtAQP1 can be found in their N- and C-termini, as well as differing hydrophobicities in loops A and C. While the former demonstrates a more hydrophilic loop A and more hydrophobic loop C, the latter shows the opposite.
In order to be able to further analyze the primary sequences of these two aquaporins and their impact on domain structure, as well as protein function, they were put into context with a selection of ten additional MIP family members. Table 13 provides an overview on the candidates.

Table 13 – Overview on NtPIP2;1, NtAQP1 and ten additional select MIP family members. Pairwise global alignments with NtPIP2;1 and NtAQP1 were performed with LALIGN. Highest scores for identity and similarity are highlighted in green, whereas lowest scores are highlighted in red.

MIP	Source Organism	Source type	Size [aa]	Database	Accession ID	NtPIP2;1		NtAQP1	
						Identity	Similarity	Identity	Similarity
NtPIP2;1	*Nicotiana tabacum*	Plant	284	GenBank	AAL33586.1	100%	100%	63%	81%
NtAQP1			287		CAA04750.1	63%	81%	100%	100%
SoPIP2;1	*Spinacia oleracea*		281	PDB	1Z98	**84%**	**94%**	65%	83%
ZmPIP1;5	*Zea mays*		288	NCBI RefSeq	NP_001105131.1	62%	79%	**82%**	**94%**
OsTIP1;2	*Oryza sativa*		252		XP_015641156.1	34%	59%	31%	57%
AtNIP2;1	*Arabidopsis thaliana*		288		NP_180986.1	23%	58%	24%	57%
bAQP0	*Bos taurus*	Mammal	263		NP_776362.1	28%	56%	28%	52%
hAQP1	*Homo sapiens*		269		NP_932766.1	34%	60%	33%	57%
hAQP9			295		NP_066190.2	**22%**	**52%**	**21%**	**49%**
Aqy1	*Pichia pastoris*	Yeast	279		XP_002492992.1	29%	58%	29%	57%
AqpZ	*Escherichia coli*	Bacteria	234	GenBank	BAJ42683.1	25%	59%	27%	56%
GlpF			295		EII23566.1	26%	54%	25%	49%

SoPIP2;1 and ZmPIP1;5 were chosen due to their high sequence identity and similarity with NtPIP2;1 and NtAQP1, respectively. Together with OsTIP1;2 and AtNIP2;1, they represent the three largest groups of plant MIPs (see chapter 1.4.1). Three additional aquaporins of bovine and human origin cover the area of mammal-derived aquaporins (bAQP0, hAQP1) and GlpF-like intrinsic proteins (hAQP9). Aqy1 from yeast and bacterial AqpZ / GlpF finalize the selection. Fig. 18 puts the twelve MIP candidates into their evolutionary context in the form of a phylogenetic tree generated via LIRMM. As expected, hAQP9 and GlpF as glyceroporins show the greatest distance from the two tobacco PIPs, whereas SoPIP2;1 and ZmPIP1;5 are the closest relatives due to their high sequence identity and similarity. The remaining six membrane proteins bridge the gap between those two extremes in successive steps of very similar lengths, thus providing an extensive cross section of the MIP family (see chapter 1.3.1). Putting the result of the phylogenetic tree in context with the substrate specificities of these MIPs (see Table 14), no discernable connection can be made between the overall sequence-based evolutionary distance of these membrane proteins with their actual function. In addition, it must be noted that not all candidates have yet been analyzed with the same range of potential substrates, thus leaving this approach to be incomplete at a high probability. So as to provide a more in-depth analysis of the domains responsible for the great disparity in water permeability between NtPIP2;1 and NtAQP1, a multiple sequence alignment was performed, together with the previously selected MIPs (see Fig. 19). The combination of this alignment with the topological analysis via CCTOP and a correlation with another multiple sequence alignment previously done by Abascal *et al.* [2014] allowed to not only identify and directly compare the individual MIP domains, but also the ar/R and P1 – P5 selectivity filters, that had already been determined to be of critical

importance to an aquaporin´s substrate specificity (see chapter 1.3.2). The comparison of the mapped domains leads to a similar conclusion as with the analysis of NtPIP2;1 and NtAQP1 listed in Table 12: Aside from the glyceroporins hAQP9 and GlpF, that demonstrate significantly elongated loops C and E_2, the only other obvious outlier can be found in AqpZ, which shows a downstream shift of its transmembrane helix 4 due to an elongated loop C and a shortened loop D. Thus, the domains of the other MIP candidates all show a remarkable conservation in their make up, location and length, with the recurrent exception of the N- and C-termini.

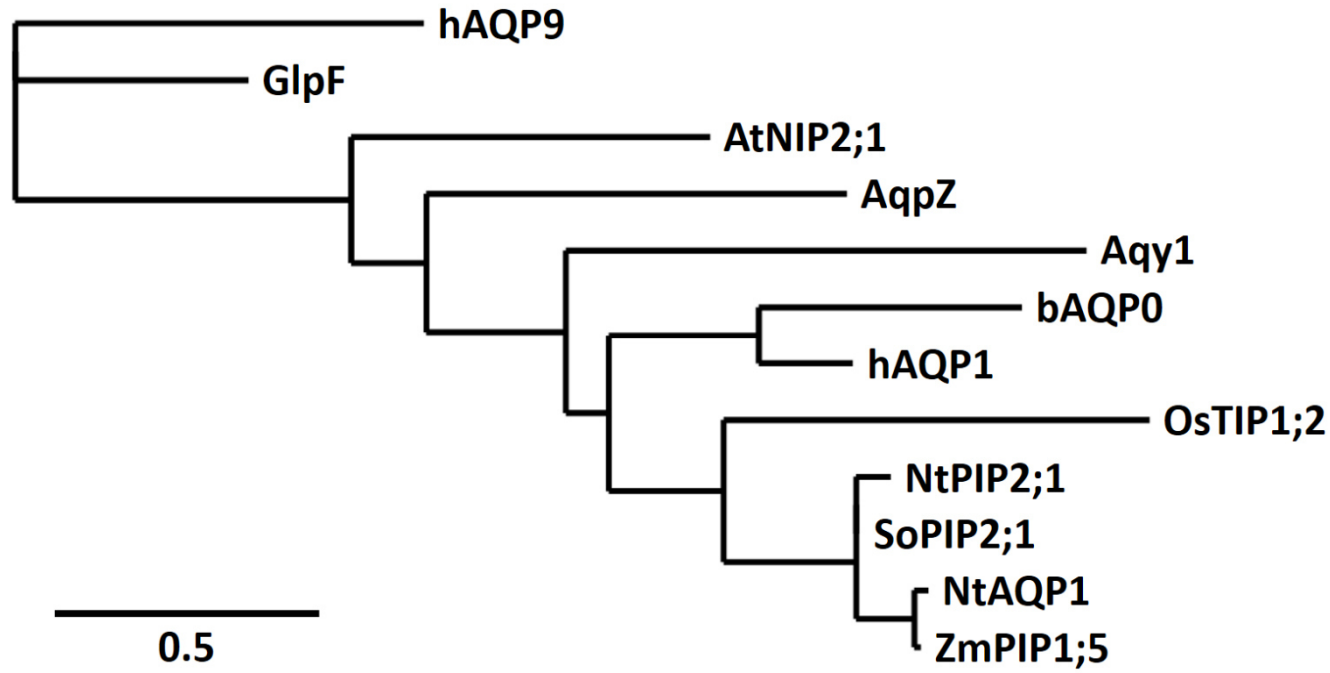

Fig. 18 – Phylogenetic tree of NtPIP2;1, NtAQP1 and ten selected MIPs generated via LIRMM. Any given branch length is proportional to the number of substitutions per site in the respective amino acid sequences (see Table 13 for details on MIPs).

Table 14 – Overview on published substrate permeabilities of NtPIP2;1, NtAQP1 and ten additional MIPs. Candidates are ordered in accordance to their distance from NtAQP1 in the phylogenetic tree. 1 = Glycerol / 2 = Urea / 3 = Carbamides / 4 = Polyols (other than glycerol) / 5 = Purines / 6 = Pyrimidines / 7 = Antimonites / 8 = Arsenites / 9 = Lactate / 10 = Ions.

MIP	Observed permeability to substrates																References
	H_2O	G^1	U^2	CO_2	H_2O_2	NO	NH_3	C^3	Po^4	Pu^5	Py^6	Sb^7	As^8	L^9	I^{10}		
NtAQP1	x	x	x	x													Biela *et al.* 1999, Eckert *et al.* 1999, Uehlein *et al.* 2003
ZmPIP1;5	x		x														Gaspar *et al.* 2003
SoPIP2;1	x																Johansson *et al.* 1998
NtPIP2;1	x																Bots *et al.* 2005a, Mahdieh *et al.* 2008, Kai & Kaldenhoff 2014
OsTIP1;2	x	x															Li *et al.* 2008, Sakurai *et al.* 2008
hAQP1	x	x		x	x	x	x								x		Preston *et al.* 1992, Abrami *et al.* 1995, Anthony *et al.* 2000, Endeward *et al.* 2006, Herrera *et al.* 2006, Musa-Aziz *et al.* 2009, Almahsalmeh *et al.* 2014
bAQP0	x			x													Zampighi *et al.* 1985, Mulders *et al.* 1995, Yang & Verkman 1997, Geyer *et al.* 2013
Aqy1	x																Fischer *et al.* 2009
AqpZ	x																Calamita *et al.* 1995
AtNIP2;1	x	x			x												Mizutani *et al.* 2006, Choi & Roberts 2007
GlpF	x	x	x						x			x	x	x			Heller *et al.* 1980, Maurel *et al.* 1994, Calamita *et al.* 1995, Sanders *et al.* 1997, Meng *et al.* 2004, Bienert *et al.* 2013
hAQP9	x	x	x					x	x	x	x		x				Ishibashi *et al.* 1998, Tsukaguchi *et al.* 1999, Dobson

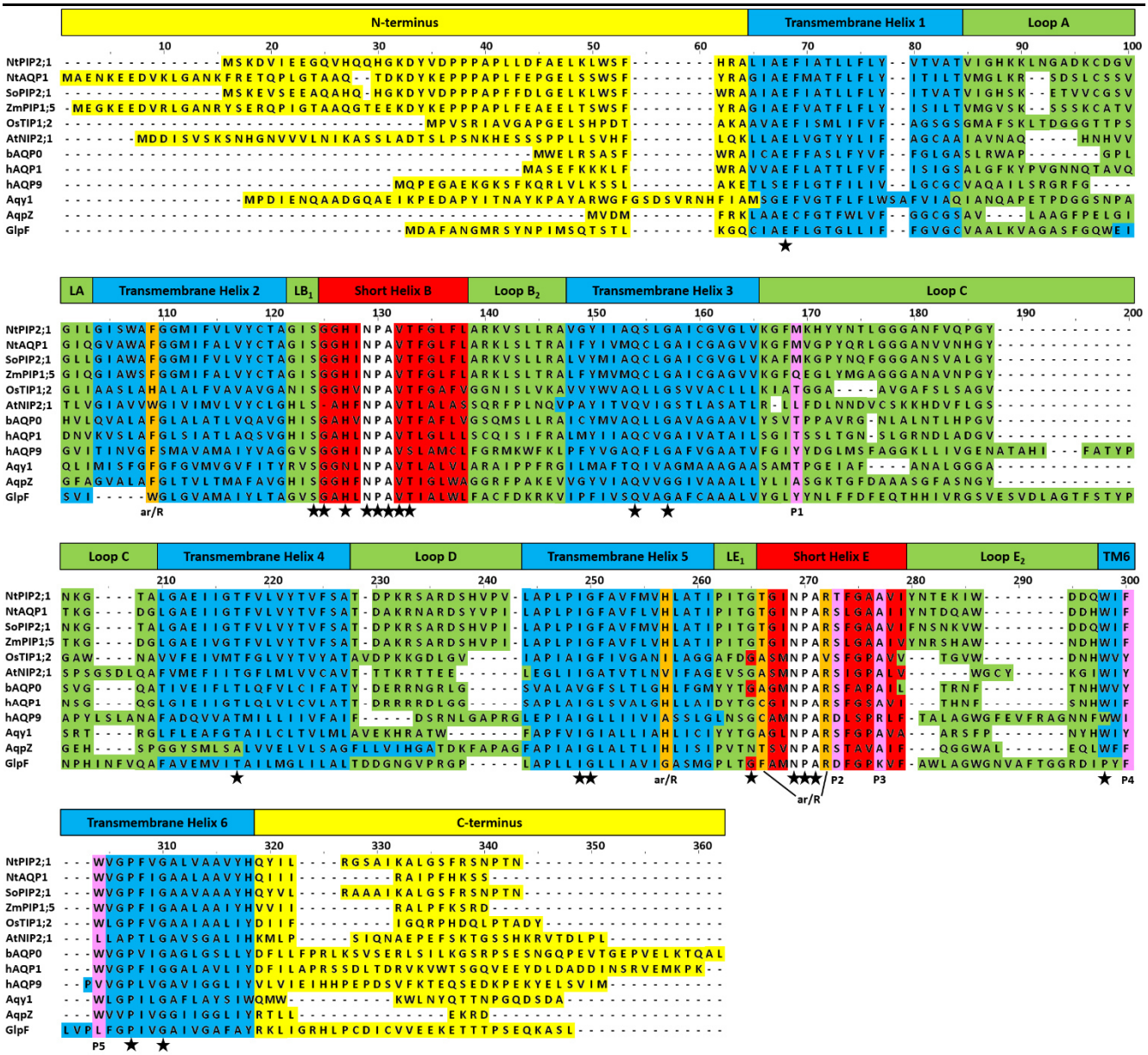

Fig. 19 – Multiple sequence alignment of NtPIP2;1, NtAQP1 and ten selected MIPs. Alignment was performed using MUSCLE and the result was visualized with JalView. CCTOP served as the tool of choice in order to classify the individual domains, whereas MIP specificity determining regions ar/R and P1 – P5 were correlated in accordance with Abascal *et al.* 2014. Residues with an alignment identity of at least 90 % are mapped with star symbols.

The positions of the identified ar/R and P1 – P5 selectivity filters fall in line with already published data (see chapter 1.3.2) and can consequently be deemed correct. Aside from these, a total of 21 highly conserved positions (identity > 90 %), including the two NPA motifs, were mapped and located exclusively inside or right next to membrane integrated domains. An isolated classification and comparison of the amino acid residues in the afore-mentioned selectivity filters is shown in Table 15. Interestingly, NtPIP2;1, NtAQP1, SoPIP2;1, ZmPIP1;5 and hAQP1 were found to share identical types of residues in their selectivity filters, with the former two differing only slightly in P2, where a threonine in NtPIP2;1 gives way to a serine residue in NtAQP1. Especially concerning the disparity in the water permeability of the two tobacco aquaporins (see chapter 1.5), this is one additional argument in favour of their N- and C-termini playing a vital role in this area.

Complementary to the introductory Table 12, Table 16 again lists a comparative make up of the individual domains in NtPIP2;1 and NtAQP1, this time in terms of their exact alignment identity and similarity as derived from LALIGN. As before, the largest differences are seen in the N- and C-termini, followed by loop A.

Table 15 – Overview on ar/R and P1 – P5 selectivity filters of NtPIP2;1, NtAQP1 and ten additional MIPs. Colored backgrounds distinguish classifications of amino acid residues: Blue = hydrophobic aromatic (F,W,Y) / Green = hydrophobic aliphatic (A,G,I,L,P,V) / Red = acidic (D,E) / Yellow = basic (R,H,K) / Pink = polar uncharged (S,T,C,M,N,Q). 1 = Amount of diverging amino acid residues in terms of their classification compared with NtPIP2;1.

MIP	ar/R 1	ar/R 2	ar/R 3	ar/R 4	P1	P2	P3	P4	P5	Δ[1]
NtPIP2;1	F	H	T	R	M	T	A	F	W	0
NtAQP1	F	H	T	R	M	S	A	F	W	0
SoPIP2;1	F	H	T	R	M	S	A	F	W	0
ZmPIP1;5	F	H	T	R	Q	S	A	F	W	0
hAQP1	F	H	C	R	T	S	A	F	W	0
AqpZ	F	H	T	R	A	S	A	F	W	1
bAQP0	F	H	A	R	T	S	A	Y	W	1
Aqy1	F	H	A	R	T	S	A	Y	W	1
AtNIP1;2	W	V	A	R	L	S	A	Y	L	4
OsTIP1;2	H	I	A	V	T	S	A	Y	W	4
GlpF	W	G	F	R	Y	D	K	F	L	6
hAQP9	F	A	C	R	Y	D	R	I	V	6

Table 16 – LALIGN derived pairwise alignment of the individual domains in NtPIP2;1 and NtAQP1. The lowest three identity and similarity scores are highlighted in red. N = Amine-terminus / TMX = Transmembrane helix X / LX = Loop X / HX = Short helix X / C = Carboxyl-terminus.

	N	TM1	LA	TM2	LB & HB	TM3	LC	TM4	LD	TM5	LE & HE	TM6	C
Identity	**35%**	67%	**37%**	83%	92%	61%	59%	100%	71%	94%	75%	83%	**24%**
Similarity	**57%**	89%	**68%**	100%	96%	83%	74%	100%	93%	100%	96%	94%	**43%**

Taken together, the presented data justify the hypothesis, that the sequence-based difference observed in the C- and N-termini of the two tobacco aquaporins NtPIP2;1 and NtAQP1 are potentially causing the former to be significantly more permeable to water than the latter.

3.2 Cloning of N- and C-terminal mutant constructs

N- and C-terminal mutant constructs of *ntpip2;1* and *ntaqp1* genes were cloned via restriction/ligation into a pET-21a plasmid backbone. After mutation of the wildtype templates via initial amplification, the mutated target genes and plasmid backbones were digested and then ligated before being transferred into *E. coli* DH5α. Constructs were then validated via PCR, digestion and sequencing before Midi-prep purification for subsequent usage in cell-free expression. All individual cloning steps underwent validation via Agarose GE (where feasible), followed by kit-assisted purification in order to remove any potentially interfering proteins and buffers. Table 17 lists templates, primers, restriction enzymes and additional info on the mutant constructs. Fig. 20 and 21 show an exemplary map of the final plasmids including their individual molecular sizes and a schematic of the resulting aquaporin configurations, respectively.

Table 17 – Overview on cloning of N- and C-terminal mutant constructs of *ntpip2;1* and *ntaqp1* genes. 1 = Clone list and primer list accession numbers in the strain collection of Prof. Dr. Ralf Kaldenhoff at Applied Plant Sciences, TU Darmstadt, Darmstadt, Germany.

Target Plasmid	Target Protein	Template[1]	Primer[1] (PCR)	REs (cloning)	Primer[1] (validation)	REs (validation)	Notes on expressed protein
pET-21a(+)::*Δ(n)_p2*(His)	Δ(N)_P2	1195	1380 / 1383	XbaI / XhoI	66 / 709	PagI / RsaI / VspI	NtPIP2;1 with N-terminus deleted
pET-21a(+)::*Δ(n)_a1*(His)	Δ(N)_A1	1303	1376 / 1379	XbaI / XhoI	66 / 709	PagI / RsaI / VspI	NtAQP1 with N-terminus deleted
pET-21a(+)::*p2_Δ(c)*(His)	P2_Δ(C)	1195	1381 / 1382	XbaI / XhoI	66 / 709	PagI / RsaI / VspI	NtPIP2;1 with C-terminus deleted

Target Plasmid	Target Protein	Template[1]	Primer[1] (PCR)	REs (cloning)	Primer[1] (validation)	REs (validation)	Notes on expressed protein
pET-21a(+)::*a1_Δ(c)*(His)	A1_Δ(C)	1303	1377 / 1378	XbaI / XhoI	66 / 709	PagI / RsaI / VspI	NtAQP1 with C-terminus deleted
pET-21a(+)::*Δ(n)_p2_Δ(c)*(His)	Δ(N)_P2_Δ(C)	1195	1380 / 1382	XbaI / XhoI	66 / 709	PagI / RsaI / VspI	NtPIP2;1 with N- and C-terminus deleted
pET-21a(+)::*Δ(n)_a1_Δ(c)*(His)	Δ(N)_A1_Δ(C)	1303	1376 / 1378	XbaI / XhoI	66 / 709	PagI / RsaI / VspI	NtAQP1 with N- and C-terminus deleted
pET-21a(+)::*(n)a1_p2*(His)	(N)A1_P2	1126	1219 / 1220	BamHI / XhoI	353 / 492, 66 / 709	BclI / PagI / PvuII	NtPIP2;1 with N-terminus of NtAQP1
pET-21a(+)::*(n)p2_a1*(His)	(N)P2_A1	667	1203 / 1208	HindIII / NotI	491 / 354, 66 / 709	PstI / PvuII	NtAQP1 with N-terminus of NtPIP2;1
pET-21a(+)::*p2_(c)a1*(His)	P2_(C)A1	1121	1215 / 1216	NheI / XhoI	491 / 354, 66 / 709	BclI / PagI / EcoRI	NtPIP2;1 with C-terminus of NtAQP1
pET-21a(+)::*a1_(c)p2*(His)	A1_(C)P2	1124	1211 / 1220	BamHI / XhoI	353 / 492, 66 / 709	PstI	NtAQP1 with C-terminus of NtPIP2;1
pET-21a(+)::*(n)a1_p2_(c)a1*(His)	(N)A1_P2_(C)A1	1128	1207 / 1208	BamHI / NotI	353 / 354, 66 / 709	BclI / PagI / PvuII	NtPIP2;1 with N- and C-terminus of NtAQP1
pET-21a(+)::*(n)p2_a1_(c)p2*(His)	(N)P2_A1_(C)P2	1100	1203 / 1220	HindIII / XhoI	491 / 492, 66 / 709	PstI	NtAQP1 with N- and C-terminus of NtPIP2;1

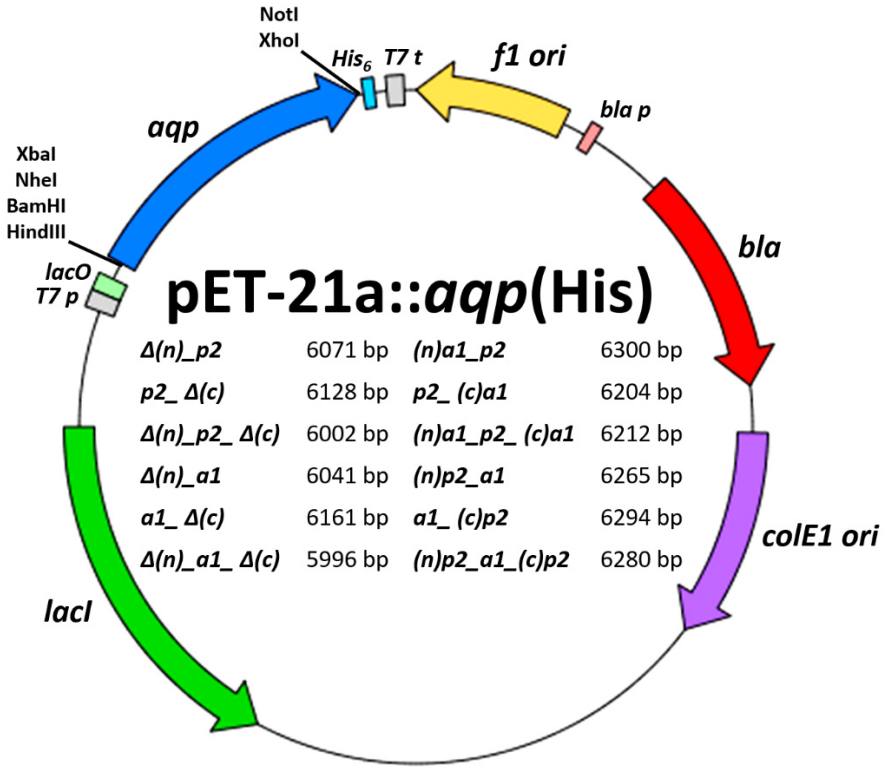

Fig. 20 – Exemplary overview on N- and C-terminal mutant constructs of *ntpip2;1* and *ntaqp1* genes in pET-21a plasmid backbones. Listed are all mutant target genes and the individual total sizes of their plasmids in amount of base pairs (bp). Δ(n/c) = mutant gene with N- or C-terminus deleted / (n)a1 = N-terminus of *ntaqp1* inserted for N-terminus of *ntpip2;1* (nomenclature analogous for other constructs) / *lacI* = Lac repressor coding region / T7 p = T7 promoter / *lacO* = Lac operator / *aqp* = *ntpip2;1* or *ntaqp1* mutated target gene / His_6 = C-terminal 6xHis tag / T7 t = T7 terminator / *f1 ori* = f1 phage origin of replication / *bla p* = β-lactamase promoter / bla = β-lactamase coding region (confers ampicillin resistance) / *colE1 ori* = *E. coli* origin of replication.

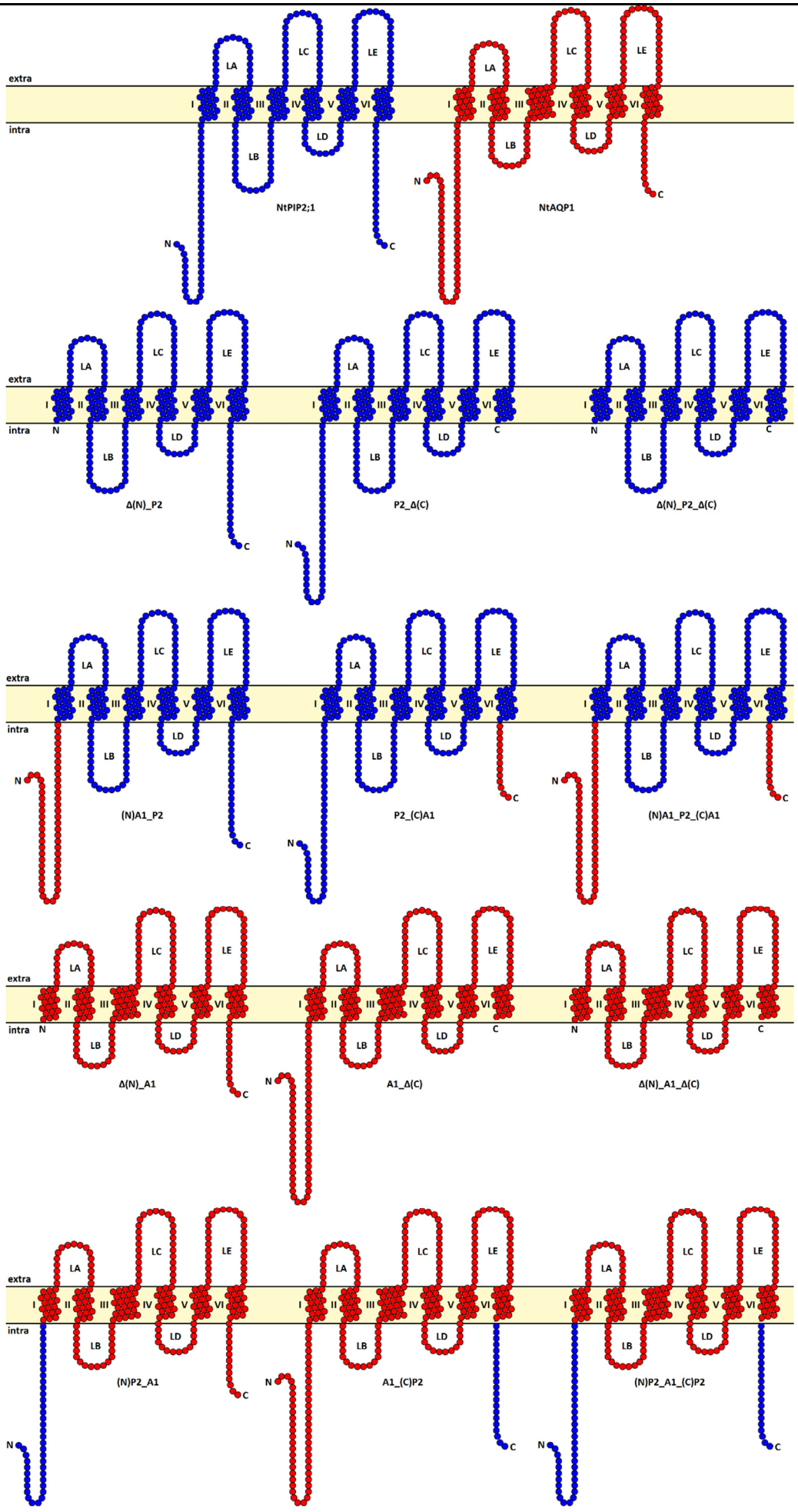
extra
intra
LA
LB
LC
LD
LE
I
II
III
IV
V
VI
N
C
NtPIP2;1
NtAQP1
Δ(N)_P2
P2_Δ(C)
Δ(N)_P2_Δ(C)
(N)A1_P2
P2_(C)A1
(N)A1_P2_(C)A1
Δ(N)_A1
A1_Δ(C)
Δ(N)_A1_Δ(C)
(N)P2_A1
A1_(C)P2
(N)P2_A1_(C)P2

Fig. 21 (previous page) – Schematic representation of wildtype and mutant aquaporin constructs integrated into lipid bilayers generated via Protter online tool [Omasits *et al.* 2014]. Wildtype derived sequences are colored in blue (NtPIP2;1) and red (NtAQP1). Transmembrane helices are depicted with roman numerals I – VI, whereas loops are designated LA – LE. Amine- (N) and Carboxy-termini (C), as well as the designations for extra- and intracellular spaces are also included.

3.3 Establishment of D-CF

3.3.1 Influence of lipid concentration and reconstitution mix on water permeability of PC liposomes

In order to analyze the impact of varying lipid concentrations and the application of a reconstitution mix on PC liposomes, 0.2 µm extrusion samples (see chapters 2.7.3 and 2.8.6) set to 1 mg/ml and 4 mg/ml in HN buffer were divided up into two groups each. One group underwent a reconstitution mix with subsequent detergent removal via SM-2 biobeads and ultra centrifugation (see chapters 2.8.1, 2.8.4 and 2.8.5) before Stopped Flow water permeability measurements (see chapter 2.9), whereas the other was measured right after dilution to its desired lipid concentration. Fig. 22 and Table 18 give an overview on the obtained water permeability results.

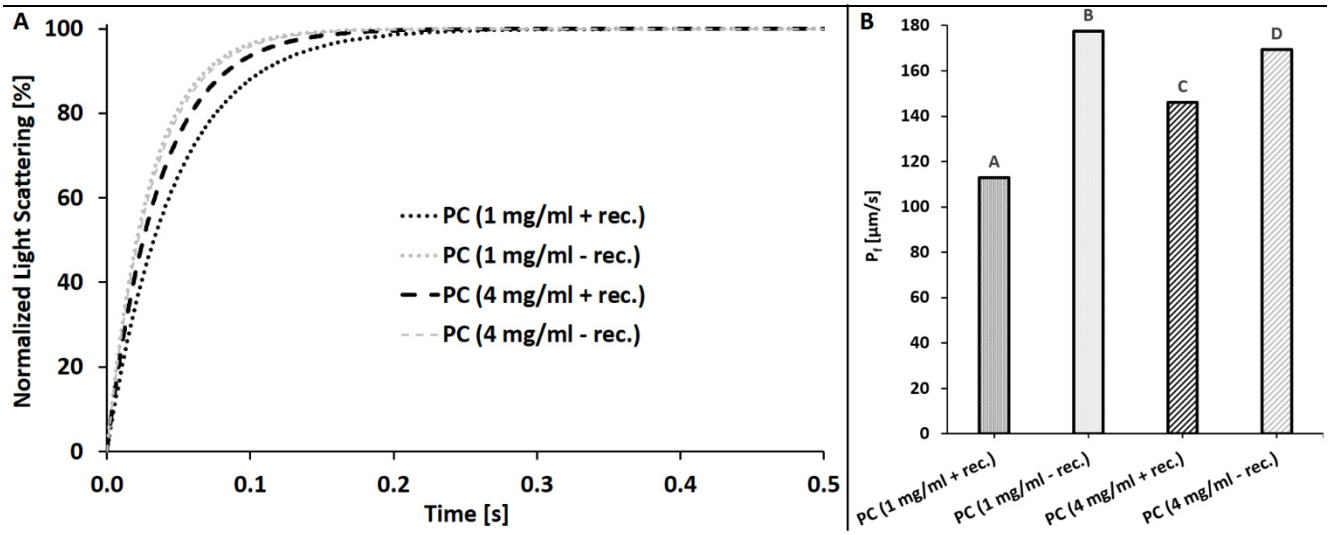

Fig. 22 – Water permeability measurements of L-α-phosphatidylcholine derived liposomes (PC) at varying lipid concentrations and in dependence of a reconstitution mix via Stopped Flow assay. Normalized light scattering kinetics measured at 436 nm are the result of shrinking liposomes via a hyperosmotically induced gradient. Each kinetic shown (A) is an average of several individual raw kinetics of one sample (see Table 18), that were fitted to an exponential rise equation. Water permeability values are based on the steepness of the slopes and are shown as distance over time in µm/s in the form of the water permeability factor P_f (B). Listed in parentheses are lipid concentrations in mg/ml, as well as the inclusion (+ rec.) or absence (- rec) of a reconstitution mix in the preparation of the liposome samples. Letters on top of the P_f columns indicate statistical significance groups determined via a two-tailed t-Test ($p < 0.05$), whereas error bars illustrate standard error.

Table 18 – Water permeability and statistical significance data of L-α-phosphatidylcholine derived liposomes (PC) at varying lipid concentrations and in dependence of a reconstitution mix via Stopped Flow assay. Given are average values ± standard error (SE) derived from n number of samples for kinetic slope steepness constant k, water permeability factor P_f and fitting distance F_D as an indicator for the quality of the fitted kinetics shown in Fig. 21. p values derived from a two-tailed t-Test are shown for each sample pair and divided up into 5 significance levels: ns = not significant ($p > 0.05$) / * = significant ($0.01 < p < 0.05$) / ** = very significant ($0.001 < p < 0.01$) / * = extremely significant ($0.0001 < p < 0.001$) / **** = extremely significant ($p < 0.0001$).**

Sample	k ± SE [s^{-1}]	P_f ± SE [µm/s]	F_D ± SE [%]	n
PC (1 mg/ml + rec.)	21.21 ± 0.04	112.95 ± 0.22	5.30 ± 0.016	24
PC (1 mg/ml - rec.)	33.34 ± 0.04	177.49 ± 0.22	2.18 ± 0.005	26
PC (4 mg/ml + rec.)	27.46 ± 0.02	146.20 ± 0.13	1.70 ± 0.004	26
PC (4 mg/ml - rec.)	31.83 ± 0.02	169.48 ± 0.13	1.24 ± 0.003	26

p	PC (4 mg/ml - rec.)	PC (4 mg/ml + rec.)	PC (1 mg/ml - rec.)
PC (1 mg/ml + rec.)	**** $1.41x10^{-34}$	**** $3.75x10^{-26}$	**** $5.24x10^{-39}$
PC (1 mg/ml - rec.)	**** $3.37x10^{-7}$	**** $2.96x10^{-25}$	- -
PC (4 mg/ml + rec.)	**** $5.06x10^{-30}$	- -	- -

It is apparent that both the lipid concentration and the application of a reconstitution mix significantly changed the water permeability of resulting PC liposomes. The inclusion of a reconstitution mix lowered the overall water permeability by 15 to 35 %, whereas a four-fold increase in lipid concentration either increased or decreased P_f values by 30 % or 5 %, respectively, when a reconstitution mix was either included or left out. In addition, the obtained fitting distance values increased by a factor of 2 to 3 when the lipid concentration was lowered from 4 to 1 mg/ml, which impacted the quality of the fitted kinetics derived from the raw data curves. These results eliminated the possibility of omitting the reconstitution mix for PC liposomes for time efficiency purposes in future experiments, when comparing them to proteoliposomes. However, the impact of the lipid concentration on the fitting distance and thus the non-linear regression quality on raw data curves necessitated further investigation with proteoliposomes.

3.3.2 Influence of lipid concentration on fitting quality and water permeability of PC + NtPIP2;1 proteoliposomes

Based on the results in chapter 3.3.1, the influence of lipid concentration on the fitting distance and water permeability of PC liposomes and PC + NtPIP2;1 proteoliposomes was investigated. NtPIP2;1 was produced in D-CF mode by using a total of seven CECF reactors (see chapters 2.7.5 and 2.8.1). After harvesting the reaction mixes, they were pooled and underwent IMAC purification (see chapter 2.8.3). The purification results are shown in Fig. 23 via SDS-PAGE analysis (see chapter 2.6.2).

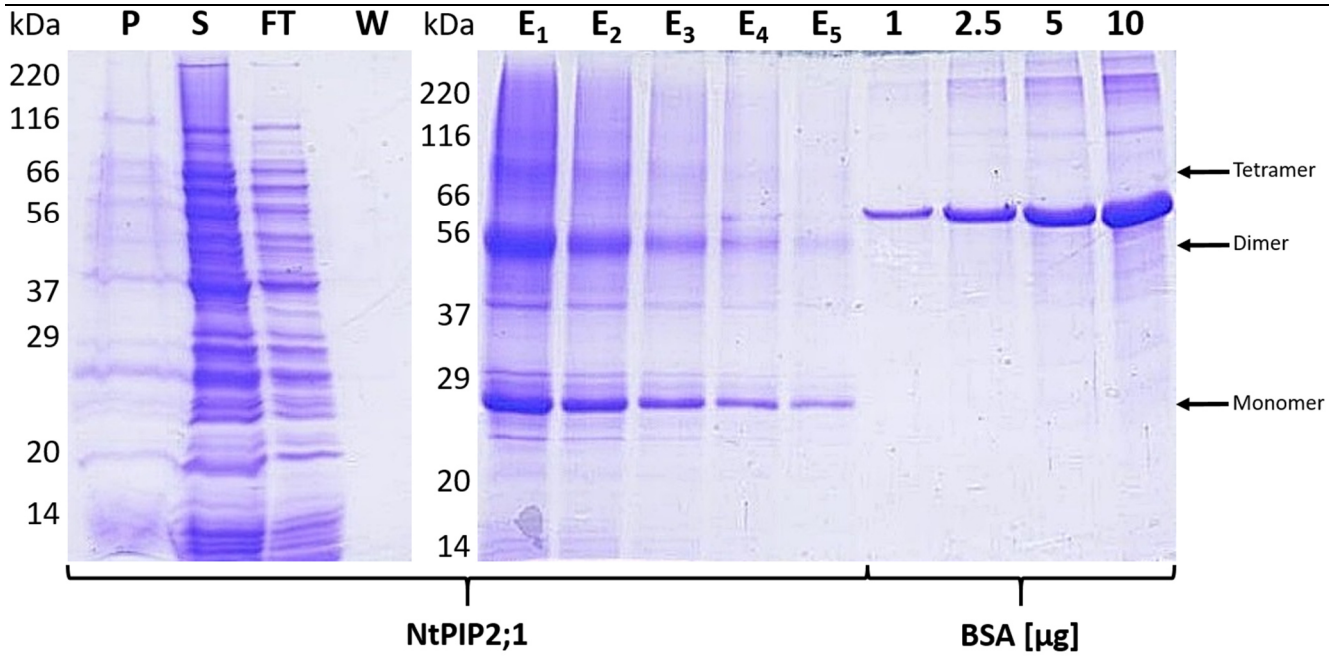

Fig. 23 – SDS-PAGE analysis of D-CF produced NtPIP2;1, which underwent subsequent IMAC purification via its C-terminally attached His_6 tag. Specific amounts of bovine serum albumin (BSA) helped determine the amount of NtPIP2;1 in elution fractions via trace quantity *in silico* analysis in Quantity One software (Bio-Rad, Hercules, California, USA). Arrows indicated approximate molecular weight of NtPIP2;1 monomeric, dimeric and tetrameric configurations. Protein standard = ProteMix (Anamed Elektrophorese GmbH, Groß-Bieberau, Germany) / P = 20 µl pellet fraction of centrifuged D-CF reaction mixes / S = 5 µl supernatant fraction of centrifuged D-CF reaction mixes / FT = 20 µl flowthrough of IMAC column after loading with supernatant RM fraction / W = 20 µl pooled wash fractions / E_1 – E_5 = 10 µl each of elution fractions 1-5.

The successful purification of D-CF produced NtPIP2;1 showed three distinct protein bands in the analyzed elution fractions at ~26 kDa, ~54 kDa and ~90 kDa representing three different aquaporin configurations as monomers, dimers and tetramers, respectively. Since SDS-PAGE samples were only heated to 37 °C for 20 min, such tertiary structures were expected. *In silico* quantification of NtPIP2;1 content in these three bands via trace quantity analysis in Quantity One software (Bio-Rad, Hercules, California, USA) and comparison to the included BSA samples resulted in a total protein amount of 620 µg with an average aquaporin concentration of 1.6 mg/ml in the initial RM. The obtained protein was then reconstituted into PC liposomes at a ratio of 100 µg protein per mg liposomes and total lipid concentrations of 1 mg/ml and 4 mg/ml (see chapter 2.8.4). Detergents were subsequently removed via SM-2 biobeads application (see chapter 2.8.5). Two additional samples of PC liposomes at 1 mg/ml and 4 mg/ml lipid concentration were included from the reconstitution step onwards without the addition of NtPIP2;1 as empty liposome controls. After detergent removal and prior to Stopped Flow water permeability measurements, all four samples were homogenized by extrusion through a 0.2 µm membrane (see chapter 2.8.6). Fig. 24 and Table 19 give an overview on the obtained data.

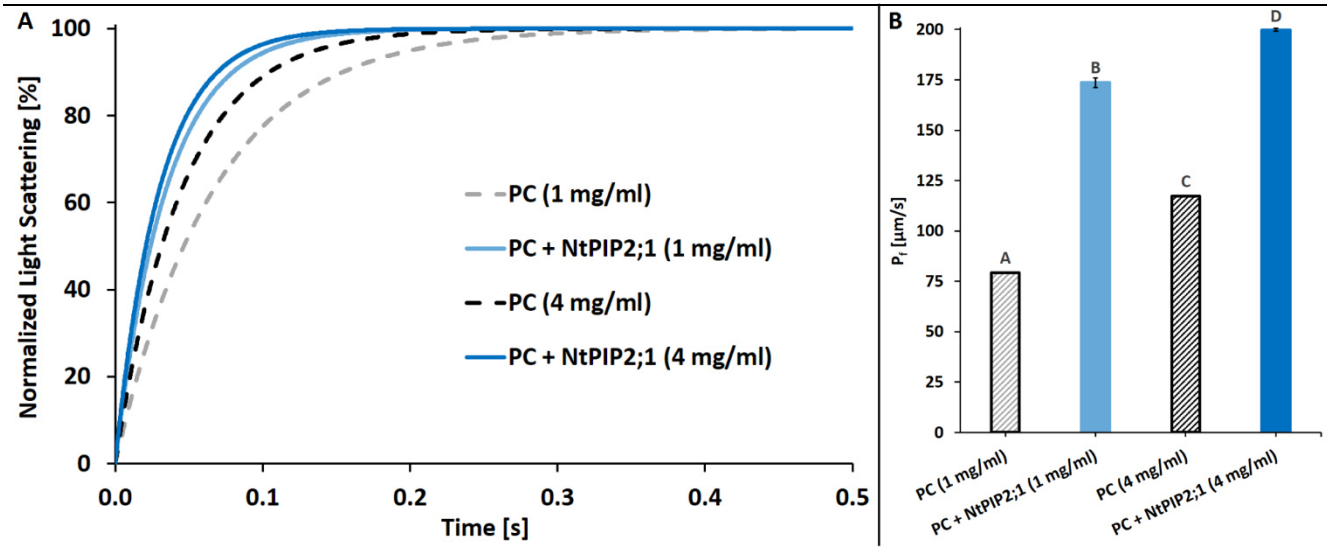

Fig. 24 – Water permeability measurements of L-α-phosphatidylcholine derived liposomes (PC) and D-CF produced NtPIP2;1 aquaporin reconstituted as proteoliposomes (PC + NtPIP2;1) at varying lipid concentrations via Stopped Flow assay. Normalized light scattering kinetics measured at 436 nm are the result of shrinking (proteo)liposomes via a hyperosmotically induced gradient. Each kinetic shown (A) is an average of several individual raw kinetics of one sample (see Table 19), that were fitted to an exponential rise equation. Water permeability values are based on the steepness of the slopes and are shown as distance over time in µm/s in the form of the water permeability factor P_f (B). Listed in parentheses are lipid concentrations in mg/ml. Letters on top of the P_f columns indicate statistical significance groups determined via a two-tailed t-Test ($p < 0.05$), whereas error bars illustrate standard error.

Table 19 – Water permeability and statistical significance data of L-α-phosphatidylcholine derived liposomes (PC) and D-CF produced NtPIP2;1 aquaporin reconstituted as proteoliposomes (PC + NtPIP2;1) at varying lipid concentrations via Stopped Flow assay. Given are average values ± standard error (SE) derived from n number of samples for kinetic slope steepness constant k, water permeability factor P_f and fitting distance F_D as an indicator for the quality of the fitted kinetics shown in Fig. 23. p values derived from a two-tailed t-Test are shown for each sample pair and divided up into 5 significance levels: ns = not significant ($p > 0.05$) / * = significant ($0.01 < p < 0.05$) / ** = very significant ($0.001 < p < 0.01$) / * = extremely significant ($0.0001 < p < 0.001$) / **** = extremely significant ($p < 0.0001$).**

Sample	k ± SE [s^{-1}]	P_f ± SE [µm/s]	F_D ± SE [%]	n
PC (1 mg/ml)	14.88 ± 0.04	79.20 ± 0.21	3.68 ± 0.011	23
PC + NtPIP2;1 (1 mg/ml)	28.85 ± 0.40	173.65 ± 2.41	12.17 ± 0.117	32
PC (4 mg/ml)	22.02 ± 0.03	117.25 ± 0.14	2.90 ± 0.008	15
PC + NtPIP2;1 (4 mg/ml)	33.21 ± 0.13	199.85 ± 0.79	1.99 ± 0.020	12

p	PC + NtPIP2;1 (4 mg/ml)	PC (4 mg/ml)	PC + NtPIP2;1 (1 mg/ml)
PC (1 mg/ml)	**** 9.01×10^{-16}	**** 2.82×10^{-34}	**** 1.06×10^{-7}
PC + NtPIP2;1 (1 mg/ml)	* 0.0189	**** 4.15×10^{-5}	- -
PC (4 mg/ml)	**** 8.16×10^{-13}	- -	- -

Analogously to the previously obtained results in chapter 3.3.1, an increase in lipid concentration from 1 mg/ml to 4 mg/ml raised the measured water permeability of PC liposomes and PC + NtPIP2;1 proteoliposomes by 50 % and 15 %, respectively. The integration of NtPIP2;1 resulted in a 70 to 110 % boost in water permeability compared to PC liposome controls, depending on the applied lipid concentration. Also, F_D values recurrently decreased significantly when the lipid concentration was increased, with PC + NtPIP2;1 samples showing a 6-fold difference, whereas their PC counterparts only showed a change of 30 %. In order to better visualize this difference in F_D values, Fig. 25 gives an overview on the obtained raw kinetics from all samples.

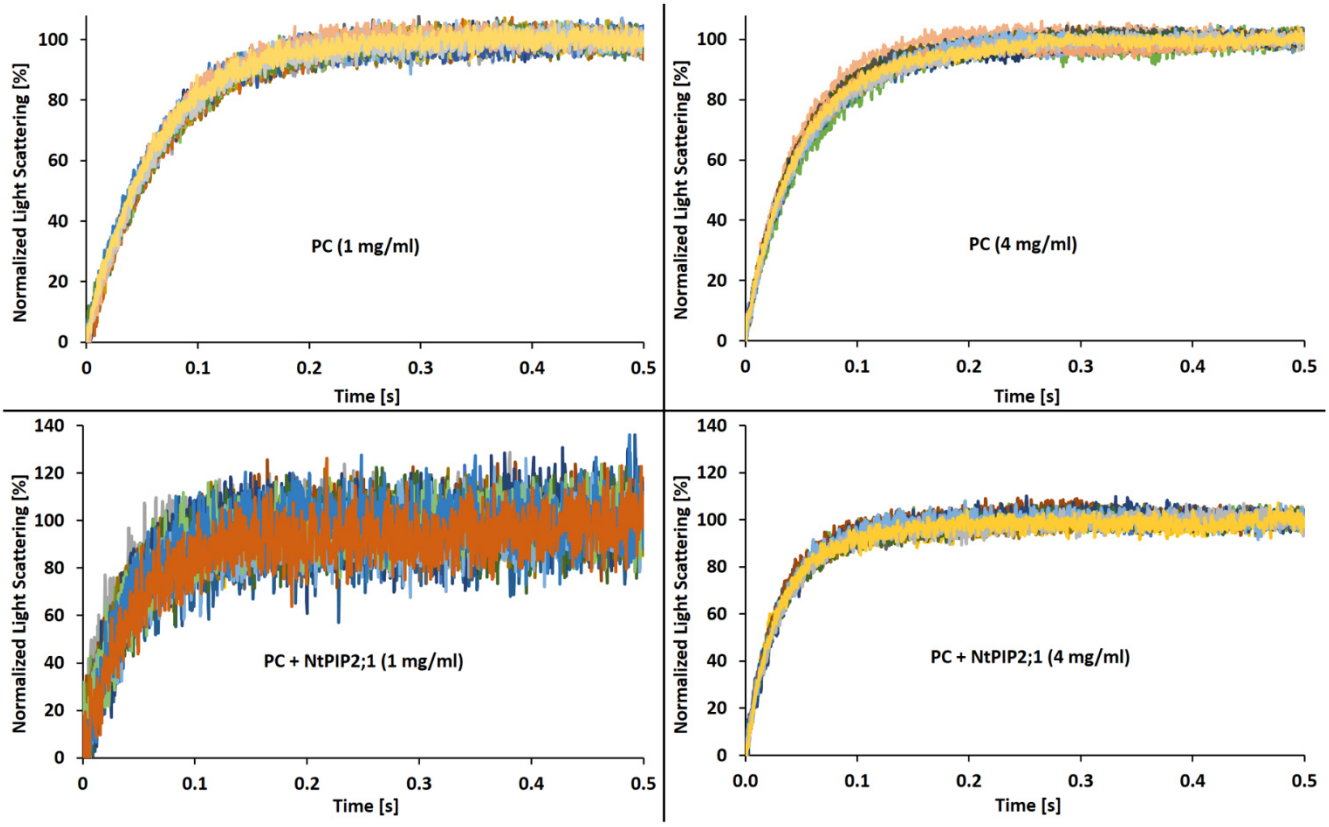

Fig. 25 – Water permeability measurements of L-α-phosphatidylcholine derived liposomes (PC) and D-CF produced NtPIP2;1 aquaporin reconstituted as proteoliposomes (PC + NtPIP2;1) at varying lipid concentrations via Stopped Flow assay. Normalized raw light scattering kinetics measured at 436 nm are the result of shrinking (proteo)liposomes via a hyperosmotically induced gradient.

The raw kinetics clearly show that the 6-fold increase in fitting distance values of PC + NtPIP2;1 proteoliposome water permeability measurements are based on a significant increase in noise when lowering the lipid concentration from 4 mg/ml to 1 mg/ml. In contrast, the 30 % difference in F_D values of PC samples is barely noticeable at the lower lipid concentration. To ensure a higher fitting quality in subsequent Stopped Flow experiments, 4 mg/ml was thus adopted as the lipid concentration of choice in the generation of (proteo)liposomes.

3.3.3 Influence of protein to liposome ratio during D-CF reconstitution on water permeability of PC + NtPIP2;1 proteoliposomes

Since the reconstitution of purified aquaporin into liposomes was found to be a critical step in the downstream processing of D-CF samples, the protein to liposome ratio was the next aspect to be analyzed. Shifting the ratio towards the protein side could potentially improve the integration into liposomes and thus provide a larger difference (and with it a wider range) in water permeability of proteoliposomes compared to empty PC liposomes. The preparation of PC + NtPIP2;1 proteoliposomes derived from a total of 24 D-CF reactors and PC liposomes was performed as described in chapter 3.3.2, with the purification results being shown in Fig. 26. NtPIP2;1 monomer and dimer signals can be discerned at ~26 and ~52 kDa, respectively, with tetramer bands not as distinctive as previously shown in Fig. 23. A comparison of the aquaporin signals with the included BSA samples resulted in a total of 993 µg purified protein and an average concentration of 0.77 mg/ml in the initial RM. Purified NtPIP2;1 to PC liposome ratios of 5, 10, 25, 50 and 75 µg/mg were applied in the subsequent reconstitution mixes and aliquots of proteoliposome samples ready for Stopped Flow measurements were analyzed via Western Blotting (see chapter 2.6.3), together with previously drawn purification samples (Fig. 27).

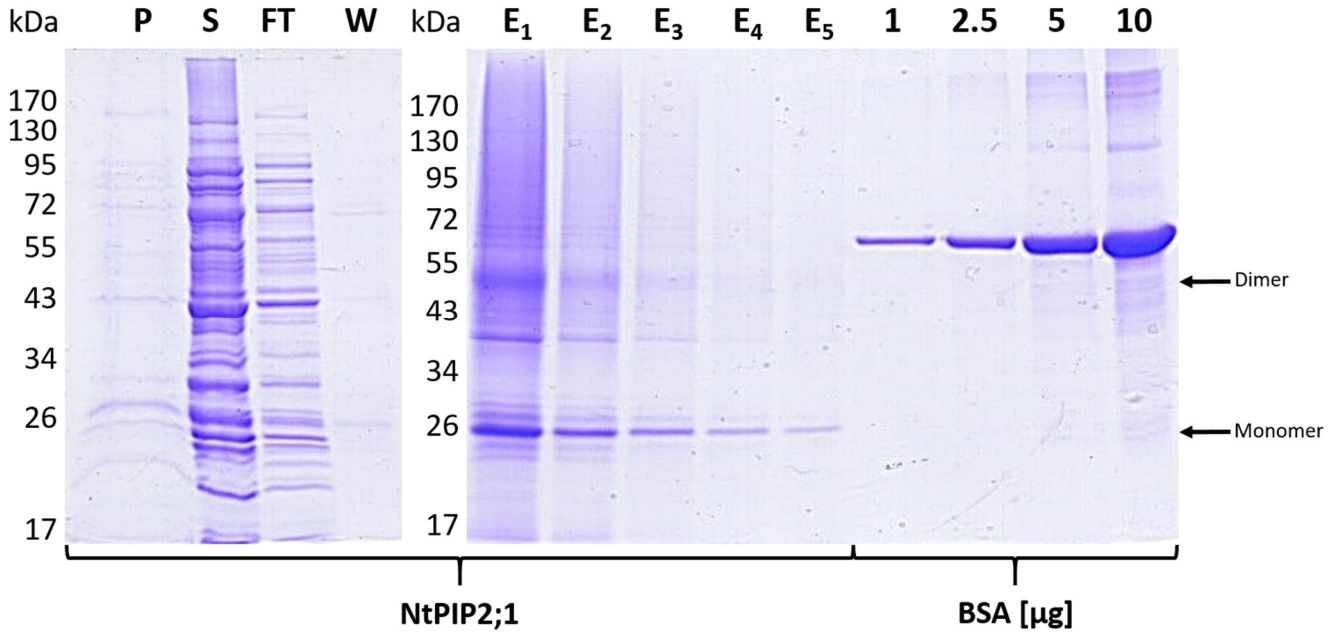

Fig. 26 – SDS-PAGE analysis of D-CF produced NtPIP2;1, which underwent subsequent IMAC purification via its C-terminally attached His_6 tag. Specific amounts of bovine serum albumin (BSA) helped determine the amount of NtPIP2;1 in elution fractions via trace quantity *in silico* analysis in Quantity One software (Bio-Rad, Hercules, California, USA). Arrows indicated approximate molecular weight of NtPIP2;1 monomeric and dimeric configurations. Protein standard = PageRuler Prestained Protein Ladder (Thermo Scientific, Waltham, Massachusetts, USA) / P = 20 µl pellet fraction of centrifuged D-CF reaction mixes / S = 5 µl supernatant fraction of centrifuged D-CF reaction mixes / FT = 20 µl flowthrough of IMAC column after loading with supernatant RM fraction / W = 20 µl pooled wash fractions / E_1 – E_5 = 10 µl each of elution fractions 1-5.

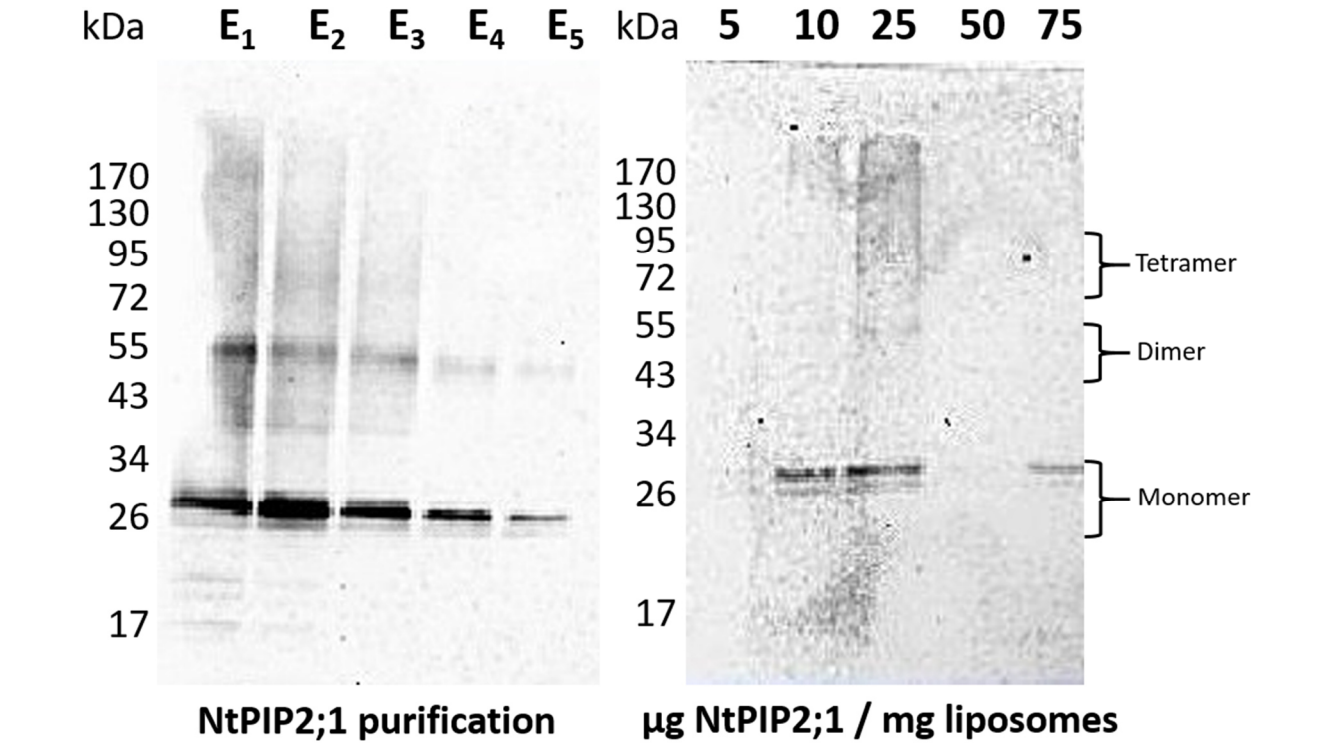

Fig. 27 – Immunological detection of C-terminal His_6 tags attached to D-CF produced NtPIP2;1 after IMAC purification (left) and chloroform / methanol extraction out of assembled PC + NtPIP2;1 proteoliposomes ready for Stopped Flow measurements (right). Brackets indicate approximate molecular weight of NtPIP2;1 monomeric, dimeric and tetrameric configurations. Primary antibody = Mouse anti-polyHis IgG / Secondary Antibody = Alkaline phosphatase-conjugated goat anti-mouse IgG / Detection type = Chemiluminescence with an exposure time of 600 s / Protein Standard = PageRuler Prestained Protein Ladder (Thermo Scientific, Waltham, Massachusetts, USA) / E_1 – E_5 = 10 µl each of elution fractions 1 -5 / 5 – 75 = Isolated protein equivalent to one D-CF RM each.

The detected signals in the purification samples correspond with the NtPIP2;1 bands pointed out in Fig. 26. Analogous signals were also detected in protein samples isolated from PC + NtPIP2;1 proteoliposomes, albeit with significantly weaker intensity. The absence of a signal at 50 µg protein per mg liposomes and the, in

comparison with 10 and 25 µg/mg, weaker signal in the 75 µg/mg sample can most likely be connected to an inherent complicacy in D-CF downstream processing, which is discussed in more detail at the end of this chapter. An overview on Stopped Flow derived water permeability data is shown in Fig. 28 and Table 20.

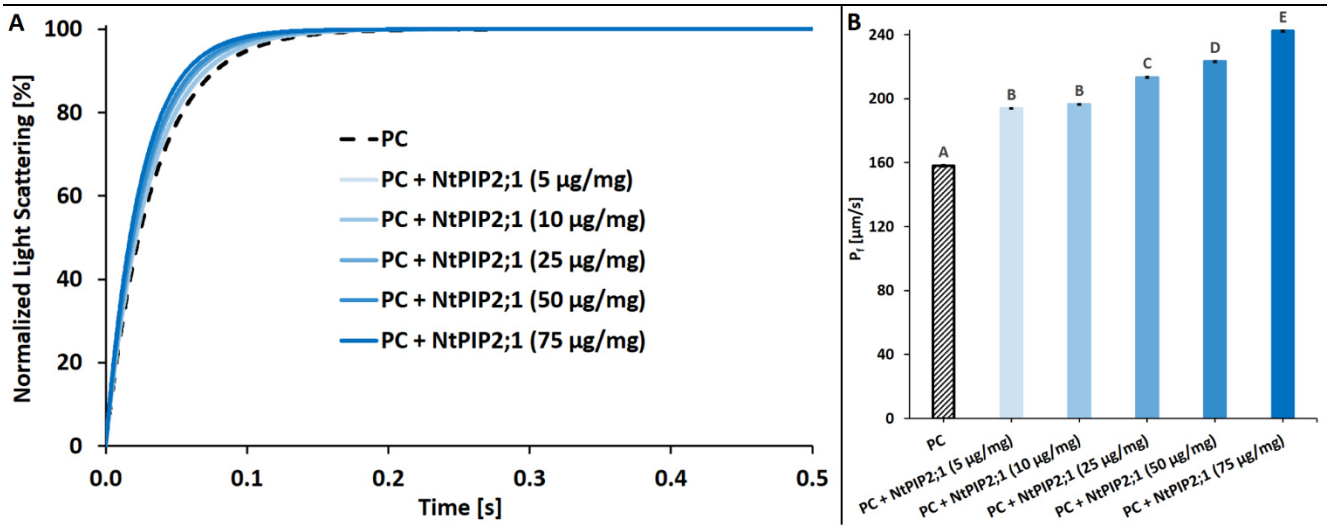

Fig. 28 – Water permeability measurements of L-α-phosphatidylcholine derived liposomes (PC) and D-CF produced NtPIP2;1 aquaporin reconstituted as proteoliposomes (PC + NtPIP2;1) at varying protein to liposome ratios via Stopped Flow assay. Normalized light scattering kinetics measured at 436 nm are the result of shrinking (proteo)liposomes via a hyperosmotically induced gradient. Each kinetic shown (A) is an average of several individual raw kinetics of one sample (see Table 20), that were fitted to an exponential rise equation. Water permeability values are based on the steepness of the slopes and are shown as distance over time in µm/s in the form of the water permeability factor P_f (B). Listed in parentheses are protein to liposomes ratios applied during reconstitution in µg/mg. Letters on top of the P_f columns indicate statistical significance groups determined via a two-tailed t-Test ($p < 0.05$), whereas error bars illustrate standard error.

Table 20 – Water permeability and statistical significance data of L-α-phosphatidylcholine derived liposomes (PC) and D-CF produced NtPIP2;1 aquaporin reconstituted as proteoliposomes (PC + NtPIP2;1) at varying protein to liposome ratios via Stopped Flow assay. Given are average values ± standard error (SE) derived from n number of samples for kinetic slope steepness constant k, water permeability factor P_f and fitting distance F_D as an indicator for the quality of the fitted kinetics shown in Fig. 27. p values derived from a two-tailed t-Test are shown for each sample pair and divided up into 5 significance levels: ns = not significant ($p > 0.05$) / * = significant ($0.01 < p < 0.05$) / ** = very significant ($0.001 < p < 0.01$) / * = extremely significant ($0.0001 < p < 0.001$) / **** = extremely significant ($p < 0.0001$).**

Sample	k ± SE [s^{-1}]	P_f ± SE [µm/s]	F_D ± SE [%]	n
PC	29.68 ± 0.12	158.00 ± 0.65	2.61 ± 0.062	14
PC + NtPIP2;1 (5 µg/mg)	32.21 ± 0.08	193.86 ± 0.49	2.69 ± 0.009	15
PC + NtPIP2;1 (10 µg/mg)	32.62 ± 0.07	196.35 ± 0.44	2.50 ± 0.010	16
PC + NtPIP2;1 (25 µg/mg)	35.45 ± 0.11	213.37 ± 0.63	2.56 ± 0.015	15
PC + NtPIP2;1 (50 µg/mg)	37.10 ± 0.09	223.31 ± 0.54	2.28 ± 0.015	13
PC + NtPIP2;1 (75 µg/mg)	40.27 ± 0.09	242.39 ± 0.55	2.38 ± 0.020	11

p	PC + NtPIP2;1 (75 µg/mg)	PC + NtPIP2;1 (50 µg/mg)	PC + NtPIP2;1 (25 µg/mg)	PC + NtPIP2;1 (10 µg/mg)	PC + NtPIP2;1 (5 µg/mg)
PC	**** 2.26×10^{-18}	**** 6.69×10^{-17}	**** 5.91×10^{-15}	**** 4.41×10^{-13}	**** 8.67×10^{-12}
PC + NtPIP2;1 (5 µg/mg)	**** 5.27×10^{-15}	**** 9.64×10^{-11}	**** 1.46×10^{-6}	ns 0.3568	- -
PC + NtPIP2;1 (10 µg/mg)	**** 2.84×10^{-15}	**** 1.74×10^{-10}	**** 6.07×10^{-6}	- -	- -
PC + NtPIP2;1 (25 µg/mg)	**** 9.81×10^{-9}	** 0.0061	- -	- -	- -
PC + NtPIP2;1 (50 µg/mg)	**** 9.35×10^{-7}	- -	- -	- -	- -

The results show a steady rise in P_f values with increasing protein to liposome ratios during reconstitution of NtPIP2;1 into PC liposomes, topping out at a 53 % higher water permeability than in control PC liposomes. In combination with F_D values in the range of 2.3 to 2.7 %, representative of a high fitting quality, this indicates an improved integration of IMAC purified aquaporin during reconstitution, when the ratio is shifted towards the protein side. However, since the purified aquaporin content in the IMAC elution fractions could only be approximated via *in silico* analysis and the maximum protein integration capacity of the applied PC liposomes is unknown, it was difficult to determine an optimal ratio during reconstitution. An additional predicament became clear during the extrusion process for the size homogenization of the proteoliposomes: with an increasing protein to liposome ratio, the resistance of the applied polycarbonate membrane increased dramatically from 50 µg/mg onwards, to the point of rupture. Even if such could be avoided by careful handling of the extruder, proteoliposome retention at the membrane due to higher concentrations of non-integrated and thus precipitated protein blocking the pores could not. This process was inevitable due to the inefficiency of reconstituting D-CF derived and IMAC purified protein into liposomes: the excessive presence of detergents (DDM from IMAC elution buffer and Triton X-100 during reconstitution itself) solubilized not only successfully generated proteoliposomes, but also a significant amount of non-integrated protein. It subsequently precipitated during detergent removal via SM-2 Biobeads application and caused the membrane blockage during extrusion. Proper adjustment of detergent volumes and biobead amounts in order to counteract this dilemma was also difficult and impractical, since these values are directly dependent on the highly variable aquaporin concentration in the IMAC elution fractions. Based on these findings, all subsequent experiments were based on L-CF instead of D-CF derived aquaporins.

3.4 Establishment of L-CF

3.4.1 Optimization of detergent to lipid ratio for the separation of proteoliposomes and precipitated protein

The direct addition of lipids to reaction mixes of L-CF reactors facilitated a more efficient and less time intensive integration of produced aquaporin into PC liposomes, as compared to D-CF. However, the previously described issue of separating successfully generated proteoliposomes from non integrated protein in order to avoid extrusion membrane blockage still remained. In contrast to the D-CF mode, a separate IMAC purification step was unnecessary for L-CF derived aquaporins, thus significantly lowering the complexity of the separation process. The omission of IMAC elution fractions highly variable in their aquaporin content in the reconstitution step created the possibility of adjusting the applied amount of Triton X-100 precisely to the amount necessary in order to solubilize exclusively proteoliposomes. A simple centrifugation was sufficient to separate the solubilized proteoliposomes from non integrated and precipitated protein. In order to determine the approximate detergent concentration necessary for separation, 4 mg/ml PC liposomes were solubilized in HN buffer (see chapter 2.7.3) and exposed to various concentrations of Triton X-100. At equal final volumes of 1.5 ml, the prepared samples were incubated at 1000 rpm for 1 h at RT, before centrifugation at 16,000 *g* for 2 h and RT. The resulting amount of precipitated liposomes would then indicate, at which detergent concentration 4 mg/ml liposomes could be completely solubilized as depicted in Fig. 29.
The first batch of samples restricted the solubility range to a value between 0.4 % and 0.7 % (v/v) Triton X-100. A second batch was then able to pinpoint the amount of detergent necessary to solubilize 4 mg/ml liposomes to 0.41 %, at which no liposome precipitation could be observed anymore. This set the basis to precisely adjust the amount of SM-2 biobeads necessary to remove 0.41 % (v/v) Triton X-100 and continue processing the proteoliposomes without the issues illustrated in connection with the D-CF mode.

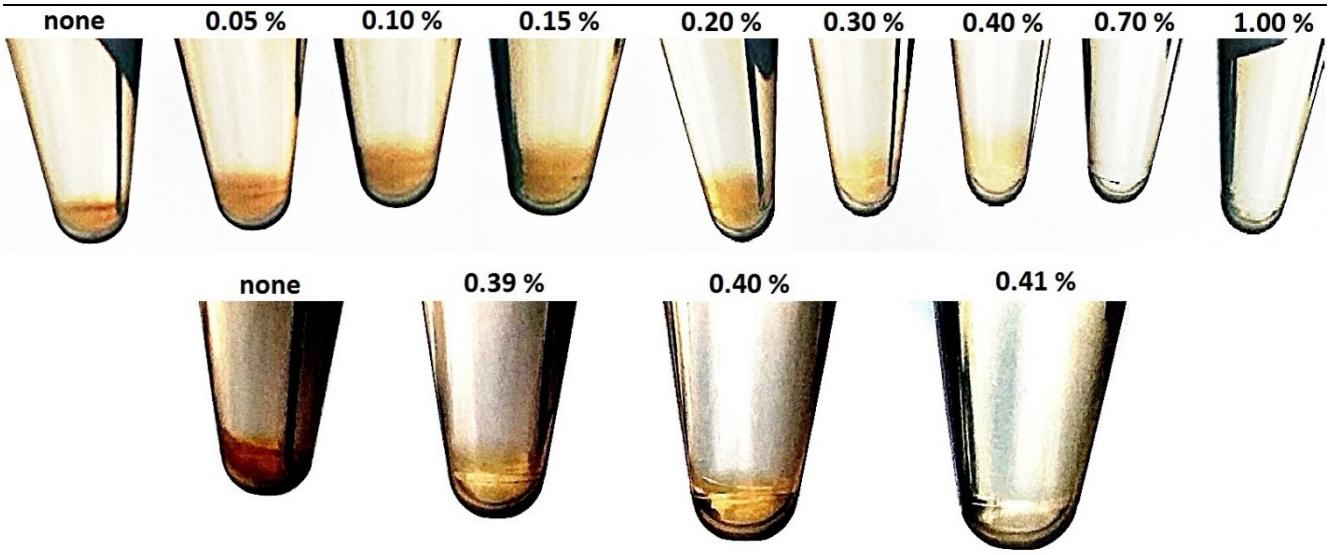

Fig. 29 – L-α-phosphatidylcholine derived liposomes (PC) and their solubility at various Triton X-100 concentrations. 4 mg/ml PC liposomes were solubilized in HN buffer and adjusted to a total volume of 1.5 ml at various Triton X-100 concentrations (v/v). Incubation of the samples at 1000 rpm for 1 h at RT preceded a centrifugation step for 2 h at 16,000 *g* and RT.

3.4.2 Optimization of Triton X-100 removal via SM-2 non-polar polystyrene biobeads in the reconstitution of PC liposomes

After determining the minimum concentration of Triton X-100 required to solubilize 4 mg/ml PC liposomes to be 0.41 % (v/v), the next step was to adjust the amount of SM-2 biobeads necessary to specifically remove the detergent and reconstitute the liposomes. For that purpose, a total of 9 samples were prepared, consisting of 4 mg/ml PC liposomes (see chapter 2.7.3) in HN buffer solubilized with 0.41 % (v/v) Triton X-100 in a total volume of 1 ml each. The samples were incubated at 1000 rpm for 1 h at RT, before SM-2 biobeads were added in steps of 20 mg, thus covering a range of 0 – 160 mg/ml sample. The beads were previously washed and equilibrated overnight in 4 mg/ml 0.2 µm extruded liposomes as described in chapter 2.8.5. Before Stopped Flow measurements, the samples were incubated with the biobeads overnight at 170 rpm, 30 °C and were subsequently extruded through a 0.2 µm membrane for size homogenization. Fig. 30 and Table 21 give an overview on the obtained results.

Based on the generated water permeability kinetics, a significant effect of remaining detergent is apparent in the samples without biobeads up to 40 mg/ml, above which a stabilization occurs at approximately 25 – 30 µm/s. The same is reflected in the F_D values, that stabilized from 60 mg/ml onwards in the range of 2.1 – 2.7 %. This indicates, that a minimum of 60 mg biobeads is necessary to remove 0.41 % (v/v) Triton X-100 from one ml sample containing 4 mg/ml PC liposomes. Supporting evidence was found during the extruding process preceding the Stopped Flow measurements: samples in the range of 0 – 40 mg/ml applied biobeads demonstrated excessive foaming inside the extruder, whereas the rest did not. Furthermore, a characteristic bend recurred exclusively in the obtained raw kinetics of the samples with 0 - 20 mg/ml biobeads (see Fig. 31). Even though that bend was missing in the raw kinetics obtained from the 40 mg/ml sample, its curves were noticeable flattened in their slope curvature when compared to those obtained from the samples in the range of 60 – 160 mg/ml applied biobeads (data not shown). In conclusion, the presented data provide a sufficient basis to continue biobead screening with PC + NtPIP2;1 proteoliposomes and the impact on their water permeability.

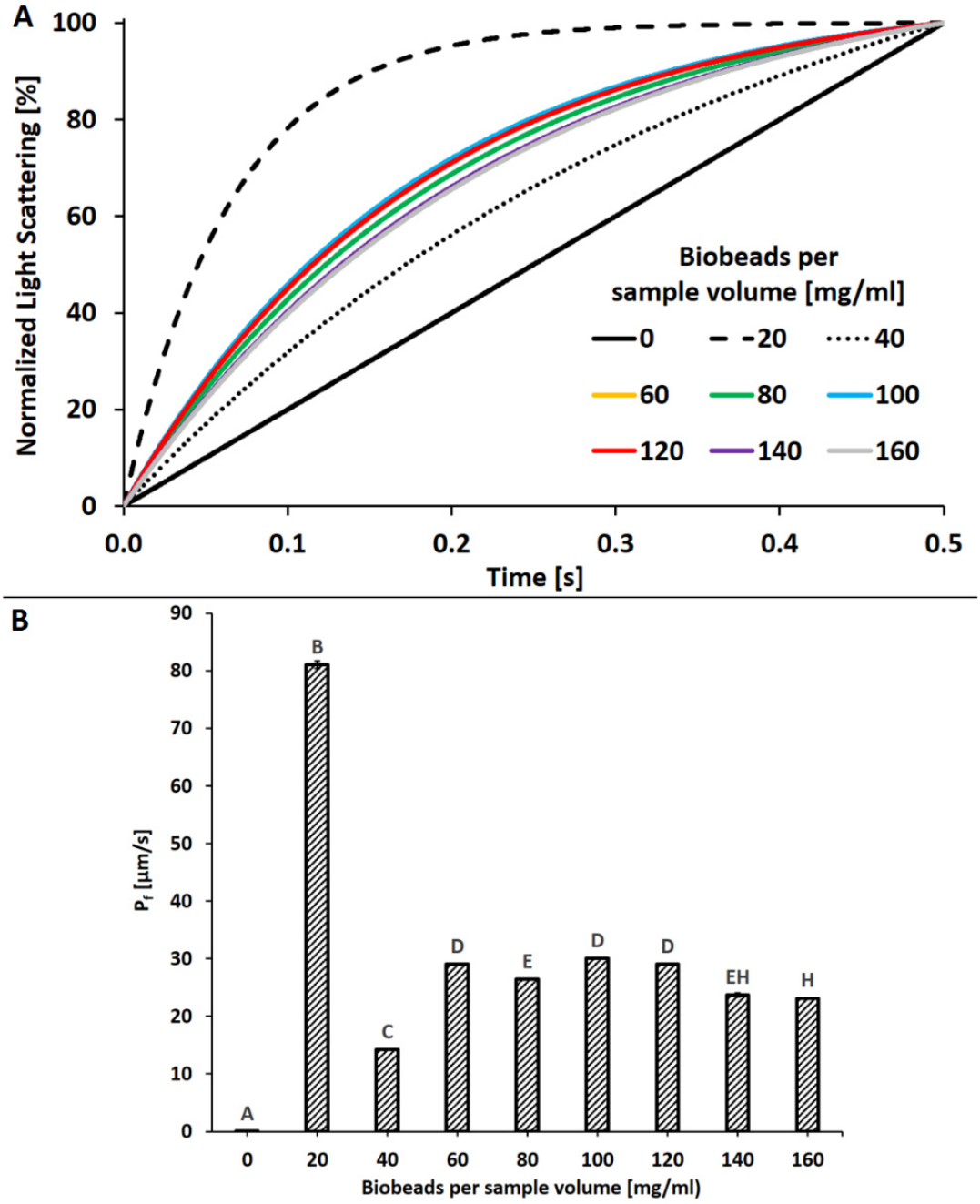

Fig. 30 – Stopped Flow water permeability measurements of L-α-phosphatidylcholine derived liposomes (PC) reconstituted with varying SM-2 biobead amounts after solubilization with Triton X-100. Normalized light scattering kinetics measured at 436 nm are the result of shrinking liposomes via a hyperosmotically induced gradient. Each kinetic shown (A) is an average of several individual raw kinetics of one sample (see Table 21), that were fitted to an exponential rise equation. Water permeability values are based on the steepness of the slopes and are shown as distance over time in µm/s in the form of the water permeability factor P_f (B). Listed are applied amounts of biobeads in mg per ml of solubilized liposomes. Letters on top of the P_f columns indicate statistical significance groups determined via a two-tailed t-Test ($p < 0.05$), whereas error bars illustrate standard error.

Table 21 – Stopped Flow water permeability and statistical significance data of L-α-phosphatidylcholine derived liposomes (PC) reconstituted with varying SM-2 biobead amounts after having been solubilized by Triton X-100. Given are average values ± standard error (SE) derived from n number of samples for kinetic slope steepness constant k, water permeability factor P_f and fitting distance F_D as an indicator for the quality of the fitted kinetics shown in Fig. 29. p values derived from a two-tailed t-Test are shown for each sample pair and divided up into 5 significance levels: ns = not significant (p > 0.05) / * = significant (0.01 < p < 0.05) / ** = very significant (0.001 < p < 0.01) / * = extremely significant (0.0001 < p < 0.001) / **** = extremely significant (p < 0.0001).**

mg/ml	k ± SE [s^{-1}]	P_f ± SE [µm/s]	F_D ± SE [%]	n
0	0.000275 ± 0.000004	0.00146 ± 0.00002	6.66 ± 0.027	33
20	15.22 ± 0.12	81.05 ± 0.64	3.26 ± 0.069	16
40	2.67 ± 0.01	14.19 ± 0.07	1.67 ± 0.004	17
60	5.47 ± 0.02	29.10 ± 0.12	2.32 ± 0.009	28
80	4.97 ± 0.02	26.45 ± 0.12	2.12 ± 0.006	27
100	5.65 ± 0.02	30.09 ± 0.11	2.20 ± 0.005	37
120	5.46 ± 0.02	29.08 ± 0.12	2.26 ± 0.006	29
140	4.45 ± 0.07	23.71 ± 0.36	2.38 ± 0.013	23
160	4.35 ± 0.02	23.17 ± 0.11	2.71 ± 0.042	36

mg/ml	160	140	120	100	80	60	40	20
0	**** $6.98x10^{-29}$	**** $3.84x10^{-12}$	**** $1.95x10^{-27}$	**** $1.17x10^{-32}$	**** $5.48x10^{-25}$	**** $3.02x10^{-27}$	**** $1.93x10^{-18}$	**** $6.35x10^{-15}$
20	**** $1.35x10^{-13}$	**** $1.55x10^{-20}$	**** $7.86x10^{-13}$	**** $8.95x10^{-13}$	**** $3.61x10^{-13}$	**** $9.11x10^{-13}$	**** $6.73x10^{-14}$	- -
40	**** $2.41x10^{-16}$	**** $1.87x10^{-5}$	**** $2.92x10^{-22}$	**** $1.35x10^{-25}$	**** $1.04x10^{-18}$	**** $1.20x10^{-22}$	- -	- -
60	**** $2.63x10^{-8}$	** 0.0073	ns 0.9806	ns 0.3096	** 0.0052	- -	- -	- -
80	*** 0.0010	ns 0.1535	** 0.0067	*** 0.0005	- -	- -	- -	- -
100	**** $4.56x10^{-10}$	** 0.0021	ns 0.3034	- -	- -	- -	- -	- -
120	**** $3.71x10^{-8}$	** 0.0078	- -	- -	- -	- -	- -	- -
140	ns 0.7736	- -	- -	- -	- -	- -	- -	- -

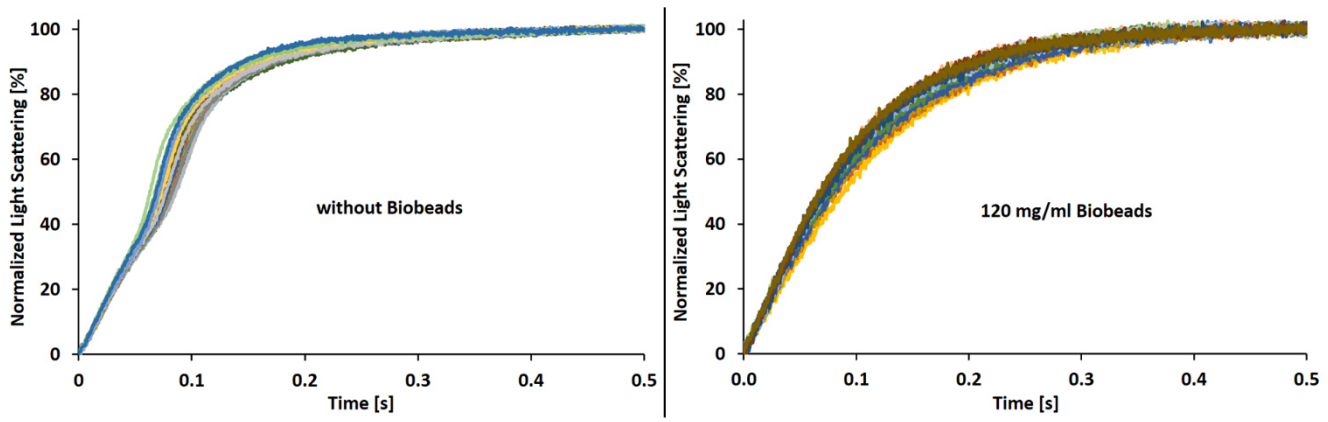

Fig. 31 – Stopped Flow water permeability measurements of 4 mg/ml L-α-phosphatidylcholine derived liposomes (PC) after being reconstituted from Triton X-100 solubilization at 0.41 % (v/v) via omission or addition of 120 mg/ml SM-2 non-polar polysterene biobeads (Bio-Rad, Hercules, California, USA). Normalized raw light scattering kinetics measured at 436 nm are the result of shrinking (proteo)liposomes via a hyperosmotically induced gradient.

3.4.3 Optimization of Triton X-100 removal via SM-2 non-polar polystyrene biobeads in the reconstitution of PC + NtPIP2;1 proteoliposomes

In order to determine the optimal application method of SM-2 biobeads in the reconstitution of L-CF produced PC + NtPIP2;1 proteoliposomes, a total of 24 L-CF reactors were set up (see chapter 2.7.5). Following the harvest, pooling and washing of the reaction mixes, the addition of 0.41 % (v/v) Triton X-100 allowed the separation of solubilized PC + NtPIP2;1 proteoliposomes from non-integrated and thus precipitated protein (see chapter 2.8.1). The equivalent of 1 RM was taken from the resulting supernatant for subsequent analysis via SDS-PAGE and Western Blotting (see chapters 2.8.7, 2.6.2 and 2.6.3), whereas the precipitated protein pellet was washed in MQ-H_2O and solubilized in 1x SDS Protein Denaturation Buffer.
The removal of detergent from the supernatant and thus the reconstitution of the solubilized proteoliposomes via SM-2 biobeads was comprised of several different application methods based on four differing factors (see chapters 2.8.5 and 2.8.6): equilibration of biobeads with 0.1 µm or 0.2 µm diameter liposomes, stepwise or direct addition of biobeads, total amount of biobeads added per sample volume and final incubation length. Diverging diameters of the liposomes used to equilibrate biobeads could potentially saturate the biobead pores more efficiently, so that unspecific absorption of proteoliposomes could be reduced or even avoided altogether. The type of addition and amount of biobeads used per sample could modulate the adsorption rate of Triton X-100 to improve the proper reconstitution of the solubilized PC + NtPIP2;1 proteoliposomes. Lastly, the incubation length could potentially improve the detergent adsorption of smaller amounts of biobeads when compared to shorter time spans with higher biobead amounts per sample volume. Based on those factors and on the results obtained in chapter 3.4.2, a total of four proteoliposome samples underwent different biobead applications:

Sample 1 = 0.1 µm liposomes for equilibration / 160 mg/ml direct addition / 1 overnight incubation
Sample 2 = 0.2 µm liposomes for equilibration / 160 mg/ml direct addition / 1 overnight incubation
Sample 3 = 0.2 µm liposomes for equilibration / 60 mg/ml direct addition / 2 overnight incubations
Sample 4 = 0.2 µm liposomes for equilibration / 4x40 mg/ml hourly stepwise addition / 1 overnight incubation

A separate PC liposome reaction without NtPIP2;1 served as a control for each application method and underwent the same subsequent downstream processing treatment as the respective proteoliposome counterparts.
Following detergent removal, the resulting sample supernatants underwent extrusion through 0.8 and 0.2 µm membranes (see chapters 2.8.1 and 2.8.6) and were diluted to identical OD_{436} values with HN buffer before Stopped Flow water permeability measurements commenced (see chapter 2.9). An equivalent of 1 RM from each proteoliposome sample was subjected to analysis of the contained protein via SDS-PAGE and Western Blotting (see chapters 2.8.7, 2.6.2 and 2.6.3). Fig. 32 and Table 22 give an overview on the obtained water permeability data, whereas Fig. 33 shows the results derived from SDS-PAGE and Western Blotting.
Based on the normalized water permeability of each proteoliposome sample, it is apparent that Sample 4 demonstrates the highest PC + NtPIP2;1 to PC water permeability ratio at 66 % higher than the included PC control. In comparison, sample 1 shows a significant 18 % higher P_f value for the PC control, whereas samples 2 and 3 do not show a statistical significance when comparing the proteoliposome samples with the empty control liposomes. The corresponding SDS-PAGE and Western Blot analysis also displays the highest detectable protein content in Sample 4 (4x40). Since current literature attests a high water permeability to NtPIP2;1 when compared to controls (see chapter 1.5.1), the stepwise addition of SM-2 biobeads seemed to provide the most efficient reconstitution of previously solubilized proteoliposomes with the highest yield of properly functioning

aquaporin. It was thus adopted as the biobead application method of choice for any ensuing water permeability experiments.

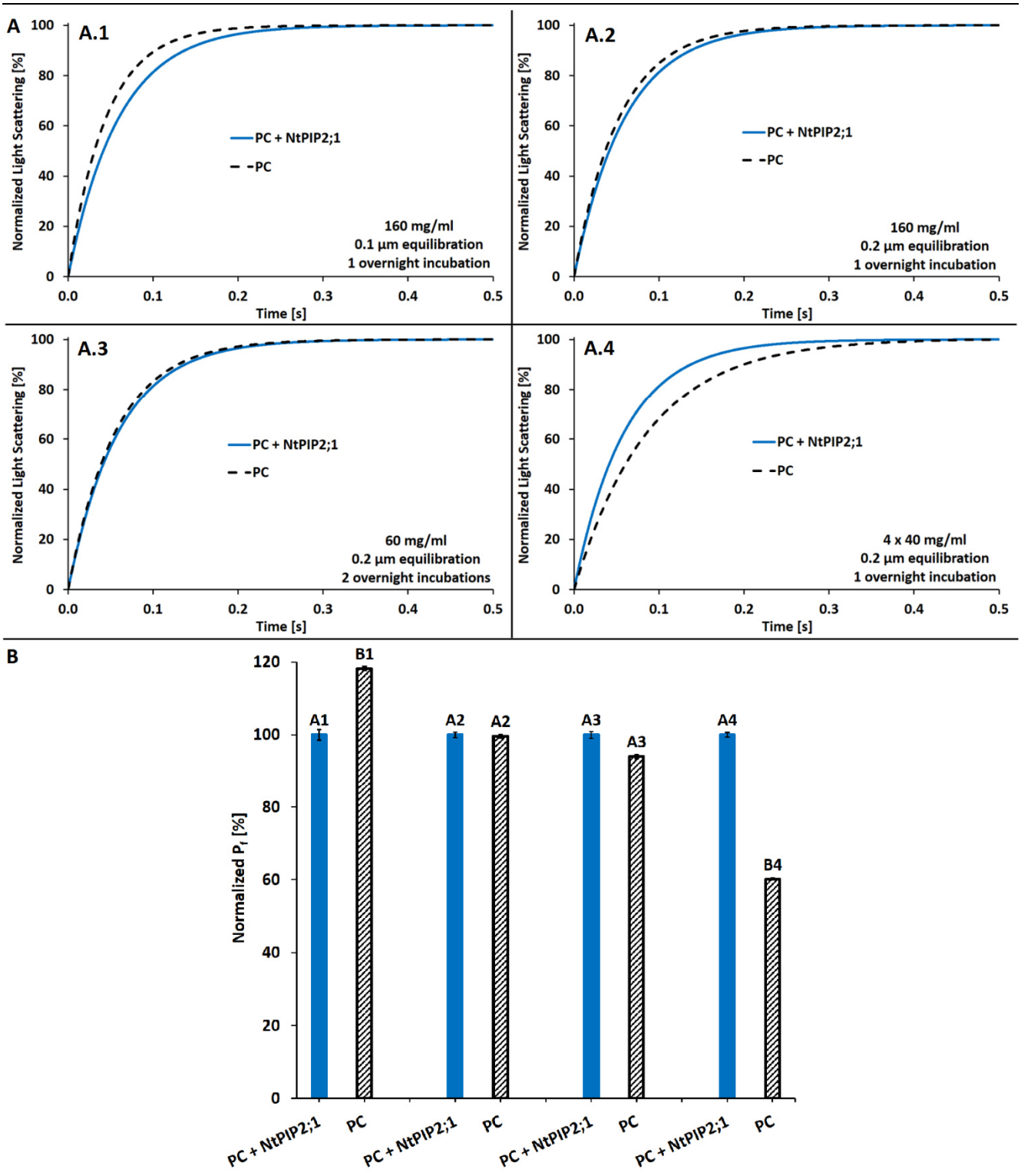

Fig. 32 – Stopped Flow water permeability measurements of L-α-phosphatidylcholine derived liposomes (PC) and L-CF derived PC + NtPIP2;1 proteoliposomes reconstituted with varying SM-2 biobead amounts after having been solubilized by Triton X-100. Normalized light scattering kinetics measured at 436 nm are the result of shrinking liposomes via a hyperosmotically induced gradient. Each kinetic shown (A) is an average of several individual raw kinetics of one sample (see Table 22), that were fitted to an exponential rise equation. Water permeability values are based on the steepness of the slopes and are shown as percentage normalized to respective PC + NtPIP2;1 proteoliposome samples in the form of the water permeability factor P_f (B). Listed are applied amounts of biobeads in mg per ml of solubilized liposomes, the diameter size of the liposomes used to equilibrate the biobeads and the length of sample incubation with the equilibrated biobeads, making up a total of four different sample configurations (A.1 – A.4). Letters on top of the P_f columns indicate statistical significance groups determined via a two-tailed t-Test ($p < 0.05$), whereas error bars illustrate standard error. Kinetic diagrams in (A) numbered 1 through 4 correspond to significance group pairs 1 through 4 in (B).

Table 22 – Stopped Flow water permeability and statistical significance data of L-α-phosphatidylcholine derived liposomes (PC) and L-CF derived PC + NtPIP2;1 proteoliposomes reconstituted with varying SM-2 biobead amounts after having been solubilized by Triton X-100. Given are average values ± standard error (SE) derived from n number of samples for kinetic slope steepness constant k, water permeability factor P_f (both normalized to respective PC + NtPIP2;1 proteoliposome samples) and fitting distance F_D as an indicator for the quality of the fitted kinetics shown in Fig. 30. p values derived from a two-tailed t-Test are shown for each sample pair and divided up into 5 significance levels: ns = not significant (p > 0.05) / * = significant (0.01 < p < 0.05) / ** = very significant (0.001 < p < 0.01) / * = extremely significant (0.0001 < p < 0.001) / **** = extremely significant (p < 0.0001). Conditions of sample preparation describe the amount of SM-2 biobeads applied in mg per sample volume, the average diameter of PC liposomes used to equilibrate the biobeads before application and the incubation time of listed (proteo)liposome samples with equilibrated biobeads in number of overnight periods.**

Sample	Conditions	k ± SE [%]	P_f ± SE [%]	F_D ± SE [%]	n	p	Significance level
PC + NtPIP2;1	160 mg/ml, 0.1 µm, 1 x overnight	100.00 ± 1.41	100.00 ± 1.41	2.38 ± 0.019	29	0.0353	*
PC		133.64 ± 0.66	118.22 ± 0.58	3.34 ± 0.018	28		
PC + NtPIP2;1	160 mg/ml, 0.2 µm, 1 x overnight	100.00 ± 0.80	100.00 ± 0.80	2.59 ± 0.018	27	0.9415	ns
PC		112.63 ± 0.57	99.63 ± 0.50	2.83 ± 0.013	26		
PC + NtPIP2;1	60 mg/ml, 0.2 µm, 2 x overnight	100.00 ± 0.97	100.00 ± 0.97	4.25 ± 0.026	29	0.2915	ns
PC		106.29 ± 0.57	94.02 ± 0.51	4.00 ± 0.021	15		
PC + NtPIP2;1	4 x 40 mg/ml, 0.2 µm, 1 x overnight	100.00 ± 0.68	100.00 ± 0.68	2.48 ± 0.007	21	$6.57x10^{-12}$	****
PC		68.01 ± 0.30	60.16 ± 0.27	3.56 ± 0.015	22		

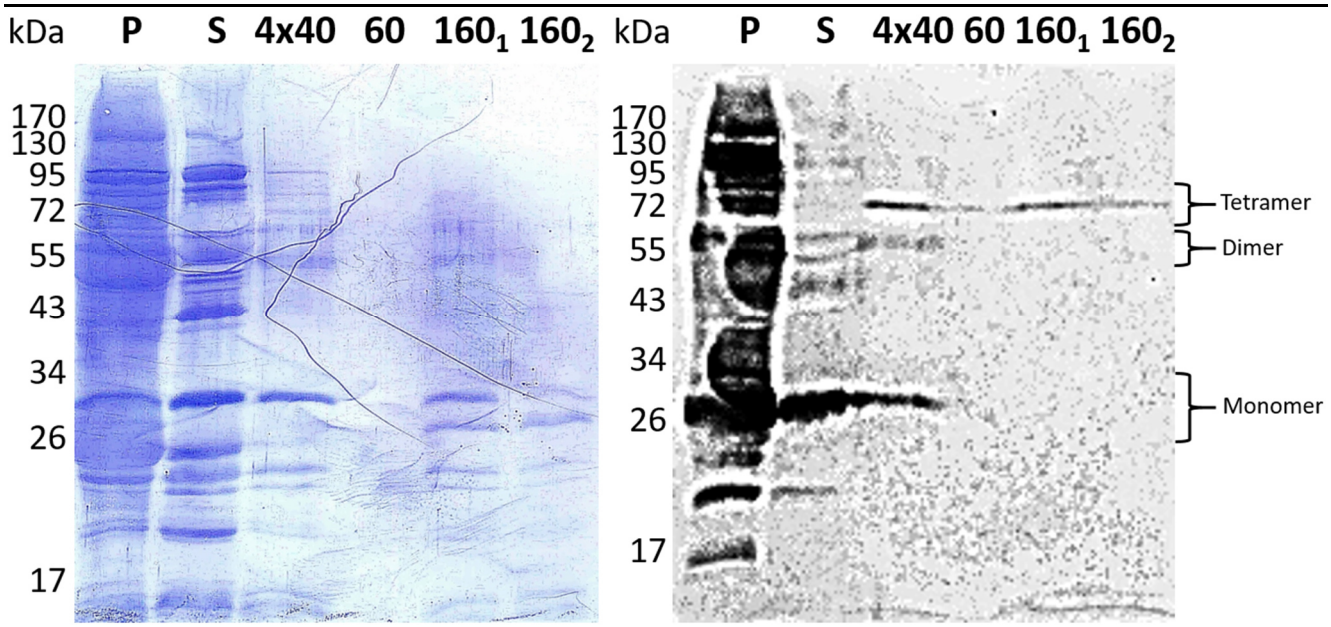

Fig. 33 –Western Blot analysis of L-CF produced NtPIP2;1, which underwent reconstitution in PC liposomes via addition of varying amounts of SM-2 non-polar polystyrene biobeads (Bio-Rad, Hercules, California, USA) after solubilization in 0.41 % (v/v) Triton X-100. Brackets indicate approximate molecular weight of NtPIP2;1 monomeric, dimeric and tetrameric configurations. Left = Coomassie Blue staining of PVDF membrane / Right = Immunological detection of PVDF membrane / Primary antibody = Mouse anti-polyHis IgG / Secondary Antibody = Alkaline phosphatase-conjugated goat anti-mouse IgG / Detection type = Chemiluminescence with an exposure time of 60 s / Protein standard = PageRuler Prestained Protein Ladder (Thermo Scientific, Waltham, Massachusetts, USA) / P = 20 µl precipitated protein fraction after addition of Triton X-100 to pooled L-CF RMs (equivalent to 0.36 RM) / S = Total protein isolated via chloroform-methanol extraction from 20 µl supernatant fraction with solubilized PC + NtPIP2;1 proteoliposomes after addition of Triton X-100 to pooled L-CF RMs (equivalent to 1 RM) / 4x40 = Total protein isolated via chloroform-methanol extraction from PC + NtPIP2;1 proteoliposomes treated with stepwise hourly addition of 4x40 mg biobeads per ml sample. Biobeads were previously equilibrated with 0.2 µm diameter PC liposomes and sample was incubated with equilibrated biobeads for 1 overnight period (equivalent to 1 RM) / 60 = Total protein isolated via chloroform-methanol extraction from PC + NtPIP2;1 proteoliposomes treated with 60 mg biobeads per ml sample. Biobeads were previously equilibrated with 0.2 µm diameter PC liposomes and sample was incubated with equilibrated biobeads for 2 overnight periods (equivalent to 1 RM) / 160_1 = Total protein isolated via chloroform-methanol extraction from PC + NtPIP2;1 proteoliposomes treated with 160 mg biobeads per ml sample. Biobeads were previously equilibrated with 0.1 µm diameter PC liposomes and sample was incubated with equilibrated biobeads for 1 overnight period (equivalent to 1 RM) / 160_2 = Total protein isolated via chloroform-methanol extraction from PC + NtPIP2;1 proteoliposomes treated with 160 mg biobeads per ml sample. Biobeads were previously equilibrated with 0.2 µm diameter PC liposomes and sample was incubated with equilibrated biobeads for 1 overnight period (equivalent to 1 RM).

3.4.4 Comparison of L-CF and liposome derived PC water permeability

After determining the optimal conditions for the separation of proteoliposomes and precipitated protein obtained from L-CF (see chapters 3.4.1 – 3.4.3), the next experiment entailed the preparation of the empty PC control. For the purpose of time and material savings, water permeability control liposomes thus far were prepared by directly diluting freshly generated stock suspensions to 4 mg/ml with HN buffer (see chapter 2.7.3). They then proceeded together with proteoliposome samples in the L-CF downstream processing from the addition of Triton X-100 onwards (see chapter 2.8.1). In order to ensure correct water permeability values, such a PC control was now compared to PC lipopomes derived from a total of six L-CF reactors containing water instead of a plasmid template coding for an aquaporin. The PC (L-CF) sample thus underwent the same experimental steps as the included PC + NtPIP2;1 proteoliposome sample, with the only difference representing the lack of a coding template (see chapters 2.7.5 and 2.8.1). Fig. 34 and Table 23 show the obtained results.
With only a 1 % difference in P_f, the L-CF derived PC control showed a water permeability statistically indistinguishable from the control diluted from a stock PC liposome suspension. The included PC + NtPIP2;1 sample demonstrated 130 % higher water permeability in comparison. It was thus concluded, that PC controls directly derived from stock suspensions for the purpose of time and material savings provided identical water permeability data to L-CF derived PC controls.

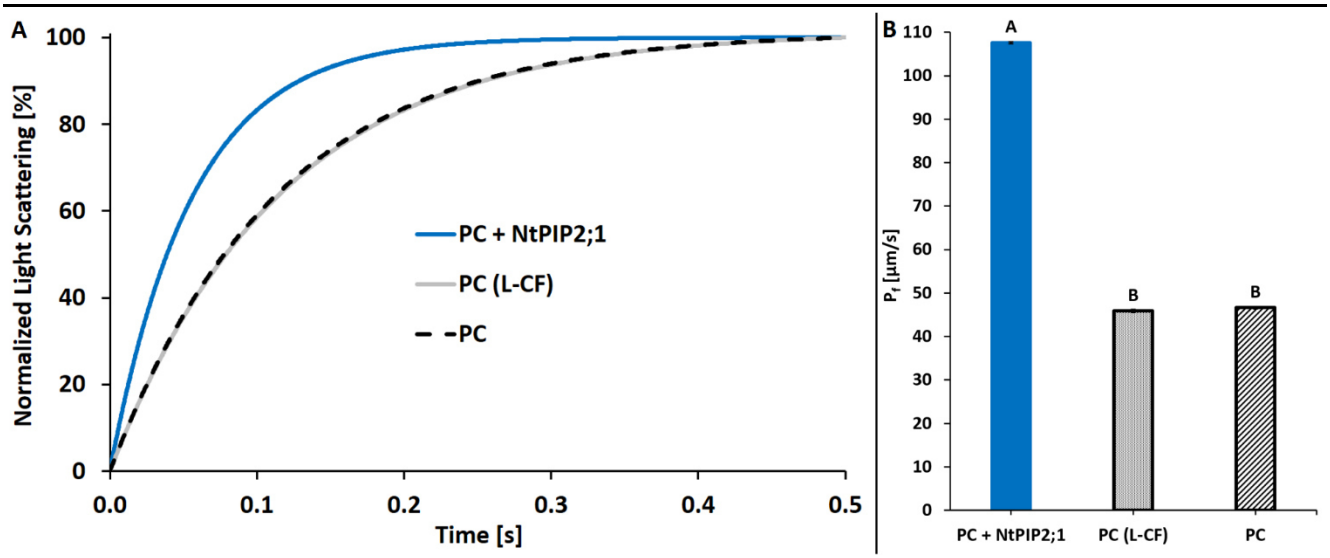

Fig. 34 – Stopped Flow water permeability measurements of L-α-phosphatidylcholine derived liposomes (PC) and L-CF derived PC and PC + NtPIP2;1 (proteo)liposomes. Normalized light scattering kinetics measured at 436 nm are the result of shrinking liposomes via a hyperosmotically induced gradient. Each kinetic shown (A) is an average of several individual raw kinetics of one sample (see Table 23), that were fitted to an exponential rise equation. Water permeability values are based on the steepness of the slopes and are shown in the form of the water permeability factor P_f (B). Letters on top of the P_f columns indicate statistical significance groups determined via a two-tailed t-Test ($p < 0.05$), whereas error bars illustrate standard error.

Table 23 – Stopped Flow water permeability and statistical significance data of L-α-phosphatidylcholine derived liposomes (PC) and L-CF derived PC and PC + NtPIP2;1 (proteo)liposomes. Given are average values ± standard error (SE) derived from n number of samples for kinetic slope steepness constant k, water permeability factor P_f and fitting distance F_D as an indicator for the quality of the fitted kinetics shown in Fig. 33. p values derived from a two-tailed t-Test are shown for each sample pair and divided up into 5 significance levels: ns = not significant ($p > 0.05$) / * = significant ($0.01 < p < 0.05$) / ** = very significant ($0.001 < p < 0.01$) / * = extremely significant ($0.0001 < p < 0.001$) / **** = extremely significant ($p < 0.0001$).**

Sample	k ± SE [s^{-1}]	P_f ± SE [µm/s]	F_D ± SE [%]	n	p	Significance
PC + NtPIP2;1	17.88 ± 0.04	107.58 ± 0.26	3.24 ± 0.009	36	2.61×10^{-35} (PC)	****
PC (L-CF)	8.62 ± 0.06	45.88 ± 0.34	2.33 ± 0.009	22	1.02×10^{-32} (PC + NtPIP2;1)	****
PC	8.76 ± 0.05	46.63 ± 0.26	3.90 ± 0.036	18	0.7211 (PC (L-CF))	ns

3.5 Overview on L-CF derived PC + NtPIP2;1 and PC + NtAQP1 water permeability, as well as overall fitting quality of protein mutant measurements

In order to determine the quality obtained from all subsequent Stopped Flow experiments involving C- and N-terminal mutants of NtPIP2;1 and NtAQP1 (see chapters 3.6 and 3.7), an overview was generated with water permeability values from the wildtype proteins and empty PC liposomes. All measurements were based on L-CF derived proteoliposomes applying the conditions determined in chapter 3.4 and described in chapters 2.7, 2.8 and 2.9. Fig. 35 and Table 24 detail the obtained wildtype and control data.

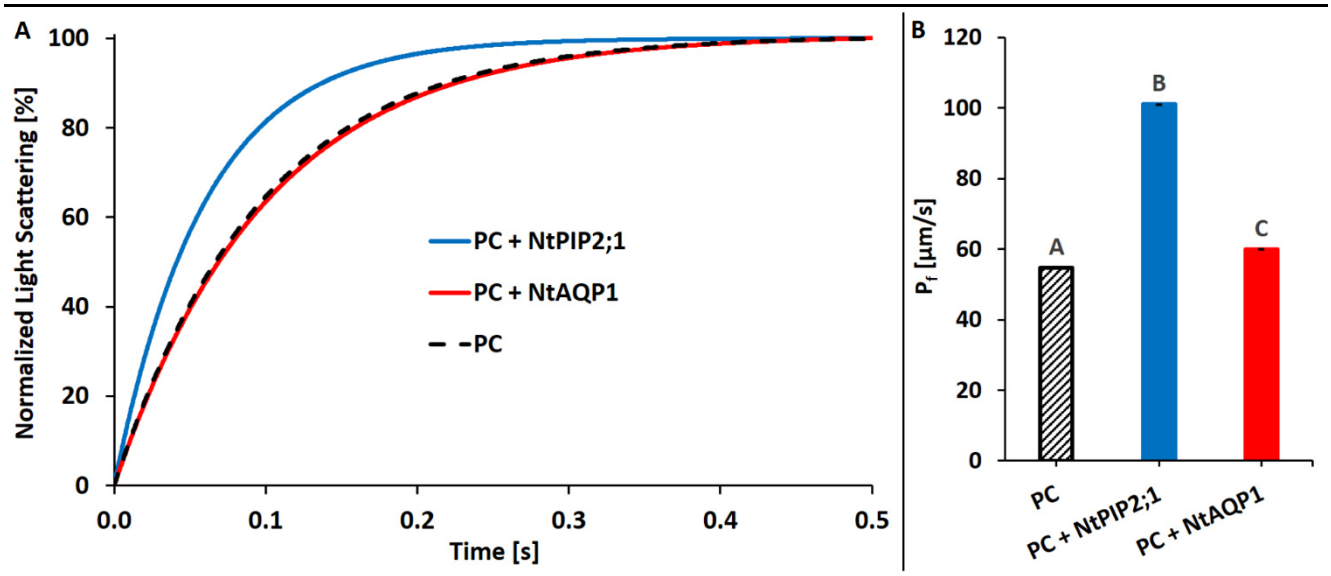

Fig. 35 – Stopped Flow water permeability measurements of L-α-phosphatidylcholine derived liposomes (PC) and L-CF derived PC + NtPIP2;1 and PC + NtAQP1 proteoliposomes. Normalized light scattering kinetics measured at 436 nm are the result of shrinking liposomes via a hyperosmotically induced gradient. Each kinetic shown (A) is an average of several individual raw kinetics of one sample (see Table 24), that were fitted to an exponential rise equation. Water permeability values are based on the steepness of the slopes and are shown in the form of the water permeability factor P_f (B). Letters on top of the P_f columns indicate statistical significance groups determined via a two-tailed t-Test ($p < 0.05$), whereas error bars illustrate standard error. Shown are averaged results of all subsequent experiments involving N- and C-terminal mutants of NtPIP2;1 and NtAQP1 (see chapters 3.6 and 3.7).

Table 24 – Stopped Flow water permeability and statistical significance data of L-α-phosphatidylcholine derived liposomes (PC) and L-CF derived PC + NtPIP2;1 and PC + NtAQP1 proteoliposomes. Given are average values ± standard error (SE) derived from n number of samples for kinetic slope steepness constant k, water permeability factor P_f and fitting distance F_D as an indicator for the quality of the fitted kinetics shown in Fig. 34. p values derived from a two-tailed t-Test are shown for each sample pair and divided up into 5 significance levels: ns = not significant ($p > 0.05$) / * = significant ($0.01 < p < 0.05$) / ** = very significant ($0.001 < p < 0.01$) / * = extremely significant ($0.0001 < p < 0.001$) / **** = extremely significant ($p < 0.0001$). Listed results are averaged data of all subsequent experiments involving N- and C- terminal mutants of NtPIP2;1 and NtAQP1 (see chapters 3.6 and 3.7).**

Sample	k ± SE [s^{-1}]	P_f ± SE [µm/s]	F_D ± SE [%]	n	p	Significance
PC	10.29 ± 0.01	54.78 ± 0.05	3.33 ± 0.003	270	1.61×10^{-104} (PC + NtPIP2;1)	****
PC + NtPIP2;1	16.79 ± 0.01	101.03 ± 0.08	3.62 ± 0.005	403	1.99×10^{-85} (PC + NtAQP1)	****
PC + NtAQP1	9.96 ± 0.01	59.96 ± 0.05	2.58 ± 0.001	383	6.69×10^{-5} (PC)	****

Based on a total of 1056 measured samples, the wildtype NtPIP2;1 aquaporin embedded as PC proteoliposomes demonstrated a water permeability of approximately 85 % higher than control PC liposomes. In comparison, PC proteoliposomes containing wildtype NtAQP1 showed only a moderate water permeability at 10 % higher than controls and 60 % of NtPIP2;1 levels. These values are in line with previous obervations described in literature (see chapter 1.5) and can thus be relied upon to put water permeability data obtained for N- and C-terminal mutants into a proper context.

Furthermore, F_D values in the range of 2.6 to 3.6 % attest an overall high fitting quality for the wildtype and liposomes controls. Fig. 36 provides an overview on the F_D ranges obtained in all 1744 individual Stopped Flow samples encompassing wildtype and liposome controls, as well as mutant constructs.

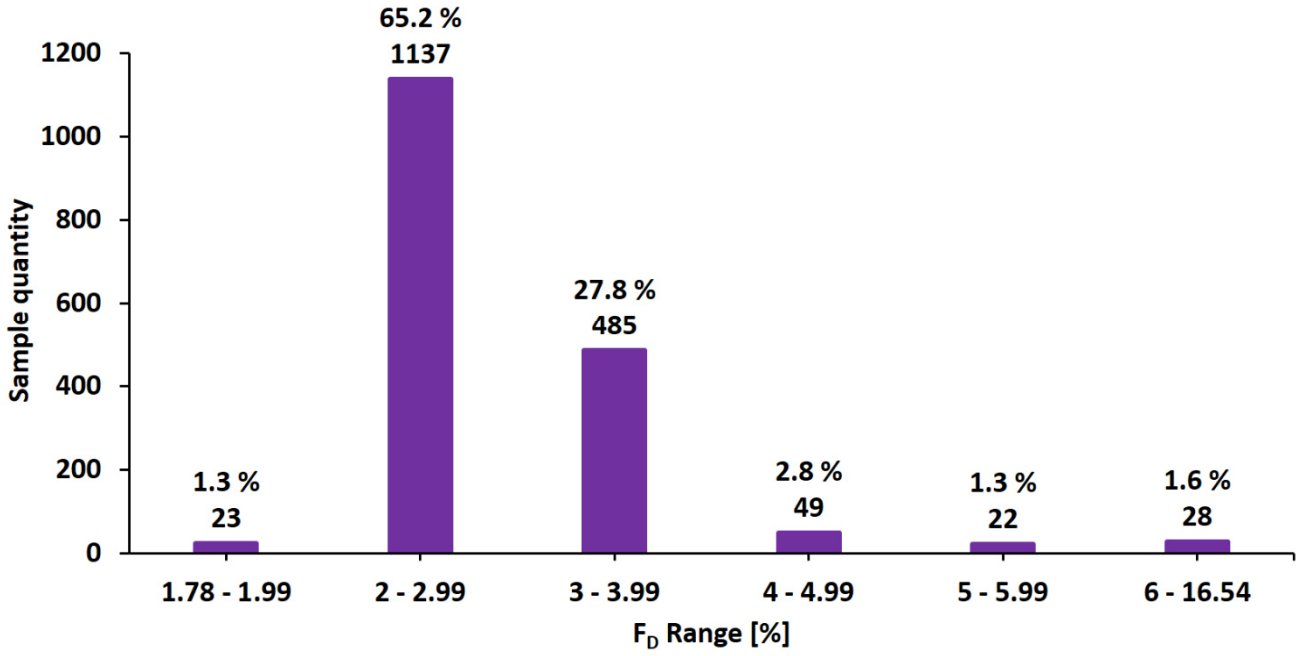

Fig. 36 – Quantity of individual Stopped Flow samples grouped into specific fitting distance (F_D) ranges as a quality measurement for mathematically fitting raw light scattering kinetics to an exponential rise equation (see chapter 2.10.1). The total of 1744 samples contain all Stopped Flow kinetics derived from NtPIP2;1 and NtAQP1 wildtype aquaporins embedded as PC proteoliposomes, as well as all measurements with empty PC liposomes and N- and C-terminal aquaporin mutants embedded as PC proteoliposomes outlined in chapters 3.6 and 3.7. Numbers on top of columns depict percentage of total sample size followed by sample quantity in respective F_D range. Min = 1.78 % / Mean = 2.96 % / Median = 2.72 % / Max = 16.54 %.

More than 97 % of all fitted raw kinetics demonstrate a fitting distance of below 5 %, indicating a very high fitting quality and thus reliability for the obtained data. A visualization of representative F_D values in this sample population is given in Fig. 16 of chapter 2.10.1, where minimum (1.78 %), mean (2.96 %), maximum (16.54 %), as well as the average value of the highest 5 % of samples (6.66 %) is shown.

3.6 Water permeability of L-CF derived NtPIP2;1 and NtAQP1 N- and C-terminal domain deletion mutants

This chapter details the water permeability of N- and C-terminal deletion mutants in comparison to their wildtype counterparts NtPIP2;1 and NtAQP1. Proteoliposome samples were produced in L-CF mode and were processed as described in chapters 2.7 through 2.9. The calculation of (proteo)liposome water permeability by non-linear regression is described in chapter 2.10.1.

3.6.1 Deletion of N-terminal domain

In order to determine the role of the N-terminus in the water permeating ability of NtPIP2;1 and NtAQP1, respective deletion mutants were generated and compared to their wildtype counterparts (see chapters 3.1 and 3.2). Fig. 37 and Table 25 summarize the data obtained for the NtPIP2;1 derived N-terminal deletion mutant Δ(N)_P2, whereas Fig. 38 and Table 26 illustrate the water permeability of the NtAQP1 derived counterpart Δ(N)_A1.

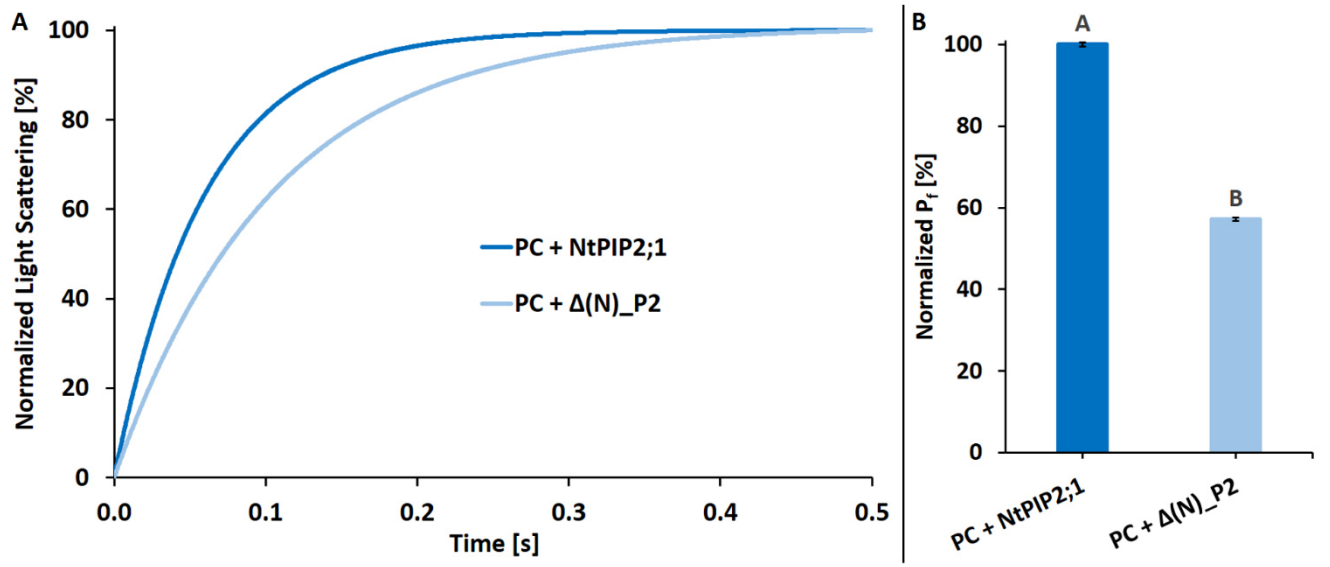

Fig. 37 – Stopped Flow water permeability measurements of L-CF produced and L-α-phosphatidylcholine derived proteoliposomes (PC) containing wildtype aquaporin NtPIP2;1 and its N-terminal deletion mutant Δ(N)_P2, respectively. Normalized light scattering kinetics measured at 436 nm are the result of shrinking liposomes via a hyperosmotically induced gradient. Each kinetic shown (A) is an average of several individual raw kinetics of one sample (see Table 25), that were fitted to an exponential rise equation. Water permeability values are based on the steepness of the slopes and are shown in the form of the water permeability factor P_f (B), which was normalized to the wildtype aquaporin. Letters on top of the P_f columns indicate statistical significance groups determined via a two-tailed t-Test ($p < 0.05$), whereas error bars illustrate standard error.

Table 25 – Stopped Flow water permeability and statistical significance data of L-CF produced and L-α-phosphatidylcholine derived proteoliposomes (PC) containing wildtype aquaporin NtPIP2;1 and its N-terminal deletion mutant Δ(N)_P2, respectively. Given are average values ± standard error (SE) derived from n number of samples for kinetic slope steepness constant k, water permeability factor P_f (both normalized to the wildtype aquaporin) and fitting distance F_D as an indicator for the quality of the fitted kinetics shown in Fig. 36. p values derived from a two-tailed t-Test are shown for each sample pair and divided up into 5 significance levels: ns = not significant ($p > 0.05$) / * = significant ($0.01 < p < 0.05$) / ** = very significant ($0.001 < p < 0.01$) / * = extremely significant ($0.0001 < p < 0.001$) / **** = extremely significant ($p < 0.0001$).**

Sample	k ± SE [%]	P_f ± SE [%]	F_D ± SE [%]	n	p	Significance
PC + NtPIP2;1	100.00 ± 0.45	100.00 ± 0.45	4.12 ± 0.033	26	6.69×10^{-20}	****
PC + Δ(N)_P2	57.16 ± 0.34	57.16 ± 0.34	3.69 ± 0.014	38		

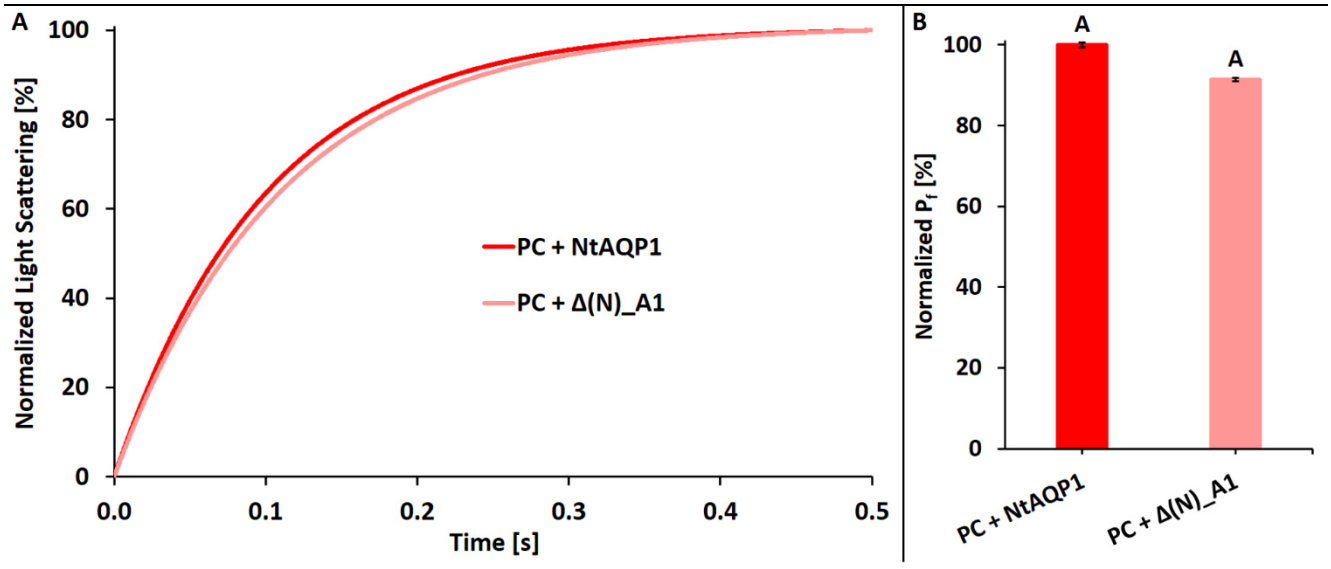

Fig. 38 – Stopped Flow water permeability measurements of L-CF produced and L-α-phosphatidylcholine derived proteoliposomes (PC) containing wildtype aquaporin NtAQP1 and its N-terminal deletion mutant Δ(N)_A1, respectively. Normalized light scattering kinetics measured at 436 nm are the result of shrinking liposomes via a hyperosmotically induced gradient. Each kinetic shown (A) is an average of several individual raw kinetics of one sample (see Table 26), that were fitted to an exponential rise equation. Water permeability values are based on the steepness of the slopes and are shown in the form of the water permeability factor P_f (B), which was normalized to the wildtype aquaporin. Letters on top of the P_f columns indicate statistical significance groups determined via a two-tailed t-Test ($p < 0.05$), whereas error bars illustrate standard error.

Table 26 – Stopped Flow water permeability and statistical significance data of L-CF produced and L-α-phosphatidylcholine derived proteoliposomes (PC) containing wildtype aquaporin NtAQP1 and its N-terminal deletion mutant Δ(N)_A1, respectively. Given are average values ± standard error (SE) derived from n number of samples for kinetic slope steepness constant k, water permeability factor P_f (both normalized to the wildtype aquaporin) and fitting distance F_D as an indicator for the quality of the fitted kinetics shown in Fig. 37. p values derived from a two-tailed t-Test are shown for each sample pair and divided up into 5 significance levels: ns = not significant (p > 0.05) / * = significant (0.01 < p < 0.05) / ** = very significant (0.001 < p < 0.01) / * = extremely significant (0.0001 < p < 0.001) / **** = extremely significant (p < 0.0001).**

Sample	k ± SE [%]	P_f ± SE [%]	F_D ± SE [%]	n	p	Significance
PC + NtAQP1	100.00 ± 0.59	100.00 ± 0.59	3.04 ± 0.010	38	0.0622	ns
PC + Δ(N)_A1	91.35 ± 0.43	91.35 ± 0.43	2.92 ± 0.007	41		

The N-terminal deletion mutant of NtPIP2;1 showed a significant reduction in water permeability compared to its wildtype counterpart, with its P_f at 57 % of the original level. In comparison, the deletion of the N-terminus in NtAQP1 also demonstrated a reduction in water permeability to 91 % of the wildtype level. However, a statistical significance was not given, thus equating the water permeating abilities of the two NtAQP1 constructs in this case.

3.6.2 Deletion of C-terminal domain

Analogously to the N-terminal deletion mutants, NtPIP2;1 and NtAQP1 constructs were generated with their C-termini deleted in order to determine the impact on their water permeability (see chapters 3.1 and 3.2). Fig. 39 and Table 27 give an overview on the data obtained for the NtPIP2;1 derived C-terminal deletion mutant P2_Δ(C), whereas Fig. 40 and Table 28 show water permeability values of the NtAQP1 derived counterpart A1_Δ(C).

Similar to their N-terminal deletion counterparts, P2_Δ(C) showed a significantly reduced water permeability at 65 % of NtPIP2;1 wildtype levels, whereas A1_Δ(C) demonstrated a slightly elevated, but not statistically significant, water permeation at 110 % of the NtAQP1 wildtype.

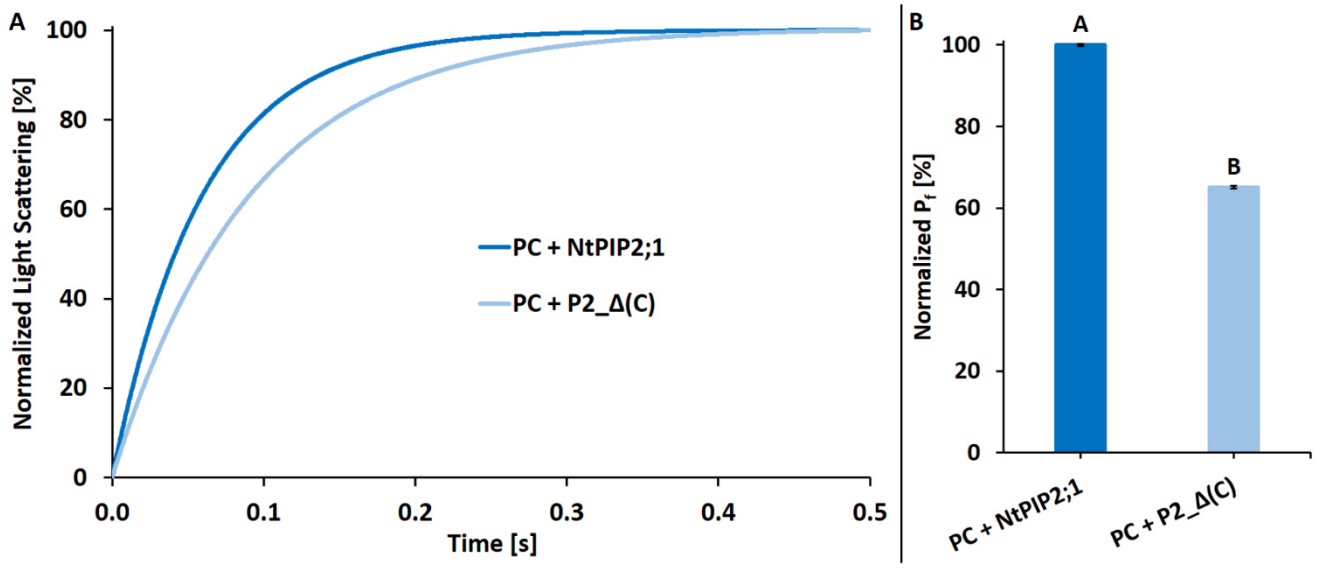

Fig. 39 – Stopped Flow water permeability measurements of L-CF produced and L-α-phosphatidylcholine derived proteoliposomes (PC) containing wildtype aquaporin NtPIP2;1 and its C-terminal deletion mutant P2_Δ(C), respectively. Normalized light scattering kinetics measured at 436 nm are the result of shrinking liposomes via a hyperosmotically induced gradient. Each kinetic shown (A) is an average of several individual raw kinetics of one sample (see Table 27), that were fitted to an exponential rise equation. Water permeability values are based on the steepness of the slopes and are shown in the form of the water permeability factor P_f (B), which was normalized to the wildtype aquaporin. Letters on top of the P_f columns indicate statistical significance groups determined via a two-tailed t-Test (p < 0.05), whereas error bars illustrate standard error.

Table 27 – Stopped Flow water permeability and statistical significance data of L-CF produced and L-α-phosphatidylcholine derived proteoliposomes (PC) containing wildtype aquaporin NtPIP2;1 and its C-terminal deletion mutant P2_Δ(C), respectively. Given are average values ± standard error (SE) derived from n number of samples for kinetic slope steepness constant k, water permeability factor P_f (both normalized to the wildtype aquaporin) and fitting distance F_D as an indicator for the quality of the fitted kinetics shown in Fig. 38. p values derived from a two-tailed t-Test are shown for each sample pair and divided up into 5 significance levels: ns = not significant (p > 0.05) / * = significant (0.01 < p < 0.05) / ** = very significant (0.001 < p < 0.01) / * = extremely significant (0.0001 < p < 0.001) / **** = extremely significant (p < 0.0001).**

Sample	k ± SE [%]	P_f ± SE [%]	F_D ± SE [%]	n	p	Significance
PC + NtPIP2;1	100.00 ± 0.27	100.00 ± 0.27	3.01 ± 0.009	35	$1.79x10^{-21}$	****
PC + P2_Δ(C)	65.10 ± 0.32	65.10 ± 0.32	2.63 ± 0.006	35		

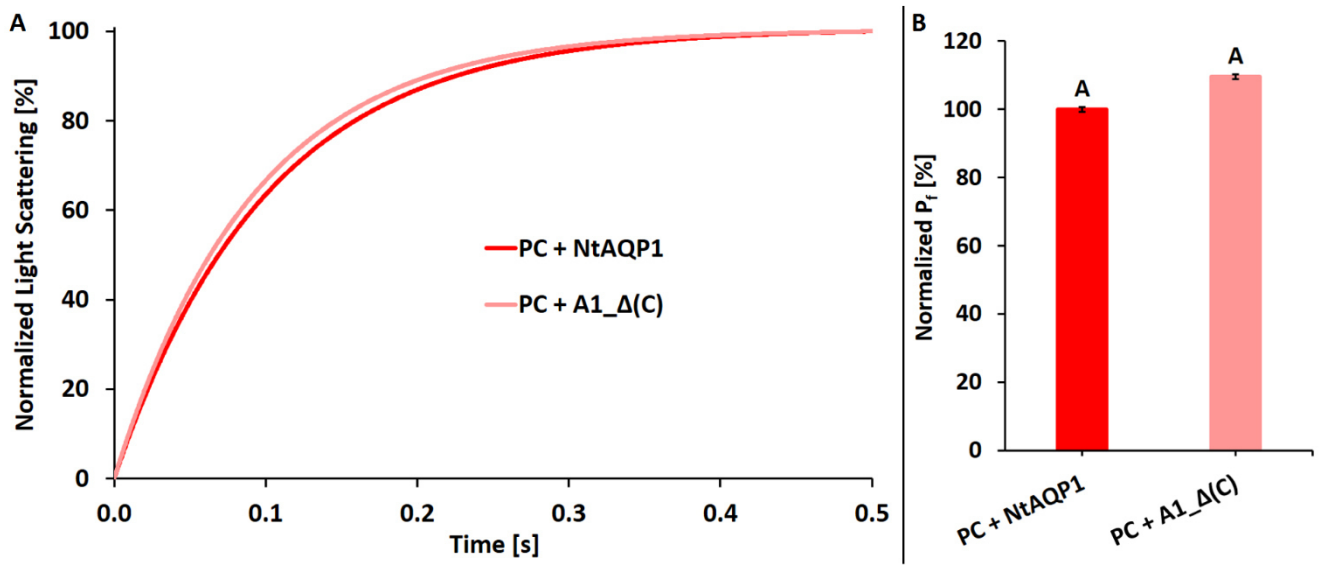

Fig. 40 – Stopped Flow water permeability measurements of L-CF produced and L-α-phosphatidylcholine derived proteoliposomes (PC) containing wildtype aquaporin NtAQP1 and its C-terminal deletion mutant A1_Δ(C), respectively. Normalized light scattering kinetics measured at 436 nm are the result of shrinking liposomes via a hyperosmotically induced gradient. Each kinetic shown (A) is an average of several individual raw kinetics of one sample (see Table 28), that were fitted to an exponential rise equation. Water permeability values are based on the steepness of the slopes and are shown in the form of the water permeability factor P_f (B), which was normalized to the wildtype aquaporin. Letters on top of the P_f columns indicate statistical significance groups determined via a two-tailed t-Test (p < 0.05), whereas error bars illustrate standard error.

Table 28 – Stopped Flow water permeability and statistical significance data of L-CF produced and L-α-phosphatidylcholine derived proteoliposomes (PC) containing wildtype aquaporin NtAQP1 and its C-terminal deletion mutant A1_Δ(C), respectively. Given are average values ± standard error (SE) derived from n number of samples for kinetic slope steepness constant k, water permeability factor P_f (both normalized to the wildtype aquaporin) and fitting distance F_D as an indicator for the quality of the fitted kinetics shown in Fig. 39. p values derived from a two-tailed t-Test are shown for each sample pair and divided up into 5 significance levels: ns = not significant (p > 0.05) / * = significant (0.01 < p < 0.05) / ** = very significant (0.001 < p < 0.01) / * = extremely significant (0.0001 < p < 0.001) / **** = extremely significant (p < 0.0001).**

Sample	k ± SE [%]	P_f ± SE [%]	F_D ± SE [%]	n	p	Significance
PC + NtAQP1	100.00 ± 0.72	100.00 ± 0.72	2.68 ± 0.009	28	0.0842	ns
PC + A1_Δ(C)	109.50 ± 0.71	109.50 ± 0.71	3.22 ± 0.027	19		

3.6.3 Deletion of N- and C-terminal domains

After determining the water permeability of their N- and C-terminal deletion mutants, respectively, double deletion mutants of NtPIP2;1 and NtAQP1 were generated in order to measure the impact on their water permeation (see chapters 3.1 and 3.2). Fig. 41 and Table 29 illustrate the data obtained for the NtPIP2;1 derived N- and C-terminal double deletion mutant Δ(N)_P2_Δ(C), whereas Fig. 42 and Table 30 summarize the water permeation capability of the NtAQP1 derived counterpart Δ(N)_A1_ Δ(C).

As with both single deletion mutants before, Δ(N)_P2_ Δ(C) as the double terminal deletion mutant of NtPIP2;1 showed a significant reduction in water permeability down to 52 % of wildtype levels. Similarly, Δ(N)_A1_ Δ(C) as the double terminal deletion mutant of NtAQP1 demonstrated a reduction in water permeation to 75 % of wildtype levels. This stands in contrast to the NtAQP1 single deletion mutants, which did not show a statistically significant change in their water permeability.

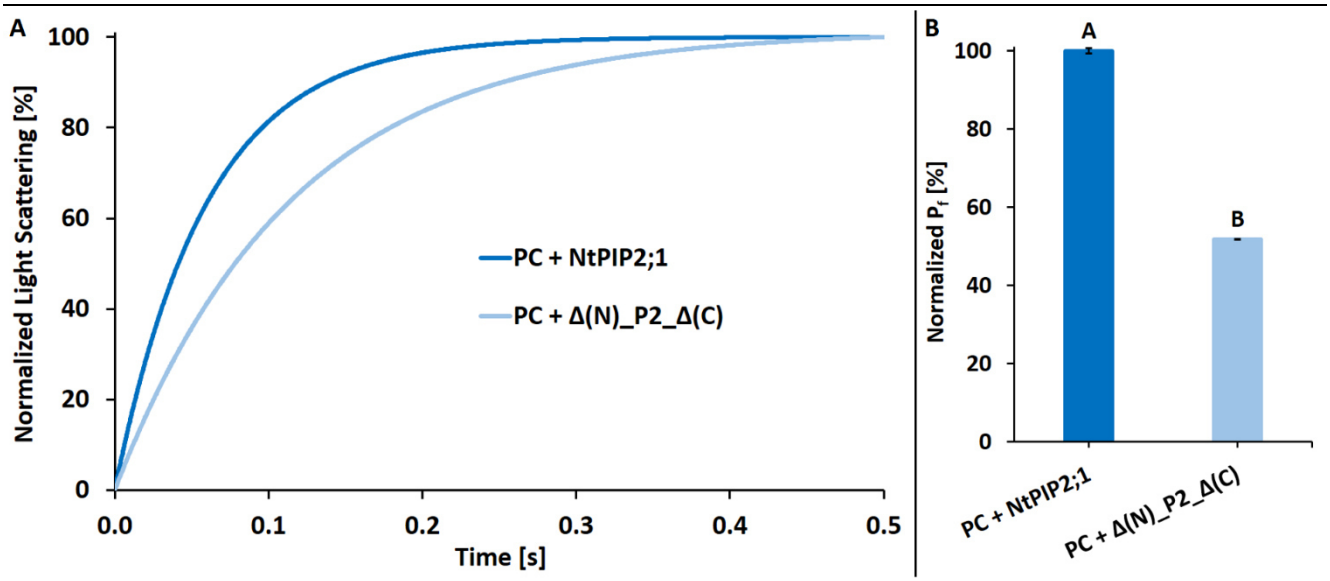

Fig. 41 – Stopped Flow water permeability measurements of L-CF produced and L-α-phosphatidylcholine derived proteoliposomes (PC) containing wildtype aquaporin NtPIP2;1 and its N- and C-terminal deletion mutant Δ(N)_P2_Δ(C), respectively. Normalized light scattering kinetics measured at 436 nm are the result of shrinking liposomes via a hyperosmotically induced gradient. Each kinetic shown (A) is an average of several individual raw kinetics of one sample (see Table 29), that were fitted to an exponential rise equation. Water permeability values are based on the steepness of the slopes and are shown in the form of the water permeability factor P_f (B), which was normalized to the wildtype aquaporin. Letters on top of the P_f columns indicate statistical significance groups determined via a two-tailed t-Test ($p < 0.05$), whereas error bars illustrate standard error.

Table 29 – Stopped Flow water permeability and statistical significance data of L-CF produced and L-α-phosphatidylcholine derived proteoliposomes (PC) containing wildtype aquaporin NtPIP2;1 and its N- and C-terminal deletion mutant Δ(N)_P2_Δ(C), respectively. Given are average values ± standard error (SE) derived from n number of samples for kinetic slope steepness constant k, water permeability factor P_f (both normalized to the wildtype aquaporin) and fitting distance F_D as an indicator for the quality of the fitted kinetics shown in Fig. 40. p values derived from a two-tailed t-Test are shown for each sample pair and divided up into 5 significance levels: ns = not significant ($p > 0.05$) / * = significant ($0.01 < p < 0.05$) / ** = very significant ($0.001 < p < 0.01$) / * = extremely significant ($0.0001 < p < 0.001$) / **** = extremely significant ($p < 0.0001$).**

Sample	k ± SE [%]	P_f ± SE [%]	F_D ± SE [%]	n	p	Significance
PC + NtPIP2;1	100.00 ± 0.66	100.00 ± 0.66	4.70 ± 0.059	24	1.97×10^{-13}	****
PC + Δ(N)_P2_Δ(C)	51.86 ± 0.10	51.86 ± 0.10	2.22 ± 0.050	32		

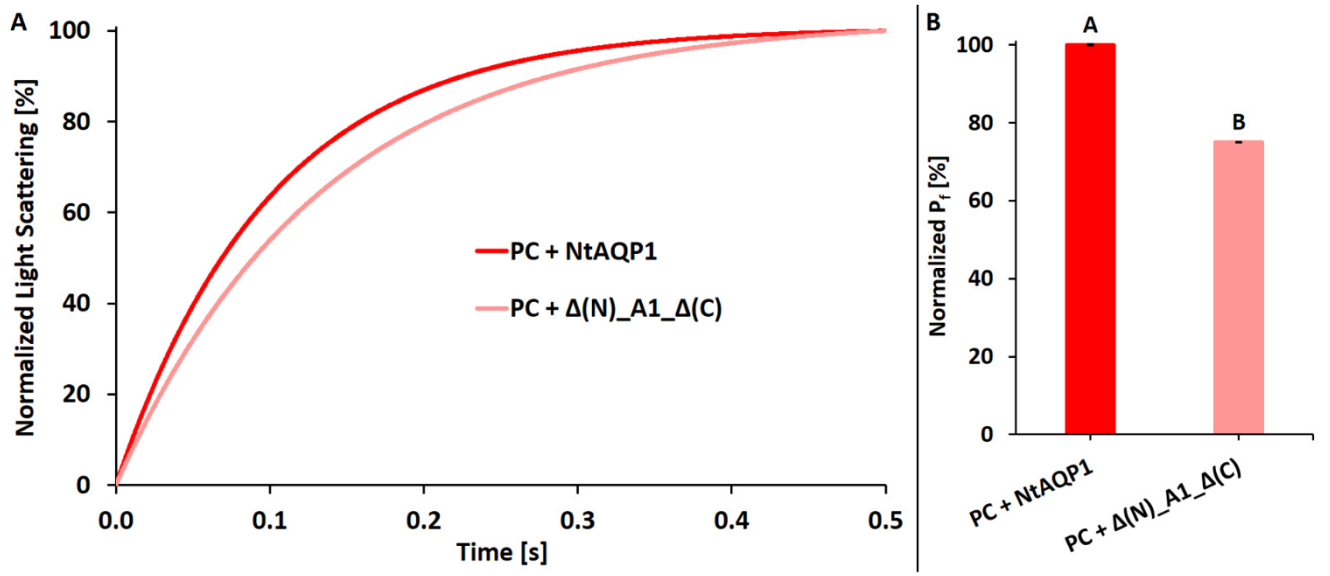

Fig. 42 – Stopped Flow water permeability measurements of L-CF produced and L-α-phosphatidylcholine derived proteoliposomes (PC) containing wildtype aquaporin NtAQP1 and its N- and C-terminal deletion mutant Δ(N)_A1_Δ(C), respectively. Normalized light scattering kinetics measured at 436 nm are the result of shrinking liposomes via a hyperosmotically induced gradient. Each kinetic shown (A) is an average of several individual raw kinetics of one sample (see Table 30), that were fitted to an exponential rise equation. Water permeability values are based on the steepness of the slopes and are shown in the form of the water permeability factor P_f (B), which was normalized to the wildtype aquaporin. Letters on top of the P_f columns indicate statistical significance groups determined via a two-tailed t-Test ($p < 0.05$), whereas error bars illustrate standard error.

Table 30 – Stopped Flow water permeability and statistical significance data of L-CF produced and L-α-phosphatidylcholine derived proteoliposomes (PC) containing wildtype aquaporin NtAQP1 and its N- and C-terminal deletion mutant Δ(N)_A1_Δ(C), respectively. Given are average values ± standard error (SE) derived from n number of samples for kinetic slope steepness constant k, water permeability factor P_f (both normalized to the wildtype aquaporin) and fitting distance F_D as an indicator for the quality of the fitted kinetics shown in Fig. 41. p values derived from a two-tailed t-Test are shown for each sample pair and divided up into 5 significance levels: ns = not significant ($p > 0.05$) / * = significant ($0.01 < p < 0.05$) / ** = very significant ($0.001 < p < 0.01$) / * = extremely significant ($0.0001 < p < 0.001$) / **** = extremely significant ($p < 0.0001$).**

Sample	k ± SE [%]	P_f ± SE [%]	F_D ± SE [%]	n	p	Significance
PC + NtAQP1	100.00 ± 0.18	100.00 ± 0.18	2.63 ± 0.007	38	9.95×10^{-28}	****
PC + Δ(N)_A1_Δ(C)	75.01 ± 0.14	75.01 ± 0.14	2.36 ± 0.006	37		

3.6.4 Summary of NtPIP2;1 N- and C-terminal domain deletion mutants

In order to put the water permeation capabilities of NtPIP2;1 derived N- and C-terminal deletion mutants into context with each other and the respective controls, the data collected from chapters 3.6.1 through 3.6.3 were summarized in Fig. 43 and Table 31.

Independently of the deletion type, all mutant constructs showed significantly lower water permeability than the NtPIP2;1 wildtype control. However, the deletion of the N-terminus indicated a significantly stronger impact on permeation than the deletion of the C-terminus, with the latter demonstrating a 13 % higher water transport rate. The deletion of both termini resulted in the lowest measured water permeability at 52 % of wildtype levels and equivalent to a significant drop of 9 % and 20 % when compared with the N- and C-terminal deletion mutants, respectively. Concerning the PC liposome and NtAQP1 wildtype controls, only the N-terminal deletion mutant Δ(N)_P2 showed statistical comparability. In contrast, both the C-terminal P2_Δ(C) and double terminal Δ(N)_P2_Δ(C) demonstrated significantly higher or lower water permeation than both controls, respectively. In conclusion, both the N- and the C-terminus are essential for NtPIP2;1 water transport function, with the absence of the Amine- having a larger impact than that of the Carboxy-terminus.

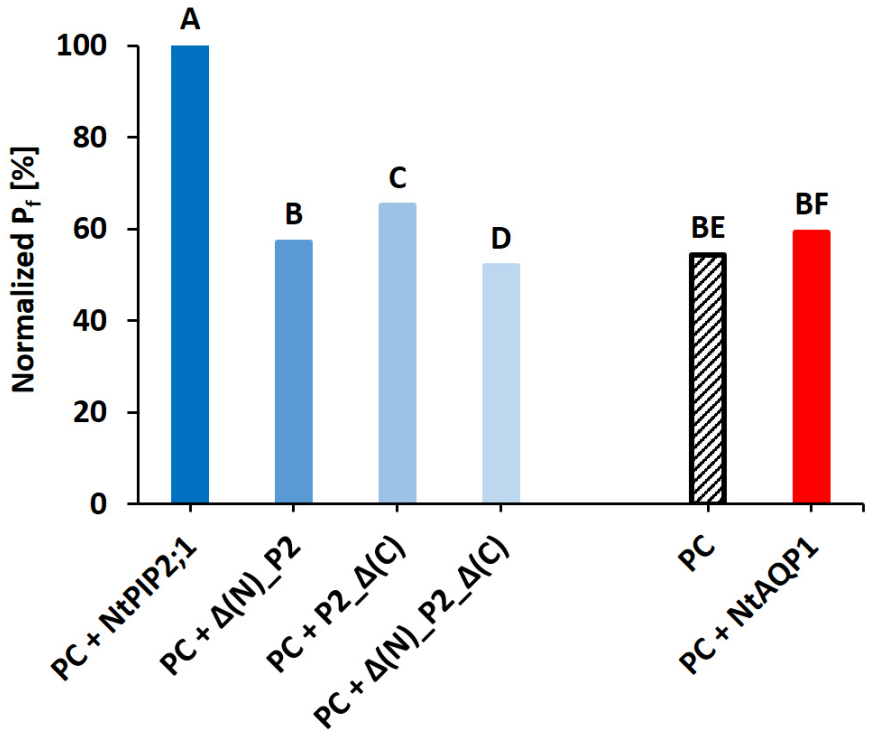

Fig. 43 – Overview on P_f based water permeation capabilities of L-CF produced and L-α-phosphatidylcholine derived proteoliposomes (PC) containing wildtype aquaporin NtPIP2;1 and its single and double N- and C-terminal deletion mutants. Empty PC liposomes and NtAQP1 wildtype proteoliposomes were also included for comparison. Water permeability values were calculated from the slope steepness of Stopped Flow light scattering kinetics by non-linear regression fitting to an exponential rise equation. They are shown in the form of the water permeability factor P_f, which was normalized to the wildtype NtPIP2;1. Letters on top of the P_f columns indicate statistical significance groups determined via a two-tailed t-Test (p < 0.05). Δ(N)_P2 = N-terminal deletion mutant / P2_Δ(C) = C-terminal deletion mutant / Δ(N)_P2_Δ(C) = N- and C-terminal double deletion mutant.

Table 31 – Overview on P_f based water permeation capabilities and statistical significance data of L-CF produced and L-α-phosphatidylcholine derived proteoliposomes (PC) containing wildtype aquaporin NtPIP2;1 and its single and double N- and C-terminal deletion mutants. Empty PC liposomes and NtAQP1 wildtype proteoliposomes were also included for comparison.Given are average values as shown in Fig. 42 for the water permeability factor P_f, which was normalized to the wildtype aquaporin. p values derived from a two-tailed t-Test are shown for each sample pair and divided up into 5 significance levels: ns = not significant (p > 0.05) / * = significant (0.01 < p < 0.05) / ** = very significant (0.001 < p < 0.01) / * = extremely significant (0.0001 < p < 0.001) / **** = extremely significant (p < 0.0001). Δ(N)_P2 = N-terminal deletion mutant / P2_Δ(C) = C-terminal deletion mutant / Δ(N)_P2_Δ(C) = N- and C-terminal double deletion mutant.**

Sample	P_f [%]	PC + NtAQP1	PC	PC + Δ(N)_P2_Δ(C)	PC + P2_Δ(C)	PC + Δ(N)_P2
PC + NtPIP2;1	100.00	**** 1.99×10^{-85}	**** 1.61×10^{-104}	**** 1.97×10^{-13}	**** 1.79×10^{-21}	**** 6.69×10^{-20}
PC + Δ(N)_P2	57.16	ns 0.3540	ns 0.2050	* 0.0201	** 0.0075	- -
PC + P2_Δ(C)	65.10	* 0.0105	**** 6.78×10^{-6}	**** 7.92×10^{-8}	- -	- -
PC + Δ(N)_P2_Δ(C)	51.86	**** 3.87×10^{-10}	* 0.0213	- -	- -	- -
PC	54.22	**** 6.69×10^{-5}	- -	- -	- -	- -
PC + NtAQP1	59.34	- -	- -	- -	- -	- -

3.6.5 Summary of NtAQP1 N- and C-terminal domain deletion mutants

Analogously to the NtPIP2;1 N- and C-terminal deletion mutants, the data collected from chapters 3.6.1 through 3.6.3 for the NtAQP1 counterparts were summarized in Fig. 44 and Table 32.

Neither the N-, nor the C-terminal deletion mutant showed a significant difference in water permeability when compared to the NtAQP1 wildtype. However, removing both domains resulted in a significant 25 % drop of transport function. Δ(N)_A1 as the N-terminal deletion construct was the only one to show a statistical comparability with the empty PC liposome control, whereas A1_Δ(C) and Δ(N)_A1_Δ(C) demonstrated a 20 % higher and an 18 % lower water transport rate, respectively. None of the mutant constructs demonstrated statistical comparability with the NtPIP2;1 wildtype, with the double deletion construct showing the lowest relative water permeability at 45 % of NtPIP2;1 levels. In conclusion, none of the individual deletion of terminal domains significantly changed NtAQP1 water permeation rates. However, removing both domains resulted in a significant drop of aquaporin function.

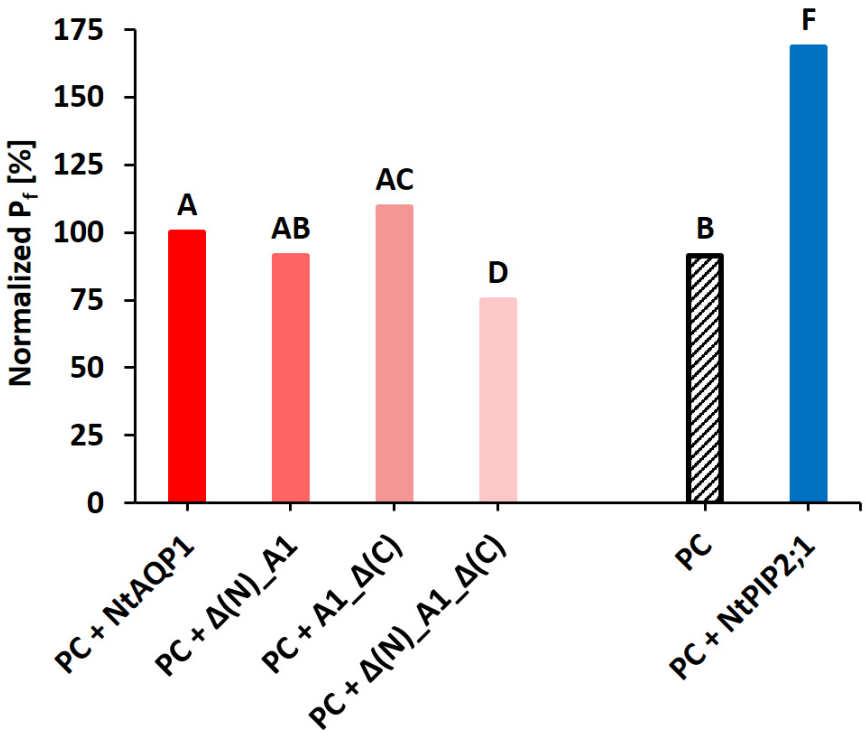

Fig. 44 – Overview on P_f based water permeation capabilities of L-CF produced and L-α-phosphatidylcholine derived proteoliposomes (PC) containing wildtype aquaporin NtAQP1 and its single and double N- and C-terminal deletion mutants. Empty PC liposomes and NtPIP2;1 wildtype proteoliposomes were also included for comparison. Water permeability values were calculated from the slope steepness of Stopped Flow light scattering kinetics by non-linear regression fitting to an exponential rise equation. They are shown in the form of the water permeability factor P_f, which was normalized to the wildtype NtAQP1. Letters on top of the P_f columns indicate statistical significance groups determined via a two-tailed t-Test ($p < 0.05$). Δ(N)_A1 = N-terminal deletion mutant / A1_Δ(C) = C-terminal deletion mutant / Δ(N)_A1_Δ(C) = N- and C-terminal double deletion mutant.

Table 32 – Overview on P_f based water permeation capabilities and statistical significance data of L-CF produced and L-α-phosphatidylcholine derived proteoliposomes (PC) containing wildtype aquaporin NtAQP1 and its single and double N- and C-terminal deletion mutants. Empty PC liposomes and NtAQP1 wildtype proteoliposomes were also included for comparison. Given are average values as shown in Fig. 43 for the water permeability factor P_f, which was normalized to the wildtype aquaporin. p values derived from a two-tailed t-Test are shown for each sample pair and divided up into 5 significance levels: ns = not significant (p > 0.05) / * = significant (0.01 < p < 0.05) / ** = very significant (0.001 < p < 0.01) / * = extremely significant (0.0001 < p < 0.001) / **** = extremely significant (p < 0.0001). Δ(N)_A1 = N-terminal deletion mutant / A1_Δ(C) = C-terminal deletion mutant / Δ(N)_A1_Δ(C) = N- and C-terminal double deletion mutant.**

Sample	P_f [%]	PC + NtPIP2;1	PC	PC + Δ(N)_A1_Δ(C)	PC + A1_Δ(C)	PC + Δ(N)_A1
PC + NtAQP1	100.00	****	****	****	ns	ns
		$1.99x10^{-85}$	$6.69x10^{-5}$	$9.95x10^{-28}$	0.0842	0.0622
PC + Δ(N)_A1	91.35	****	ns	****	***	-
		$3.66x10^{-42}$	0.9980	$9.13x10^{-7}$	0.0002	-
PC + A1_Δ(C)	109.50	****	****	****	-	-
		$4.22x10^{-19}$	$1.86x10^{-5}$	$9.32x10^{-10}$	-	-
PC + Δ(N)_A1_Δ(C)	75.01	****	****	-	-	-
		$2.22x10^{-128}$	$5.76x10^{-20}$	-	-	-
PC	91.36	****	-	-	-	-
		$1.61x10^{-104}$	-	-	-	-
PC + NtPIP2;1	168.51	-	-	-	-	-
		-	-	-	-	-

3.7 Water permeability of L-CF derived NtPIP2;1 and NtAQP1 N- and C-terminal domain exchange mutants

This chapter details the water permeability of N- and C-terminal domain exchange mutants in comparison to their wildtype counterparts NtPIP2;1 and NtAQP1 and their respective terminal domain deletion mutants. Proteoliposome samples were produced in L-CF mode and were processed as described in chapters 2.7 through 2.9. The calculation of (proteo)liposome water permeability by non-linear regression is described in chapter 2.10.1.

3.7.1 Exchange of N-terminal domain

In order to further specify the role of the N-terminus in the water permeating ability of NtPIP2;1 and NtAQP1, respective domain exchange mutants were generated and compared to their wildtype counterparts (see chapters 3.1 and 3.2). Previously obtained results of the corresponding N-terminal deletion constructs were also added for comparison. Fig. 45 and Table 33 summarize the data obtained for the NtPIP2;1 derived N-terminal domain exchange mutant (N)A1_P2, whereas Fig. 46 and Table 34 illustrate the water permeability of the NtAQP1 derived counterpart (N)P2_A1.

Exchanging the native N-terminal domain of NtPIP2;1 with that of NtAQP1 resulted in a significant drop of aquaporin function down to 60 % of wildtype levels. In comparison with the previously obtained data from the N-terminal deletion mutant Δ(N)_P2, there was no significant difference. This equates the functional contribution of the NtAQP1 N-terminus to NtPIP2;1 water permeability to that of an altogether absent N-terminal domain. In contrast, the exchange of the native NtAQP1 N-terminus with that of NtPIP2;1 in (N)P2_A1 showed a significant 8 % rise in water permeation when compared to wildtype levels. Comparing this P_f value with that of the corresponding N-terminal deletion mutant Δ(N)_A1, the difference increases to almost 20 %. However, deleting the N-terminal domain did not demonstrate a statistical significance when compared to wildtype NtAQP1.

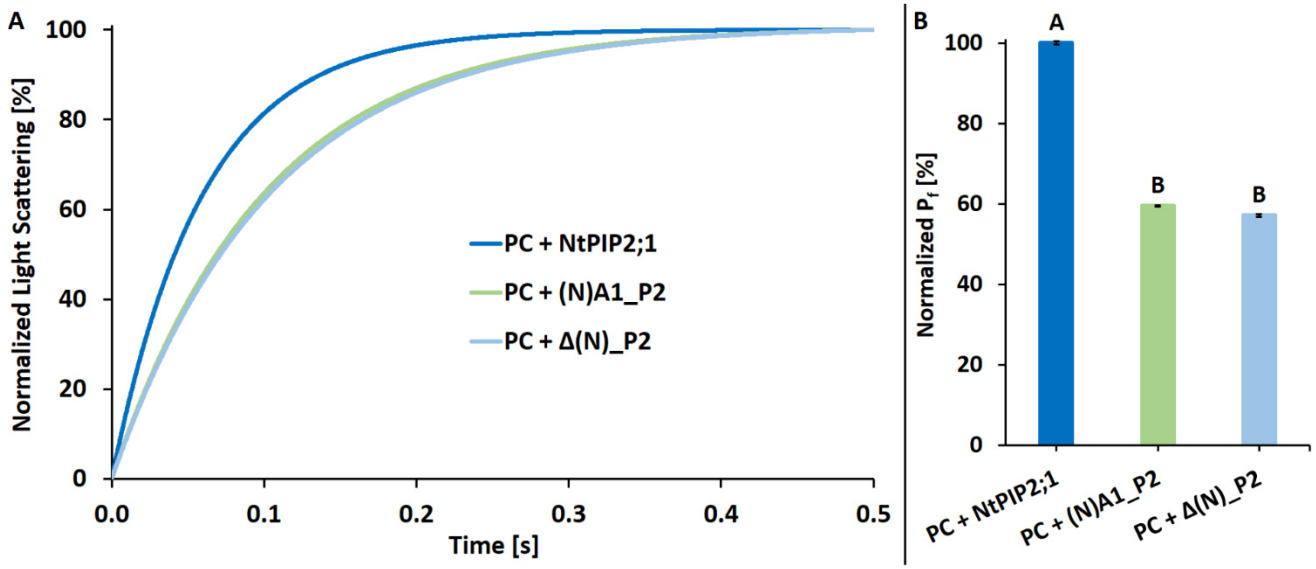

Fig. 45 – Stopped Flow water permeability measurements of L-CF produced and L-α-phosphatidylcholine derived proteoliposomes (PC) containing wildtype aquaporin NtPIP2;1 and its N-terminal domain exchange mutant (N)A1_P2, respectively. In addition to the exchange mutant, which has the NtAQP1 N-terminus instead of its native domain in place (see chapters 3.1 and 3.2), the corresponding N-terminal deletion construct Δ(N)_P2 was included for comparison. Normalized light scattering kinetics measured at 436 nm are the result of shrinking liposomes via a hyperosmotically induced gradient. Each kinetic shown (A) is an average of several individual raw kinetics of one sample (see Table 33), that were fitted to an exponential rise equation. Water permeability values are based on the steepness of the slopes and are shown in the form of the water permeability factor P_f (B), which was normalized to the wildtype aquaporin. Letters on top of the P_f columns indicate statistical significance groups determined via a two-tailed t-Test ($p < 0.05$), whereas error bars illustrate standard error.

Table 33 – Stopped Flow water permeability and statistical significance data of L-CF produced and L-α-phosphatidylcholine derived proteoliposomes (PC) containing wildtype aquaporin NtPIP2;1, its N-terminal domain exchange mutant (N)A1_P2 and the corresponding N-terminal deletion construct Δ(N)_P2, respectively. Given are average values ± standard error (SE) derived from n number of samples for kinetic slope steepness constant k, water permeability factor P_f (both normalized to the wildtype aquaporin) and fitting distance F_D as an indicator for the quality of the fitted kinetics shown in Fig. 44. p values derived from a two-tailed t-Test are shown for each sample pair and divided up into 5 significance levels: ns = not significant ($p > 0.05$) / * = significant ($0.01 < p < 0.05$) / ** = very significant ($0.001 < p < 0.01$) / * = extremely significant ($0.0001 < p < 0.001$) / **** = extremely significant ($p < 0.0001$).**

Sample	k ± SE [%]	P_f ± SE [%]	F_D ± SE [%]	n	p	Significance
PC + NtPIP2;1	100.00 ± 0.43	100.00 ± 0.43	3.11 ± 0.015	65	1.54×10^{-17} (PC + (N)A1_P2)	****
PC + (N)A1_P2	59.47 ± 0.18	59.47 ± 0.18	2.17 ± 0.003	60	0.3438 (PC + Δ(N)_P2)	ns
PC + Δ(N)_P2	57.16 ± 0.34	57.16 ± 0.34	3.69 ± 0.014	38	6.69×10^{-20} (PC + NtPIP2;1)	****

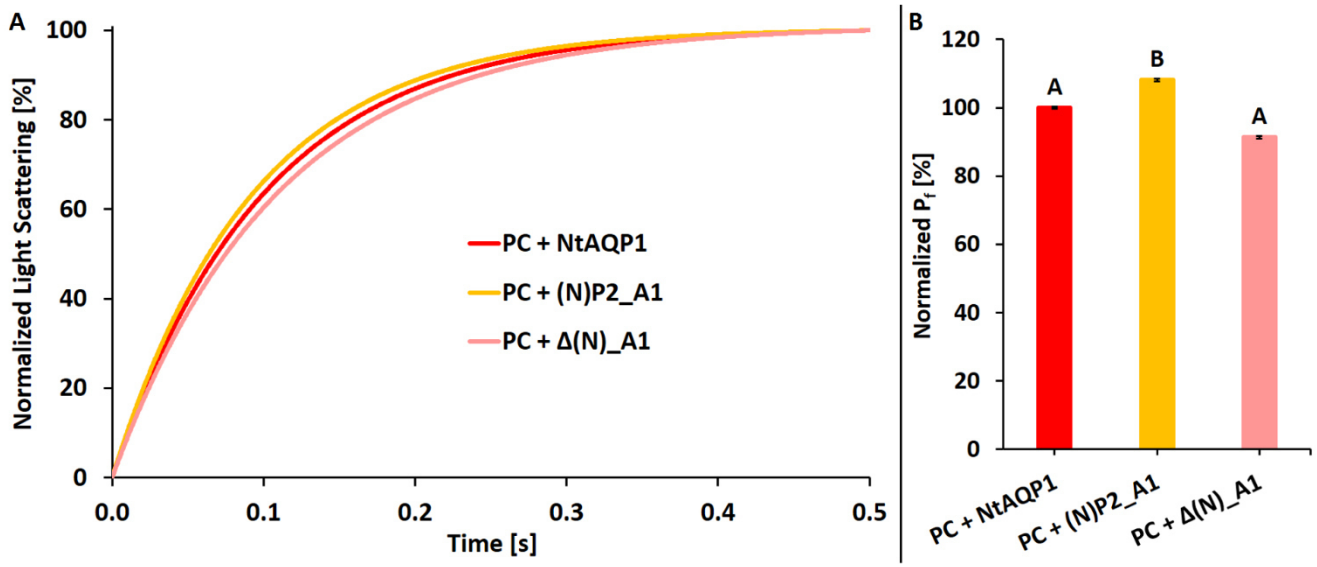

Fig. 46 – Stopped Flow water permeability measurements of L-CF produced and L-α-phosphatidylcholine derived proteoliposomes (PC) containing wildtype aquaporin NtAQP1 and its N-terminal domain exchange mutant (N)P2_A1, respectively. In addition to the exchange mutant, which has the NtPIP2;1 N-terminus instead of its native domain in place (see chapters 3.1 and 3.2), the corresponding N-terminal deletion construct Δ(N)_A1 was included for comparison. Normalized light scattering kinetics measured at 436 nm are the result of shrinking liposomes via a hyperosmotically induced gradient. Each kinetic shown (A) is an average of several individual raw kinetics of one sample (see Table 34), that were fitted to an exponential rise equation. Water permeability values are based on the steepness of the slopes and are shown in the form of the water permeability factor P_f (B), which was normalized to the wildtype aquaporin. Letters on top of the P_f columns indicate statistical significance groups determined via a two-tailed t-Test ($p < 0.05$), whereas error bars illustrate standard error.

Table 34 – Stopped Flow water permeability and statistical significance data of L-CF produced and L-α-phosphatidylcholine derived proteoliposomes (PC) containing wildtype aquaporin NtAQP1, its N-terminal domain exchange mutant (N)P2_A1 and the corresponding N-terminal deletion construct Δ(N)_A1, respectively. Given are average values ± standard error (SE) derived from n number of samples for kinetic slope steepness constant k, water permeability factor P_f (both normalized to the wildtype aquaporin) and fitting distance F_D as an indicator for the quality of the fitted kinetics shown in Fig. 45. p values derived from a two-tailed t-Test are shown for each sample pair and divided up into 5 significance levels: ns = not significant ($p > 0.05$) / * = significant ($0.01 < p < 0.05$) / ** = very significant ($0.001 < p < 0.01$) / * = extremely significant ($0.0001 < p < 0.001$) / **** = extremely significant ($p < 0.0001$).**

Sample	k ± SE [%]	P_f ± SE [%]	F_D ± SE [%]	n	p	Significance
PC + NtAQP1	100.00 ± 0.28	100.00 ± 0.28	2.32 ± 0.011	59	0.0175 (PC + (N)P2_A1)	*
PC + (N)P2_A1	108.19 ± 0.40	108.19 ± 0.40	2.69 ± 0.007	53	3.86×10^{-5} (PC + Δ(N)_A1)	****
PC + Δ(N)_A1	91.35 ± 0.43	91.35 ± 0.43	2.92 ± 0.007	41	0.0622 (PC + NtAQP1)	ns

3.7.2 Exchange of C-terminal domain

Analogously to the N-terminal domain exchange mutants, NtPIP2;1 and NtAQP1 constructs were generated with their C-termini replaced in order to determine the impact on their water permeability (see chapters 3.1 and 3.2). Respective C-terminal deletion constructs were added for comparison. Fig. 47 and Table 35 give an overview on the data obtained for the NtPIP2;1 derived C-terminal domain exchange mutant P2_(C)A1, whereas Fig. 48 and Table 36 show water permeability values of the NtAQP1 derived counterpart A1_(C)P2.

As was the case with the exchange of its native N-terminus, replacing the C-terminal domain of NtPIP2;1 with that of NtAQP1 resulted in a significantly lowered water permeation at 63 % of wildtype levels. When compared to the C-terminal deletion mutant P2_Δ(C), no statistical significance could be determined. In opposition to that, the implementation of the NtPIP2;1 C-terminus provided A1_(C)P2 with a significant 18 % boost in water permeability when compared to wildtype levels. This diverged from the C-terminal deletion mutant A1_Δ(C), which did not show a statistically significant change in aquaporin function when compared to NtAQP1.

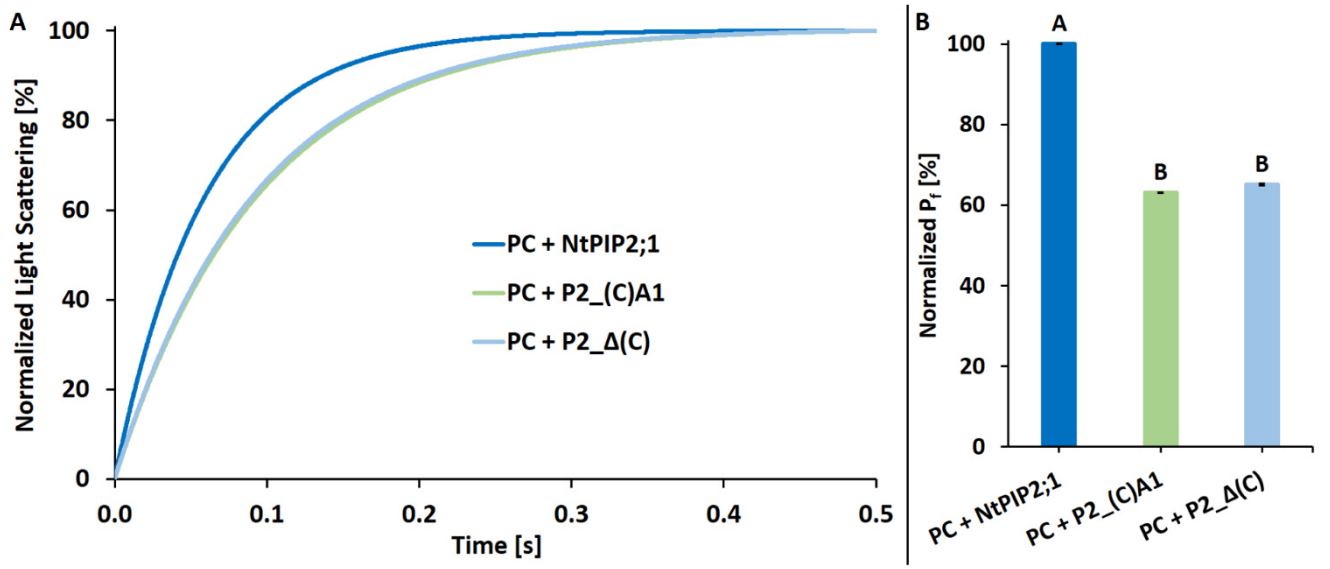

Fig. 47 – Stopped Flow water permeability measurements of L-CF produced and L-α-phosphatidylcholine derived proteoliposomes (PC) containing wildtype aquaporin NtPIP2;1 and its C-terminal domain exchange mutant P2_(C)A1, respectively. In addition to the exchange mutant, which has the NtAQP1 C-terminus instead of its native domain in place (see chapters 3.1 and 3.2), the corresponding C-terminal deletion construct P2_ Δ (C) was included for comparison. Normalized light scattering kinetics measured at 436 nm are the result of shrinking liposomes via a hyperosmotically induced gradient. Each kinetic shown (A) is an average of several individual raw kinetics of one sample (see Table 35), that were fitted to an exponential rise equation. Water permeability values are based on the steepness of the slopes and are shown in the form of the water permeability factor P_f (B), which was normalized to the wildtype aquaporin. Letters on top of the P_f columns indicate statistical significance groups determined via a two-tailed t-Test ($p < 0.05$), whereas error bars illustrate standard error.

Table 35 – Stopped Flow water permeability and statistical significance data of L-CF produced and L-α-phosphatidylcholine derived proteoliposomes (PC) containing wildtype aquaporin NtPIP2;1, its C-terminal domain exchange mutant P2_(C)A1 and the corresponding C-terminal deletion construct P2_Δ(C), respectively. Given are average values ± standard error (SE) derived from n number of samples for kinetic slope steepness constant k, water permeability factor P_f (both normalized to the wildtype aquaporin) and fitting distance F_D as an indicator for the quality of the fitted kinetics shown in Fig. 46. p values derived from a two-tailed t-Test are shown for each sample pair and divided up into 5 significance levels: ns = not significant ($p > 0.05$) / * = significant ($0.01 < p < 0.05$) / ** = very significant ($0.001 < p < 0.01$) / * = extremely significant ($0.0001 < p < 0.001$) / **** = extremely significant ($p < 0.0001$).**

Sample	k ± SE [%]	P_f ± SE [%]	F_D ± SE [%]	n	p	Significance
PC + NtPIP2;1	100.00 ± 0.14	100.00 ± 0.14	2.82 ± 0.003	129	4.60×10^{-49} (PC + P2_(C)A1)	****
PC + P2_(C)A1	63.13 ± 0.08	63.13 ± 0.08	2.37 ± 0.002	119	0.3128 (PC + P2_Δ(C))	ns
PC + P2_Δ(C)	65.10 ± 0.32	65.10 ± 0.32	2.63 ± 0.006	35	1.79×10^{-21} (PC + NtPIP2;1)	****

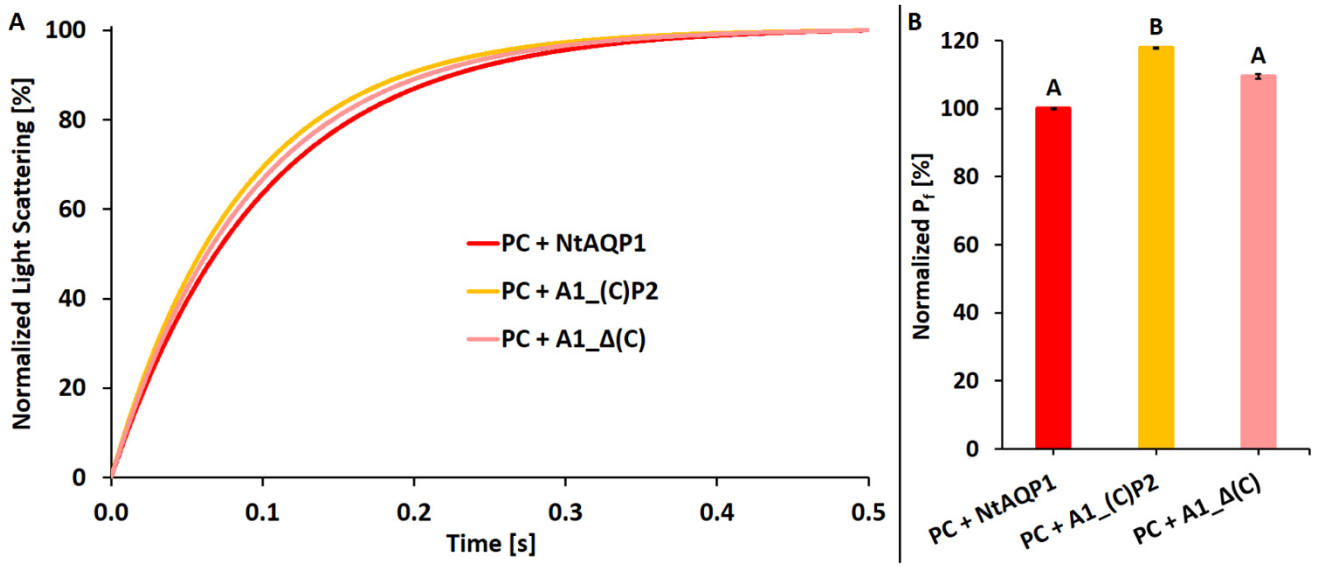

Fig. 48 – Stopped Flow water permeability measurements of L-CF produced and L-α-phosphatidylcholine derived proteoliposomes (PC) containing wildtype aquaporin NtAQP1 and its C-terminal domain exchange mutant A1_(C)P2, respectively. In addition to the exchange mutant, which has the NtPIP2;1 C-terminus instead of its native domain in place (see chapters 3.1 and 3.2), the corresponding C-terminal deletion construct A1_ Δ(C) was included for comparison. Normalized light scattering kinetics measured at 436 nm are the result of shrinking liposomes via a hyperosmotically induced gradient. Each kinetic shown (A) is an average of several individual raw kinetics of one sample (see Table 36), that were fitted to an exponential rise equation. Water permeability values are based on the steepness of the slopes and are shown in the form of the water permeability factor P_f (B), which was normalized to the wildtype aquaporin. Letters on top of the P_f columns indicate statistical significance groups determined via a two-tailed t-Test ($p < 0.05$), whereas error bars illustrate standard error.

Table 36 – Stopped Flow water permeability and statistical significance data of L-CF produced and L-α-phosphatidylcholine derived proteoliposomes (PC) containing wildtype aquaporin NtAQP1, its C-terminal domain exchange mutant A1_(C)P2 and the corresponding C-terminal deletion construct A1_Δ(C), respectively. Given are average values ± standard error (SE) derived from n number of samples for kinetic slope steepness constant k, water permeability factor P_f (both normalized to the wildtype aquaporin) and fitting distance F_D as an indicator for the quality of the fitted kinetics shown in Fig. 47. p values derived from a two-tailed t-Test are shown for each sample pair and divided up into 5 significance levels: ns = not significant ($p > 0.05$) / * = significant ($0.01 < p < 0.05$) / ** = very significant ($0.001 < p < 0.01$) / * = extremely significant ($0.0001 < p < 0.001$) / **** = extremely significant ($p < 0.0001$).**

Sample	k ± SE [%]	P_f ± SE [%]	F_D ± SE [%]	n	p	Significance
PC + NtAQP1	100.00 ± 0.18	100.00 ± 0.18	2.35 ± 0.002	108	1.03×10^{-7} (PC + A1_(C)P2)	****
PC + A1_(C)P2	117.84 ± 0.22	117.84 ± 0.22	2.61 ± 0.003	129	0.0480 (PC + A1_Δ(C))	*
PC + A1_Δ(C)	109.50 ± 0.71	109.50 ± 0.71	3.22 ± 0.027	19	0.0842 (PC + NtAQP1)	ns

3.7.3 Exchange of N- and C-terminal domains

After determining the water permeability of their N- and C-terminal domain exchange mutants, respectively, double exchange mutants of NtPIP2;1 and NtAQP1 were generated in order to measure the impact on their water permeation (see chapters 3.1 and 3.2). Corresponding N- and C-terminal deletion constructs were added for comparison. Fig. 49 and Table 37 illustrate the data obtained for the NtPIP2;1 derived N- and C-terminal double deletion mutant (N)A1_P2_(C)A1, whereas Fig. 50 and Table 38 summarize the water permeation capability of the NtAQP1 derived counterpart (N)P2_A1_ (C)P2.

The combined replacement of both terminal domains in NtPIP2;1 demonstrated a significantly reduced water permeation at 61 % of wildtype levels. This resulted in an 18 % higher aquaporin function than the double deletion construct Δ(N)_P2_Δ(C), which was calculated to be statistically significant. In comparison, the exchange of both terminal domains in NtAQP1 enhanced the water transport rate of (N)P2_A1_(C)P2 to 145 % of its wildtype. This stands in significant contrast to its double deletion counterpart Δ(N)_A1_Δ(C), which is overtaken by 93 %.

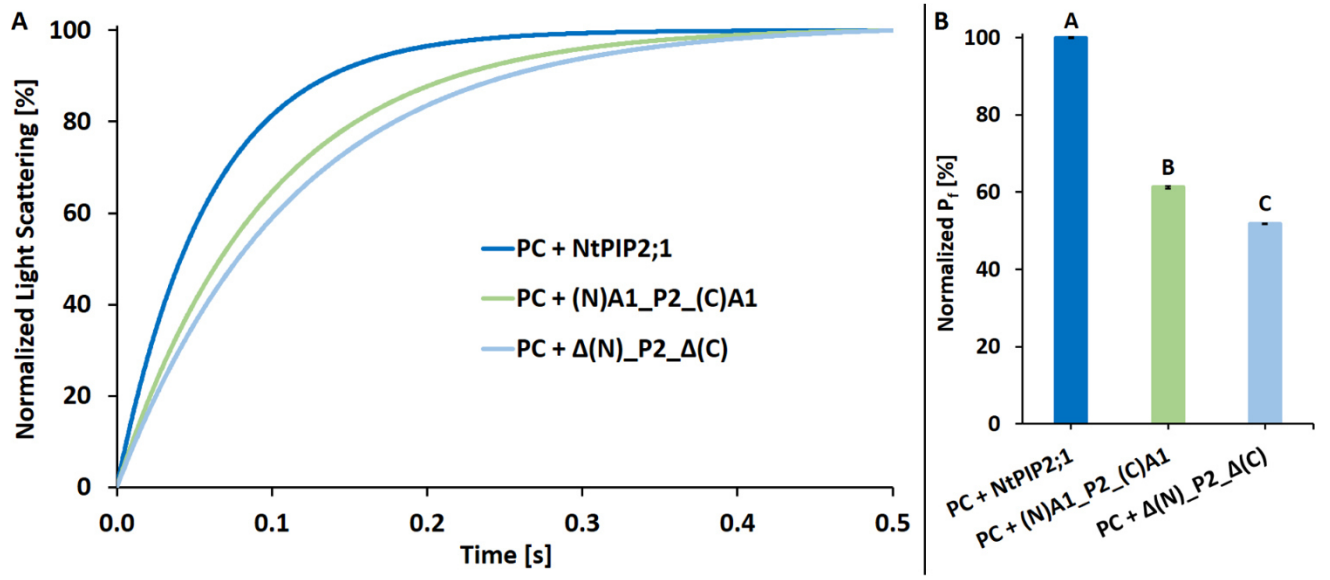

Fig. 49 – Stopped Flow water permeability measurements of L-CF produced and L-α-phosphatidylcholine derived proteoliposomes (PC) containing wildtype aquaporin NtPIP2;1 and its N- and C-terminal domain exchange mutant (N)A1_P2_(C)A1, respectively. In addition to the exchange mutant, which has the NtAQP1 N- and C-termini instead of its native domains in place (see chapters 3.1 and 3.2), the corresponding N- and C-terminal deletion construct Δ(N)_P2_ Δ(C) was included for comparison. Normalized light scattering kinetics measured at 436 nm are the result of shrinking liposomes via a hyperosmotically induced gradient. Each kinetic shown (A) is an average of several individual raw kinetics of one sample (see Table 37), that were fitted to an exponential rise equation. Water permeability values are based on the steepness of the slopes and are shown in the form of the water permeability factor P_f (B), which was normalized to the wildtype aquaporin. Letters on top of the P_f columns indicate statistical significance groups determined via a two-tailed t-Test ($p < 0.05$), whereas error bars illustrate standard error.

Table 37 – Stopped Flow water permeability and statistical significance data of L-CF produced and L-α-phosphatidylcholine derived proteoliposomes (PC) containing wildtype aquaporin NtPIP2;1, its N- and C-terminal domain exchange mutant (N)A1_P2_(C)A1 and the corresponding N- and C-terminal deletion construct Δ(N)_P2_Δ(C), respectively. Given are average values ± standard error (SE) derived from n number of samples for kinetic slope steepness constant k, water permeability factor P_f (both normalized to the wildtype aquaporin) and fitting distance F_D as an indicator for the quality of the fitted kinetics shown in Fig. 48. p values derived from a two-tailed t-Test are shown for each sample pair and divided up into 5 significance levels: ns = not significant ($p > 0.05$) / * = significant ($0.01 < p < 0.05$) / ** = very significant ($0.001 < p < 0.01$) / * = extremely significant ($0.0001 < p < 0.001$) / **** = extremely significant ($p < 0.0001$).**

Sample	k ± SE [%]	P_f ± SE [%]	F_D ± SE [%]	n	p	Significance
PC + NtPIP2;1	100.00 ± 0.22	100.00 ± 0.22	3.32 ± 0.006	72	1.19×10^{-26} (PC + (N)A1_P2_(C)A1)	****
PC + (N)A1_P2_(C)A1	61.25 ± 0.28	61.25 ± 0.28	2.76 ± 0.011	51	3.80×10^{-5} (PC + Δ(N)_P2_Δ(C))	****
PC + Δ(N)_P2_Δ(C)	51.86 ± 0.10	51.86 ± 0.10	2.22 ± 0.050	32	1.97×10^{-13} (PC + NtPIP2;1)	****

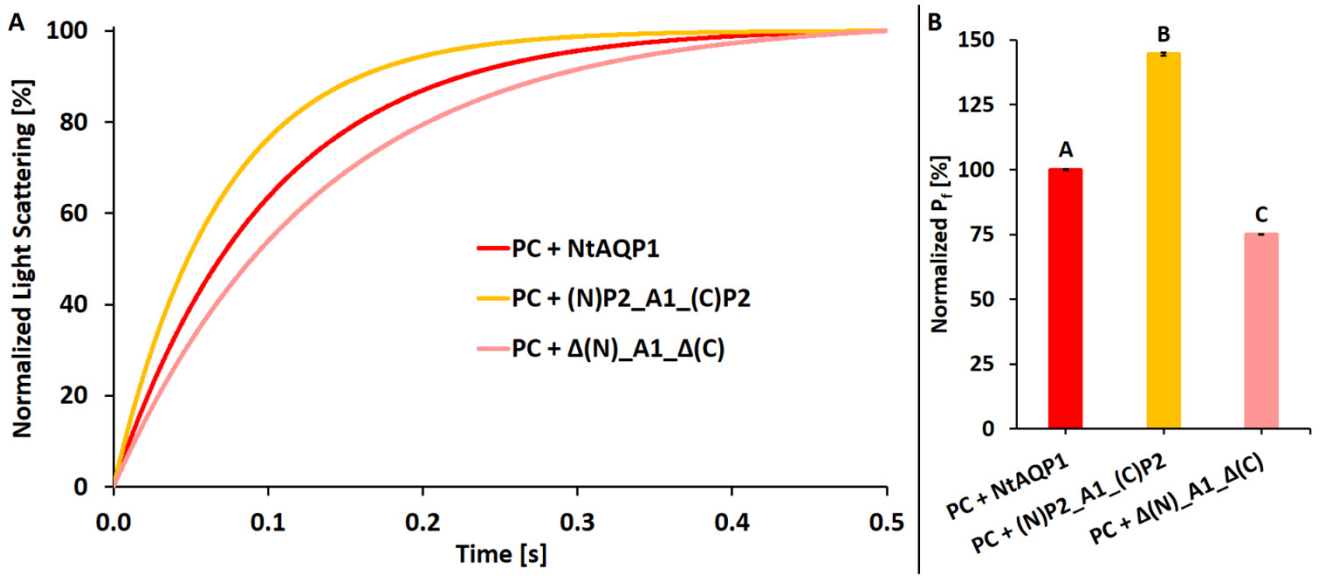

Fig. 50 – Stopped Flow water permeability measurements of L-CF produced and L-α-phosphatidylcholine derived proteoliposomes (PC) containing wildtype aquaporin NtAQP1 and its N- and C-terminal domain exchange mutant (N)P2_A1_(C)P2, respectively. In addition to the exchange mutant, which has the NtPIP2;1 N- and C-termini instead of its native domains in place (see chapters 3.1 and 3.2), the corresponding N- and C-terminal deletion construct Δ(N)_A1_Δ(C) was included for comparison. Normalized light scattering kinetics measured at 436 nm are the result of shrinking liposomes via a hyperosmotically induced gradient. Each kinetic shown (A) is an average of several individual raw kinetics of one sample (see Table 38), that were fitted to an exponential rise equation. Water permeability values are based on the steepness of the slopes and are shown in the form of the water permeability factor P_f (B), which was normalized to the wildtype aquaporin. Letters on top of the P_f columns indicate statistical significance groups determined via a two-tailed t-Test ($p < 0.05$), whereas error bars illustrate standard error.

Table 38 – Stopped Flow water permeability and statistical significance data of L-CF produced and L-α-phosphatidylcholine derived proteoliposomes (PC) containing wildtype aquaporin NtAQP1, its N- and C-terminal domain exchange mutant (N)P2_A1_(C)P2 and the corresponding N- and C-terminal deletion construct Δ(N)_A1_Δ(C), respectively. Given are average values ± standard error (SE) derived from n number of samples for kinetic slope steepness constant k, water permeability factor P_f (both normalized to the wildtype aquaporin) and fitting distance F_D as an indicator for the quality of the fitted kinetics shown in Fig. 49. p values derived from a two-tailed t-Test are shown for each sample pair and divided up into 5 significance levels: ns = not significant ($p > 0.05$) / * = significant ($0.01 < p < 0.05$) / ** = very significant ($0.001 < p < 0.01$) / * = extremely significant ($0.0001 < p < 0.001$) / **** = extremely significant ($p < 0.0001$).**

Sample	k ± SE [%]	P_f ± SE [%]	F_D ± SE [%]	n	p	Significance
PC + NtAQP1	100.00 ± 0.35	100.00 ± 0.35	2.75 ± 0.003	112	$8.54x10^{-10}$ (PC + (N)P2_A1_(C)P2)	****
PC + (N)P2_A1_(C)P2	144.54 ± 0.65	144.54 ± 0.65	2.81 ± 0.010	74	$1.22x10^{-19}$ (PC + Δ(N)_A1_Δ(C))	****
PC + Δ(N)_A1_Δ(C)	75.01 ± 0.14	75.01 ± 0.14	2.36 ± 0.006	37	$9.95x10^{-28}$ (PC + NtAQP1)	****

3.7.4 Summary of NtPIP2;1 N- and C-terminal domain exchange mutants

In order to put the water permeation capabilities of NtPIP2;1 derived N- and C-terminal exchange mutants into context with each other and the respective controls, as well as the corresponding deletion constructs, the data collected from chapters 3.6.1 through 3.6.3 and 3.7.1 through 3.7.3 were summarized in Fig. 51 and Table 39. Independently from the type of terminal domain exchange with NtAQP1, a significant loss of water permeation capability was observed in each NtPIP2;1 protein mutant. This goes in line with their deletion counterparts, encompassing an overall range of 52 to 65 % of NtPIP2;1 wildtype levels. A direct comparison among single deletion and exchange constructs revealed, that the terminal domains of NtAQP1 equate in functionality to the absence of NtPIP2;1 native termini. Thus, there was no statistical difference between a single terminal domain exchange with NtAQP1 or outright deletion of a native NtPIP2;1 terminus. Another similarity between single deletion and single exchange constructs was the slight but significantly higher impact of an N-terminal deletion / exchange when compared with its respective C-terminal counterpart. On average, an N-terminal modification resulted in an approximately 10 % lower water permeability than a C-terminal modification. However, replacing both NtPIP2;1 termini with those of NtAQP1 resulted in a water permeation intermediate to the single exchange

mutants and thus without a statistically significant difference to either of them. In contrast, the deletion of both NtPIP2;1 terminal domains resulted in a significantly lower water permeability than all of the other NtPIP2;1 based constructs. Interestingly, any N-terminal modification or the exchange of both NtPIP2;1 termini essentially reprogrammed NtPIP2;1 into NtAQP1 with no significant difference in their water transport rates. In conclusion, both terminal NtPIP2;1 domains are fundamental for the aquaporin´s capability for high water transport rates, with NtAQP1 terminal substitutes being basically superfluous in their functional contribution.

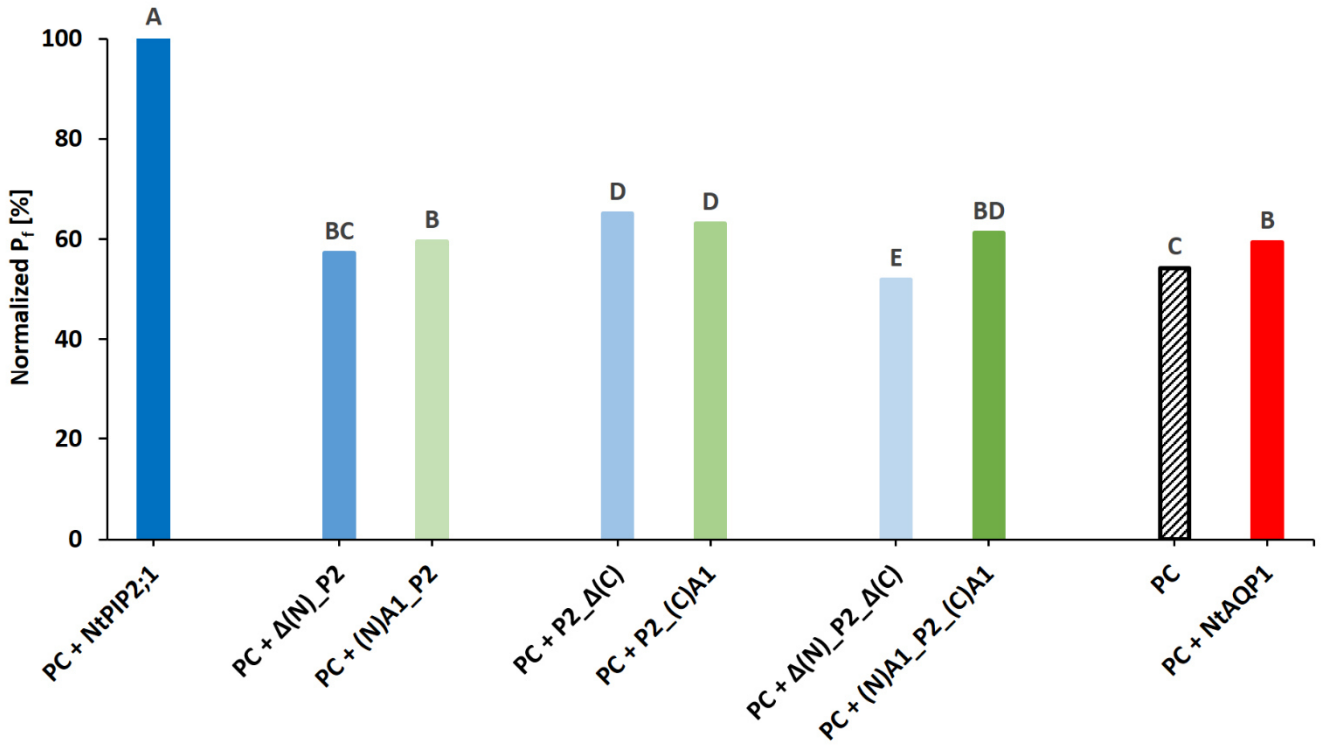

Fig. 51 – Overview on P_f based water permeation capabilities of L-CF produced and L-α-phosphatidylcholine derived proteoliposomes (PC) containing wildtype aquaporin NtPIP2;1 and its single and double N- and C-terminal deletion (blue) and exchange (green) mutants. Empty PC liposomes and NtAQP1 wildtype proteoliposomes were also included for comparison. Water permeability values were calculated from the slope steepness of Stopped Flow light scattering kinetics by non-linear regression fitting to an exponential rise equation. They are shown in the form of the water permeability factor P_f, which was normalized to the wildtype NtPIP2;1. Letters on top of the P_f columns indicate statistical significance groups determined via a two-tailed t-Test ($p < 0.05$). Δ(N)_P2 = N-terminal deletion mutant / P2_Δ(C) = C-terminal deletion mutant / Δ(N)_P2_Δ(C) = N- and C-terminal double deletion mutant / (N)A1_P2 = NtPIP2;1 with its native N-terminus replaced by that of NtAQP1 / P2_(C)A1 = NtPIP2;1 with its native C-terminus replaced by that of NtAQP1 / (N)A1_P2_(C)A1 = NtPIP2;1 with its native N- and C-terminal domains replaced by those of NtAQP1.

Table 39 – Overview on P_f based water permeation capabilities and statistical significance data of L-CF produced and L-α-phosphatidylcholine derived proteoliposomes (PC) containing wildtype aquaporin NtPIP2;1 and its single and double N- and C-terminal deletion and exchange mutants. Empty PC liposomes and NtAQP1 wildtype proteoliposomes were also included for comparison. Given are average values as shown in Fig. 50 for the water permeability factor P_f, which was normalized to the wildtype NtPIP2;1. p values derived from a two-tailed t-Test are shown for each sample pair and divided up into 5 significance levels: ns = not significant ($p > 0.05$) / * = significant ($0.01 < p < 0.05$) / ** = very significant ($0.001 < p < 0.01$) / * = extremely significant ($0.0001 < p < 0.001$) / **** = extremely significant ($p < 0.0001$). Δ(N)_P2 = N-terminal deletion mutant / P2_Δ(C) = C-terminal deletion mutant / Δ(N)_P2_Δ(C) = N- and C-terminal double deletion mutant / (N)A1_P2 = NtPIP2;1 with its native N-terminus replaced by that of NtAQP1 / P2_(C)A1 = NtPIP2;1 with its native C-terminus replaced by that of NtAQP1 / (N)A1_P2_(C)A1 = NtPIP2;1 with its native N- and C-terminal domains replaced by those of NtAQP1.**

Sample	P_f [%]	PC + NtAQP1	PC	PC + (N)A1_P2_(C)A1	PC + Δ(N)_P2_Δ(C)	PC + P2_(C)A1	PC + P2_Δ(C)	PC + (N)A1_P2	PC + Δ(N)_P2
PC + NtPIP2;1	100.00	**** 1.99×10^{-85}	**** 1.61×10^{-104}	**** 1.19×10^{-26}	**** 1.97×10^{-13}	**** 4.60×10^{-49}	**** 1.79×10^{-21}	**** 1.54×10^{-17}	**** 6.69×10^{-20}
PC + Δ(N)_P2	57.16	ns 0.3540	ns 0.2050	ns 0.1717	* 0.0201	* 0.0122	** 0.0075	ns 0.3438	- -
PC + (N)A1_P2	59.47	ns 0.9430	** 0.0015	ns 0.4680	**** 2.97×10^{-6}	* 0.0228	* 0.0180	- -	- -

Sample	P_f [%]	PC + NtAQP1	PC	PC + (N)A1_P2_(C)A1	PC + Δ(N)_P2_Δ(C)	PC + P2_(C)A1	PC + P2_Δ(C)	PC + (N)A1_P2	PC + Δ(N)_P2
PC + P2_Δ(C)	65.10	* 0.0105	**** $6.78x10^{-6}$	ns 0.1911	**** $7.92x10^{-8}$	ns 0.3128	- -	- -	- -
PC + P2_(C)A1	63.13	** 0.0046	**** $1.58x10^{-12}$	ns 0.3990	**** $2.25x10^{-19}$	- -	- -	- -	- -
PC + Δ(N)_P2_Δ(C)	51.86	**** $3.87x10^{-10}$	* 0.0213	**** $3.80x10^{-5}$	- -	- -	- -	- -	- -
PC + (N)A1_P2_(C)A1	61.25	ns 0.3980	*** 0.0008	- -	- -	- -	- -	- -	- -
PC	54.22	**** $6.69x10^{-5}$	- -	- -	- -	- -	- -	- -	- -
PC + NtAQP1	59.34	- -	- -	- -	- -	- -	- -	- -	- -

3.7.5 Summary of NtAQP1 N- and C-terminal domain exchange mutants

Analogously to the NtPIP2;1 N- and C-terminal exchange and deletion mutants, the data collected from chapters 3.6.1 through 3.6.3 and 3.7.1 through 3.7.3 for the NtAQP1 counterparts were summarized in Fig. 52 and Table 40.

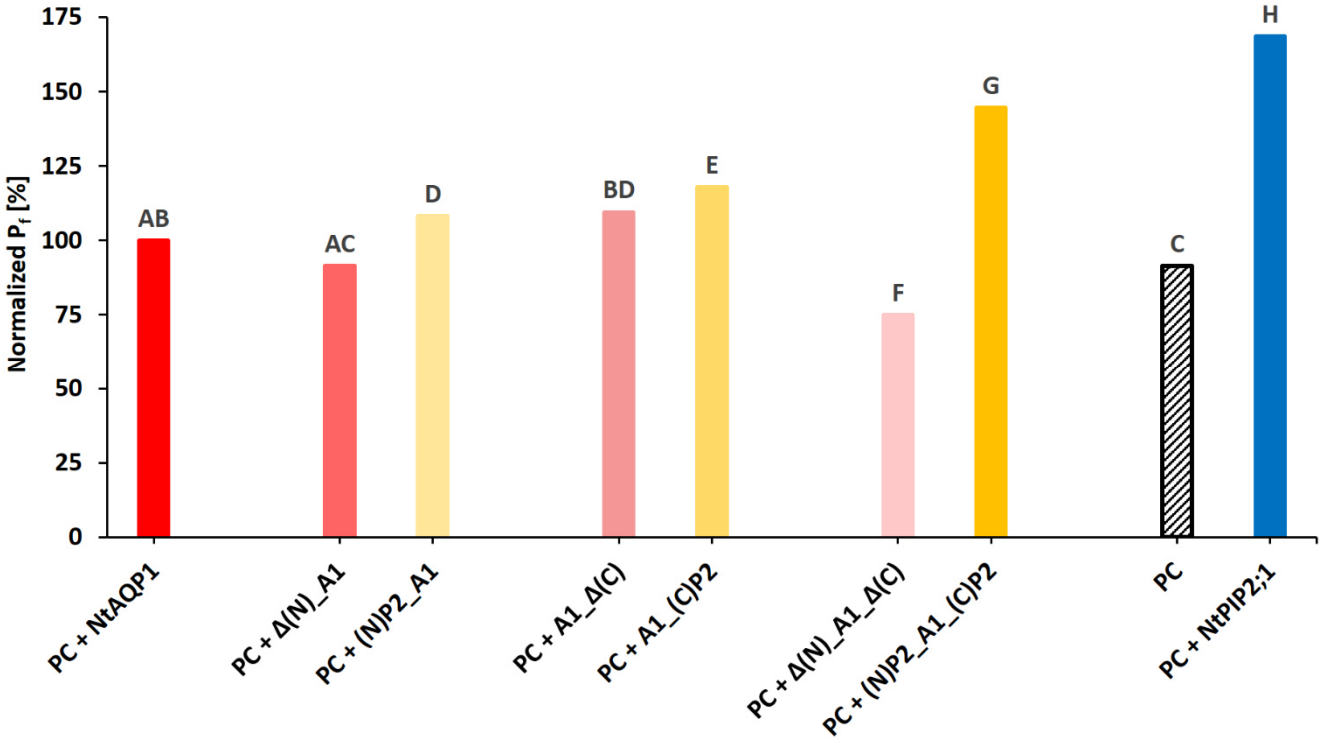

Fig. 52 – Overview on P_f based water permeation capabilities of L-CF produced and L-α-phosphatidylcholine derived proteoliposomes (PC) containing wildtype aquaporin NtAQP1 and its single and double N- and C-terminal deletion (red) and exchange (yellow/orange) mutants. Empty PC liposomes and NtPIP2;1 wildtype proteoliposomes were also included for comparison. Water permeability values were calculated from the slope steepness of Stopped Flow light scattering kinetics by non-linear regression fitting to an exponential rise equation. They are shown in the form of the water permeability factor P_f, which was normalized to the wildtype NtAQP1. Letters on top of the P_f columns indicate statistical significance groups determined via a two-tailed t-Test ($p < 0.05$). Δ(N)_A1 = N-terminal deletion mutant / A1_Δ(C) = C-terminal deletion mutant / Δ(N)_A1_Δ(C) = N- and C-terminal double deletion mutant / (N)P2_A1 = NtAQP1 with its native N-terminus replaced by that of NtPIP2;1 / A1_(C)P2 = NtAQP1 with its native C-terminus replaced by that of NtPIP2;1 / (N)P2_A1_(C)P2 = NtAQP1 with its native N- and C-terminal domains replaced by those of NtPIP2;1.

Table 40 – Overview on P_f based water permeation capabilities and statistical significance data of L-CF produced and L-α-phosphatidylcholine derived proteoliposomes (PC) containing wildtype aquaporin NtAQP1 and its single and double N- and C-terminal deletion and exchange mutants. Empty PC liposomes and NtPIP2;1 wildtype proteoliposomes were also included for comparison. Given are average values as shown in Fig. 51 for the water permeability factor P_f, which was normalized to the wildtype NtAQP1. p values derived from a two-tailed t-Test are shown for each sample pair and divided up into 5 significance levels: ns = not significant (p > 0.05) / * = significant (0.01 < p < 0.05) / ** = very significant (0.001 < p < 0.01) / * = extremely significant (0.0001 < p < 0.001) / **** = extremely significant (p < 0.0001). Δ(N)_A1 = N-terminal deletion mutant / A1_Δ(C) = C-terminal deletion mutant / Δ(N)_A1_Δ(C) = N- and C-terminal double deletion mutant / (N)P2_A1 = NtAQP1 with its native N-terminus replaced by that of NtPIP2;1 / A1_(C)P2 = NtAQP1 with its native C-terminus replaced by that of NtPIP2;1 / (N)P2_A1_(C)P2 = NtAQP1 with its native N- and C-terminal domains replaced by those of NtPIP2;1.**

Sample	P_f [%]	PC + NtPIP2;1	PC	PC + (N)P2_A1_(C)P2	PC + Δ(N)_A1_Δ(C)	PC + A1_(C)P2	PC + A1_Δ(C)	PC + (N)P2_A1	PC + Δ(N)_A1
PC + NtAQP1	100.00	**** $1.99x10^{-85}$	**** $6.69x10^{-5}$	**** $8.54x10^{-10}$	**** $9.95x10^{-28}$	**** $1.03x10^{-7}$	ns 0.0842	* 0.0175	ns 0.0622
PC + Δ(N)_A1	91.35	**** $3.66x10^{-42}$	ns 0.9980	**** $1.84x10^{-13}$	**** $9.13x10^{-7}$	**** $2.22x10^{-10}$	*** 0.0002	**** $3.86x10^{-5}$	- -
PC + (N)P2_A1	108.19	**** $9.49x10^{-37}$	**** $7.16x10^{-7}$	**** $6.38x10^{-8}$	**** $1.49x10^{-17}$	* 0.0109	ns 0.7884	- -	- -
PC + A1_Δ(C)	109.50	**** $4.22x10^{-19}$	**** $1.86x10^{-5}$	**** $4.83x10^{-7}$	**** $9.32x10^{-10}$	* 0.0480	- -	- -	- -
PC + A1_(C)P2	117.84	**** $7.53x10^{-36}$	**** $2.22x10^{-16}$	**** $3.78x10^{-5}$	**** $3.78x10^{-33}$	- -	- -	- -	- -
PC + Δ(N)_A1_Δ(C)	75.01	**** $2.22x10^{-128}$	**** $5.76x10^{-20}$	**** $1.22x10^{-19}$	- -	- -	- -	- -	- -
PC + (N)P2_A1_(C)P2	144.54	*** 0.0002	**** $3.18x10^{-14}$	- -	- -	- -	- -	- -	- -
PC	91.36	**** $1.61x10^{-104}$	- -	- -	- -	- -	- -	- -	- -
PC + NtPIP2;1	168.51	- -	- -	- -	- -	- -	- -	- -	- -

Every type of terminal domain exchange with NtPIP2;1 resulted in a significant boost of water permeability in NtAQP1 mutant constructs. This stands in contrast to the NtAQP1 single deletion mutants, which did not significantly differ from the wildtype; and the double deletion mutant, which demonstrated a significant loss in function at 75 % of wildtype levels. N- and C-terminal single exchange with NtPIP2;1 demonstrated 8 % and 18 % higher aquaporin function, respectively. When both terminal domains were exchanged with those of NtPIP2;1, water permeability rose to 45 % above NtAQP1 levels. This effectively doubled transport rates when compared to the double deletion construct Δ(N)_A1_Δ(C), while reaching 86 % of NtPIP2;1 wildtype levels. In conclusion, NtPIP2;1´s water transport capabilities were successfully transferred in part to NtAQP1 via terminal domain replacements, whereas deletion of the native termini only had an impact on NtAQP1 water transport when both were absent.

3.8 Immunological His_6 tag detection of NtPIP2;1 and NtAQP1 wildtypes and mutants

Samples drawn from the L-CF and Stopped Flow derived water permeability measurements of NtPIP2;1, NtAQP1 and their respective deletion, as well as domain exchange mutants (see chapter 3.6 and 3.7), were analyzed via SDS-PAGE and Western Blotting. The detection of the C-terminal His_6 tag in each protein construct took place via chemiluminescence as described in chapter 2.6.3. Fig. 53 illustrates the obtained results.

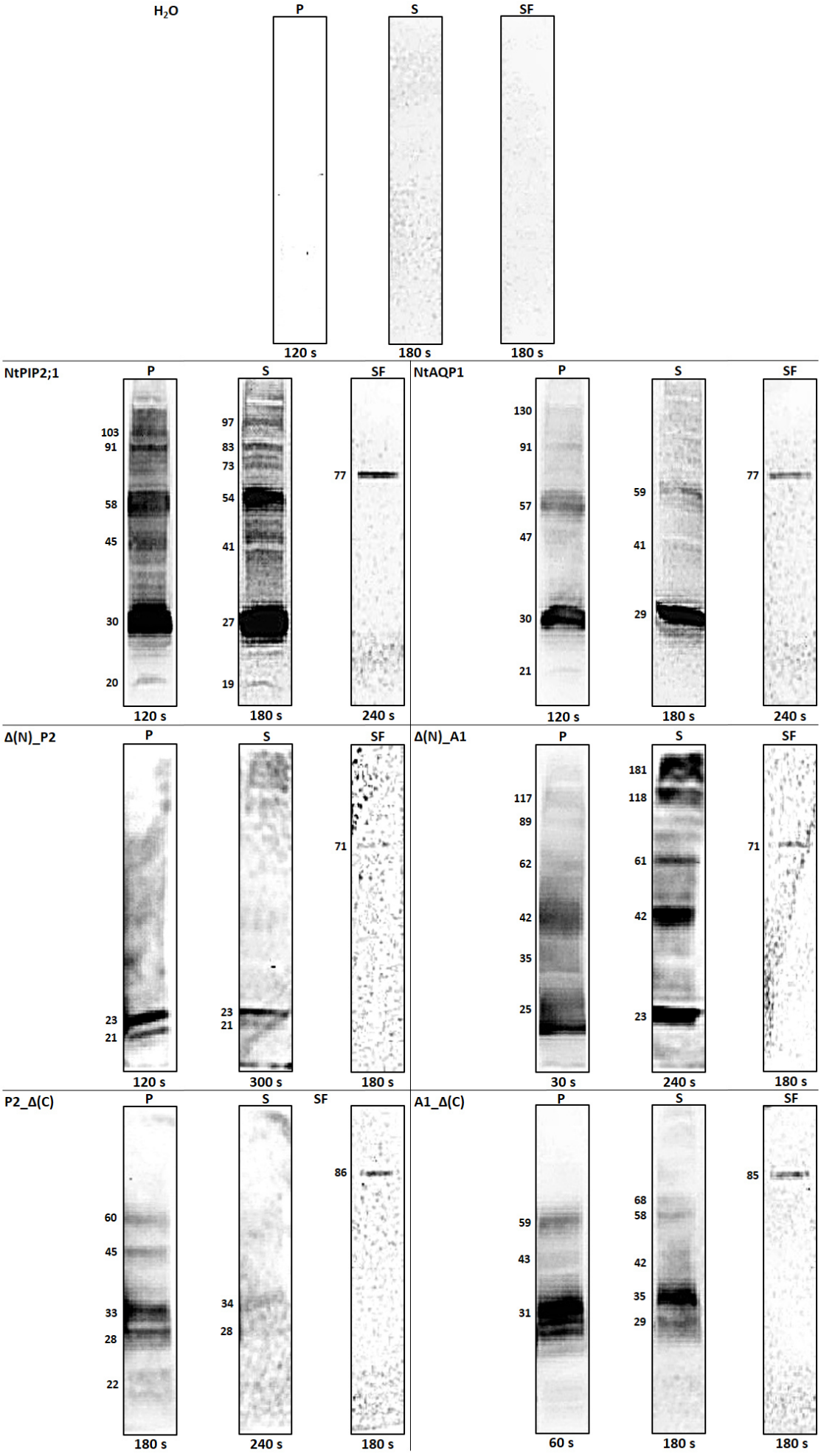
H2O
P
S
SF
120 s
180 s
180 s
NtPIP2;1
103
91
58
45
30
20
120 s
97
83
73
54
41
27
19
180 s
77
240 s
NtAQP1
130
91
57
47
30
21
120 s
59
41
29
180 s
77
240 s
Δ(N)_P2
23
21
120 s
23
21
300 s
71
180 s
Δ(N)_A1
117
89
62
42
35
25
30 s
181
118
61
42
23
240 s
71
180 s
P2_Δ(C)
60
45
33
28
22
180 s
34
28
240 s
86
180 s
A1_Δ(C)
59
43
31
60 s
68
58
42
35
29
180 s
85
180 s

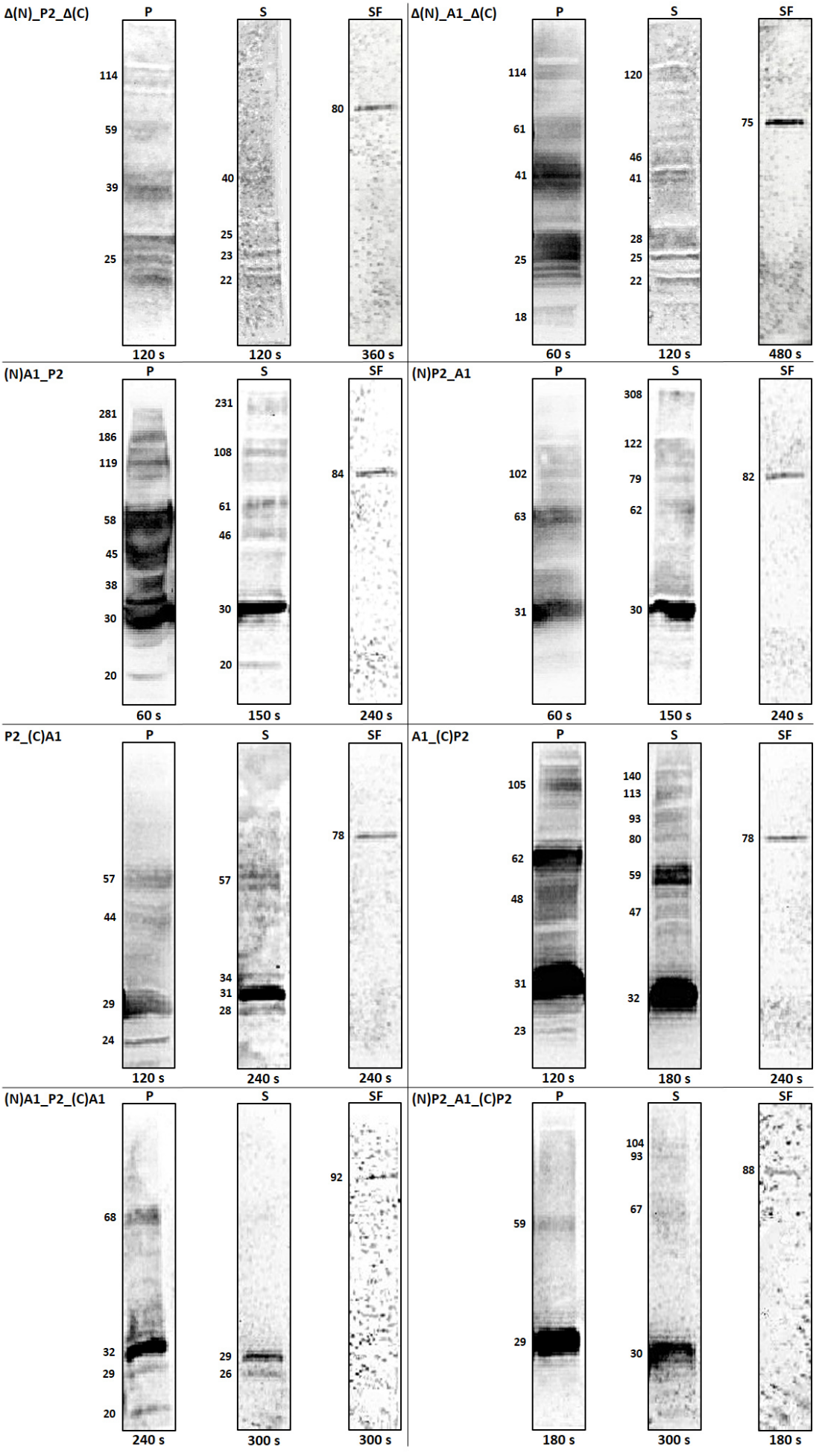
Δ(N)_P2_Δ(C)
P
S
SF
114
59
39
25
40
25
23
22
80
120 s
120 s
360 s
Δ(N)_A1_Δ(C)
P
S
SF
114
61
41
25
18
120
46
41
28
25
22
75
60 s
120 s
480 s
(N)A1_P2
P
S
SF
281
186
119
58
45
38
30
20
231
108
61
46
30
20
84
60 s
150 s
240 s
(N)P2_A1
P
S
SF
102
63
31
308
122
79
62
30
82
60 s
150 s
240 s
P2_(C)A1
P
S
SF
57
44
29
24
57
34
31
28
78
120 s
240 s
240 s
A1_(C)P2
P
S
SF
105
62
48
31
23
140
113
93
80
59
47
32
78
120 s
180 s
240 s
(N)A1_P2_(C)A1
P
S
SF
68
32
29
20
29
26
92
240 s
300 s
300 s
(N)P2_A1_(C)P2
P
S
SF
59
29
104
93
67
30
88
180 s
300 s
180 s

Fig. 53 (previous two pages) – Immunological His_6 tag detection of samples from L-CF based NtPIP2;1 and NtAQP1 terminal deletion and exchange experiments. Pellets (P) and supernatants (S) were drawn after addition of Triton X-100 to pooled L-CF reaction mixes and subsequent centrifugation, thus separating solubilized proteoliposomes from non-integrated and precipitated protein. SF samples represent aliquots of proteoliposomes ready for Stopped Flow assay after Triton X-100 removal and successful reconstitution via SM-2 biobeads treatment, as well as extrusion through a 0.2 µm membrane. S and SF samples underwent chloroform/methanol extraction to isolate the protein contained in the liposomes (see chapter 2.8.7) prior to SDS-PAGE and Western Blotting. Protein quantity of loaded samples is equivalent to 0.36 (P) and 1 (S and SF) L-CF reaction mix. Numbers on the left indicate the molecular weight in kDa of the most prominent signals detected in each sample, calculated via Quantity One software analysis of trace quantities (Bio-Rad, Hercules, California, USA). Numbers below each sample indicate exposure time in seconds. Primary antibody = Mouse anti-polyHis IgG / Secondary Antibody = Alkaline phosphatase-conjugated goat anti-mouse IgG / Detection type = Chemiluminescence with indicated exposure times / Protein standard = PageRuler Prestained Protein Ladder (Thermo Scientific, Waltham, Massachusetts, USA). H_2O = Samples drawn from L-CF reaction mixes containing water instead of a protein-coding plasmid / NtPIP2;1 & NtAQP1 = wildtype aquaporins / Δ(N)_P2 = N-terminal deletion mutant / Δ(N)_A1 = N-terminal deletion mutant / P2_Δ(C) = C-terminal deletion mutant / A1_Δ(C) = C-terminal deletion mutant / Δ(N)_P2_Δ(C) = N- and C-terminal double deletion mutant / Δ(N)_A1_Δ(C) = N- and C-terminal double deletion mutant / (N)A1_P2 = NtPIP2;1 with its native N-terminus replaced by that of NtAQP1 / (N)P2_A1 = NtAQP1 with its native N-terminus replaced by that of NtPIP2;1 / P2_(C)A1 = NtPIP2;1 with its native C-terminus replaced by that of NtAQP1 / A1_(C)P2 = NtAQP1 with its native C-terminus replaced by that of NtPIP2;1 / (N)A1_P2_(C)A1 = NtPIP2;1 with its native N- and C-terminal domains replaced by those of NtAQP1 / (N)P2_A1_(C)P2 = NtAQP1 with its native N- and C-terminal domains replaced by those of NtPIP2;1.

No signal was detected in either of the included H_2O samples, that served as negative control baselines. This meant that all detected signals in the other samples originated conclusively from protein products encoded by pET-21a vectors with aquaporin genes (see chapter 3.1) and not from any other compounds involved in the cell-free expression system. Pellet fractions containing precipitated protein, which was translated, but not integrated into liposomes, showed predominant signals ranging 20 – 30 kDa, 40 – 65 kDa and somewhat less frequent at 70 – 120 kDa. The evident exception here was the N-terminal deletion mutant Δ(N)_P2, which only demonstrated signals at the lowest molecular size range. These three range brackets fall in line with molecular weights previously determined for purified aquaporin monomers, dimers and tetramers (see chapter 3.3). Supernatant samples derived from proteoliposomes solubilized via Triton X-100 were very similar to their pellet counterparts, with the most prominent signals again falling into the three determined molecular size ranges. However, an overall shift down to lower molecular sizes was observed, with monomer and dimer signals increasing in frequency, while tetramer signals declined. Most evident exceptions included the two single terminal deletion mutants Δ(N)_P2 and P2_Δ(C), as well as the double domain mutant (N)A1_P2_(C)A1, that only demonstrated signals in the range of 20 – 30 kDa. The analyzed SF samples represented via SM-2 biobeads reconstituted and extruded proteoliposomes ready for Stopped Flow measurement. Their overall appearance was very uniform, in each case demonstrating a very distinct signal in the range of 70 – 90 kDa, which falls in line with the range determined for tetrameric aquaporin configuration. In conclusion, the analyzed Western Blot samples document a vast array of various aquaporin configurations during the downstream processing of L-CF produced proteoliposomes, that culminate in a very homogeneous appearance after biobead reconstitution and extrusion and directly preceding Stopped Flow measurements.

4. Discussion

4.1 Establishment of cell-free expression workflows for the generation of proteoliposomes

E. coli derived extracts have been established as the "workhorse" of currently available cell-free expression systems for prokaryotic, as well as eukaryotic membrane protein production [Zemella *et al.* 2015]. Since the lack of a natural membrane impedes the production of such targets in this system, the supplementation of mimicking structures becomes necessary [Geller & Wickner 1985 / Junge *et al.* 2011]. During this work, liposomes represented the artificial hydrophobic environment of choice for improved folding and functionality of the expressed aquaporin targets. Their predominant use in functional studies encompassing transporter assays and ion channel characterization has established liposomes as a handy tool to analyze processes involving the regulated passage of solutes across lipid bilayers [Geller & Wickner 1985].

The application of three different *E. coli* based cell-free expression modes during the course of this work allowed for their comparison in terms of yield and practicality for Stopped-Flow derived water permeability measurements. In the absence of hydrophobic environments, the precipitation based cell-free expression (P-CF) is a remnant of the first described CF systems with steady yields [Klammt *et al.* 2007]. It requires the use of harsh detergents for resolubilization, additional protein purification and complex refolding protocols, making this approach quite laborious while obtaining comparatively low yields of functional targets. Facing such obstacles, P-CF was thus only applied as a quick test to establish an expression baseline for individual target plasmids and to ensure the efficiency of CF components (data not shown).
In order to circumvent the refolding process, the use of milder detergents during transcription / translation enabled a detergent based cell free expression mode (D-CF) to be applied. Previously published data on screening of potential candidates therein resulted in Brij S20 being used during D-CF transcription / translation in this work [Berrier *et al.* 2004]. Its and others´ suitability was based on these detergents´ ability to form micelles at defined concentrations in order to enclose the membrane protein, while still allowing for a native configuration. With harsh detergents and refolding protocols out of the way, D-CF thus allowed for higher functional yields than P-CF. However, a purification step following cell-free expression was still necessary, during which Brij S20 was exchanged with DDM. Obtained NiNTA derived results from this work turned out to be comparable in quality with previously published data [Kai & Kaldenhoff 2014]. The main culprit in the establishment of D-CF during the course of this thesis turned out to be the reconstitution of purified aquaporin into liposomes after their purification (see chapter 3.3) via the addition of Triton X-100. While determination of obtained aquaporin amount in eluates via SDS-PAGE quantification was possible, fine-tuning all individual components in the resulting reconstitution mix was quite complex. An optimal total protein to liposome ratio was necessary to ensure saturation of the latter and thus the quality of ensuing water permeability data. Lower ratios could potentially leave a high number of liposomes "empty", i.e. without aquaporin. High ratios, on the other hand, were problematic due to non-incorporated protein significantly increasing pressure during extruder homogenization (see chapter 2.8.6) and thus causing a high risk of membrane rupture. In addition, varying aquaporin concentrations in the eluates meant that the amount of detergent during reconstitution was not constant, even at comparable protein to liposome ratios. This made the proper adjustment of SM-2 biobeads for the removal of DDM and Triton X-100 difficult (see chapter 2.8.5). Consequently, water permeability data was found to be highly fluctuating and unreliable between individual experiments or even samples of the same experiment.
For the stated reasons, a liposome based cell-free expression mode (L-CF) was adopted as the strategy of choice to obtain reproducible Stopped Flow data (see chapter 3.4). The lack of need for a protein purification step

significantly lowered the complexity of L-CF downstream processing in terms of time and material demands. A manual adjustment of protein to liposome ratio like in D-CF was not necessary, since the presence of liposomes during transcription / translation caused an automatic equilibrium to take place during aquaporin integration. Also, fine-tuning the eventual reconstitution of proteoliposomes and their separation from non-integrated protein prior to Stopped Flow measurements was just a matter of determining two factors: namely, the minimal amount of Triton X-100 necessary to solubilize the proteoliposomes and the application strategy for SM-2 biobeads in order to remove the detergent. Both factors turned out to be relatively straight-forward, especially due to the presence of only one instead of three different detergents as in D-CF. The application of Triton X-100 on preformed proteoliposomes was not problematic due to its non-denaturing quality when it comes to aquaporin oligomeric configuration [Le Caherec *et al.* 1996 / Lagree *et al.* 1998 / Duchesne *et al.* 2001]. This was also evident from Western Blot signals obtained in this work (see chapters 3.4.3 and 3.8). The type of SM-2 biobead application turned out to be crucial for the water permeability of reconstituted proteoliposomes (see chapters 3.4.2 & 3.4.3). It suggests that the speed of detergent removal could play a role in the eventual aquaporin oligomerization state. Especially in the case of NtPIP2;1, it has been indicated that a tetrameric configuration is responsible for maximum water permeability rates, as opposed to mono- or dimeric structures [Otto *et al.* 2010]. In addition, any leftover detergent would naturally interfere with the water permeability of liposome vesicles and also potentially influence native aquaporin folding [Lyukmanova *et al.* 2012].

There are several main factors contributing to protein yield in CF systems [Roos *et al.* 2013]. First and foremost, the quality and purity of the template DNA has a great influence in this regard. Circular templates have a higher efficiency than linear ones and midi or maxi prep purification kits trump mini prep equivalents or manual, column-independent protocols in terms of purity. Both strategies were employed in this work to ensure high protein yields and transcription / translation efficiency. A second factor is the total concentration of free Mg^{2+} cations in the reaction and feeding mixtures. As one of the main enzyme cofactors, it can be fine-tuned to improve the overall transcription / translation efficiency for each type of protein target. However, Mg^{2+} screening done in the range of 12 to 20 mM during the course of this thesis resulted in barely discernible differences in aquaporin yields (data not shown), thus it was set at 16 mM for all subsequent experiments. Lastly, properly designed DNA templates ensured sufficient expression of all protein constructs via codon optimization, as well as the use of promoter / terminator and ribosome binding site sequences for maximum compatibility with the applied *E. coli* extracts. Raw aquaporin yields obtained in all three expression modes ranged at several mg per ml reaction mix and were thus in line with previously published data on this system [Spirin *et al.* 1988]. The amount of protein necessary to saturate the utilized liposomes could approximately be determined via the obtained SDS-PAGE and Western Blot analyses (see chapters 3.3 and 3.8). Since it was found to be in the range of single to double digit µg amounts per ml, the thousand-fold higher raw aquaporin yields were sufficient for L-CF purposes.

The integration of aquaporins into liposomes took place with disregard to their final orientation in the membrane in both D-CF and L-CF (N- and C-terminal domains are cytosolic in native configuration, see chapter 1.3.2). While this may be interpreted as a non-native configuration for potentially 50 % of the total integrated protein, it was of no importance for the obtained water permeability values. Bidirectional water transport is a given for aquaporins [Agre 2004] and has specifically been demonstrated for both mammalian and plant aquaporins, among others [Meinild *et al.* 1998 / Horie *et al.* 2011]. A non-native orientation would thus have no influence on the shrinking kinetics obtained via Stopped Flow methodology. However, a study into this area demonstrated that a directed integration of mammalian AQP0 was indeed possible by using specific asymmetric ABC-triblock copolymers [Stoenescu *et al.* 2014]. When compared to liposomes, such copolymers showed a

native integration rate of 80 % as opposed to 50 %, making this a promising approach for future aquaporin studies, where native orientation is of greater importance.

Looking at the SDS-PAGE and Western Blot analyses of aquaporin samples in this work, it became apparent that quaternary configurations in mainly mono-, di- and tetramer groups were common. This was due to their high detergent stability even in the presence of SDS, as was previously demonstrated [To & Torres 2015]. However, thermal stability was another matter altogether. The spinach aquaporin SoPIP2;1, for example, was shown to undergo temperature dependent aggregation into very high molecular size ranges, thus preventing the samples to enter gel pockets and making analysis difficult [Plasencia *et al.* 2011]. The preparation of aquaporin samples for SDS-PAGE analysis was thus restricted to a 37 °C incubation instead of the usual 80 to 95 °C in this work. Although this allowed an approximate molecular size determination of the oligomeric structures, a precise comparison to the respective protein standards was prevented by the half-denatured state of the aquaporin samples. Nevertheless, the observed molecular sizes for NtPIP2;1 and NtAQP1 monomers at ~ 20 – 35 kDa and dimers at ~ 40 – 65 kDa (see chapter 3.8) are in line with previously published results for these two plant aquaporins [Kai & Kaldenhoff 2014 / Mahdieh & Mostajeran 2009 / Flexas *et al.* 2006].

4.2 Differences between NtPIP2;1 and NtAQP1 in terms of sequence and water permeability

Although the majority of prokaryotic and eukaryotic aquaporins are capable of water transport, there are several exceptions that include, but are not restricted to: fungal Aqy2 [Laize *et al.* 2000 / Carbrey *et al.* 2001], type-6 nodulin intrinsic proteins (NIP6) [Wallace & Roberts 2005], drosophila big brain (BIB) [Yanochko & Yool 2002 / Tatsumi *et al.* 2009] and plant type-1 plasma membrane intrinsic proteins (PIP1) [Chaumont *et al.* 2000 / Dordas *et al.* 2000 / Temmei *et al.* 2005]. As their nomenclature implies, PIPs are mainly located in the plasma membrane of all plant parts like roots or leaves [Kaldenhoff & Fischer 2006]. Their phylogenetic group is divided into two subclasses PIP1 and PIP2 [Zardoya 2005], that differ in the length of their N- and C-termini, as well as their apparent water permeability as measured in different heterologous systems. PIP2 members possess a shorter N- and a longer C-terminal domain, as well as additional amino acid residues in loop A, while showing a significantly higher water permeability than their PIP1 counterparts [Weig *et al.* 1997 / Daniels *et al.* 1994]. They are thus suggested to be the major pathways for symplastic and apoplastic water transport in plants. In contrast, PIP1 aquaporins demonstrate an overall low intrinsic water permeability [Moshelion *et al.* 2002 / Temmei *et al.* 2005], but divergent functionality when it comes to gas and small solute transport [Gaspar *et al.* 2003 / Heckwolf *et al.* 2011]. Putting that information into context with the sequence analyses of NtPIP2;1 and NtAQP1 (see chapter 3.1), it is apparent that both proteins are typical representatives of their respective PIP subclasses. Their sequence-based variations were isolated to differences in length of N-terminus (NtPIP2;1 shorter), C-terminus (NtPIP2;1 longer) and loop A (NtPIP2;1 longer), that were also the most differing domains in terms of amino acid identity and similarity. Seeing that a previous study could not find an increase in NtAQP1 water permeability when its loop A was elongated [Siefritz *et al.* 2001], the focus was placed on the differing terminal domains of the two tobacco aquaporins.

It had been shown before that specific sequence motifs play a critical role as selectivity filters for permeates in the MIP protein family. With the central two NPA motifs serving to exclude cations and protons [Murata *et al.* 2000 / Ho *et al.* 2009 / Tani *et al.* 2009 / Wree *et al.* 2011], two additional aromatic / arginine (ar/R) amino acid clusters located in the outer channel vestibule determined, which substrate can traverse the pore [Fu *et al.* 2000 / Sui *et al.* 2001 / Beitz *et al.* 2006 / Almasalmeh *et al.* 2014]. Aside from those two selectivity determinants, five relatively conserved sites named Froger´s positions or P1 – P5 discriminate between classical water-selective aquaporins and aquaglyceroporins by also adjusting the pore diameter [Froger *et al.* 1998]. Interestingly, the *in silico* analysis of NtPIP2;1 and NtAQP1 revealed an almost identical configuration in the listed selectivity filters, with the only discernible difference being a Thr_{229} to Ser_{240} exchange at the P2 site when comparing the former

to the latter (see chapter 3.1). That particular site, located directly downstream of the second NPA box, had been demonstrated to be of crucial importance in the case of aspartic acid increasing the size of the central monomer pore in order to permeate larger molecules such as glycerol [Hub & de Groot 2008]. However, the difference in side chains between the two stated residues in this case is limited to a mere methyl moiety. It is unlikely to be the cause of steric hinderance to water permeation, especially considering that it is part of the significantly more permeable NtPIP2;1 aquaporin. This again pointed to a role of the two PIPs´ terminal domains rather than their selectivity filters for their overall intrinsic water permeation capabilities.

The water permeability results of wildtype NtPIP2;1 and NtAQP1 obtained in this work (see chapter 3.5) were also in line with the levels expected for their respective PIP subclasses, as well as with previous reports on these specific aquaporins. NtAQP1 showed intrinsic water permeability near that of control levels, but significantly lower than NtPIP2;1, which had been demonstrated to be an efficient water channel [Biela *et al.* 1999 / Bots *et al.* 2005a / Mahdieh *et al.* 2008 / Otto *et al.* 2010 / Kai & Kaldenhoff 2014]. Since NtAQP1 did not generally lower intrinsic liposome water permeability by much, if at all, it can be assumed that its water transport rate is just sufficient enough to compensate for the resistance added via its membrane integration. Depending on the heterologous expression system used in previous publications, stated absolute P_f values differred greatly. This can be attributed to a varying intrinsic resistance to water permeation of the membranes used to incorporate the aquaporins. Yeast membranes showed the lowest water permeability control values [Otto *et al.* 2010] and thus demonstrated the highest increase after the integration of a functional water channel. In comparison, *Xenopus* oocytes [Biela *et al.* 1999 / Mahdieh *et al.* 2008] and soybean derived liposomes [Kai & Kaldenhoff 2014] did not show such a great disparity between NtPIP2;1 and control levels. This did not, however, change the relative water transport characteristics typical for the respective PIP1 and PIP2 phylogenetic subclasses.

4.3 Regulation of NtPIP2;1 and NtAQP1 intrinsic water permeability by terminal domains

Based on the Stopped Flow results obtained from terminal deletion (see chapter 3.6) and terminal exchange mutants of NtPIP2;1 and NtAQP1 (see chapter 3.7), it can be surmised that their terminal domains play a significant role in the intrinsic water permeability of these aquaporins.

Any modification of a single terminal domain in NtPIP2;1 led to a significant drop in water transport to levels comparable to that of controls and NtAQP1 (N-terminal deletion / exchange) or slightly above that (C-terminal deletion / exchange). The deletion of both terminal domains lowered the water permeability even further to below empty liposome control levels. In comparison, a double exchange with NtAQP1 N- and C-terminal sequences led to water transport rates statistically equal to the PIP1 tobacco aquaporin.

In contrast to that, single deletion mutants of NtAQP1 did not show significant differences in water permeability when compared to the wildtype. However, when both terminal domains were removed, P_f values dropped significantly as with the NtPIP2;1 counterpart, but to even lower absolute levels. The most intriguing results were obtained, when NtPIP2;1 terminal domains were transferred to NtAQP1. Both single exchange mutants showed significantly higher water permeability than the wildtype, with the double exchange mutant surpassing even those values.

These results suggest that the specific make up of the terminal domains plays a more important role in the regulation of intrinsic water permeability in each protein than the mere presence of the same. On one hand, the transfer of a single NtAQP1 terminal domain to NtPIP2;1 did not alter water transport rates compared to single deletion mutants of NtPIP2;1. The transfer of both terminal domains, however, led to a significantly higher P_f value than the double deletion mutant of NtPIP2;1. This basically suggests that the low, but existent water permeability of NtAQP1, which barely compensates for the aquaporin´s membrane resistance upon integration, is transferred onto NtPIP2;1. This kept the NtPIP2;1 double exchange mutant (N)A1_P2_(C)A1 more permeable than its double deletion counterpart Δ(N)_P2_Δ(C). In contrast to its native terminal domains though, the mere

presence of NtAQP1 terminal sequences was not sufficient to restore the NtPIP2;1 exchange mutants to their wildtype water permeability levels. On the other hand, the transfer of NtPIP2;1 termini led to significantly increased water permeation in both single and double exchange mutants of NtAQP1. In the most extreme case, the transfer of both NtPIP2;1 termini essentially doubled water transport rates when compared to the NtAQP1 double deletion mutant. Although that did not completely close the initial gap seen between the PIP1 and PIP2 wildtypes, these results still strongly suggest that the terminal domains of both aquaporins are capable of transferring the bulk of their respective water permeabilities to one another. This is reflected in the high sequence similarity found in the central transmembrane regions between the two wildtypes, whereas their terminal domains were found to be quite diverse (see chapter 3.1).

Siefritz *et al.* [2001] is to date the only reference published, which discusses the impact of terminal modification on the water permeability of either NtPIP2;1 or NtAQP1. There, the deletion of 81 N-terminal amino acid residues did not result in any significant change of NtAQP1 water permeability, which corresponds with the results obtained in this work (see chapter 3.6.1). In order to properly interpret the potential impact of terminal domain regulation in these two tobacco aquaporins, additional sources were researched, opening up a range of possibilities in terms of regulation mechanisms. These include, but are not restricted to: blockage of the central monomer pore due to interactions with terminal domains [Fischer *et al.* 2009], conformational changes in the transmembrane regions due to absence of native or presence of non-native terminal domains [Verdoucq *et al.* 2008], regulation via post-translational modifications [Santoni *et al.* 2006], modified adhesion of monomers to oligomeric configurations due to terminal modification [Gonen *et al.* 2004], pH gating [Alleva *et al.* 2006], regulation via divalent cations [Törnroth-Horsefield *et al.* 2006] and gating through high solute concentration and pressure pulses (mechanosensitivity) [Wan *et al.* 2004 / Fischer *et al.* 2009]. The following chapters will discuss the listed regulation mechanisms in detail and evaluate their individual potential for applicability for the two tobacco aquaporins. Although subcellular trafficking is also a common aquaporin regulation mechanism [Prak *et al.* 2008 / Zelazny *et al.* 2009], it is not included due to its absent role in the cell free expression system applied in this work.

4.3.1 Post-translational modifications

In order to investigate the potential role of post-translational modifications in the regulation of water permeability in NtPIP2;1 and NtAQP1 via their terminal domains, several tools have been applied to the respective sequences. Table 41 shows a summary of N- and C-terminal amino acid residues and potential modifications thereof for both aquaporins.

Table 41 – Overview on potential post-translational modification sites in the N- and C-terminal domains of the tobacco aquaporins NtPIP2;1 and NtAQP1. Highlighted in red are residues that correspond to each other according to the global multiple sequence alignment shown in chapter 3.1. 1 = WuXi PharmaTech (Cayman) Inc., Shanghai, China.

Tool	PTM Type	NtPIP2;1	NtAQP1	References
DISULFIND	Disulfide bond	-	-	Ceroni *et al.* 2006
ISOGlyP	Glycosylation	Ser_{270}, Ser_{277}, **Ser_{280}**, Thr_{283}	**Ser_{286}**, Ser_{287}	Gerken *et al.* 2006/2008/2011, Perrine *et al.* 2009
NetPhos 3.1	Phosphorylation	Ser_2, **Tyr_{19}**, Ser_{37}, Ser_{270}, Ser_{277}	Thr_{19}, Thr_{28}, **Tyr_{32}**, Ser_{48}, Ser_{287}	Blom *et al.* 2004
Sulfinator	Sulfation	-	Tyr_{32}	Monigatti *et al.* 2002
SUMOPlot	Sumoylation	-	Val_9-Lys_{10}-Leu_{11}-Gly_{12}	WuXi PharmaTech[1]
TermiNator	N-terminal: Met excision, acetylation, myristoylation, S-palmitoylation	Ac-Ser_2	Ac-Ala_2	Martinez *et al.* 2008, Frottin *et al.* 2006

Due to the complete absence of cysteine residues in the terminal domains of both aquaporins, there is no likelihood for their involvement in the formation of disulfide bonds.

As for glycosylation, a total of 6 amino acid residues were identified in the C-terminal domains of NtPIP2;1 and NtAQP1, out of which one site corresponded to identical positions in both aquaporin sequences. This type of post-translational modification has previously been demonstrated to be important for proper routing and membrane integration of mammalian AQP1 and AQP2 [Smith *et al.* 1994 / Baumgarten *et al.* 1998 / Hendriks *et al.* 2004]. In the plant kingdom, the first instance of aquaporin regulation via glycosylation was reported in 2004 with McTIP1;2 from the Ice Plant (*Mesembryanthemum crystallinum*) [Vera-Estrella *et al.* 2004]. It was found to be glycosylated in situations of osmotic stress and as a consequence was redistributed to endosomal compartments instead of the tonoplast membrane. However, membrane routing does not play a role in *E. coli* derived cell-free expression systems and the integration of the aquaporin targets was successful in each case (see chapter 3.8). It is therefore impossible, that the presence or absence of this type of post-translational modification is responsible for the change in water permeation seen in the data obtained from the deletion and exchange mutants. In addition, the lack of glycosyltransferases in the *E. coli* cell-free expression system used in this work [Fernandez & Hoeffler 1999] makes such post-translational modifications unfeasible.

Phosphorylation is a very common type of post-translational aquaporin regulation and both tobacco aquaporins show a total of ten potential residues in both their N- and C-terminal domains. Known examples of such regulation in the plant kingdom include SoPIP2;1 (formerly PM28A) from spinach [Johansson *et al.* 1998 / Törnroth-Horsefield *et al.* 2006] and RsPIP1;3, as well as RsPIP2;2 from radish [Suga & Maeshima 2004]. The water channel activity of the former was shown to be regulated by phosphorylation of Ser_{274} in its C-terminus, which corresponds to Ser_{277} in NtPIP2;1 and Phe_{283} in NtAQP1. Permeability was enhanced by 30 % when the residue was phosphorylated and returned to control levels when dephosphorylated. In an *in vivo* context, this was suggested to take place in response to increasing apoplastic water potential and cell turgor. As for the latter two aquaporin examples from radish, they showed low (PIP1;3) and high (PIP2;2) water permeability as expected for isoforms of their respective PIP subclasses. The exchange of Ser_{27}Ala in the N-terminus of RsPIP1;3 increased its intrinsic water permeability by two thirds. This residue corresponds to Gln_{13} in NtPIP2;1, whereas NtAQP1 lacks this position as shown in the multiple sequence alignment in chapter 3.1. In contrast, a Ser_{277}Ala/Asp mutation in the C-terminus of RsPIP2;2 decreased its relative water permeability by a third. The corresponding sites in NtPIP2;1 and NtAQP1 are Ser_{277} and Phe_{283}, respectively, matching the previously stated phosphorylation site in SoPIP2;1. Based on these findings, Ser_{277} in NtPIP2;1 could be surmised as a potential phosphorylation site lacking in NtAQP1, that is responsible for the differences in water permeability. However, both tobacco aquaporins had previously been demonstrated to be impervious to protein kinase and protein phosphatase inhibitors [Biela *et al.* 1999 / Eckert *et al.* 1999 / Mahdieh *et al.* 2008]. Thus, regulation by this type of post-translational modification is also not feasible. In addition, the applied *E. coli* derived expression system is not capable of such modifications [Fernandez & Hoeffler 1999].

Even though one potential site was found for sulfation and sumoylation in NtAQP1, respectively, neither modification has yet been described in the context of aquaporin regulation. Furthermore, the cell-free expression system used in this work is not capable of such modifications [Fernandez & Hoeffler 1999], further disqualifying them as a potential basis for interpreting the terminal domain regulation of water permeability in NtPIP2;1 and NtAQP1.

Lastly, the amino acid sequences of the two tobacco MIPs were analyzed for potential N-terminal modifications in terms of Met_1 excision, acetylation, myristoylation and S-palmytoylation.

S-palmytoylation of two N-terminal Cys residues in AQP4 from rat had previously been determined to hinder the formation of tetramer arrays [Suzuki *et al.* 2008], that provide water transport across the blood-brain interface. However, both NtPIP2;1 and NtAQP1 lack any such residues in their terminal domains.

A possible role of N-terminal methylation and acetylation in the regulation of aquaporin water transport was described by Santoni *et al.* in 2006. Lys_3 dimethylation in AtPIP2;1 from *Arabidopsis*, which is also present in NtPIP2;1, was shown to be crucial for its intrinsic water permeability. An exchange with Ala at that position decreased P_f values to 60 % of wildtype levels. Since members of the PIP1 subfamily, including NtAQP1, lack Lys_3, their initial methionine is acetylated [Polevoda & Sherman 2003]. This N_α acetylation, in turn, is prevented in PIP2 proteins by the Lys_3 methylation. Even though the TermiNator analysis shown in Table 41 lists potential acetylation of both tobacco aquaporin´s second residue position, the stated Lys_3 methylation (or lack thereof) could serve as a pointer for future experiments. This especially in light of the fact that both methylation and acetylation are viable post-translational modifications in an *E. coli* based expression system [Nesterchuk *et al.* 2011 / Brown *et al.* 2016].

4.3.2 Domain interactions

Another possibility of terminal domains regulating intrinsic water permeability in NtPIP2;1 and NtAQP1 is their interaction with other domains of the same monomer or even those of neighboring subunits in an oligomeric configuration.

One example for such regulation can be found in AtPIP2;1, where the N-terminal Asp_{28} and Glu_{31} residues have been suggested to contribute to ion binding and the stabilization of a closed-pore conformation [Verdoucq *et al.* 2008]. The process is triggered via the modulation of Ca^{2+} and proton concentration in plant cells, which in turn was demonstrated to transduce developmental, hormonal or stress signals [Fan *et al.* 2004 / Israelsson *et al.* 2006 / Shimazaki *et al.* 2007 / Yakir *et al.* 2007]. Corresponding residues are present in NtPIP2;1 with Asp_{29} and Glu_{32}, whereas NtAQP1 has Glu_{42} and Glu_{45} incorporated in its N-terminus (see chapter 3.1). However, such a mechanism would enable NtPIP2;1 to enter a closed-pore configuration and have a lower water transport rate than NtAQP1, which was clearly not the case. In addition, the absence of divalent cations and a pH set at a rather neutral 7.5 would hinder such a mechanism to take place during Stopped Flow assay measurements (see chapters 2.7.3 and 2.9).

Similar principles of regulation via domain interaction were postulated for the spinach aquaporin SoPIP2;1 by Törnroth-Horsefield *et al.* in 2006. A divalent cation binding motif in loop D would result in anchoring onto a short alpha helix in the N-terminus in the presence of Ca^{2+} or Cd^{2+} ions and thereby occlude the cytosolic pore entrance. More precisely, Arg_{190} and Asp_{191} in loop D would connect to Arg_{118} located in loop B_2 and Gly_{30} in the N-terminus through a hydrogen bond network containing three water molecules. Arg_{118} would then form hydrogen bonds with Glu_{31} in the N-terminus and ligate the divalent cation. Interestingly, NtAQP1 has identical amino acid residues at all corresponding positions, whereas NtPIP2;1 exhibits Ala_{31} in its N-terminus equating to the spinach aquaporin´s Gly_{30} (see chapter 3.1). In theory, that disparity could hinder loop D to be anchored to the N-terminus and occlude the pore, consequently providing NtPIP2;1 with a much higher water permeability than NtAQP1. However, as with AtPIP2;1 before, the presence of divalent cations would be necessary in order to activate this mechanism, which was not the case in this work. A second potential mechanism was presented in that same publication, involving Ser_{274} in the C-terminus of SoPIP2;1 [Törnroth-Horsefield *et al.* 2006]. The residue would interact with Pro_{199} and Leu_{200} of an adjacent monomer subunit in a tetramer configuration in order to stabilize the terminal domain. When these interactions are lost, Leu_{197} takes the place of Ser_{274} with the consequence of the TM5 N-terminal end extending an additional half-turn into the cytoplasm and opening the channel by displacing Leu_{197}. Transferring this to the context of the two tobacco aquaporins, NtPIP2;1 exhibits identical amino acid residues at all corresponding positions, while NtAQP1 bears a Phe_{283} in correspondence to the C-terminal Ser_{274} in the spinach aquaporin. In addition, the required tetrameric configuration was demonstrated to be given in all constructs via Western Blot analysis (see chapter 3.8). If that mechanism was indeed applicable, both the C-terminal deletion and exchange mutants of NtAQP1 should demonstrate increased

water permeability when compared to the wildtype, while the corresponding NtPIP2;1 constructs should exhibit the opposite. Interestingly, the obtained results correspond well to that, although the measured water permeability for A1_Δ(C) is not significantly different from the wildtype, albeit in direct proximity of the set p value (see chapter 3.7.4 and 3.7.5).
Fischer *et al.* discussed another case of domain interaction regulation in 2009, in which the central monomer pore of Aqy1 from the yeast *Pichia pastoris* was occluded by an elongated N-terminus. The terminal domain would arrange in a tightly wound helical bundle, in which Tyr_{31} forms hydrogen bond interactions with a water molecule inside the pore. Although an intriguing principle, the corresponding Leu_{33} and Leu_{46} in NtPIP2;1 and NtAQP1, respectively, could probably hinder such a mechanism to function properly.

4.3.3 Oligomerization of monomers

As indicated by studies involving aquaporins from mammals [Verbavatz *et al.* 1993 / Neely *et al.* 1999] and plants [Fetter *et al.* 2004 / Mahdieh *et al.* 2008 / Otto *et al.* 2010 / Murozuka *et al.* 2013], the oligomerization of monomers could play an important role in the regulation of their intrinsic water transport capabilities. Assemblies of homo- or heterotetramers could therefore enable multiple molecular and functional combinations.
One publication discussed the critical role of loop A in plant plasma membrane proteins in particular, whereby oligomer interactions were initiated by disulfide bonds. These would stabilize PIP dimers and consequently allow the formation of tetramers [Bienert *et al.* 2012]. Site-directed mutations in this loop modified the interaction behavior of PIP1 and PIP2 members from *Beta vulgaris*, thus confirming that mechanism [Jozefkowicz *et al.* 2013]. This is interesting insofar, as loop A is the only domain that shows considerable differences in sequence identity / similarity and length between NtPIP2;1 and NtAQP1 (see chapter 3.1). However, mutational analysis in loop A of NtAQP1 did not result in a modulation of its water permeability [Siefritz *et al.* 2001]. In addition, a tetrameric configuration was observed for all aquaporin constructs in this work (see chapter 3.8). Hence, a conformational change in loop A by terminal domain modification leading to subsequent oligomerization hinderance can be ruled out for NtPIP2;1 and NtAQP1.
An opposite effect was reported by Gonen *et al.* in 2004, where terminal domain deletion led to increased adhesion of tetramers. The deletion of the complete cytoplasmic C-terminal tail in AQP0 from sheep caused conformational changes and facilitated enhanced adhesive properties of the aquaporin´s extracellular surface. This, in turn promoted an increased pairing of tetramers and changed the water pore into an adhesive molecule in the lens core, where fiber cells are densely packed together. Although this type of regulation cannot be ruled out for NtPIP2;1 and NtAQP1, it would be difficult to verify in the absence of structural analyses, such as X-ray crystallography, ECM, NMR or AFM (see chapter 1.1.2). Furthermore, it is unlikely that this mechanism is exclusively responsible for the water transport modulation in all tested terminal domain mutants of the two tobacco aquaporins.

4.3.4 pH dependent gating

For the purpose of finding MIP family members with high N- and C-terminal sequence identity to NtPIP2;1 and NtAQP1, a pBLAST search was performed. Putative, predicted or hypothetical matches were sorted out and only candidates with high identity scores in both N- (> 76 %) and C-terminal domains (> 77 %) were included. A literature search ensued, looking for published results on biochemical characterization related to their water transport regulation.
A PIP2 candidate from *Beta vulgaris* matched the above criteria, exhibiting high sequence similarity with the terminal domains of NtPIP2;1 (N = 78 % identity, 93 % similarity / C = 91 % identity, 100 % similarity). Alleva *et*

al. demonstrated that cytoplasmic pH levels regulate the water channel activity of BvPIP2;2 in 2006. More precisely, intracellular acidification shut down water permeability of aquaporins in plasma membrane vesicles isolated from *Beta vulgaris* roots. (De)phosphorylation was discounted as a regulatory mechanism, while cytoplasmic Ca^{2+} concentrations were able to up- or downregulate water channel activity. Building upon that work, Bellati *et al.* further demonstrated a regulation mechanism in plasma membrane water permeability through a combination of cytosolic pH and PIP1/PIP2 co-expression in 2010. Intracellular acidification lowered the intrinsic water permeability, whereas the parallel expression of BvPIP1;1 and BvPIP2;2 enhanced it and reinforced pH inhibitory response. Since the localization of those mechanisms was restricted to the cytosolic side, the results pointed towards a potential involvement of N- and C-terminal domains, as well as loop D (see chapter 1.3.2). Interestingly, NtPIP2;1 exhibited a similar behavior to BvPIP2;2 in terms of phosphorylation insensitivity [Mahdieh *et al.* 2008] and acidification dependent down-regulation of its intrinsic water permeability [Fischer & Kaldenhoff 2008]. However, its pH regulation was found to be linked to His_{196} located in loop D and was independent of its terminal domains. Nevertheless, a C-terminal Ser_{277}Ala exchange surprisingly enhanced NtPIP2;1 water permeability by 20 to 75 %, depending on the pH, without changing the aquaporin´s overall pH sensitivity.

The role of the histidine residue in loop D had previously been described in proton dependent gating of the spinach aquaporin SoPIP2;1 [Törnroth-Horsefield *et al.* 2006]. Building on that work, a subsequent publication managed to resolve the crystal structure of SoPIP2;1 at low cytosolic pH levels [Frick *et al.* 2013b]. During flooding, anoxia initiated cytosolic acidification would lead to a simoultaneous closing of plasma membrane aquaporins via the above mentioned histidine residue in loop D. This was the first proof that loop D is involved in aquaporin gating at low pH, even when divalent cations are not present (see chapter 4.3.2). Due to the absence of such ions, the N-terminus would thus not be involved in the stabilization of the closed pore formation.

4.3.5 Mechanical gating

Although not commonly described in the context of aquaporins, mechanical gating was proposed to play a role in young corn roots [Wan *et al.* 2004]. Elevated turgor pressure simulated by pressure pulses lead to a decrease in hydraulic conductivity in root tissues. The plant stress hormone ABA was able to reverse these effects inside of short time spans. It was concluded that aquaporins played a vital role in the observed water transport changes with the potential regulation mechanism involving mechanical gating. The kinetic energy presumably impacts the channel constriction at the NPA motifs (see chapter 1.3.2) and hence the overall protein conformation in a way that water transport is restricted. Activating pressure limits for mechanical gating in this case were found to be above 0.1 MPa. It is highly unlikely that NtPIP2;1 and NtAQP1 constructs underwent this type of regulation during Stopped Flow measurements, since the calculated osmotic pressure difference between the two buffers used was 4.65 kPa and thus barely 5 % of the stated limit (see chapters 2.7.3 and 2.9, calculation based on osmotic pressure calculator: hyperphysics.phy-astr.gsu.edu/hbase/kinetic/ospcal.html). Nevertheless, terminal domain modifications could potentially have contributed to the destabilization of the protein conformation in some constructs, thus leading to a higher mechanosensitivity.

4.3.6 Conformational changes in transmembrane structure - Homology modeling analysis

All regulation mechanisms discussed thus far presupposed a direct involvement of terminal domains. However, there is still the possibility of terminal domain modifications inducing conformational changes in the overall protein structure of NtPIP2;1 and NtAQP1 and thus modulating their water permeability. In order to examine this possibility, 3D homology models were generated with Phyre2 [Kelley *et al.* 2015] for the two tobacco

aquaporin wildtypes, as well as their respective double deletion and double exchange mutants. The results of the initial model generation are shown in Table 42.

Table 42 – Overview on Phyre2 homology model generation [Kelley *et al.* 2015] for the tobacco aquaporins NtPIP2;1 and NtAQP1, as well as their terminal domain double deletion and double exchange mutants (see chapter 3.2). Templates used for the generation of the respective homology models are listed by their PDB ID. Template identity gives an individual template´s aa sequence identity to the respective construct in %, as well as overall average values per construct. Template confidence gives the probability in % that the template is a homology match to the respective construct. Lastly, homology model confidence lists the accuracy, with which individual segments or the whole of the resulting homology model were generated. Δ(N)_P2_Δ(C) = NtPIP2;1 with N- and C-terminal domains deleted / Δ(N)_A1_Δ(C) = NtAQP1 with N- and C-terminal domains deleted / (N)A1_P2_(C)A1 = NtPIP2;1 with N- and C-terminal domains of NtAQP1 / (N)P2_A1_(C)P2 = NtAQP1 with N-and C-terminal domains of NtPIP2;1.

Construct	Templates (PDB ID)	Template Identity		Template confidence	Homology model confidence	
		individual	overall		individual	overall
NtPIP2;1	2B6P	33 %	35 %	100 %	aa 1-28 = 0 - 10 % aa 29 - 284 = 90 - 100 %	81 - 91 %
	5I32	37 %				
	1J4N	40 %				
	1LDA	30 %				
	2F2B	35 %				
	3D9S	37 %				
NtAQP1	2W2E	31 %	45 %		aa 1 - 19 = 0 - 10 % aa 20 - 279 = 90 - 100 % aa 280 - 287 = 0 - 10 %	82 - 92 %
	2B5F	74 %				
	2F2B	31 %				
Δ(N)_P2_Δ(C)	5I32	38 %	49 %		aa 1 - 218 = 90 - 100 %	90 - 100 %
	1H6I	43 %				
	1J4N	43 %				
	2B5F	83 %				
	2F2B	36 %				
Δ(N)_A1_Δ(C)	2B5F	74 %	74 %		aa 1 - 216 = 90 - 100 %	90 - 100 %
(N)A1_P2_(C)A1	5I32	36 %	35 %		aa 1 - 41 = 0 - 10 % aa 42 - 287 = 90 - 100 % aa 288 - 289 = 0 - 10 %	77 - 87 %
	2B6P	33 %				
	1J4N	41 %				
	1LDA	31 %				
	2F2B	35 %				
	1FX8	31 %				
(N)P2_A1_(C)P2	2B5F	75 %	75 %		aa 1 - 31 = 0 - 10 % aa 32 - 264 = 90 - 100 % aa 265 - 282 = 0 - 10 %	74 - 84 %

According to Phyre2 documentation, extremely high accruracy models require a sequence identity with their templates of at least 30 %. This was given in all cases, with NtPIP2;1 and its double exchange mutant having the lowest average sequence identity at 35 %. In addition, the throughout perfect template confidence was another good indication for high accuracy homology models, that adopt the general template fold with high confidence. While the core of the protein was modeled with an accuracy of up to 2 angström (Å) from the true, native configuration, non-membrane integrated domains, such as surface loops, are stated to very likely deviate more singificantly from the native structure. As for the obtained homology model confidence values, any regions with 0 – 10 % confidence were modeled *ab initio*, hence based on a purely computational derivation and without a proper template. These regions were restricted to the outermost parts of the terminal domains and therefore

did not affect the core transmembrane parts of the models. In conclusion, the obtained homology models were of high accuracy and could subsequently be used to determine conformational differences between the constructs.

For that purpose, the acquired PDB files of the respective homology models were loaded into Molecular Operating Environment (MOE) v2014.09 (Chemical Computing Group, Montreal, Quebec, Canada) and superimposed onto each other. All atoms of the respective models were first aligned based on their sequence and then superimposed with the option set to accent secondary structure matches. Any detected structural deviations could then be extracted via text files listing individual root mean square distance (RMSD) values as a function of 3D positioning of amino acid residues in Ångström (Å). Since the maximum attainable accuracy of the homology models was stated around 2 Å and surface loops were said to deviate from the native structure in a wider manner (see above), highlighted residues were restricted to values ≥ 3 Å located in transmembrane domains. Fig. 54 shows the superimposition of the two wildtype constructs NtPIP2;1 and NtAQP1, while Table 43 gives a summary on the obtained RMSD values.

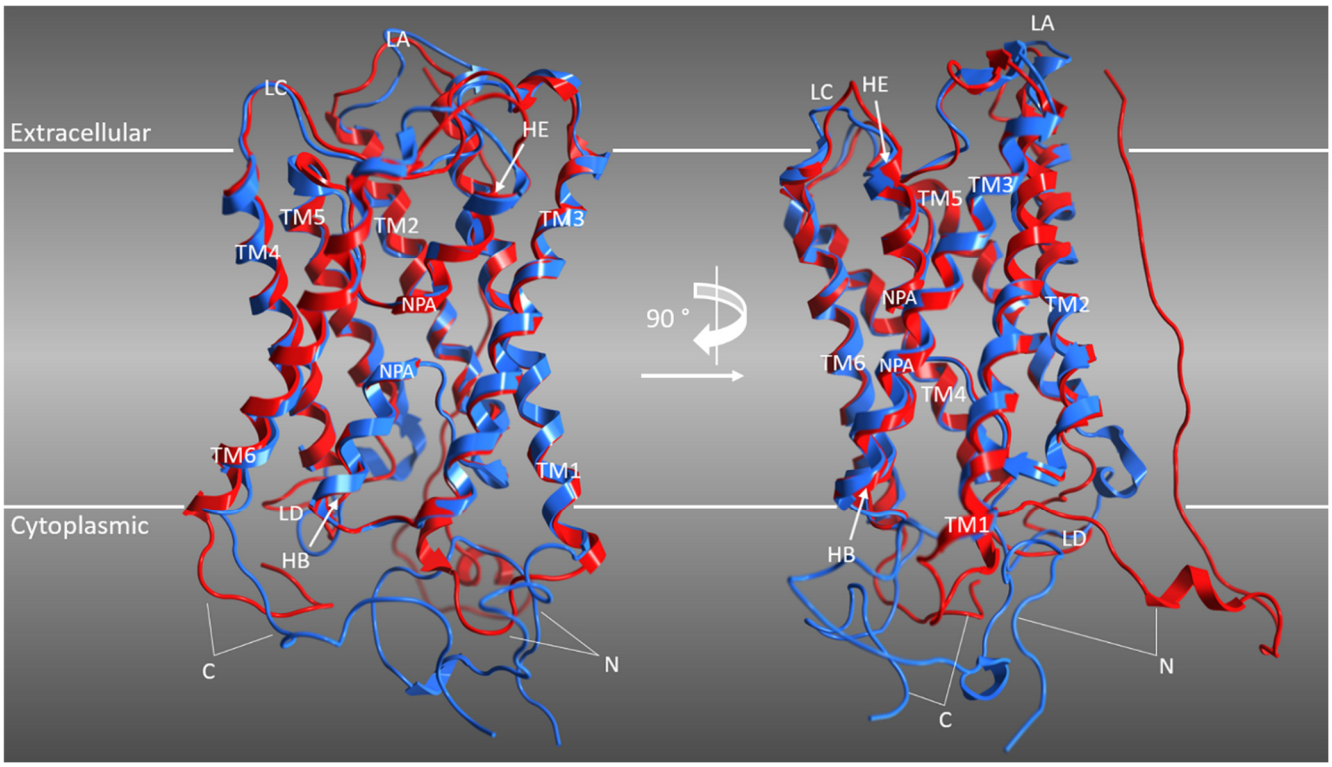

Fig. 54 – Superimposition of Phyre2 derived [Kelley *et al.* 2015] monomer homology models of tobacco aquaporins NtPIP2;1 (blue) and NtAQP1 (red). Visualization was generated using Molecular Operating Environment (MOE) v2014.09 (Chemical Computing Group, Montreal, Quebec, Canada). Indicated are individual protein domains including transmembrane helices 1 through 6 (TM1 – TM6), short helices B and E (HB, HE), loops A, C, D (LA, LC, LD), N- and C-terminus (N, C), as well as the two Asn-Ala-Pro (NPA) motifs at the center of the monomer pore. Horizontal white lines illustrate approximate positions of membrane boundaries with designated extracellular and cytoplasmic space. The structure on the left is adjusted for HB, HE and the NPA motifs to face the observer, whereas the structure on the right is rotated clockwise by 90 ° around its vertical axis. Contrary to the appearance, the NtAQP1 N-terminus does not project into the membrane, but most likely into the central axis of a tetrameric aquaporin configuration.

Based on the superimposed homology models of the wildtype NtPIP2;1 and NtAQP1, it is indicated that the transmembrane domains do not differ much, while terminal domains and surface loops do so in a more significant manner. This was expected, since transmembrane domains were stated to be modeled with a higher accuracy than surface loops via Phyre2, while N- and C-terminal domains were modeled *ab initio* in some parts (see Table 42). Nevertheless, a closer look at individual RMSD values of the respective domains revealed additional conformational disparities in the HB, TM3, TM5, HE and TM6 domains. Interestingly, all amino acid residues located in transmembrane domains with RMSD values ≥ 3 Å are identical in both NtPIP2;1 and NtAQP1. They include the selectivity filters ar/R 4, P4 and P5 (see chapter 1.3.2), as well as three amino acid residues that

are either highly conserved, in close proximity to one of the NPA motifs, or both (see multiple sequence alignment in chapter 3.1). *In silico* sequence analysis of the two wildtypes in chapter 3.1 indicated that their selectivity filters exhibit identical types of amino acids on all positions. Based on these results it can be assumed that shifted amino acid residues at critical sequence positions might very well be responsible for a difference in water permeability between NtPIP2;1 and NtAQP1.

Table 43 – Overview on root mean square distance (RMSD) values after superimposing Phyre2 derived [Kelley *et al.* 2015] homology models of NtPIP2;1 and NtAQP1 via MOE 2014.09 (Chemical Computing Group, Montreal, Quebec, Canada). RMSD values in Å indicate differing 3D positions of structural regions and thus conformational differences between the two aquaporins. Results are grouped into whole domain (left) and amino acid residue specific RMSD values (right). Maximum attainable model accuracy via Phyre2 was stated to be 2 Å and surface loops were said to deviate from the native structure in a wider manner than transmembrane domains. Hence, the fraction of amino acid residues with RMSD values ≥ 3 Å is indicated (left), while individual residues located in TM domains are singled out on the right.

Domain	NtPIP2;1 / NtAQP1	
	avg. RMSD [Å]	aa with ≥ 3 Å RMSD
N	2.4	44%
TM1	0.9	0%
LA	1.8	19%
TM2	1.1	0%
LB1	0.7	0%
HB	1.2	14%
LB2	1.4	11%
TM3	0.6	6%
LC	1.9	12%
TM4	1.0	0%
LD	3.1	67%
TM5	1.2	11%
LE1	1.5	0%
HE	1.1	7%
LE2	2.5	38%
TM6	1.6	22%
C	3.9	75%
Total	**1.5**	**14%**

NtPIP2;1	NtAQP1	RMSD [Å]	Domain	Notes
His_{102}	His_{113}	3.4	HB	highly conserved, 2 aa upstream of NPA1
Phe_{109}	Phe_{120}	4.1		3 aa downstream of NPA1
Tyr_{125}	Tyr_{136}	3.0	TM3	-
Leu_{200}	Leu_{211}	3.2	TM5	
Phe_{207}	Phe_{218}	3.4		
Arg_{228}	Arg_{239}	3.0	HE	ar/R 4, directly downstream of NPA2
Trp_{246}	Trp_{257}	5.3	TM6	highly conserved
Phe_{248}	Phe_{259}	3.7		P4
Trp_{249}	Trp_{260}	4.1		P5
His_{263}	His_{274}	3.5		-

In order to analyze, whether terminal domain modifications could be responsible for such shifts of critical amino acid residues, each wildtype aquaporin was superimposed onto its respective double deletion and double exchange mutant. Fig. 55, Table 44 and Table 45 summarize the results obtained for NtPIP2;1, Δ(N)_P2_Δ(C) and (N)A1_P2_(C)A1.

As with the superimposition of the two wildtypes, the three-dimensional visualization indicates an overall high conformational transmembrane identity between NtPIP2;1 and its terminal domain mutants. Nevertheless, significant shifts of individual amino acid residues were found in the TM2, HB, TM5, HE and TM6 transmembrane domains. Interestingly, seven out of the nine amino acid residues found to be significantly shifted between NtPIP2;1 and its double deletion mutant Δ(N)_P2_Δ(C) are identical to those found between the two wildtypes (see highlighted residues in Table 45). This includes the selectivity filters ar/R 4, P4 and P5 and suggests a change in conformation towards NtAQP1`s native structure, triggered by the deletion of NtPIP2;1´s terminal domains. The significant drop in water permeability measured for that mutant in comparison to the wildtype also supports that hypothesis (see chapter 3.6.3).

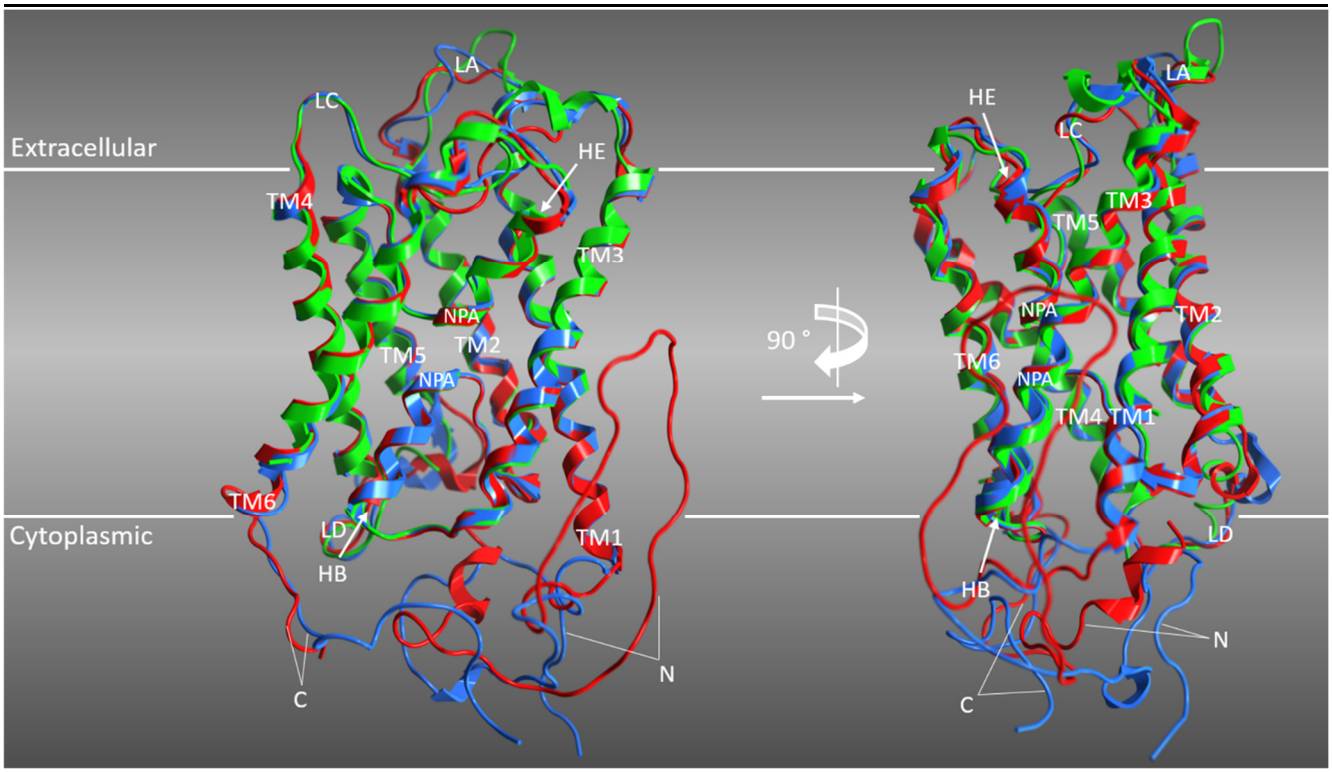

Fig. 55 – Superimposition of Phyre2 derived [Kelley *et al.* 2015] monomer homology models of wildtype tobacco aquaporin NtPIP2;1 (blue), its terminal domain double deletion mutant Δ(N)_P2_Δ(C) (green) and the terminal domain double exchange mutant (N)A1_P2_(C)A1 (red). Visualization was generated using Molecular Operating Environment (MOE) v2014.09 (Chemical Computing Group, Montreal, Quebec, Canada). Indicated are individual protein domains including transmembrane helices 1 through 6 (TM1 – TM6), short helices B and E (HB, HE), loops A, C, D (LA, LC, LD), N- and C-terminus (N, C), as well as the two Asn-Ala-Pro (NPA) motifs at the center of the monomer pore. Horizontal white lines illustrate approximate positions of membrane boundaries with designated extracellular and cytoplasmic space. The structure on the left is adjusted for HB, HE and the NPA motifs to face the observer, whereas the structure on the right is rotated clockwise by 90 ° around its vertical axis. Contrary to the appearance, the (N)A1_P2_(C)A1 N-terminus does not project into the membrane, but is most likely located on the cytosolic side of the membrane.

Table 44 – Overview on root mean square distance (RMSD) values after superimposing Phyre2 derived [Kelley *et al.* 2015] homology models of NtPIP2;1 and its terminal domain mutants via MOE v2014.09 (Chemical Computing Group, Montreal, Quebec, Canada). RMSD values in Å indicate differing 3D positions of structural regions and thus conformational differences between the aquaporin constructs. Results are grouped into domain specific RMSD values. Maximum attainable model accuracy via Phyre2 was stated to be 2 Å. Hence, the fraction of amino acid residues with RMSD values ≥ 3 Å is indicated.

Domain	NtPIP2;1 / Δ(N)_P2_Δ(C)		NtPIP2;1 / (N)A1_P2_(C)A1		Δ(N)_P2_Δ(C) / (N)A1_P2_(C)A1	
	avg. RMSD [Å]	aa with ≥ 3 Å RMSD	avg. RMSD [Å]	aa with ≥ 3 Å RMSD	avg. RMSD [Å]	aa with ≥ 3 Å RMSD
TM1	0.9	0%	0.2	0%	0.9	0%
LA	4.1	42%	2.5	32%	4.4	53%
TM2	1.3	6%	0.5	0%	1.3	6%
LB1	1.6	0%	0.7	0%	1.2	0%
HB	1.3	14%	0.5	7%	1.2	7%
LB2	1.6	22%	1.6	22%	1.4	11%
TM3	0.9	0%	0.3	0%	0.9	0%
LC	2.3	26%	1.9	30%	2.8	44%
TM4	1.0	0%	0.5	0%	1.1	0%
LD	4.4	71%	3.1	36%	4.3	64%
TM5	1.5	11%	1.2	11%	1.6	6%
LE1	1.0	0%	0.3	0%	1.1	0%
HE	1.1	7%	0.5	0%	1.1	7%
LE2	2.6	30%	2.1	20%	3.2	40%
TM6	1.7	19%	0.6	6%	1.8	19%
Total	**1.9**	**18%**	**1.1**	**12%**	**2.0**	**20%**

Table 45 – Overview on root mean square distance (RMSD) values after superimposing Phyre2 derived [Kelley *et al.* 2015] homology models of NtPIP2;1 (WT) and its terminal domain mutants via MOE v2014.09 (Chemical Computing Group, Montreal, Quebec, Canada). RMSD values in Å indicate differing 3D positions of structural regions and thus conformational differences between the aquaporin constructs. Results are in amino acid residue specific RMSD values. Maximum attainable model accuracy via Phyre2 was stated to be 2 Å and surface loops were said to deviate from the native structure in a wider manner than transmembrane domains. Hence, only amino acid residues with RMSD values ≥ 3 Å and located in TM domains are listed. Amino acid residues corresponding in their alignment position are listed in the same row. Residues that were also found to be significantly shifted in the superimposition of NtPIP2;1 and NtAQP1 are highlighted in blue. 1 = NtPIP2;1 wildtype / 2 = upstream / 3 = downstream.

WT[1]	Δ(N)_P2_Δ(C)	RMSD [Å]	WT[1]	(N)A1_P2_(C)A1	RMSD [Å]	Δ(N)_P2_Δ(C)	(N)A1_P2_(C)A1	RMSD [Å]	Domain	Notes
Trp_{82}	Trp_{39}	4.4		-		Trp_{39}	Trp_{95}	4.5	TM2	-
His_{102}	His_{59}	3.5	His_{102}	His_{115}	3.2		-		HB	highly conserved, 2 aa us[2] of NPA1
Phe_{109}	Phe_{66}	4.3		-		Phe_{66}	Phe_{122}	4.2		3 aa ds[3] of NPA1
Leu_{200}	Leu_{157}	5.3	Leu_{200}	Leu_{213}	9.6	Leu_{157}	Leu_{213}	6.6	TM5	-
Ala_{201}	Ala_{158}	3.5	Ala_{201}	Ala_{214}	4.9		-			
Arg_{228}	Arg_{185}	3.0				Arg_{185}	Arg_{241}	3.0	HE	ar/R 4, directly ds[3] of NPA2
Trp_{246}	Trp_{203}	5.3		-		Trp_{203}	Trp_{259}	5.2	TM6	highly conserved
Phe_{248}	Phe_{205}	3.8				Phe_{205}	Phe_{261}	3.9		P4
Trp_{249}	Trp_{206}	4.3				Trp_{206}	Trp_{262}	4.2		P5
	-		Phe_{253}	Phe_{266}	3.6		-			-

The attachment of NtAQP1´s terminal domains to the core of NtPIP2;1 significantly reduces the amount of shifted residues seen between the wildtype and its double deletion mutant. This translates to an almost 20 % higher water permeability compared to Δ(N)_P2_Δ(C) (see chapter 3.7.4), indicating that the mere presence of terminal domains is sufficient to change the conformation of the double deletion mutant towards improved water transport. However, this does not fully restore the native conformation of NtPIP2;1, as seen in four significantly shifted amino acid residues still present in the HB, TM5 and TM6 (see Table 45) domains. In addition, the water transport rate of the double exchange mutant (N)A1_P2_(C)A1 is more comparable to NtAQP1 than its wildtype progenitor NtPIP2;1 (see chapter 3.7.4).

Lastly, NtAQP1 was superimposed onto its terminal domain double deletion and double exchange mutants. The obtained results are shown in Fig. 56, Table 46 and Table 47.

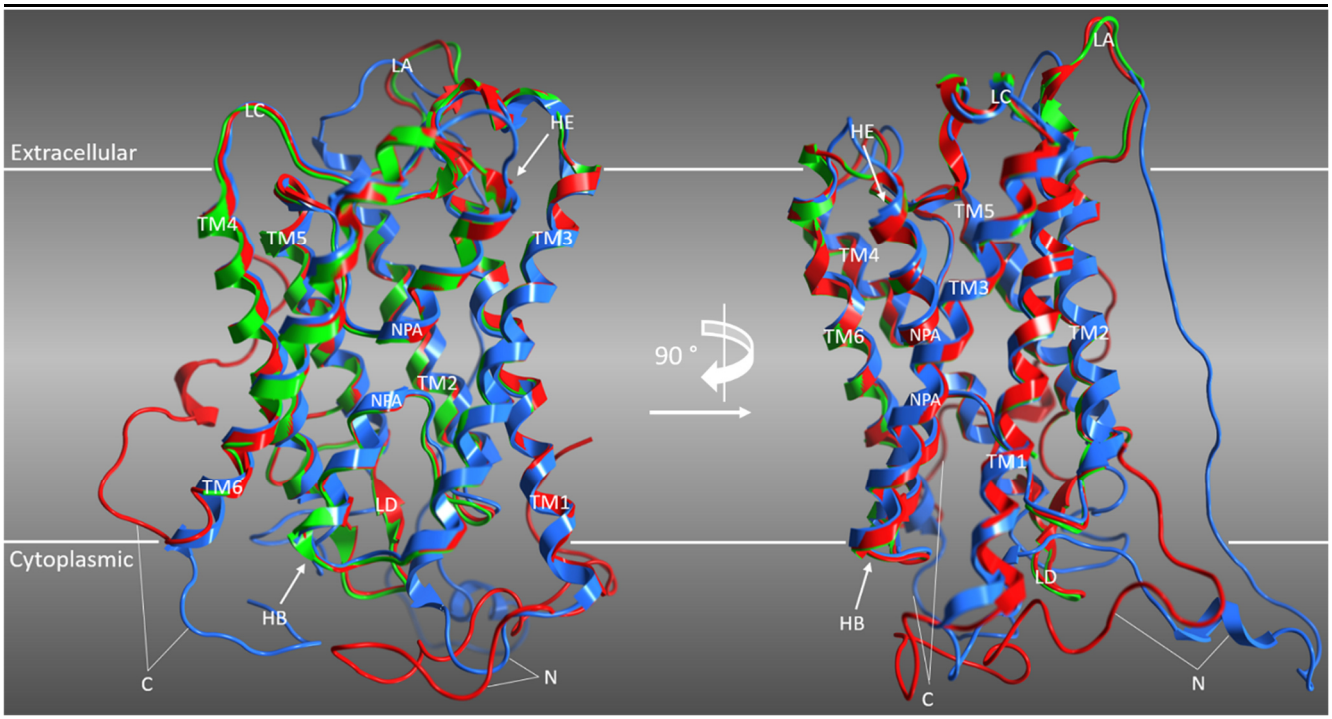

Fig. 56 – Superimposition of Phyre2 derived [Kelley *et al.* 2015] monomer homology models of wildtype tobacco aquaporin NtAQP1 (blue), its terminal domain double deletion mutant Δ(N)_A1_Δ(C) (green) and the terminal domain double exchange mutant (N)P2_A1_(C)P2 (red). Visualization was generated using Molecular Operating Environment (MOE) v2014.09 (Chemical Computing Group, Montreal, Quebec, Canada). Indicated are individual protein domains including transmembrane helices 1 through 6 (TM1 – TM6), short helices B and E (HB, HE), loops A, C, D (LA, LC, LD), N- and C-terminus (N, C), as well as the two Asn-Ala-Pro (NPA) motifs at the center of the monomer pore. Horizontal white lines illustrate approximate positions of membrane boundaries with designated extracellular and cytoplasmic space. The structure on the left is adjusted for HB, HE and the NPA motifs to face the observer, whereas the structure on the right is rotated clockwise by 90 ° around its vertical axis. Contrary to the appearance, the NtAQP1 N-terminus does not project into the membrane, but most likely into the central axis of a tetrameric aquaporin configuration.

Table 46 – Overview on root mean square distance (RMSD) values after superimposing Phyre2 derived [Kelley *et al.* 2015] homology models of NtAQP1 and its terminal domain mutants via MOE v2014.09 (Chemical Computing Group, Montreal, Quebec, Canada). RMSD values in Å indicate differing 3D positions of structural regions and thus conformational differences between the aquaporin constructs. Results are grouped into domain specific RMSD values. Maximum attainable model accuracy via Phyre2 was stated to be 2 Å. Hence, the fraction of amino acid residues with RMSD values ≥ 3 Å is indicated.

Domain	NtAQP1 / Δ(N)_A1_Δ(C)		NtAQP1 / (N)P2_A1_(C)P2		Δ(N)_A1_Δ(C) / (N)P2_A1_(C)P2	
	avg. RMSD [Å]	aa with >3 Å RMSD	avg. RMSD [Å]	aa with >3 Å RMSD	avg. RMSD [Å]	aa with >3 Å RMSD
TM1	0.9	0%	0.8	0%	0.7	0%
LA	5.0	47%	4.8	47%	1.1	6%
TM2	1.0	0%	1.1	0%	0.5	0%
LB1	1.4	0%	1.2	0%	0.6	0%
HB	0.7	0%	0.7	0%	0.4	0%
LB2	1.4	0%	1.1	0%	0.8	0%
TM3	1.0	6%	0.7	0%	0.9	6%
LC	1.7	4%	1.5	7%	0.9	4%
TM4	1.2	0%	1.1	0%	0.5	0%
LD	6.3 - 7.9	75 - 100%	6.4 - 8.1	75 - 100%	0.6	0%
TM5	1.1 - 1.5	0 - 6%	1.1 - 1.6	0 - 6%	0.4	0%
LE1	0.9	0%	1.1	0%	0.5	0%
HE	0.9	0%	0.9	0%	0.5	0%
LE2	3.4	50%	3.5	50%	0.8	0%
TM6	1.0	0%	1.0	0%	0.5	0%
Total	**1.8**	**11%**	**1.8**	**11%**	**0.7**	**1%**

Table 47 – Overview on root mean square distance (RMSD) values after superimposing Phyre2 derived [Kelley *et al.* 2015] homology models of NtAQP1 and its terminal domain mutants via MOE v2014.09 (Chemical Computing Group, Montreal, Quebec, Canada). RMSD values in Å indicate differing 3D positions of structural regions and thus conformational differences between the two aquaporins. Results are in amino acid residue specific RMSD values. Maximum attainable model accuracy via Phyre2 was stated to be 2 Å and surface loops were said to deviate from the native structure in a wider manner than transmembrane domains. Hence, only amino acid residues with RMSD values ≥ 3 Å and located in TM domains are listed. Amino acid residues corresponding in their alignment position are listed in the same row. Residues that were also found to be significantly shifted in the superimposition of NtPIP2;1 and NtAQP1 are highlighted in red.

NtAQP1	Δ(N)_A1_Δ(C)	RMSD [Å]	NtAQP1	(N)P2_A1_(C)P2	RMSD [Å]	Δ(N)_A1_Δ(C)	(N)P2_A1_(C)P2	RMSD [Å]	Domain	Notes
Phe_{135}	Phe_{79}	4.2		-		Phe_{79}	Phe_{122}	3.1	TM3	-
Leu_{211}	Asp_{149}	6.8	Leu_{211}	Asp_{192}	6.8		-		TM5/LD	

As with the previous superimpositions, the three-dimensional visualizations in this case show significant conformational differences in surface loops and terminal domains, whereas transmembrane regions do not seem to differ much. Looking at the alignment of the individual amino acid positions in more detail, however, reveals a shift of the N-terminal transmembrane helix 5. In both Δ(N)_A1_Δ(C) and (N)P2_A1_(C)P2 mutants, the amino acid residues corresponding to NtAQP1´s Ala_{203}-Val_{208} in loop D align with the N-terminal residues in the wildtype´s TM5 domain, namely Pro_{209}-Leu_{214}. As a consequence, their TM5 helix is elongated by an additional half turn and protrudes into the cytosol. Tables 46 and 47 list both domains for specific amino acid positions and giving ranges for RMSD values instead of exact numbers. A similar phenomenon was reported by Törnroth-Horsefield *et al.* in 2006, where the spinach aquaporin SoPIP2;1 underwent a TM5 half turn shift into the cytosol. Interestingly, this was as a consequence of its C-terminal Ser_{274} losing interaction with an adjacent monomer, in turn causing the TM shift and setting an open-pore configuration. Although NtAQP1 exhibits a Phe_{283} instead of a Ser at the corresponding position, its C-terminus is intriguingly rendered to project into the central axis of a tetrameric aquaporin configuration (see Fig. 56 and 54). This would certainly make direct interactions with adjacent monomers possible, for instance with one of the two C-terminal serines at positions 286 and 287, which are in close proximity to Phe_{283}. The domain-specific and overall RMSD values between the wildtype and its mutants demonstrate a striking similarity between the latter. Although the double exchange mutant´s water permeability was determined to be basically twice that of NtAQP1´s double deletion mutant (see chapter 3.7.5), their overall average RMSD is only 0.7 Å (see Table 47). Significantly shifted amino acid residues between the mutant constructs are restricted to their LA, TM3 and LC domains with only one phenylalanine located in a transmembrane region (see Table 47). Even though these conformational differences seem minor in comparison with the observed water permeability, previous studies indicated that a large change in water transport rate can be achieved by subtle effects. For instance, mutational and crystal structure analyses of PfAQP from *Plasmodium falciparum* revealed that changes in hydrogen bond interactions in the ar/R filter [Newby *et al.* 2008] or in the electrostatic environment of the pore entrance [Beitz *et al.* 2004] could have a significant effect on an aquaporin´s water permeability. A few conformational changes in combination with differing terminal domain interactions with other domains of the same monomer or adjacent monomers might thus have a modulation effect as strong as observed with Δ(N)_A1_Δ(C) and (N)P2_A1_(C)P2 in this case.

Potential conformational changes of loops were not considered in either of the homology analyses, since their heightened flexibility in comparison with the transmembrane domains made their RMSD data significantly harder to interpret. However, they cannot be ruled out to play a role in influencing these aquaporins´ water permeation capabilities in combination with terminal domain modifications.

4.4 Conclusion

The establishment of the *E. coli* based cell-free expression system in this work demonstrated its power as a handy tool for the characterization of aquaporin mediated water transport. Its open system allowed full control

over individual components and thus made the application of various protocols possible (P-CF, D-CF, L-CF). However, obligatory requirements included very precise handling and strict accordance to established protocols due to the sensitivity of the experimental steps involved.

Initial analyses of NtPIP2;1 and NtAQP1 wildtype permeability turned out to be as expected for members of their respective PIP subfamilies. Furthermore, liposomes showed a comparably low resistance to water diffusion in contrast to other, more native membranes equipped with various proteins and carbohydrates, i.e. yeast or *Xenopus* derived oocytes. *In silico* analyses of the two wildtype aquaporins revealed identical selectivity filters for both proteins, as well as high sequence similarities in their cores, thus pointing towards a potential modulation of their water permeability by their terminal domains. The ensuing deletion and exchange mutations ascribed low water transport rates to a total absence of terminal domains, whereas NtAQP1 sequences allowed for water permeability at control or PIP1 levels. NtPIP2;1 terminal domains, however, enabled permeation rates significantly higher than all other constructs, except for the NtPIP2;1 wildtype.

As a consequence from these results, potential regulation mechanisms were discussed for their viability in terms of terminal domain dependence in the two tobacco aquaporins. The majority of post-translational modifications and domain interactions, as well as oligomerization mechanisms discussed in aquaporin related literature was discarded. This was due to incompatibilities found in either the amino acid sequence, the experimental setup or results obtained in this work or other publications for NtPIP2;1 and NtAQP1. The same was found to be true for the possibility of pH dependent and mechanical gating. Though the latter could not be completely dismissed due to potentially increased mechanosensitivity via terminal domain modifications. Increased adhesive properties derived from terminal cleavage and N-terminal methylation / acetylation, respectively, were found to be in the realm of possibility, with additional mutation and structure analysis based experiments necessary to determine their viability. Homology based modeling of NtPIP2;1, NtAQP1 and their respective double mutation constructs opened up the possibility of conformational changes in the transmembrane core structures induced by terminal domain modifications. In the case of NtPIP2;1 mutants, the removal or exchange of termini resulted in a “reprogramming” towards a more PIP1-like configuration, with water permeabilities being adjusted accordingly. The NtAQP1 double deletion and double exchange mutants, however, demonstrated a striking similarity in transmembrane conformation in contrast to their vastly differing permeation capabilities. An elongation of their TM5 domain into the cytosol was curiously reminiscent of a previously described domain interaction mechanism involving a C-terminal serine interacting with an adjacent monomer. Thus, rather subtle, terminal domain derived deviations from the wildtype could potentially induce a disproportionally large difference in water transport.

Structural changes due to terminal domain modifications had previously been shown to modify water permeation in aquaporins [Fotiadis *et al.* 2002]. A potential explanation for this type of conformational aquaporin modulation could be based on the evolutional history of plant MIPs. Since their protein subfamily consists exclusively of aquaporins without sequence motifs pointing towards aquaglyceroporins like in animals [Maurel *et al.* 2015], their sequence and functional diversification was likely based on gene duplications [Zardoya 2005]. This eventually led to subfunctionalization in various tissues [Ishibashi *et al.* 2011], while at the same time conserving the ubiquitous aquaporin hourglass shape, which is thought to be a natural selection towards efficient hydrodynamic transport [Gravelle *et al.* 2013]. Thus far, its cytosolic side has been shown to be highly conserved, while pore selectivity is determined on the extracellular half [Abascal *et al.* 2014]. However, sequence based diversification at the terminal domain level adds the possibility to modulate aquaporin mediated permeation of solutes without direct modification of the transmembrane core. It would be highly

interesting to see, whether the modifications to the tobacco aquaporins presented in this work also have the potential to alter or expand their functionality with different solutes. With NtAQP1, CO_2 mediation certainly catches the attention [Uehlein *et al.* 2003], with NtPIP2;1´s capabilities so far being restricted to water transport [Bots *et al.* 2005a / Otto *et al.* 2010 / Kai & Kaldenhoff 2014], thus being a potential target for expansion in specificity. In addition, an investigation into the PIP1 specific isoleucine corresponding to NtAQP1 position 245 reported to be a steric hinderance to water transport could potentially close the small gap left between its double exchange mutant and the NtPIP2;1 wildtype [Suga & Maeshima 2004]. Lastly, the introduction of double exchange mutants *in planta* could shed a light on their tissue localization and membrane integration capabilities, as well as analyze their impact on overall physiology.

References

Abascal F, Irisarri I, Zardoya R. 2014. Diversity and evolution of membrane intrinsic proteins. *Biochim Biophys Acta* **1840:** 1468-1481.

Abrami L, Tacnet F, Ripoche P. 1995. Evidence for a glycerol pathway through aquaporin 1 (CHIP28) channels. *Pflugers Arch* **430:** 447-458.

Agre P. 2004. Aquaporin water channels (Nobel Lecture). *Angew Chem Int Ed Engl* **43:** 4278-4290.

Agre P, Preston GM, Smith BL, Jung JS, Raina S, Moon C, Guggino WB, Nielsen S. 1993. Aquaporin CHIP: the archetypal molecular water channel. *Am J Physiol* **265:** F463-476.

Aharon R, Shahak Y, Wininger S, Bendov R, Kapulnik Y, Galili G. 2003. Overexpression of a plasma membrane aquaporin in transgenic tobacco improves plant vigor under favorable growth conditions but not under drought or salt stress. *Plant Cell* **15:** 439-447.

Ajit Walter P, Muthukumar T, Reddy BS. 2015. Assessment of antifouling efficacy of polyhedral oligomeric silsesquioxane based poly (urea-urethane-imide) hybrid membranes. *Lett Appl Microbiol* **61:** 274-282.

Alleva K, Chara O, Amodeo G. 2012. Aquaporins: another piece in the osmotic puzzle. *FEBS Lett* **586:** 2991-2999.

Alleva K, Niemietz CM, Sutka M, Maurel C, Parisi M, Tyerman SD, Amodeo G. 2006. Plasma membrane of Beta vulgaris storage root shows high water channel activity regulated by cytoplasmic pH and a dual range of calcium concentrations. *J Exp Bot* **57:** 609-621.

Almasalmeh A, Krenc D, Wu B, Beitz E. 2014. Structural determinants of the hydrogen peroxide permeability of aquaporins. *FEBS J* **281:** 647-656.

Anderberg HI, Danielson JA, Johanson U. 2011. Algal MIPs, high diversity and conserved motifs. *BMC Evol Biol* **11:** 110.

Anderberg HI, Kjellbom P, Johanson U. 2012. Annotation of Selaginella moellendorffii Major Intrinsic Proteins and the Evolution of the Protein Family in Terrestrial Plants. *Front Plant Sci* **3:** 33.

Anthony TL, Brooks HL, Boassa D, Leonov S, Yanochko GM, Regan JW, Yool AJ. 2000. Cloned human aquaporin-1 is a cyclic GMP-gated ion channel. *Mol Pharmacol* **57:** 576-588.

Arthur J, Huang J, Nomura N, Jin WW, Li W, Cheng X, Brown D, Lu HJ. 2015. Characterization of the putative phosphorylation sites of the AQP2 C terminus and their role in AQP2 trafficking in LLC-PK1 cells. *Am J Physiol Renal Physiol* **309:** F673-679.

Ball LE, Little M, Nowak MW, Garland DL, Crouch RK, Schey KL. 2003. Water permeability of C-terminally truncated aquaporin 0 (AQP0 1-243) observed in the aging human lens. *Invest Ophthalmol Vis Sci* **44:** 4820-4828.

Baumgarten R, Van De Pol MH, Wetzels JF, Van Os CH, Deen PM. 1998. Glycosylation is not essential for vasopressin-dependent routing of aquaporin-2 in transfected Madin-Darby canine kidney cells. *J Am Soc Nephrol* **9:** 1553-1559.

Bayburt TH, Sligar SG. 2010. Membrane protein assembly into Nanodiscs. *FEBS Lett* **584:** 1721-1727.

Beebo A, Mathai JC, Schoefs B, Spetea C. 2013. Assessment of the requirement for aquaporins in the thylakoid membrane of plant chloroplasts to sustain photosynthetic water oxidation. *FEBS Lett* **587:** 2083-2089.

Beebo A, Thomas D, Der C, Sanchez L, Leborgne-Castel N, Marty F, Schoefs B, Bouhidel K. 2009. Life with and without AtTIP1;1, an Arabidopsis aquaporin preferentially localized in the apposing tonoplasts of adjacent vacuoles. *Plant Mol Biol* **70:** 193-209.

Beitz E. 2005. Aquaporins from pathogenic protozoan parasites: structure, function and potential for chemotherapy. *Biol Cell* **97:** 373-383.

Beitz E, Pavlovic-Djuranovic S, Yasui M, Agre P, Schultz JE. 2004. Molecular dissection of water and glycerol permeability of the aquaglyceroporin from Plasmodium falciparum by mutational analysis. *Proc Natl Acad Sci U S A* **101:** 1153-1158.

Beitz E, Wu B, Holm LM, Schultz JE, Zeuthen T. 2006. Point mutations in the aromatic/arginine region in aquaporin 1 allow passage of urea, glycerol, ammonia, and protons. *Proc Natl Acad Sci U S A* **103:** 269-274.

Bellati J, Alleva K, Soto G, Vitali V, Jozefkowicz C, Amodeo G. 2010. Intracellular pH sensing is altered by plasma membrane PIP aquaporin co-expression. *Plant Mol Biol* **74:** 105-118.

Benga G. 2012. On the definition, nomenclature and classification of water channel proteins (aquaporins and relatives). *Mol Aspects Med* **33:** 514-517.

Bernhard F, Tozawa Y. 2013. Cell-free expression--making a mark. *Curr Opin Struct Biol* **23:** 374-380.

Berrier C, Park KH, Abes S, Bibonne A, Betton JM, Ghazi A. 2004. Cell-free synthesis of a functional ion channel in the absence of a membrane and in the presence of detergent. *Biochemistry* **43:** 12585-12591.

Besse M, Knipfer T, Miller AJ, Verdeil JL, Jahn TP, Fricke W. 2011. Developmental pattern of aquaporin expression in barley (Hordeum vulgare L.) leaves. *J Exp Bot* **62:** 4127-4142.

Biela A, Grote K, Otto B, Hoth S, Hedrich R, Kaldenhoff R. 1999. The Nicotiana tabacum plasma membrane aquaporin NtAQP1 is mercury-insensitive and permeable for glycerol. *Plant J* **18:** 565-570.

Bienert GP, Bienert MD, Jahn TP, Boutry M, Chaumont F. 2011. Solanaceae XIPs are plasma membrane aquaporins that facilitate the transport of many uncharged substrates. *Plant J* **66:** 306-317.

Bienert GP, Cavez D, Besserer A, Berny MC, Gilis D, Rooman M, Chaumont F. 2012. A conserved cysteine residue is involved in disulfide bond formation between plant plasma membrane aquaporin monomers. *Biochem J* **445:** 101-111.

Bienert GP, Desguin B, Chaumont F, Hols P. 2013. Channel-mediated lactic acid transport: a novel function for aquaglyceroporins in bacteria. *Biochem J* **454:** 559-570.

Bienert GP, Moller AL, Kristiansen KA, Schulz A, Moller IM, Schjoerring JK, Jahn TP. 2007. Specific aquaporins facilitate the diffusion of hydrogen peroxide across membranes. *J Biol Chem* **282:** 1183-1192.

Bienert GP, Schussler MD, Jahn TP. 2008. Metalloids: essential, beneficial or toxic? Major intrinsic proteins sort it out. *Trends Biochem Sci* **33:** 20-26.

BioLogic Science Instruments C, France. 2008. SFM-300/400 User´s Manual Version 2.4 - August 2008.

Birnboim HC. 1983. A rapid alkaline extraction method for the isolation of plasmid DNA. *Methods Enzymol* **100:** 243-255.

Biswas SK, Brako L, Gu S, Jiang JX, Lo WK. 2014. Regional changes of AQP0-dependent square array junction and gap junction associated with cortical cataract formation in the Emory mutant mouse. *Exp Eye Res* **127:** 132-142.

Blom N, Sicheritz-Ponten T, Gupta R, Gammeltoft S, Brunak S. 2004. Prediction of post-translational glycosylation and phosphorylation of proteins from the amino acid sequence. *Proteomics* **4:** 1633-1649.

Boassa D, Yool AJ. 2003. Single amino acids in the carboxyl terminal domain of aquaporin-1 contribute to cGMP-dependent ion channel activation. *BMC Physiol* **3:** 12.

Borgnia MJ, Kozono D, Calamita G, Maloney PC, Agre P. 1999. Functional reconstitution and characterization of AqpZ, the E. coli water channel protein. *J Mol Biol* **291:** 1169-1179.

Bots M, Feron R, Uehlein N, Weterings K, Kaldenhoff R, Mariani T. 2005a. PIP1 and PIP2 aquaporins are differentially expressed during tobacco anther and stigma development. *J Exp Bot* **56:** 113-121.

Bots M, Vergeldt F, Wolters-Arts M, Weterings K, van As H, Mariani C. 2005b. Aquaporins of the PIP2 class are required for efficient anther dehiscence in tobacco. *Plant Physiol* **137:** 1049-1056.

Boursiac Y, Chen S, Luu DT, Sorieul M, van den Dries N, Maurel C. 2005. Early effects of salinity on water transport in Arabidopsis roots. Molecular and cellular features of aquaporin expression. *Plant Physiol* **139:** 790-805.

Brown CW, Sridhara V, Boutz DR, Person MD, Marcotte EM, Barrick JE, Wilke CO. 2016. Large-scale analysis of post-translational modifications in *E. coli* under glucose-limiting conditions. *bioRxiv*.

Bullock WO, Fernandez JM, Stuart JM. 1987. XL1-Blue: a high efficiency plasmid transforming *rec A Escherichia coli* strain with β-galactosidase selection. *Biotechniques***:** 376-379.

Burnette WN. 1981. "Western blotting": electrophoretic transfer of proteins from sodium dodecyl sulfate--polyacrylamide gels to unmodified nitrocellulose and radiographic detection with antibody and radioiodinated protein A. *Anal Biochem* **112:** 195-203.

Calamita G, Bishai WR, Preston GM, Guggino WB, Agre P. 1995. Molecular cloning and characterization of AqpZ, a water channel from Escherichia coli. *J Biol Chem* **270:** 29063-29066.

Cancedda R, Schlesinger MJ. 1974. Formation of Sindbis virus capsid protein in mammalian cell-free extracts programmed with viral messenger RNA. *Proc Natl Acad Sci U S A* **71:** 1843-1847.

Carbrey JM, Gorelick-Feldman DA, Kozono D, Praetorius J, Nielsen S, Agre P. 2003. Aquaglyceroporin AQP9: solute permeation and metabolic control of expression in liver. *Proc Natl Acad Sci U S A* **100:** 2945-2950.

Carlisle EM. 1982. The nutritional essentiality of silicon. *Nutr Rev* **40:** 193-198.

Carlson ED, Gan R, Hodgman CE, Jewett MC. 2012. Cell-free protein synthesis: applications come of age. *Biotechnol Adv* **30:** 1185-1194.

Carpenter EP, Beis K, Cameron AD, Iwata S. 2008. Overcoming the challenges of membrane protein crystallography. *Curr Opin Struct Biol* **18:** 581-586.

Carvajal M, Cooke DT, Clarkson DT. 1996. Responses of wheat plants to nutrient deprivation may involve the regulation of water-channel function. *Planta***:** 372-381.

Ceroni A, Passerini A, Vullo A, Frasconi P. 2006. DISULFIND: a disulfide bonding state and cysteine connectivity prediction server. *Nucleic Acids Res* **34:** W177-181.

CGSC, Mattice L, Whitehead N, Wertz J. 2016. CGSC - Coli Genetic Stock Center Website, Yale University, New Haven, Conncecticut, USA. *cgsc.biology.yale.edu/*.

Chaumont F, Barrieu F, Jung R, Chrispeels MJ. 2000. Plasma membrane intrinsic proteins from maize cluster in two sequence subgroups with differential aquaporin activity. *Plant Physiol* **122:** 1025-1034.

Chaumont F, Moshelion M, Daniels MJ. 2005. Regulation of plant aquaporin activity. *Biol Cell* **97:** 749-764.

Chi Y, Fan Y, He L, Liu W, Wen X, Zhou S, Wang X, Zhang C, Kong H, Sonoda L, Tripathi P, Li CJ, Yu MS, Su C, Hu G. 2011. Novel role of aquaporin-4 in CD4+ CD25+ T regulatory cell development and severity of Parkinson's disease. *Aging Cell* **10:** 368-382.

Chin JW, Cropp TA, Anderson JC, Mukherji M, Zhang Z, Schultz PG. 2003. An expanded eukaryotic genetic code. *Science* **301:** 964-967.

Choi WG, Roberts DM. 2007. Arabidopsis NIP2;1, a major intrinsic protein transporter of lactic acid induced by anoxic stress. *J Biol Chem* **282:** 24209-24218.

Commons W, Foobar. 2016. Integral monotopic protein, Transmembrane protein, Wikipedia Articles Website, Wikimedia Foundations Inc. *upload.wikimedia.org/wikipedia/commons/c/c3/Monotopic_membrane_protein.svg and Polytopic_membrane_protein.png*.

Cui XH, Hao FS, Chen H, Chen J, Wang XC. 2008. Expression of the Vicia faba VfPIP1 gene in Arabidopsis thaliana plants improves their drought resistance. *J Plant Res* **121:** 207-214.

Dabeka RW, McKenzie AD, Lacroix GM, Cleroux C, Bowe S, Graham RA, Conacher HB, Verdier P. 1993. Survey of arsenic in total diet food composites and estimation of the dietary intake of arsenic by Canadian adults and children. *J AOAC Int* **76:** 14-25.

Daniels MJ, Chrispeels MJ, Yeager M. 1999. Projection structure of a plant vacuole membrane aquaporin by electron cryo-crystallography. *J Mol Biol* **294:** 1337-1349.

Daniels MJ, Mirkov TE, Chrispeels MJ. 1994. The plasma membrane of Arabidopsis thaliana contains a mercury-insensitive aquaporin that is a homolog of the tonoplast water channel protein TIP. *Plant Physiol* **106:** 1325-1333.

Danielson JA, Johanson U. 2008. Unexpected complexity of the aquaporin gene family in the moss Physcomitrella patens. *BMC Plant Biol* **8:** 45.

Davis RW, Botstein D, Roth JR. 1980. Advanced bacterial genetics, a manual for genetic engineering. *Cold Spring Harbor Laboratory Press, Cold Spring Harbor, New York, USA*.

de Groot BL, Grubmuller H. 2001. Water permeation across biological membranes: mechanism and dynamics of aquaporin-1 and GlpF. *Science* **294:** 2353-2357.

Deen PM, Verdijk MA, Knoers NV, Wieringa B, Monnens LA, van Os CH, van Oost BA. 1994. Requirement of human renal water channel aquaporin-2 for vasopressin-dependent concentration of urine. *Science* **264:** 92-95.

Denker BM, Smith BL, Kuhajda FP, Agre P. 1988. Identification, purification, and partial characterization of a novel Mr 28,000 integral membrane protein from erythrocytes and renal tubules. *J Biol Chem* **263:** 15634-15642.

Dereeper A, Guignon V, Blanc G, Audic S, Buffet S, Chevenet F, Dufayard JF, Guindon S, Lefort V, Lescot M, Claverie JM, Gascuel O. 2008. Phylogeny.fr: robust phylogenetic analysis for the non-specialist. *Nucleic Acids Res* **36:** W465-469.

di Pietro M, Vialaret J, Li GW, Hem S, Prado K, Rossignol M, Maurel C, Santoni V. 2013. Coordinated post-translational responses of aquaporins to abiotic and nutritional stimuli in Arabidopsis roots. *Mol Cell Proteomics* **12:** 3886-3897.

Dobson L, Remenyi I, Tusnady GE. 2015a. CCTOP: a Consensus Constrained TOPology prediction web server. *Nucleic Acids Res* **43:** W408-412.

Dobson L, Remenyi I, Tusnady GE. 2015b. The human transmembrane proteome. *Biol Direct* **10:** 31.

Dordas C, Chrispeels MJ, Brown PH. 2000. Permeability and channel-mediated transport of boric acid across membrane vesicles isolated from squash roots. *Plant Physiol* **124:** 1349-1362.

Drake LL, Rodriguez SD, Hansen IA. 2015. Functional characterization of aquaporins and aquaglyceroporins of the yellow fever mosquito, Aedes aegypti. *Sci Rep* **5:** 7795.

Duchesne L, Deschamps S, Pellerin I, Lagree V, Froger A, Thomas D, Bron P, Delamarche C, Hubert JF. 2001. Oligomerization of water and solute channels of the major intrinsic protein (MIP) family. *Kidney Int* **60:** 422-426.

Duchesne L, Pellerin I, Delamarche C, Deschamps S, Lagree V, Froger A, Bonnec G, Thomas D, Hubert JF. 2002. Role of C-terminal domain and transmembrane helices 5 and 6 in function and quaternary structure of major intrinsic proteins: analysis of aquaporin/glycerol facilitator chimeric proteins. *J Biol Chem* **277:** 20598-20604.

Durbak AR, Phillips KA, Pike S, O'Neill MA, Mares J, Gallavotti A, Malcomber ST, Gassmann W, McSteen P. 2014. Transport of boron by the tassel-less1 aquaporin is critical for vegetative and reproductive development in maize. *Plant Cell* **26:** 2978-2995.

Eckert M, Biela A, Siefritz F, Kaldenhoff R. 1999. New aspects of plant aquaporin regulation and specificity. *J Exp Bot* **50:** 1541-1546.

Edgar RC. 2004a. MUSCLE: a multiple sequence alignment method with reduced time and space complexity. *BMC Bioinformatics* **5:** 113.

Edgar RC. 2004b. MUSCLE: multiple sequence alignment with high accuracy and high throughput. *Nucleic Acids Res* **32:** 1792-1797.

Eisch AJ, Petrik D. 2012. Depression and hippocampal neurogenesis: a road to remission? *Science* **338:** 72-75.

Endeward V, Musa-Aziz R, Cooper GJ, Chen LM, Pelletier MF, Virkki LV, Supuran CT, King LS, Boron WF, Gros G. 2006. Evidence that aquaporin 1 is a major pathway for CO2 transport across the human erythrocyte membrane. *FASEB J* **20:** 1974-1981.

Engelund MB, Madsen SS. 2015. Tubular localization and expressional dynamics of aquaporins in the kidney of seawater-challenged Atlantic salmon. *J Comp Physiol B* **185:** 207-223.

Evans JR, Kaldenhoff R, Genty B, Terashima I. 2009. Resistances along the CO2 diffusion pathway inside leaves. *J Exp Bot* **60:** 2235-2248.

Faghiri Z, Camargo SM, Huggel K, Forster IC, Ndegwa D, Verrey F, Skelly PJ. 2010. The tegument of the human parasitic worm Schistosoma mansoni as an excretory organ: the surface aquaporin SmAQP is a lactate transporter. *PLoS One* **5:** e10451.

Fan LM, Zhao Z, Assmann SM. 2004. Guard cells: a dynamic signaling model. *Curr Opin Plant Biol* **7:** 537-546.

Fernandez JM, Hoeffler JP. 1999. Gene Expression Systems. Using nature for the art of expression. *Academic Press, San Diego, California, USA*.

Ferro M, Brugiere S, Salvi D, Seigneurin-Berny D, Court M, Moyet L, Ramus C, Miras S, Mellal M, Le Gall S, Kieffer-Jaquinod S, Bruley C, Garin J, Joyard J, Masselon C, Rolland N. 2010. AT_CHLORO, a comprehensive chloroplast proteome database with subplastidial localization and curated information on envelope proteins. *Mol Cell Proteomics* **9:** 1063-1084.

Ferro M, Salvi D, Brugiere S, Miras S, Kowalski S, Louwagie M, Garin J, Joyard J, Rolland N. 2003. Proteomics of the chloroplast envelope membranes from Arabidopsis thaliana. *Mol Cell Proteomics* **2:** 325-345.

Fetter K, Van Wilder V, Moshelion M, Chaumont F. 2004. Interactions between plasma membrane aquaporins modulate their water channel activity. *Plant Cell* **16:** 215-228.

Finn RN, Cerda J. 2015. Evolution and functional diversity of aquaporins. *Biol Bull* **229:** 6-23.

Finn RN, Chauvigne F, Hlidberg JB, Cutler CP, Cerda J. 2014. The lineage-specific evolution of aquaporin gene clusters facilitated tetrapod terrestrial adaptation. *PLoS One* **9:** e113686.

Fischer G, Kosinska-Eriksson U, Aponte-Santamaria C, Palmgren M, Geijer C, Hedfalk K, Hohmann S, de Groot BL, Neutze R, Lindkvist-Petersson K. 2009. Crystal structure of a yeast aquaporin at 1.15 angstrom reveals a novel gating mechanism. *PLoS Biol* **7:** e1000130.

Fischer M. 2007. Untersuchungen zur Modifikation von Aquaporinen aus *Nicotiana tabacum*. *Doctoral dissertation in the Department of Biology at the Darmstadt University of Technology, Darmstadt, Germany*.

Fischer M, Kaldenhoff R. 2008. On the pH regulation of plant aquaporins. *J Biol Chem* **283:** 33889-33892.

Fleishman SJ, Harrington SE, Enosh A, Halperin D, Tate CG, Ben-Tal N. 2006. Quasi-symmetry in the cryo-EM structure of EmrE provides the key to modeling its transmembrane domain. *J Mol Biol* **364:** 54-67.

Flexas J, Ribas-Carbo M, Hanson DT, Bota J, Otto B, Cifre J, McDowell N, Medrano H, Kaldenhoff R. 2006. Tobacco aquaporin NtAQP1 is involved in mesophyll conductance to CO2 in vivo. *Plant J* **48:** 427-439.

Fortin MG, Zelechowska M, Verma DP. 1985. Specific targeting of membrane nodulins to the bacteroid-enclosing compartment in soybean nodules. *EMBO J* **4:** 3041-3046.

Fotiadis D, Suda K, Tittmann P, Jeno P, Philippsen A, Muller DJ, Gross H, Engel A. 2002. Identification and structure of a putative Ca2+-binding domain at the C terminus of AQP1. *J Mol Biol* **318:** 1381-1394.

Frick A, Jarva M, Ekvall M, Uzdavinys P, Nyblom M, Tornroth-Horsefield S. 2013a. Mercury increases water permeability of a plant aquaporin through a non-cysteine-related mechanism. *Biochem J* **454:** 491-499.

Frick A, Jarva M, Tornroth-Horsefield S. 2013b. Structural basis for pH gating of plant aquaporins. *FEBS Lett* **587:** 989-993.

Frigeri A, Gropper MA, Turck CW, Verkman AS. 1995. Immunolocalization of the mercurial-insensitive water channel and glycerol intrinsic protein in epithelial cell plasma membranes. *Proc Natl Acad Sci U S A* **92:** 4328-4331.

Froger A, Tallur B, Thomas D, Delamarche C. 1998. Prediction of functional residues in water channels and related proteins. *Protein Sci* **7:** 1458-1468.

Frottin F, Martinez A, Peynot P, Mitra S, Holz RC, Giglione C, Meinnel T. 2006. The proteomics of N-terminal methionine cleavage. *Mol Cell Proteomics* **5:** 2336-2349.

Fu D, Libson A, Miercke LJ, Weitzman C, Nollert P, Krucinski J, Stroud RM. 2000. Structure of a glycerol-conducting channel and the basis for its selectivity. *Science* **290:** 481-486.

Garneau AP, Carpentier GA, Marcoux AA, Frenette-Cotton R, Simard CF, Remus-Borel W, Caron L, Jacob-Wagner M, Noel M, Powell JJ, Belanger R, Cote F, Isenring P. 2015. Aquaporins Mediate Silicon Transport in Humans. *PLoS One* **10:** e0136149.

Gaspar M, Bousser A, Sissoëff I, Roche O, Hoarau J, Mahé A. 2003. Cloning and characterization of *ZmPIP1-5b,* an aquaporin transporting water and urea. *Plant Sci* **165:** 21-31.

Gasteiger E, Hoogland C, Gattiker A, Duvaud S, Wilkins MR, Appel RD, Bairoch A. 2005. The Proteomics Protocols Handbook, Chapter 52: Protein Identification and Analysis Tools on the ExPASy Server. *Totowa, NJ: Humana Press Inc.***:** 571-607.

Gavrin A, Kaiser BN, Geiger D, Tyerman SD, Wen Z, Bisseling T, Fedorova EE. 2014. Adjustment of host cells for accommodation of symbiotic bacteria: vacuole defunctionalization, HOPS suppression, and TIP1g retargeting in Medicago. *Plant Cell* **26:** 3809-3822.

Geller BL, Wickner W. 1985. M13 procoat inserts into liposomes in the absence of other membrane proteins. *J Biol Chem* **260:** 13281-13285.

Gerbeau P, Guclu J, Ripoche P, Maurel C. 1999. Aquaporin Nt-TIPa can account for the high permeability of tobacco cell vacuolar membrane to small neutral solutes. *Plant J* **18:** 577-587.

Gerken TA, Jamison O, Perrine CL, Collette JC, Moinova H, Ravi L, Markowitz SD, Shen W, Patel H, Tabak LA. 2011. Emerging paradigms for the initiation of mucin-type protein O-glycosylation by the polypeptide GalNAc transferase family of glycosyltransferases. *J Biol Chem* **286:** 14493-14507.

Gerken TA, Raman J, Fritz TA, Jamison O. 2006. Identification of common and unique peptide substrate preferences for the UDP-GalNAc:polypeptide alpha-N-acetylgalactosaminyltransferases T1 and T2 derived from oriented random peptide substrates. *J Biol Chem* **281:** 32403-32416.

Gerken TA, Ten Hagen KG, Jamison O. 2008. Conservation of peptide acceptor preferences between Drosophila and mammalian polypeptide-GalNAc transferase ortholog pairs. *Glycobiology* **18:** 861-870.

Gesteland RF. 1966. Isolation and characterization of ribonuclease I mutants of Escherichia coli. *J Mol Biol* **16:** 67-84.

Geyer RR, Musa-Aziz R, Qin X, Boron WF. 2013. Relative CO(2)/NH(3) selectivities of mammalian aquaporins 0-9. *Am J Physiol Cell Physiol* **304:** C985-994.

Gonen T, Cheng Y, Kistler J, Walz T. 2004. Aquaporin-0 membrane junctions form upon proteolytic cleavage. *J Mol Biol* **342:** 1337-1345.

Gonen T, Walz T. 2006. The structure of aquaporins. *Q Rev Biophys* **39:** 361-396.

Gourbal B, Sonuc N, Bhattacharjee H, Legare D, Sundar S, Ouellette M, Rosen BP, Mukhopadhyay R. 2004. Drug uptake and modulation of drug resistance in Leishmania by an aquaglyceroporin. *J Biol Chem* **279:** 31010-31017.

GraphPad Software Inc. LJ, California, USA. 2014. GraphPad Statistics Guide for GraphPad Prism v6.

Gravelle S, Joly L, Detcheverry F, Ybert C, Cottin-Bizonne C, Bocquet L. 2013. Optimizing water permeability through the hourglass shape of aquaporins. *Proc Natl Acad Sci U S A* **110:** 16367-16372.

Guenther JF, Roberts DM. 2000. Water-selective and multifunctional aquaporins from Lotus japonicus nodules. *Planta* **210:** 741-748.

Gustavsson S, Lebrun AS, Norden K, Chaumont F, Johanson U. 2005. A novel plant major intrinsic protein in Physcomitrella patens most similar to bacterial glycerol channels. *Plant Physiol* **139:** 287-295.

Habel J, Hansen M, Kynde S, Larsen N, Midtgaard SR, Jensen GV, Bomholt J, Ogbonna A, Almdal K, Schulz A, Helix-Nielsen C. 2015. Aquaporin-Based Biomimetic Polymeric Membranes: Approaches and Challenges. *Membranes (Basel)* **5:** 307-351.

Hachez C, Veselov D, Ye Q, Reinhardt H, Knipfer T, Fricke W, Chaumont F. 2012. Short-term control of maize cell and root water permeability through plasma membrane aquaporin isoforms. *Plant Cell Environ* **35:** 185-198.

Hall AR, Scott A, Rotem D, Mehta KK, Bayley H, Dekker C. 2010. Hybrid pore formation by directed insertion of alpha-haemolysin into solid-state nanopores. *Nat Nanotechnol* **5:** 874-877.

Hamdi M, Sanchez MA, Beene LC, Liu Q, Landfear SM, Rosen BP, Liu Z. 2009. Arsenic transport by zebrafish aquaglyceroporins. *BMC Mol Biol* **10:** 104.

Hanahan D. 1983. Studies on transformation of Escherichia coli with plasmids. *J Mol Biol* **166:** 557-580.

Heckwolf M, Pater D, Hanson DT, Kaldenhoff R. 2011. The Arabidopsis thaliana aquaporin AtPIP1;2 is a physiologically relevant CO(2) transport facilitator. *Plant J* **67:** 795-804.

Heller KB, Lin EC, Wilson TH. 1980. Substrate specificity and transport properties of the glycerol facilitator of Escherichia coli. *J Bacteriol* **144:** 274-278.

Hendriks G, Koudijs M, van Balkom BW, Oorschot V, Klumperman J, Deen PM, van der Sluijs P. 2004. Glycosylation is important for cell surface expression of the water channel aquaporin-2 but is not essential for tetramerization in the endoplasmic reticulum. *J Biol Chem* **279:** 2975-2983.

Herrera M, Garvin JL. 2007. Novel role of AQP-1 in NO-dependent vasorelaxation. *Am J Physiol Renal Physiol* **292:** F1443-1451.

Herrera M, Garvin JL. 2011. Aquaporins as gas channels. *Pflugers Arch* **462:** 623-630.

Herrera M, Hong NJ, Garvin JL. 2006. Aquaporin-1 transports NO across cell membranes. *Hypertension* **48:** 157-164.

HGVS, Den Dunnen JT, Hong W. 2016. HGVS - Human Genome Variation Society: Sequence Variant Nomenclature Website. *varnomen.hgvs.org/*.

Hibuse T, Maeda N, Nagasawa A, Funahashi T. 2006. Aquaporins and glycerol metabolism. *Biochim Biophys Acta* **1758:** 1004-1011.

Hill T, Taylor BW. 2012. Use of Aquaporins to Achieve Needed Water Purity On ISS for the EMU Space Suit System. *ICES 42nd; 15019 Jul. 2012;*.

Hiroaki Y, Tani K, Kamegawa A, Gyobu N, Nishikawa K, Suzuki H, Walz T, Sasaki S, Mitsuoka K, Kimura K, Mizoguchi A, Fujiyoshi Y. 2006. Implications of the aquaporin-4 structure on array formation and cell adhesion. *J Mol Biol* **355:** 628-639.

Hirsch AM, Lum MR, Downie JA. 2001. What makes the rhizobia-legume symbiosis so special? *Plant Physiol* **127:** 1484-1492.

Ho JD, Yeh R, Sandstrom A, Chorny I, Harries WE, Robbins RA, Miercke LJ, Stroud RM. 2009. Crystal structure of human aquaporin 4 at 1.8 A and its mechanism of conductance. *Proc Natl Acad Sci U S A* **106:** 7437-7442.

Hofmann K, Stoffel W. 1993. TMBase - A Database of Membrane Spanning Protein Segments. *Biol Chem Hoppe-Seyler***:** 166.

Holm LM, Jahn TP, Moller AL, Schjoerring JK, Ferri D, Klaerke DA, Zeuthen T. 2005. NH3 and NH4+ permeability in aquaporin-expressing Xenopus oocytes. *Pflugers Arch* **450:** 415-428.

Horie T, Kaneko T, Sugimoto G, Sasano S, Panda SK, Shibasaka M, Katsuhara M. 2011. Mechanisms of water transport mediated by PIP aquaporins and their regulation via phosphorylation events under salinity stress in barley roots. *Plant Cell Physiol* **52:** 663-675.

Horsefield R, Norden K, Fellert M, Backmark A, Tornroth-Horsefield S, Terwisscha van Scheltinga AC, Kvassman J, Kjellbom P, Johanson U, Neutze R. 2008. High-resolution x-ray structure of human aquaporin 5. *Proc Natl Acad Sci U S A* **105:** 13327-13332.

Hove RM, Bhave M. 2011. Plant aquaporins with non-aqua functions: deciphering the signature sequences. *Plant Mol Biol* **75:** 413-430.

Hu S, Wang B, Qi Y, Lin H. 2012. The Arg233Lys AQP0 mutation disturbs aquaporin0-calmodulin interaction causing polymorphic congenital cataract. *PLoS One* **7:** e37637.

Huang X, Miller W. 1991. A Time-Efficient, Linear-Space Local Similarity Algorithm. *Adv Appl Math***:** 337-357.

Hub JS, de Groot BL. 2008. Mechanism of selectivity in aquaporins and aquaglyceroporins. *Proc Natl Acad Sci U S A* **105:** 1198-1203.

Huber VJ, Tsujita M, Nakada T. 2012. Aquaporins in drug discovery and pharmacotherapy. *Mol Aspects Med* **33:** 691-703.

Ignarro LJ. 2002. Nitric oxide as a unique signaling molecule in the vascular system: a historical overview. *J Physiol Pharmacol* **53:** 503-514.

Ikai A. 1980. Thermostability and aliphatic index of globular proteins. *J Biochem* **88:** 1895-1898.

Ikeda M, Beitz E, Kozono D, Guggino WB, Agre P, Yasui M. 2002. Characterization of aquaporin-6 as a nitrate channel in mammalian cells. Requirement of pore-lining residue threonine 63. *J Biol Chem* **277:** 39873-39879.

Iliff JJ, Wang M, Liao Y, Plogg BA, Peng W, Gundersen GA, Benveniste H, Vates GE, Deane R, Goldman SA, Nagelhus EA, Nedergaard M. 2012. A paravascular pathway facilitates CSF flow through the brain parenchyma and the clearance of interstitial solutes, including amyloid beta. *Sci Transl Med* **4:** 147ra111.

Innis MA, Gelfand DH, Sninsky JJ, White TJ. 1990. PCR protocols: a guide to methods and applications. *Academic Press, New York City, New York, USA*.

Ishibashi K. 2006. Aquaporin superfamily with unusual npa boxes: S-aquaporins (superfamily, sip-like and subcellular-aquaporins). *Cell Mol Biol (Noisy-le-grand)* **52:** 20-27.

Ishibashi K, Kondo S, Hara S, Morishita Y. 2011. The evolutionary aspects of aquaporin family. *Am J Physiol Regul Integr Comp Physiol* **300:** R566-576.

Ishibashi K, Kuwahara M, Gu Y, Tanaka Y, Marumo F, Sasaki S. 1998. Cloning and functional expression of a new aquaporin (AQP9) abundantly expressed in the peripheral leukocytes permeable to water and urea, but not to glycerol. *Biochem Biophys Res Commun* **244:** 268-274.

Ishikawa F, Suga S, Uemura T, Sato MH, Maeshima M. 2005. Novel type aquaporin SIPs are mainly localized to the ER membrane and show cell-specific expression in Arabidopsis thaliana. *FEBS Lett* **579:** 5814-5820.

Israelsson M, Siegel RS, Young J, Hashimoto M, Iba K, Schroeder JI. 2006. Guard cell ABA and CO2 signaling network updates and Ca2+ sensor priming hypothesis. *Curr Opin Plant Biol* **9:** 654-663.

Itel F, Al-Samir S, Oberg F, Chami M, Kumar M, Supuran CT, Deen PM, Meier W, Hedfalk K, Gros G, Endeward V. 2012. CO2 permeability of cell membranes is regulated by membrane cholesterol and protein gas channels. *FASEB J* **26:** 5182-5191.

Jang HY, Rhee J, Carlson JE, Ahn SJ. 2014. The Camelina aquaporin CsPIP2;1 is regulated by phosphorylation at Ser273, but not at Ser277, of the C-terminus and is involved in salt- and drought-stress responses. *J Plant Physiol* **171:** 1401-1412.

Jang JY, Rhee JY, Kim DG, Chung GC, Lee JH, Kang H. 2007. Ectopic expression of a foreign aquaporin disrupts the natural expression patterns of endogenous aquaporin genes and alters plant responses to different stress conditions. *Plant Cell Physiol* **48:** 1331-1339.

Jarius S, Paul F, Franciotta D, Waters P, Zipp F, Hohlfeld R, Vincent A, Wildemann B. 2008. Mechanisms of disease: aquaporin-4 antibodies in neuromyelitis optica. *Nat Clin Pract Neurol* **4:** 202-214.

Jiang X, Ookubo Y, Fujii I, Nakano H, Yamane T. 2002. Expression of Fab fragment of catalytic antibody 6D9 in an Escherichia coli in vitro coupled transcription/translation system. *FEBS Lett* **514:** 290-294.

Johanson U, Gustavsson S. 2002. A new subfamily of major intrinsic proteins in plants. *Mol Biol Evol* **19:** 456-461.

Johanson U, Karlsson M, Johansson I, Gustavsson S, Sjovall S, Fraysse L, Weig AR, Kjellbom P. 2001. The complete set of genes encoding major intrinsic proteins in Arabidopsis provides a framework for a new nomenclature for major intrinsic proteins in plants. *Plant Physiol* **126:** 1358-1369.

Johansson I, Karlsson M, Shukla VK, Chrispeels MJ, Larsson C, Kjellbom P. 1998. Water transport activity of the plasma membrane aquaporin PM28A is regulated by phosphorylation. *Plant Cell* **10:** 451-459.

Jozefkowicz C, Rosi P, Sigaut L, Soto G, Pietrasanta LI, Amodeo G, Alleva K. 2013. Loop A is critical for the functional interaction of two Beta vulgaris PIP aquaporins. *PLoS One* **8:** e57993.

Jugdaohsingh R, Tucker KL, Qiao N, Cupples LA, Kiel DP, Powell JJ. 2004. Dietary silicon intake is positively associated with bone mineral density in men and premenopausal women of the Framingham Offspring cohort. *J Bone Miner Res* **19:** 297-307.

Junge F, Haberstock S, Roos C, Stefer S, Proverbio D, Dotsch V, Bernhard F. 2011. Advances in cell-free protein synthesis for the functional and structural analysis of membrane proteins. *N Biotechnol* **28:** 262-271.

Junge F, Schneider B, Reckel S, Schwarz D, Dotsch V, Bernhard F. 2008. Large-scale production of functional membrane proteins. *Cell Mol Life Sci* **65:** 1729-1755.

Kadohira I, Abe Y, Nuriya M, Sano K, Tsuji S, Arimitsu T, Yoshimura Y, Yasui M. 2008. Phosphorylation in the C-terminal domain of Aquaporin-4 is required for Golgi transition in primary cultured astrocytes. *Biochem Biophys Res Commun* **377:** 463-468.

Kai L, Bernhard F, Kaldenhoff R. 2014. Characterization of aquaporins produced from an *E. coli* cell-free expression systems. *Poster presentation, CRC 807 - International Symposium on Membrane Transport and Communication, Goethe-University Frankfurt, Frankfurt am Main, Germany*.

Kai L, Kaldenhoff R. 2014. A refined model of water and CO(2) membrane diffusion: effects and contribution of sterols and proteins. *Sci Rep* **4:** 6665.

Kai L, Kaldenhoff R, Lian J, Zhu X, Dotsch V, Bernhard F, Cen P, Xu Z. 2010. Preparative scale production of functional mouse aquaporin 4 using different cell-free expression modes. *PLoS One* **5:** e12972.

Kai L, Roos C, Haberstock S, Proverbio D, Ma Y, Junge F, Karbyshev M, Dotsch V, Bernhard F. 2012. Systems for the cell-free synthesis of proteins. *Methods Mol Biol* **800:** 201-225.

Kaldenhoff R, Fischer M. 2006. Functional aquaporin diversity in plants. *Biochim Biophys Acta* **1758:** 1134-1141.

Kamaluddin M, Zwiazek JJ. 2004. Effects of root medium pH on water transport in paper birch (Betula papyrifera) seedlings in relation to root temperature and abscisic acid treatments. *Tree Physiol* **24:** 1173-1180.

Kamiya T, Tanaka M, Mitani N, Ma JF, Maeshima M, Fujiwara T. 2009. NIP1;1, an aquaporin homolog, determines the arsenite sensitivity of Arabidopsis thaliana. *J Biol Chem* **284:** 2114-2120.

Karp G. 2009. Cell and Molecular Biology: Concepts and Experiments, Chapter 4 - The Structure and Function of the Plasma Membrane. *John Wiley & Sons, Hoboken, New Jersey, USA*.

Kato J, Hayashi MK, Aizu S, Yukutake Y, Takeda J, Yasui M. 2013. A general anaesthetic propofol inhibits aquaporin-4 in the presence of Zn(2)(+). *Biochem J* **454:** 275-282.

Katsuhara M, Sasano S, Horie T, Matsumoto T, Rhee J, Shibasaka M. 2014. Functional and molecular characteristics of rice and barley NIP aquaporins transporting water, hydrogen peroxide and arsenite. *Plant Biotechnol***:** 213-219.

Kelley LA, Mezulis S, Yates CM, Wass MN, Sternberg MJ. 2015. The Phyre2 web portal for protein modeling, prediction and analysis. *Nat Protoc* **10:** 845-858.

Kelly G, Sade N, Attia Z, Secchi F, Zwieniecki M, Holbrook NM, Levi A, Alchanatis V, Moshelion M, Granot D. 2014. Relationship between hexokinase and the aquaporin PIP1 in the regulation of photosynthesis and plant growth. *PLoS One* **9:** e87888.

Kim DM, Choi CY. 1996. A semicontinuous prokaryotic coupled transcription/translation system using a dialysis membrane. *Biotechnol Prog* **12:** 645-649.

Kim DM, Swartz JR. 1999. Prolonging cell-free protein synthesis with a novel ATP regeneration system. *Biotechnol Bioeng* **66:** 180-188.

Kim RG, Choi CY. 2001. Expression-independent consumption of substrates in cell-free expression system from Escherichia coli. *J Biotechnol* **84:** 27-32.

Kita-Tokarczyk K, Meier W. 2008. Biomimetic Block Copolymer Membranes. *CHIMIA* **62:** 820-825.

Klammt C, Schwarz D, Eifler N, Engel A, Piehler J, Haase W, Hahn S, Dotsch V, Bernhard F. 2007. Cell-free production of G protein-coupled receptors for functional and structural studies. *J Struct Biol* **158:** 482-493.

Kong H, Sha LL, Fan Y, Xiao M, Ding JH, Wu J, Hu G. 2009. Requirement of AQP4 for antidepressive efficiency of fluoxetine: implication in adult hippocampal neurogenesis. *Neuropsychopharmacology* **34:** 1263-1276.

Krogh A, Larsson B, von Heijne G, Sonnhammer EL. 2001. Predicting transmembrane protein topology with a hidden Markov model: application to complete genomes. *J Mol Biol* **305:** 567-580.

Kuehnelt D, Goessler W, Francesconi KA. 2003. Nitrogen purity influences the occurrence of As+ ions in high-performance liquid chromatography/electrospray ionization mass spectrometric analysis of four common arsenosugars. *Rapid Commun Mass Spectrom* **17:** 654-659.

Kuhlbrandt W. 1988. Three-dimensional crystallization of membrane proteins. *Q Rev Biophys* **21:** 429-477.

Kukulski W, Schenk AD, Johanson U, Braun T, de Groot BL, Fotiadis D, Kjellbom P, Engel A. 2005. The 5A structure of heterologously expressed plant aquaporin SoPIP2;1. *J Mol Biol* **350:** 611-616.

Kumar M, Grzelakowski M, Zilles J, Clark M, Meier W. 2007. Highly permeable polymeric membranes based on the incorporation of the functional water channel protein Aquaporin Z. *Proc Natl Acad Sci U S A* **104:** 20719-20724.

Kumari SS, Gandhi J, Mustehsan MH, Eren S, Varadaraj K. 2013. Functional characterization of an AQP0 missense mutation, R33C, that causes dominant congenital lens cataract, reveals impaired cell-to-cell adhesion. *Exp Eye Res* **116:** 371-385.

Kuwahara M, Asai T, Terada Y, Sasaki S. 2005. The C-terminal tail of aquaporin-2 determines apical trafficking. *Kidney Int* **68:** 1999-2009.

Kuwahara M, Iwai K, Ooeda T, Igarashi T, Ogawa E, Katsushima Y, Shinbo I, Uchida S, Terada Y, Arthus MF, Lonergan M, Fujiwara TM, Bichet DG, Marumo F, Sasaki S. 2001. Three families with autosomal dominant nephrogenic diabetes insipidus caused by aquaporin-2 mutations in the C-terminus. *Am J Hum Genet* **69:** 738-748.

Kyte J, Doolittle RF. 1982. A simple method for displaying the hydropathic character of a protein. *J Mol Biol* **157:** 105-132.

Laemmli UK. 1970. Cleavage of structural proteins during the assembly of the head of bacteriophage T4. *Nature* **227:** 680-685.

Laforenza U. 2012. Water channel proteins in the gastrointestinal tract. *Mol Aspects Med* **33:** 642-650.

Lagree V, Froger A, Deschamps S, Pellerin I, Delamarche C, Bonnec G, Gouranton J, Thomas D, Hubert JF. 1998. Oligomerization state of water channels and glycerol facilitators. Involvement of loop E. *J Biol Chem* **273:** 33949-33953.

Laize V, Gobin R, Rousselet G, Badier C, Hohmann S, Ripoche P, Tacnet F. 1999. Molecular and functional study of AQY1 from Saccharomyces cerevisiae: role of the C-terminal domain. *Biochem Biophys Res Commun* **257:** 139-144.

Lau KK, Yang Y, Cook GA, Wyatt RJ, Nishimura H. 2009. Control of aquaporin 2 expression in collecting ducts of quail kidneys. *Gen Comp Endocrinol* **160:** 288-294.

Le Caherec F, Deschamps S, Delamarche C, Pellerin I, Bonnec G, Guillam MT, Thomas D, Gouranton J, Hubert JF. 1996. Molecular cloning and characterization of an insect aquaporin functional comparison with aquaporin 1. *Eur J Biochem* **241:** 707-715.

Li GW, Peng YH, Yu X, Zhang MH, Cai WM, Sun WN, Su WA. 2008. Transport functions and expression analysis of vacuolar membrane aquaporins in response to various stresses in rice. *J Plant Physiol* **165:** 1879-1888.

Li W, Cowley A, Uludag M, Gur T, McWilliam H, Squizzato S, Park YM, Buso N, Lopez R. 2015. The EMBL-EBI bioinformatics web and programmatic tools framework. *Nucleic Acids Res* **43:** W580-584.

Li Y, Wang E, Wang Y. 1999. A modified procedure for fast purification of T7 RNA polymerase. *Protein Expr Purif* **16:** 355-358.

Li Z, Gao L, Liu Q, Cao C, Sun XL, Ding JH, Hu G. 2006. Aquaporin-4 knockout regulated cocaine-induced behavior and neurochemical changes in mice. *Neurosci Lett* **403:** 294-298.

Liu C, Fukumoto T, Matsumoto T, Gena P, Frascaria D, Kaneko T, Katsuhara M, Zhong S, Sun X, Zhu Y, Iwasaki I, Ding X, Calamita G, Kitagawa Y. 2013. Aquaporin OsPIP1;1 promotes rice salt resistance and seed germination. *Plant Physiol Biochem* **63:** 151-158.

Liu LH, Ludewig U, Gassert B, Frommer WB, von Wiren N. 2003. Urea transport by nitrogen-regulated tonoplast intrinsic proteins in Arabidopsis. *Plant Physiol* **133:** 1220-1228.

Liu P, Yin L, Deng X, Wang S, Tanaka K, Zhang S. 2014. Aquaporin-mediated increase in root hydraulic conductance is involved in silicon-induced improved root water uptake under osmotic stress in Sorghum bicolor L. *J Exp Bot* **65:** 4747-4756.

Liu W, Eilers M, Patel AB, Smith SO. 2004a. Helix packing moments reveal diversity and conservation in membrane protein structure. *J Mol Biol* **337:** 713-729.

Liu Z, Carbrey JM, Agre P, Rosen BP. 2004b. Arsenic trioxide uptake by human and rat aquaglyceroporins. *Biochem Biophys Res Commun* **316:** 1178-1185.

Liu Z, Shen J, Carbrey JM, Mukhopadhyay R, Agre P, Rosen BP. 2002. Arsenite transport by mammalian aquaglyceroporins AQP7 and AQP9. *Proc Natl Acad Sci U S A* **99:** 6053-6058.

Long SB, Campbell EB, Mackinnon R. 2005. Crystal structure of a mammalian voltage-dependent Shaker family K+ channel. *Science* **309:** 897-903.

Lopez D, Bronner G, Brunel N, Auguin D, Bourgerie S, Brignolas F, Carpin S, Tournaire-Roux C, Maurel C, Fumanal B, Martin F, Sakr S, Label P, Julien JL, Gousset-Dupont A, Venisse JS. 2012. Insights into Populus XIP aquaporins: evolutionary expansion, protein functionality, and environmental regulation. *J Exp Bot* **63:** 2217-2230.

Loque D, Ludewig U, Yuan L, von Wiren N. 2005. Tonoplast intrinsic proteins AtTIP2;1 and AtTIP2;3 facilitate NH3 transport into the vacuole. *Plant Physiol* **137:** 671-680.

Lorenz A, Kaldenhoff R, Hertel R. 2003. A major integral protein of the plant plasma membrane binds flavin. *Protoplasma* **221:** 19-30.

Lovisolo C, Schubert A. 2006. Mercury hinders recovery of shoot hydraulic conductivity during grapevine rehydration: evidence from a whole-plant approach. *New Phytol* **172:** 469-478.

Luis P, Van Gerven T, Van der Bruggen B. 2012. Recent developments in membrane-based technologies for CO_2 capture. *Prog Energy Combust Sci* **38:** 419-448.

Lyukmanova EN, Shenkarev ZO, Khabibullina NF, Kopeina GS, Shulepko MA, Paramonov AS, Mineev KS, Tikhonov RV, Shingarova LN, Petrovskaya LE, Dolgikh DA, Arseniev AS, Kirpichnikov MP. 2012. Lipid-protein nanodiscs for cell-free production of integral membrane proteins in a soluble and folded state: comparison with detergent micelles, bicelles and liposomes. *Biochim Biophys Acta* **1818:** 349-358.

Ma JF, Tamai K, Yamaji N, Mitani N, Konishi S, Katsuhara M, Ishiguro M, Murata Y, Yano M. 2006. A silicon transporter in rice. *Nature* **440:** 688-691.

Ma JF, Yamaji N, Mitani N, Xu XY, Su YH, McGrath SP, Zhao FJ. 2008. Transporters of arsenite in rice and their role in arsenic accumulation in rice grain. *Proc Natl Acad Sci U S A* **105:** 9931-9935.

Ma T, Gao H, Fang X, Yang H. 2012. Water channel proteins in the peripheral nervous system in health and disease. *Mol Aspects Med* **33:** 605-611.

MacRobbie EA. 2006. Osmotic effects on vacuolar ion release in guard cells. *Proc Natl Acad Sci U S A* **103:** 1135-1140.

Maggio A, Joly RJ. 1995. Effects of Mercuric Chloride on the Hydraulic Conductivity of Tomato Root Systems (Evidence for a Channel-Mediated Water Pathway). *Plant Physiol* **109:** 331-335.

Mahdieh M, Mostajeran A. 2009. Abscisic acid regulates root hydraulic conductance via aquaporin expression modulation in Nicotiana tabacum. *J Plant Physiol* **166:** 1993-2003.

Mahdieh M, Mostajeran A, Horie T, Katsuhara M. 2008. Drought stress alters water relations and expression of PIP-type aquaporin genes in Nicotiana tabacum plants. *Plant Cell Physiol* **49:** 801-813.

Manley GT, Fujimura M, Ma T, Noshita N, Filiz F, Bollen AW, Chan P, Verkman AS. 2000. Aquaporin-4 deletion in mice reduces brain edema after acute water intoxication and ischemic stroke. *Nat Med* **6:** 159-163.

Marcoux J, Wang SC, Politis A, Reading E, Ma J, Biggin PC, Zhou M, Tao H, Zhang Q, Chang G, Morgner N, Robinson CV. 2013. Mass spectrometry reveals synergistic effects of nucleotides, lipids, and drugs binding to a multidrug resistance efflux pump. *Proc Natl Acad Sci U S A* **110:** 9704-9709.

Martinez A, Traverso JA, Valot B, Ferro M, Espagne C, Ephritikhine G, Zivy M, Giglione C, Meinnel T. 2008. Extent of N-terminal modifications in cytosolic proteins from eukaryotes. *Proteomics* **8:** 2809-2831.

Martinez-Ballesta Mdel C, Carvajal M. 2014. New challenges in plant aquaporin biotechnology. *Plant Sci* **217-218:** 71-77.

Masalkar P, Wallace IS, Hwang JH, Roberts DM. 2010. Interaction of cytosolic glutamine synthetase of soybean root nodules with the C-terminal domain of the symbiosome membrane nodulin 26 aquaglyceroporin. *J Biol Chem* **285:** 23880-23888.

Matsuzaki T, Yaguchi T, Shimizu K, Kita A, Ishibashi K, Takata K. 2016. The distribution and function of aquaporins in the kidney: resolved and unresolved questions. *Anat Sci Int*.

Matthaei H, Nirenberg MW. 1961. The dependence of cell-free protein synthesis in E. coli upon RNA prepared from ribosomes. *Biochem Biophys Res Commun* **4:** 404-408.

Maurel C, Boursiac Y, Luu DT, Santoni V, Shahzad Z, Verdoucq L. 2015. Aquaporins in Plants. *Physiol Rev* **95:** 1321-1358.

Maurel C, Reizer J, Schroeder JI, Chrispeels MJ. 1993. The vacuolar membrane protein gamma-TIP creates water specific channels in Xenopus oocytes. *EMBO J* **12:** 2241-2247.

Maurel C, Reizer J, Schroeder JI, Chrispeels MJ, Saier MH, Jr. 1994. Functional characterization of the Escherichia coli glycerol facilitator, GlpF, in Xenopus oocytes. *J Biol Chem* **269:** 11869-11872.

Maurel C, Tacnet F, Guclu J, Guern J, Ripoche P. 1997. Purified vesicles of tobacco cell vacuolar and plasma membranes exhibit dramatically different water permeability and water channel activity. *Proc Natl Acad Sci U S A* **94:** 7103-7108.

McWilliam H, Li W, Uludag M, Squizzato S, Park YM, Buso N, Cowley AP, Lopez R. 2013. Analysis Tool Web Services from the EMBL-EBI. *Nucleic Acids Res* **41:** W597-600.

Meinild AK, Klaerke DA, Zeuthen T. 1998. Bidirectional water fluxes and specificity for small hydrophilic molecules in aquaporins 0-5. *J Biol Chem* **273:** 32446-32451.

Meng G, Fronzes R, Chandran V, Remaut H, Waksman G. 2009. Protein oligomerization in the bacterial outer membrane (Review). *Mol Membr Biol* **26:** 136-145.

Meng YL, Liu Z, Rosen BP. 2004. As(III) and Sb(III) uptake by GlpF and efflux by ArsB in Escherichia coli. *J Biol Chem* **279:** 18334-18341.

Mitani N, Yamaji N, Ma JF. 2008. Characterization of substrate specificity of a rice silicon transporter, Lsi1. *Pflugers Arch* **456:** 679-686.

Mizutani M, Watanabe S, Nakagawa T, Maeshima M. 2006. Aquaporin NIP2;1 is mainly localized to the ER membrane and shows root-specific accumulation in Arabidopsis thaliana. *Plant Cell Physiol* **47:** 1420-1426.

Monigatti F, Gasteiger E, Bairoch A, Jung E. 2002. The Sulfinator: predicting tyrosine sulfation sites in protein sequences. *Bioinformatics* **18:** 769-770.

Moshelion M, Becker D, Biela A, Uehlein N, Hedrich R, Otto B, Levi H, Moran N, Kaldenhoff R. 2002. Plasma membrane aquaporins in the motor cells of Samanea saman: diurnal and circadian regulation. *Plant Cell* **14:** 727-739.

mpstruc, White SH. 2016. mpstruc - Database for Membrane Protein of Known 3D Structure Website, University of California, Irvine, California, USA. *http://blanco.biomol.uci.edu/mpstruc/*.

Mubarakshina Borisova MM, Kozuleva MA, Rudenko NN, Naydov IA, Klenina IB, Ivanov BN. 2012. Photosynthetic electron flow to oxygen and diffusion of hydrogen peroxide through the chloroplast envelope via aquaporins. *Biochim Biophys Acta* **1817:** 1314-1321.

Mulders SM, Preston GM, Deen PM, Guggino WB, van Os CH, Agre P. 1995. Water channel properties of major intrinsic protein of lens. *J Biol Chem* **270:** 9010-9016.

Murad F. 2004. Discovery of some of the biological effects of nitric oxide and its role in cell signaling. *Biosci Rep* **24:** 452-474.

Murata K, Mitsuoka K, Hirai T, Walz T, Agre P, Heymann JB, Engel A, Fujiyoshi Y. 2000. Structural determinants of water permeation through aquaporin-1. *Nature* **407:** 599-605.

Murozuka E, Hanisch S, Pomorski TG, Jahn TP, Schjoerring JK. 2013. Bimolecular fluorescence complementation and interaction of various Arabidopsis major intrinsic proteins expressed in yeast. *Physiol Plant* **148:** 422-431.

Musa-Aziz R, Chen LM, Pelletier MF, Boron WF. 2009. Relative CO2/NH3 selectivities of AQP1, AQP4, AQP5, AmtB, and RhAG. *Proc Natl Acad Sci U S A* **106:** 5406-5411.

Nakahama K, Fujioka A, Nagano M, Satoh S, Furukawa K, Sasaki H, Shigeyoshi Y. 2002. A role of the C-terminus of aquaporin 4 in its membrane expression in cultured astrocytes. *Genes Cells* **7:** 731-741.

Nakhoul NL, Davis BA, Romero MF, Boron WF. 1998. Effect of expressing the water channel aquaporin-1 on the CO2 permeability of Xenopus oocytes. *Am J Physiol* **274:** C543-548.

Neely JD, Christensen BM, Nielsen S, Agre P. 1999. Heterotetrameric composition of aquaporin-4 water channels. *Biochemistry* **38:** 11156-11163.

Nesterchuk MV, Sergiev PV, Dontsova OA. 2011. Post-translational Modifications of Ribosomal Proteins in Escherichia coli. *Acta Naturae* **3:** 22-33.

Newby ZE, O'Connell J, 3rd, Robles-Colmenares Y, Khademi S, Miercke LJ, Stroud RM. 2008. Crystal structure of the aquaglyceroporin PfAQP from the malarial parasite Plasmodium falciparum. *Nat Struct Mol Biol* **15:** 619-625.

Nishi H, Hashimoto K, Madej T, Panchenko AR. 2013. Evolutionary, physicochemical, and functional mechanisms of protein homooligomerization. *Prog Mol Biol Transl Sci* **117:** 3-24.

Nogales E, Wolf SG, Downing KH. 1997. Visualizing the secondary structure of tubulin: three-dimensional map at 4 A. *J Struct Biol* **118:** 119-127.

Noronha H, Agasse A, Martins AP, Berny MC, Gomes D, Zarrouk O, Thiebaud P, Delrot S, Soveral G, Chaumont F, Geros H. 2014. The grape aquaporin VvSIP1 transports water across the ER membrane. *J Exp Bot* **65:** 981-993.

Nozaki K, Ishii D, Ishibashi K. 2008. Intracellular aquaporins: clues for intracellular water transport? *Pflugers Arch* **456:** 701-707.

Oberai A, Ihm Y, Kim S, Bowie JU. 2006. A limited universe of membrane protein families and folds. *Protein Sci* **15:** 1723-1734.

Ohashi Y, Tsuzaka K, Takeuchi T, Sasaki Y, Tsubota K. 2008. Altered distribution of aquaporin 5 and its C-terminal binding protein in the lacrimal glands of a mouse model for Sjogren's syndrome. *Curr Eye Res* **33:** 621-629.

Omasits U, Ahrens C H, Muller S, Wollscheid B. 2014. Protter: interactive protein feature visualization and integration with experimental proteomic data. *Bioinformatics* **30:** 884-886.

Opella SJ. 2013. Structure determination of membrane proteins in their native phospholipid bilayer environment by rotationally aligned solid-state NMR spectroscopy. *Acc Chem Res* **46:** 2145-2153.

OpenWetWare, Brock J, Kosuri S, Cumbers J. 2016. OpenWetWare - Nomenclature & Abbreviations of *E. coli* genotypes Website, BioBricks Foundation, San Francisco, California, USA. *openwetware.org/wiki/E._coli_genotypes#Nomenclature_.26_Abbreviations*.

Otto B, Kaldenhoff R. 2000. Cell-specific expression of the mercury-insensitive plasma-membrane aquaporin NtAQP1 from Nicotiana tabacum. *Planta* **211:** 167-172.

Otto B, Uehlein N, Sdorra S, Fischer M, Ayaz M, Belastegui-Macadam X, Heckwolf M, Lachnit M, Pede N, Priem N, Reinhard A, Siegfart S, Urban M, Kaldenhoff R. 2010. Aquaporin tetramer composition modifies the function of tobacco aquaporins. *J Biol Chem* **285:** 31253-31260.

Otto R, Sonnenberg AS, Veldkamp H, Konings WN. 1980. Generation of an electrochemical proton gradient in Streptococcus cremoris by lactate efflux. *Proc Natl Acad Sci U S A* **77:** 5502-5506.

Overington JP, Al-Lazikani B, Hopkins AL. 2006. How many drug targets are there? *Nat Rev Drug Discov* **5:** 993-996.

Pacher P, Beckman JS, Liaudet L. 2007. Nitric oxide and peroxynitrite in health and disease. *Physiol Rev* **87:** 315-424.

Palmer RM, Ferrige AG, Moncada S. 1987. Nitric oxide release accounts for the biological activity of endothelium-derived relaxing factor. *Nature* **327:** 524-526.

Pavlovic-Djuranovic S, Schultz JE, Beitz E. 2003. A single aquaporin gene encodes a water/glycerol/urea facilitator in Toxoplasma gondii with similarity to plant tonoplast intrinsic proteins. *FEBS Lett* **555:** 500-504.

PDBTM. PDBTM - Protein Data Bank of Transmembrane Proteins growth statistics Website, The Institute of Enzymology, Hungarian Academy of Sciences, Budapest, Hungary. *pdbtm.enzim.hu/?_=/statistics/growth*.

Pedersen BP, Buch-Pedersen MJ, Morth JP, Palmgren MG, Nissen P. 2007. Crystal structure of the plasma membrane proton pump. *Nature* **450:** 1111-1114.

Perez Di Giorgio J, Soto G, Alleva K, Jozefkowicz C, Amodeo G, Muschietti JP, Ayub ND. 2014. Prediction of aquaporin function by integrating evolutionary and functional analyses. *J Membr Biol* **247:** 107-125.

Perrine CL, Ganguli A, Wu P, Bertozzi CR, Fritz TA, Raman J, Tabak LA, Gerken TA. 2009. Glycopeptide-preferring polypeptide GalNAc transferase 10 (ppGalNAc T10), involved in mucin-type O-glycosylation, has a unique GalNAc-O-Ser/Thr-binding site in its catalytic domain not found in ppGalNAc T1 or T2. *J Biol Chem* **284:** 20387-20397.

Perrone I, Gambino G, Chitarra W, Vitali M, Pagliarani C, Riccomagno N, Balestrini R, Kaldenhoff R, Uehlein N, Gribaudo I, Schubert A, Lovisolo C. 2012. The grapevine root-specific aquaporin VvPIP2;4N controls root hydraulic conductance and leaf gas exchange under well-watered conditions but not under water stress. *Plant Physiol* **160:** 965-977.

Perry M, Madsen SU, Jorgensen T, Braekevelt S, Lauritzen K, Helix-Nielsen C. 2015. Challenges in Commercializing Biomimetic Membranes. *Membranes (Basel)* **5:** 685-701.

Pienkowska JR, Kosicka E, Wojtkowska M, Kmita H, Lesicki A. 2014. Molecular identification of first putative aquaporins in snails. *J Membr Biol* **247:** 239-252.

Pierce Biotechnology Inc. R, Illinois, USA. 2004. Acetone precipitation of proteins (Technical Resource TR0049.0).

Plasencia I, Survery S, Ibragimova S, Hansen JS, Kjellbom P, Helix-Nielsen C, Johanson U, Mouritsen OG. 2011. Structure and stability of the spinach aquaporin SoPIP2;1 in detergent micelles and lipid membranes. *PLoS One* **6:** e14674.

Pogozheva ID, Mosberg HI, Lomize AL. 2014. Life at the border: adaptation of proteins to anisotropic membrane environment. *Protein Sci* **23:** 1165-1196.

Polevoda B, Sherman F. 2003. N-terminal acetyltransferases and sequence requirements for N-terminal acetylation of eukaryotic proteins. *J Mol Biol* **325:** 595-622.

Porcel R, Gomez M, Kaldenhoff R, Ruiz-Lozano JM. 2005. Impairment of NtAQP1 gene expression in tobacco plants does not affect root colonisation pattern by arbuscular mycorrhizal fungi but decreases their symbiotic efficiency under drought. *Mycorrhiza* **15:** 417-423.

Prado K, Boursiac Y, Tournaire-Roux C, Monneuse JM, Postaire O, Da Ines O, Schaffner AR, Hem S, Santoni V, Maurel C. 2013. Regulation of Arabidopsis leaf hydraulics involves light-dependent phosphorylation of aquaporins in veins. *Plant Cell* **25:** 1029-1039.

Prak S, Hem S, Boudet J, Viennois G, Sommerer N, Rossignol M, Maurel C, Santoni V. 2008. Multiple phosphorylations in the C-terminal tail of plant plasma membrane aquaporins: role in subcellular trafficking of AtPIP2;1 in response to salt stress. *Mol Cell Proteomics* **7:** 1019-1030.

Preston GM, Carroll TP, Guggino WB, Agre P. 1992. Appearance of water channels in Xenopus oocytes expressing red cell CHIP28 protein. *Science* **256:** 385-387.

Prive GG. 2007. Detergents for the stabilization and crystallization of membrane proteins. *Methods* **41:** 388-397.

Quast RB, Claussnitzer I, Merk H, Kubick S, Gerrits M. 2014. Synthesis and site-directed fluorescence labeling of azido proteins using eukaryotic cell-free orthogonal translation systems. *Anal Biochem* **451:** 4-9.

Quigley F, Rosenberg JM, Shachar-Hill Y, Bohnert HJ. 2002. From genome to function: the Arabidopsis aquaporins. *Genome Biol* **3:** RESEARCH0001.

Raaijmakers MJ, Hempenius MA, Schon PM, Vancso GJ, Nijmeijer A, Wessling M, Benes NE. 2014. Sieving of hot gases by hyper-cross-linked nanoscale-hybrid membranes. *J Am Chem Soc* **136:** 330-335.

Radoicic J, Lu GJ, Opella SJ. 2014. NMR structures of membrane proteins in phospholipid bilayers. *Q Rev Biophys* **47:** 249-283.

Rai T, Sasaki S, Uchida S. 2006. Polarized trafficking of the aquaporin-3 water channel is mediated by an NH2-terminal sorting signal. *Am J Physiol Cell Physiol* **290:** C298-304.

Reffitt DM, Ogston N, Jugdaohsingh R, Cheung HF, Evans BA, Thompson RP, Powell JJ, Hampson GN. 2003. Orthosilicic acid stimulates collagen type 1 synthesis and osteoblastic differentiation in human osteoblast-like cells in vitro. *Bone* **32:** 127-135.

Rice P, Longden I, Bleasby A. 2000. EMBOSS: the European Molecular Biology Open Software Suite. *Trends Genet* **16:** 276-277.

Rigaud JL, Levy D, Mosser G, Lambert O. 1998. Detergent removal by non-polar polystyrene beads. *Eur Biophys J***:** 305-319.

Ritchie TK, Grinkova YV, Bayburt TH, Denisov IG, Zolnerciks JK, Atkins WM, Sligar SG. 2009. Methods in Enzymology. *Academic Press. New York City, New York, USA* **464: Liposomes, Part F**.

Rodriguez A, Catalan V, Gomez-Ambrosi J, Fruhbeck G. 2006. Role of aquaporin-7 in the pathophysiological control of fat accumulation in mice. *FEBS Lett* **580:** 4771-4776.

Rollauer SE, Tarry MJ, Graham JE, Jaaskelainen M, Jager F, Johnson S, Krehenbrink M, Liu SM, Lukey MJ, Marcoux J, McDowell MA, Rodriguez F, Roversi P, Stansfeld PJ, Robinson CV, Sansom MS, Palmer T, Hogbom M, Berks BC, Lea SM. 2012. Structure of the TatC core of the twin-arginine protein transport system. *Nature* **492:** 210-214.

Roos C, Kai L, Proverbio D, Ghoshdastider U, Filipek S, Dotsch V, Bernhard F. 2013. Co-translational association of cell-free expressed membrane proteins with supplied lipid bilayers. *Mol Membr Biol* **30:** 75-89.

Rosenblum G, Cooperman BS. 2014. Engine out of the chassis: cell-free protein synthesis and its uses. *FEBS Lett* **588:** 261-268.

Ryabova LA, Desplancq D, Spirin AS, Pluckthun A. 1997. Functional antibody production using cell-free translation: effects of protein disulfide isomerase and chaperones. *Nat Biotechnol* **15:** 79-84.

Saadoun S, Papadopoulos MC, Hara-Chikuma M, Verkman AS. 2005. Impairment of angiogenesis and cell migration by targeted aquaporin-1 gene disruption. *Nature* **434:** 786-792.

Sachse R, Wüstenhagen D, Šamalíková M, Gerrits M, Bier FF, Kubick S. 2013. Synthesis of membrane proteins in eukaryotic cell-free systems. *Eng Life Sci* **13:** 39-48.

Sade N, Galle A, Flexas J, Lerner S, Peleg G, Yaaran A, Moshelion M. 2014. Differential tissue-specific expression of NtAQP1 in Arabidopsis thaliana reveals a role for this protein in stomatal and mesophyll conductance of CO(2) under standard and salt-stress conditions. *Planta* **239:** 357-366.

Sade N, Gebretsadik M, Seligmann R, Schwartz A, Wallach R, Moshelion M. 2010. The role of tobacco Aquaporin1 in improving water use efficiency, hydraulic conductivity, and yield production under salt stress. *Plant Physiol* **152:** 245-254.

Sade N, Vinocur BJ, Diber A, Shatil A, Ronen G, Nissan H, Wallach R, Karchi H, Moshelion M. 2009. Improving plant stress tolerance and yield production: is the tonoplast aquaporin SlTIP2;2 a key to isohydric to anisohydric conversion? *New Phytol* **181:** 651-661.

Saito C, Ueda T, Abe H, Wada Y, Kuroiwa T, Hisada A, Furuya M, Nakano A. 2002. A complex and mobile structure forms a distinct subregion within the continuous vacuolar membrane in young cotyledons of Arabidopsis. *Plant J* **29:** 245-255.

Sakr S, Alves G, Morillon R, Maurel K, Decourteix M, Guilliot A, Fleurat-Lessard P, Julien JL, Chrispeels MJ. 2003. Plasma membrane aquaporins are involved in winter embolism recovery in walnut tree. *Plant Physiol* **133:** 630-641.

Sakurai J, Ahamed A, Murai M, Maeshima M, Uemura M. 2008. Tissue and cell-specific localization of rice aquaporins and their water transport activities. *Plant Cell Physiol* **49:** 30-39.

Sambrook J, Russell DW. 2001. Molecular Cloning: A Laboratory Manual. *Cold Spring Harbor Laboratory Press, Cold Spring Harbor, New York, USA*.

Sanders OI, Rensing C, Kuroda M, Mitra B, Rosen BP. 1997. Antimonite is accumulated by the glycerol facilitator GlpF in Escherichia coli. *J Bacteriol* **179:** 3365-3367.

Santoni V, Verdoucq L, Sommerer N, Vinh J, Pflieger D, Maurel C. 2006. Methylation of aquaporins in plant plasma membrane. *Biochem J* **400:** 189-197.

Saparov SM, Kozono D, Rothe U, Agre P, Pohl P. 2001. Water and ion permeation of aquaporin-1 in planar lipid bilayers. Major differences in structural determinants and stoichiometry. *J Biol Chem* **276:** 31515-31520.

Sarda X, Tousch D, Ferrare K, Legrand E, Dupuis JM, Casse-Delbart F, Lamaze T. 1997. Two TIP-like genes encoding aquaporins are expressed in sunflower guard cells. *Plant J* **12:** 1103-1111.

Sawasaki T, Ogasawara T, Morishita R, Endo Y. 2002. A cell-free protein synthesis system for high-throughput proteomics. *Proc Natl Acad Sci U S A* **99:** 14652-14657.

Schaffner AR. 1998. Aquaporin function, structure, and expression: are there more surprises to surface in water relations? *Planta* **204:** 131-139.

Schey KL, Grey AC, Nicklay JJ. 2013. Mass spectrometry of membrane proteins: a focus on aquaporins. *Biochemistry* **52:** 3807-3817.

Schrank E, Wagner GE, Zangger K. 2013. Solution NMR studies on the orientation of membrane-bound peptides and proteins by paramagnetic probes. *Molecules* **18:** 7407-7435.

Schüssler MD, Alexandersson E, Bienert GP, Kichey T, Laursen KH, Johanson U, Kjellbom P, Schjoerring JK, Jahn TP. 2008. The effects of the loss of TIP1;1 and TIP1;2 aquaporins in Arabidopsis thaliana. *Plant J* **56:** 756-767.

Schuurmans JA, van Dongen JT, Rutjens BP, Boonman A, Pieterse CM, Borstlap AC. 2003. Members of the aquaporin family in the developing pea seed coat include representatives of the PIP, TIP, and NIP subfamilies. *Plant Mol Biol* **53:** 633-645.

Secchi F, Zwieniecki MA. 2010. Patterns of PIP gene expression in Populus trichocarpa during recovery from xylem embolism suggest a major role for the PIP1 aquaporin subfamily as moderators of refilling process. *Plant Cell Environ* **33:** 1285-1297.

Sfera A, Osorio C. 2014. Water for thought: is there a role for aquaporin channels in delirium? *Front Psychiatry* **5:** 57.

Shachar-Hill B, Hill AE, Powell J, Skepper JN, Shachar-Hill Y. 2013. Mercury-sensitive water channels as possible sensors of water potentials in pollen. *J Exp Bot* **64:** 5195-5205.

Shi PP, Cao XR, Qu J, Volk KA, Kirby P, Williamson RA, Stokes JB, Yang B. 2007. Nephrogenic diabetes insipidus in mice caused by deleting COOH-terminal tail of aquaporin-2. *Am J Physiol Renal Physiol* **292:** F1334-1344.

Shi Y. 2013. Common folds and transport mechanisms of secondary active transporters. *Annu Rev Biophys* **42:** 51-72.

Shimazaki K, Doi M, Assmann SM, Kinoshita T. 2007. Light regulation of stomatal movement. *Annu Rev Plant Biol* **58:** 219-247.

Siefritz F, Biela A, Eckert M, Otto B, Uehlein N, Kaldenhoff R. 2001. The tobacco plasma membrane aquaporin NtAQP1. *J Exp Bot* **52:** 1953-1957.

Siefritz F, Otto B, Bienert GP, van der Krol A, Kaldenhoff R. 2004. The plasma membrane aquaporin NtAQP1 is a key component of the leaf unfolding mechanism in tobacco. *Plant J* **37:** 147-155.

Siefritz F, Tyree MT, Lovisolo C, Schubert A, Kaldenhoff R. 2002. PIP1 plasma membrane aquaporins in tobacco: from cellular effects to function in plants. *Plant Cell* **14:** 869-876.

Sjohamn J, Hedfalk K. 2014. Unraveling aquaporin interaction partners. *Biochim Biophys Acta* **1840:** 1614-1623.

Skelton LA, Boron WF, Zhou Y. 2010. Acid-base transport by the renal proximal tubule. *J Nephrol* **23 Suppl 16:** S4-18.

Smith BL, Preston GM, Spring FA, Anstee DJ, Agre P. 1994. Human red cell aquaporin CHIP. I. Molecular characterization of ABH and Colton blood group antigens. *J Clin Invest* **94:** 1043-1049.

Spirin AS, Baranov VI, Ryabova LA, Ovodov SY, Alakhov YB. 1988. A continuous cell-free translation system capable of producing polypeptides in high yield. *Science* **242:** 1162-1164.

Stech M, Merk H, Schenk JA, Stocklein WF, Wustenhagen DA, Micheel B, Duschl C, Bier FF, Kubick S. 2012. Production of functional antibody fragments in a vesicle-based eukaryotic cell-free translation system. *J Biotechnol* **164:** 220-231.

Stech M, Quast RB, Sachse R, Schulze C, Wustenhagen DA, Kubick S. 2014. A continuous-exchange cell-free protein synthesis system based on extracts from cultured insect cells. *PLoS One* **9:** e96635.

Stoenescu R, Graff A, Meier W. 2004. Asymmetric ABC-triblock copolymer membranes induce a directed insertion of membrane proteins. *Macromol Biosci* **4:** 930-935.

Stougaard J. 2000. Regulators and regulation of legume root nodule development. *Plant Physiol* **124:** 531-540.

Studier FW, Moffatt BA. 1986. Use of bacteriophage T7 RNA polymerase to direct selective high-level expression of cloned genes. *J Mol Biol* **189:** 113-130.

Subramaniam S, Henderson R. 2000. Molecular mechanism of vectorial proton translocation by bacteriorhodopsin. *Nature* **406:** 653-657.

Suga S, Maeshima M. 2004. Water channel activity of radish plasma membrane aquaporins heterologously expressed in yeast and their modification by site-directed mutagenesis. *Plant Cell Physiol* **45:** 823-830.

Sui H, Han BG, Lee JK, Walian P, Jap BK. 2001. Structural basis of water-specific transport through the AQP1 water channel. *Nature* **414:** 872-878.

Sun G, Chung T, Jeyaseelan K, Armugam A. 2013. A layer-by-layer self-assembly approach to developing an aquaporin-embedded mixed matrix membrane. *RSC Adv***:** 473-481.

Sundell KS, Sundh H. 2012. Intestinal fluid absorption in anadromous salmonids: importance of tight junctions and aquaporins. *Front Physiol* **3:** 388.

Sutka M, Li G, Boudet J, Boursiac Y, Doumas P, Maurel C. 2011. Natural variation of root hydraulics in Arabidopsis grown in normal and salt-stressed conditions. *Plant Physiol* **155:** 1264-1276.

Suzuki H, Nishikawa K, Hiroaki Y, Fujiyoshi Y. 2008. Formation of aquaporin-4 arrays is inhibited by palmitoylation of N-terminal cysteine residues. *Biochim Biophys Acta* **1778:** 1181-1189.

Tait MJ, Saadoun S, Bell BA, Papadopoulos MC. 2008. Water movements in the brain: role of aquaporins. *Trends Neurosci* **31:** 37-43.

Takano J, Wada M, Ludewig U, Schaaf G, von Wiren N, Fujiwara T. 2006. The Arabidopsis major intrinsic protein NIP5;1 is essential for efficient boron uptake and plant development under boron limitation. *Plant Cell* **18:** 1498-1509.

Takata K, Matsuzaki T, Tajika Y. 2004. Aquaporins: water channel proteins of the cell membrane. *Prog Histochem Cytochem* **39:** 1-83.

Tan S, Tan HT, Chung MC. 2008. Membrane proteins and membrane proteomics. *Proteomics* **8:** 3924-3932.

Tang C, Wang Z, Petrinić I, Fane AG, Hélix-Nielsen C. 2015. Biomimetic aquaporin membranes coming of age. *Desalination***:** 89-105.

Tani K, Mitsuma T, Hiroaki Y, Kamegawa A, Nishikawa K, Tanimura Y, Fujiyoshi Y. 2009. Mechanism of aquaporin-4's fast and highly selective water conduction and proton exclusion. *J Mol Biol* **389:** 694-706.

Temmei Y, Uchida S, Hoshino D, Kanzawa N, Kuwahara M, Sasaki S, Tsuchiya T. 2005. Water channel activities of Mimosa pudica plasma membrane intrinsic proteins are regulated by direct interaction and phosphorylation. *FEBS Lett* **579:** 4417-4422.

Terryn S, Ho A, Beauwens R, Devuyst O. 2011. Fluid transport and cystogenesis in autosomal dominant polycystic kidney disease. *Biochim Biophys Acta* **1812:** 1314-1321.

Thenral ST, Vanisree AJ. 2012. Peripheral assessment of the genes AQP4, PBP and TH in patients with Parkinson's disease. *Neurochem Res* **37:** 512-515.

Thogersen L, Nissen P. 2012. Flexible P-type ATPases interacting with the membrane. *Curr Opin Struct Biol* **22:** 491-499.

Tingaud-Sequeira A, Calusinska M, Finn RN, Chauvigne F, Lozano J, Cerda J. 2010. The zebrafish genome encodes the largest vertebrate repertoire of functional aquaporins with dual paralogy and substrate specificities similar to mammals. *BMC Evol Biol* **10:** 38.

To J, Torres J. 2015. Can Stabilization and Inhibition of Aquaporins Contribute to Future Development of Biomimetic Membranes? *Membranes (Basel)* **5:** 352-368.

To J, Yeo CY, Soon CH, Torres J. 2015. A generic high-throughput assay to detect aquaporin functional mutants: Potential application to discovery of aquaporin inhibitors. *Biochim Biophys Acta* **1850:** 1869-1876.

Tomkowiak E, Pienkowska JR. 2010. The current knowledge of invertebrate aquaporin water channels with particular emphasis on insect AQPs. *Adv Cell Biol* **2:** 91-104.

Tong J, Canty JT, Briggs MM, McIntosh TJ. 2013. The water permeability of lens aquaporin-0 depends on its lipid bilayer environment. *Exp Eye Res* **113:** 32-40.

Törnroth-Horsefield S, Hedfalk K, Fischer G, Lindkvist-Petersson K, Neutze R. 2010. Structural insights into eukaryotic aquaporin regulation. *FEBS Lett* **584:** 2580-2588.

Törnroth-Horsefield S, Wang Y, Hedfalk K, Johanson U, Karlsson M, Tajkhorshid E, Neutze R, Kjellbom P. 2006. Structural mechanism of plant aquaporin gating. *Nature* **439:** 688-694.

Tourdias T, Mori N, Dragonu I, Cassagno N, Boiziau C, Aussudre J, Brochet B, Moonen C, Petry KG, Dousset V. 2011. Differential aquaporin 4 expression during edema build-up and resolution phases of brain inflammation. *J Neuroinflammation* **8:** 143.

Tournaire-Roux C, Sutka M, Javot H, Gout E, Gerbeau P, Luu DT, Bligny R, Maurel C. 2003. Cytosolic pH regulates root water transport during anoxic stress through gating of aquaporins. *Nature* **425:** 393-397.

Towbin H, Staehelin T, Gordon J. 1979. Electrophoretic transfer of proteins from polyacrylamide gels to nitrocellulose sheets: procedure and some applications. *Proc Natl Acad Sci U S A* **76:** 4350-4354.

Trinh MH, Odorico M, Pique ME, Teulon JM, Roberts VA, Ten Eyck LF, Getzoff ED, Parot P, Chen SW, Pellequer JL. 2012. Computational reconstruction of multidomain proteins using atomic force microscopy data. *Structure* **20:** 113-120.

Tsukaguchi H, Weremowicz S, Morton CC, Hediger MA. 1999. Functional and molecular characterization of the human neutral solute channel aquaporin-9. *Am J Physiol* **277:** F685-696.

Tyerman SD, Bohnert HJ, Maurel C, Steudle E, Smith JAC. 1999. Plant aquaporins: their molecular biology, biophysics and significance for plant water relations. *J Exp Bot* **50:** 1055-1071.

Uehlein N, Lovisolo C, Siefritz F, Kaldenhoff R. 2003. The tobacco aquaporin NtAQP1 is a membrane CO2 pore with physiological functions. *Nature* **425:** 734-737.

Uehlein N, Otto B, Eilingsfeld A, Itel F, Meier W, Kaldenhoff R. 2012. Gas-tight triblock-copolymer membranes are converted to CO(2) permeable by insertion of plant aquaporins. *Sci Rep* **2:** 538.

Uehlein N, Otto B, Hanson DT, Fischer M, McDowell N, Kaldenhoff R. 2008. Function of Nicotiana tabacum aquaporins as chloroplast gas pores challenges the concept of membrane CO2 permeability. *Plant Cell* **20:** 648-657.

van Heeswijk MP, van Os CH. 1986. Osmotic water permeabilities of brush border and basolateral membrane vesicles from rat renal cortex and small intestine. *J Membr Biol* **92:** 183-193.

Venkatakrishnan AJ, Levy ED, Teichmann SA. 2010. Homomeric protein complexes: evolution and assembly. *Biochem Soc Trans* **38:** 879-882.

Vera-Estrella R, Barkla BJ, Bohnert HJ, Pantoja O. 2004. Novel regulation of aquaporins during osmotic stress. *Plant Physiol* **135:** 2318-2329.

Verbavatz JM, Brown D, Sabolic I, Valenti G, Ausiello DA, Van Hoek AN, Ma T, Verkman AS. 1993. Tetrameric assembly of CHIP28 water channels in liposomes and cell membranes: a freeze-fracture study. *J Cell Biol* **123:** 605-618.

Verdoucq L, Grondin A, Maurel C. 2008. Structure-function analysis of plant aquaporin AtPIP2;1 gating by divalent cations and protons. *Biochem J* **415:** 409-416.

Verkman AS. 2005. More than just water channels: unexpected cellular roles of aquaporins. *J Cell Sci* **118:** 3225-3232.

Verma RK, Prabh ND, Sankararamakrishnan R. 2015. Intra-helical salt-bridge and helix destabilizing residues within the same helical turn: Role of functionally important loop E half-helix in channel regulation of major intrinsic proteins. *Biochim Biophys Acta* **1848:** 1436-1449.

Vinothkumar KR, Henderson R. 2010. Structures of membrane proteins. *Q Rev Biophys* **43:** 65-158.

Virkki LV, Franke C, Somieski P, Boron WF. 2002. Cloning and functional characterization of a novel aquaporin from Xenopus laevis oocytes. *J Biol Chem* **277:** 40610-40616.

Vojdani A, Mukherjee PS, Berookhim J, Kharrazian D. 2015. Detection of Antibodies against Human and Plant Aquaporins in Patients with Multiple Sclerosis. *Autoimmune Dis* **2015:** 905208.

von Heijne G. 2006. Membrane-protein topology. *Nat Rev Mol Cell Biol* **7:** 909-918.

Wallace IS, Roberts DM. 2005. Distinct transport selectivity of two structural subclasses of the nodulin-like intrinsic protein family of plant aquaglyceroporin channels. *Biochemistry* **44:** 16826-16834.

Wan X, Steudle E, Hartung W. 2004. Gating of water channels (aquaporins) in cortical cells of young corn roots by mechanical stimuli (pressure pulses): effects of ABA and of HgCl2. *J Exp Bot* **55:** 411-422.

Wang HL, Chung T, Tong YW, Jeyaseelan K, Armugam A, Phuoc Duong HH, Fu F, Seah H, Yang J, Hong M. 2013. Mechanically robust and highly permeable AquaporinZ biomimetic membranes. *J Memb Sci***:** 130-136.

Wang LL, Chen AP, Zhong NQ, Liu N, Wu XM, Wang F, Yang CL, Romero MF, Xia GX. 2014. The Thellungiella salsuginea tonoplast aquaporin TsTIP1;2 functions in protection against multiple abiotic stresses. *Plant Cell Physiol* **55:** 148-161.

Wang Y, Tajkhorshid E. 2010. Nitric oxide conduction by the brain aquaporin AQP4. *Proteins* **78:** 661-670.

Waterhouse AM, Procter JB, Martin DM, Clamp M, Barton GJ. 2009. Jalview Version 2--a multiple sequence alignment editor and analysis workbench. *Bioinformatics* **25:** 1189-1191.

Weaver CD, Crombie B, Stacey G, Roberts DM. 1991. Calcium-dependent phosphorylation of symbiosome membrane proteins from nitrogen-fixing soybean nodules : evidence for phosphorylation of nodulin-26. *Plant Physiol* **95:** 222-227.

Weber K, Osborn M. 1969. The reliability of molecular weight determinations by dodecyl sulfate-polyacrylamide gel electrophoresis. *J Biol Chem* **244:** 4406-4412.

Weig A, Deswarte C, Chrispeels MJ. 1997. The major intrinsic protein family of Arabidopsis has 23 members that form three distinct groups with functional aquaporins in each group. *Plant Physiol* **114:** 1347-1357.

Wellner RB, Cotrim AP, Hong S, Swaim WD, Baum BJ. 2005. Localization of AQP5/AQP8 chimeras in MDCK-II cells: exchange of the N- and C-termini. *Biochem Biophys Res Commun* **330:** 172-177.

Wessel D, Flugge UI. 1984. A method for the quantitative recovery of protein in dilute solution in the presence of detergents and lipids. *Anal Biochem* **138:** 141-143.

Wree D, Wu B, Zeuthen T, Beitz E. 2011. Requirement for asparagine in the aquaporin NPA sequence signature motifs for cation exclusion. *FEBS J* **278:** 740-748.

Wudick MM, Luu DT, Maurel C. 2009. A look inside: localization patterns and functions of intracellular plant aquaporins. *New Phytol* **184:** 289-302.

Wysocki R, Chery CC, Wawrzycka D, Van Hulle M, Cornelis R, Thevelein JM, Tamas MJ. 2001. The glycerol channel Fps1p mediates the uptake of arsenite and antimonite in Saccharomyces cerevisiae. *Mol Microbiol* **40:** 1391-1401.

Xie LL, Sun XL, Fan Y, Kong H, Ding JH, Hu G. 2009. Aquaporin 4 knockout resists negative regulation of neural cell proliferation by cocaine in mouse hippocampus. *Int J Neuropsychopharmacol* **12:** 843-850.

Xu L, Zhou Y, Boron WF. 2011. Role of aquaporin 1 (AQP1) as a CO_2 channel in chronic metabolic acidosis. *FASEB J*: 834-835.

Yakir E, Hilman D, Harir Y, Green RM. 2007. Regulation of output from the plant circadian clock. *FEBS J* **274:** 335-345.

Yang B, Verkman AS. 1997. Water and glycerol permeabilities of aquaporins 1-5 and MIP determined quantitatively by expression of epitope-tagged constructs in Xenopus oocytes. *J Biol Chem* **272:** 16140-16146.

Yang W, Wu Q, Yuan C, Gao J, Xiao M, Gu M, Ding J, Hu G. 2012. Aquaporin-4 mediates astrocyte response to beta-amyloid. *Mol Cell Neurosci* **49:** 406-414.

Yool AJ, Weinstein AM. 2002. New roles for old holes: ion channel function in aquaporin-1. *News Physiol Sci* **17:** 68-72.

Yoon Y, Lueptow RM. 2005. Removal of organic contaminants by RO and NF membranes. *J Memb Sci* **261:** 76-86.

Yukutake Y, Yasui M. 2010. Regulation of water permeability through aquaporin-4. *Neuroscience* **168:** 885-891.

Zampighi GA, Hall JE, Kreman M. 1985. Purified lens junctional protein forms channels in planar lipid films. *Proc Natl Acad Sci U S A* **82:** 8468-8472.

Zardoya R. 2005. Phylogeny and evolution of the major intrinsic protein family. *Biol Cell* **97:** 397-414.

Zeidel ML, Nielsen S, Smith BL, Ambudkar SV, Maunsbach AB, Agre P. 1994. Ultrastructure, pharmacologic inhibition, and transport selectivity of aquaporin channel-forming integral protein in proteoliposomes. *Biochemistry* **33:** 1606-1615.

Zelazny E, Miecielica U, Borst JW, Hemminga MA, Chaumont F. 2009. An N-terminal diacidic motif is required for the trafficking of maize aquaporins ZmPIP2;4 and ZmPIP2;5 to the plasma membrane. *Plant J* **57:** 346-355.

Zemella A, Thoring L, Hoffmeister C, Kubick S. 2015. Cell-Free Protein Synthesis: Pros and Cons of Prokaryotic and Eukaryotic Systems. *Chembiochem* **16:** 2420-2431.

Zeuthen T, Wu B, Pavlovic-Djuranovic S, Holm LM, Uzcategui NL, Duszenko M, Kun JF, Schultz JE, Beitz E. 2006. Ammonia permeability of the aquaglyceroporins from Plasmodium falciparum, Toxoplasma gondii and Trypansoma brucei. *Mol Microbiol* **61:** 1598-1608.

Zhang WH, Tyerman SD. 1999. Inhibition of water channels by HgCl2 in intact wheat root cells. *Plant Physiol* **120:** 849-858.

Zhao XQ, Mitani N, Yamaji N, Shen RF, Ma JF. 2010. Involvement of silicon influx transporter OsNIP2;1 in selenite uptake in rice. *Plant Physiol* **153:** 1871-1877.

Zhao Y, Qiu C, Li X, Vararattanavech A, Shen W, Torres J, Helix-Nielsen C, Wang R, Hu X, Fane AG, Tang C. 2012. Synthesis of robust and high-performance auqaporin-based biomimetic membranes by interfacial polymerization-membrane preparation and RO performance characterization. *J Memb Sci* **423-424:** 422-428.

Zhou HX, Cross TA. 2013. Influences of membrane mimetic environments on membrane protein structures. *Annu Rev Biophys* **42:** 361-392.

Zhou S, Hu W, Deng X, Ma Z, Chen L, Huang C, Wang C, Wang J, He Y, Yang G, He G. 2012. Overexpression of the wheat aquaporin gene, TaAQP7, enhances drought tolerance in transgenic tobacco. *PLoS One* **7:** e52439.

Zuo G, Shen R, Ma S, Guo W. 2010. Transport properties of single-file water molecules inside a carbon nanotube biomimicking water channel. *ACS Nano* **4:** 205-210.

Acknowledgements

First and foremost, I would like to thank Dr. Lei Kai for the supervision of my thesis. His dedication towards methodical precision and vast knowledge on all things regarding cell-free protein expression and aquaporins helped me immensely during the course of this work.

Next, I would like to thank Dr. Anastassia Boudichevskaia and her husband for her invaluable input on statistics, as well as their combined, outrageous skills in programming the makros necessary for the mathematical fitting of my raw data curves on aquaporin water permeability. Thanks to them, I was able to cut the required computing time for the collected 6,000 raw data curves down to just 3 days as opposed to approximately a month. Aside from that, I can vouch for the fact that statisticians and programmers have a good sense of humor!

I would also like to thank Magdalena Lachnit, Dr. Simon Heppel, Nam Trung Tran and Dr. Norbert Uehlein for providing me with everyday advice on lab work, equipment maintenance and repair, as well as the occasional jokes to lift the spirit during the more difficult days of my thesis.

A very special thanks is dedicated to Dr. Christoph Schwarz, Prof. Dr. Heribert Warzecha and Sebastian Hoeler for helping me out during my “final sprint towards the finish line” of my doctoral thesis. Not only did they provide priceless input in terms of proofreading my thesis and defence presentation / preparation, but they also ensured a fairer implementation of due process than would otherwise have been possible.

Last, but the very opposite of least, I would like to send a heartful THANK YOU to my girlfriend Renata, my parents (in Germany, as well as in Denmark), my best friends Julia and Andreas, as well as all family members and friends who were the actual reason all of this was made possible. I could not have done this without your never-ending emotional, financial and general support in all things that make a difference in my life.

Curriculum Vitae – Gabriel Glitsos

WORK EXPERIENCE

04/2013 – 03/2017 **RESEARCH ASSISTANT / PHD (DR. RER. NAT.) IN APPLIED PLANT SCIENCES AT THE DARMSTADT UNIVERSITY OF TECHNOLOGY, GERMANY**

- PhD thesis topic involved the molecular characterization of tobacco derived aquaporins with regard to their water mediation through liposomes via domain exchange, Cell-Free expression, Stopped Flow measurements and *In Silico* analyses
- Other responsibilities included organization and supervision of student courses, IT administration, technical maintenance of laboratory equipment and management of liquid nitrogen transport and storage

10/2012 – 03/2013 **LABORATORY TECHNICIAN FOR WENO WERKZEUG & MASCHINENBAU GMBH, BASED IN VIERSEN, GERMANY**

- Involvement in a project for the optimization of a fully automated, climate-controlled imaging system to be deployed in the area of medical diagnostics and bacterial cell growth
- Responsibilities as liaison between construction team and medical diagnostics client included the preparation, handling and analysis of bacterial culture samples and providing input for optimizing the imaging system

04/2012 – 09/2012 **BIOPROCESS TECHNICIAN FOR BIOPLASTECH LTD., BASED IN MALAHIDE, COUNTY DUBLIN, IRELAND**

- Management of a research based pilot scale fermentation project for the production of polyhydroxyalkanoate (PHA) derived biodegradable plastics in *Pseudomonas putida*
- Responsibilities included the preparation of precultures & media and the day to day operation of 30 l and 650 l fermentors

10/2007 – 05/2008 **TRAINEE AT S*BIO PTE LTD. IN SCIENCE PARK II, SINGAPORE**

- Position inside the company's Biology R&D department with the focus on small molecule drug design for the treatment of cancer
- Project topic: Cloning, expression and GST-Tag purification of EZH2 human methyltransferase truncation mutants by use of a combined *E. coli / Baculovirus - Spodoptera frugiperda* insect cell cultivation system

EDUCATION

10/2009 – 03/2012 **MASTER OF SCIENCE IN BIOTECHNOLOGY AT THE WESTFÄLISCHE WILHELMS-UNIVERSITY IN MÜNSTER, GERMANY**

- Master thesis: Expression, Purification and Characterization of different Cyanophycin Synthetases in *E. coli* with Regard to Substrate Specificity
- Most relevant courses: Purification & characterization of biotechnically relevant enzymes, large-scale fermentation and biosynthesis of various polymers, innovation management & patent law
- Certified attendance of a course on safety measures and occupational safety during genetic engineering operations

05/2010 – 10/2010 **DAAD SCHOLARSHIP PROGRAM "A NEW PASSAGE TO INDIA" AT THE UNIVERSITY OF HYDERABAD, HYDERABAD, ANDHRA PRADESH, INDIA**

- Completion of a research project: Cloning of a GFP marker into Bacterial Broad Host Range Plasmids for Labelling of Wildtype and *opd*$^{-}$ Mutant Strains of *Brevundimonas diminuta*
- Attendance of classes in bioinformatics, as well as Hindi language and culture

10/2008 – 09/2009 **MASTER OF SCIENCE STUDENT IN LIFE SCIENCE AT THE UNIVERSITY OF KONSTANZ, KONSTANZ, GERMANY (DISCONTINUED)**

10/2004 – 08/2007 **BACHELOR OF SCIENCE IN BIOTECHNOLOGY AT RWTH AACHEN UNIVERSITY, AACHEN, GERMANY**

- Bachelor thesis: Integrative establishment of a production process for recombinant proteins in *E. coli*

Statutatory Declaration (Ehrenwörtliche Erklärung)

Ich erkläre hiermit ehrenwörtlich, dass ich die vorliegende Arbeit entsprechend den Regeln guter wissenschaftlicher Praxis selbstständig und ohne unzulässige Hilfe Dritter angefertigt habe.

Sämtliche aus fremden Quellen direkt oder indirekt übernommenen Gedanken sowie sämtliche von Anderen direkt oder indirekt übernommenen Daten, Techniken und Materialien sind als solche kenntlich gemacht. Die Arbeit wurde bisher bei keiner anderen Hochschule zu Prüfungszwecken eingereicht.

Darmstadt, den